

REPORT DOCUMENTATION PAGE

Form Approved OMB No. 0704-0188

Public reporting burden for this collection of information is estimated to average 1 hour per response, including the time for reviewing instructions, searching existing data sources, gathering and maintaining the data needed, and completing and reviewing the collection of information. Send comments regarding this burden estimate or any other aspect of this collection of information, including suggestions for reducing this burden to Washington Headquarters Services, Directorate for Information Operations and Reports, 1215 Jefferson Davis Highway, Suite 1204, Arlington, VA 22202-4302, and to the Office of Management and Budget, Paperwork Reduction Project (0704-0188), Washington, DC 20503.

1. AGENCY USE ONLY (Leave blank)		2. REPORT DATE 21 April 1998	3. REPORT TYPE AND DATES COVERED Conference Proceedings	
4. TITLE AND SUBTITLE Quantum Optics IV			5. FUNDING NUMBERS F6170897W0093	
6. AUTHOR(S) Jan Mostowski and Arkadiusz Orlowski				
7. PERFORMING ORGANIZATION NAME(S) AND ADDRESS(ES) Center for Theoretical Physics, Polish Academy of Sciences Al. Lotnikow 32/46 Warsaw 02 668 Poland			8. PERFORMING ORGANIZATION REPORT NUMBER N/A	
9. SPONSORING/MONITORING AGENCY NAME(S) AND ADDRESS(ES) EOARD PSC 802 BOX 14 FPO 09499-0200			10. SPONSORING/MONITORING AGENCY REPORT NUMBER CSP 97-1041	
11. SUPPLEMENTARY NOTES				
12a. DISTRIBUTION/AVAILABILITY STATEMENT Approved for public release; distribution is unlimited.			12b. DISTRIBUTION CODE A	
13. ABSTRACT (Maximum 200 words) The Final Proceedings for Quantum Optics IV, 17 June 1997 - 24 June 1997. The leading themes of the meeting were: cold atoms, strong laser field-atom interactions, and quantum chaos.				
14. SUBJECT TERMS Atom Optics, Physics, Quantum Coherence, Non-linear Optics			15. NUMBER OF PAGES 251	
			16. PRICE CODE N/A	
17. SECURITY CLASSIFICATION OF REPORT UNCLASSIFIED	18. SECURITY CLASSIFICATION OF THIS PAGE UNCLASSIFIED	19. SECURITY CLASSIFICATION OF ABSTRACT UNCLASSIFIED	20. LIMITATION OF ABSTRACT UL	

NSN 7540-01-280-5500

Standard Form 298 (Rev. 2-89)
Prescribed by ANSI Std. Z39-18
298-102

19980501 198

Contents

INTRODUCTION	2
CHAPTER I. A MODEL OF THE ATMOSPHERE	4
1.1. Altitude profiles of atmospheric parameters	4
1.2. Intercomparison of models of the atmospheric turbulence spectrum	19
1.3. Effective outer scale of atmospheric turbulence	27
References to Chapter I	33
CHAPTER II. MATHEMATICAL SIMULATION OF LASER BEAM PROPAGATION IN THE ATMOSPHERE	35
2.1. Problem of coherent radiation propagation	35
2.2. Generation of random 2D phase screens by Fourier transform	47
2.3. Dynamic simulation of large-scale turbulent aberrations of optical phase	56
2.4. Modification of the numeric model to the case of partially coherent beams	63
2.5. Modeling the wavefront dislocations	68
References to Chapter II	74

INTRODUCTION

The present report is the first in a series to be written according to contract F61708-97-W0126. It was assumed that at this stage a method of solution of the wave equation governing propagation of beams in the atmosphere should be described. The atmosphere must be considered as a turbulent, scattering, and absorbing medium. Accurate description of phase and intensity fluctuations of optical waves should also be included in the method.

The splitting algorithm of solution that we chose gives one the possibility to realize efficient computational algorithms that take into account all important parameters of optical experiment.

Randomly inhomogeneous atmosphere was described using models for the main atmospheric parameters.

A model of atmospheric turbulence. Modeling atmospheric turbulence on the path of propagation we used Kolmogorov - Obukhov model. Characteristic feature of this model is infinite outer scale of turbulence. Models allowing for deviations of turbulent spectrum in low frequency region were also introduced in our algorithm.

A finite size of the outer scale and possibility to use von Karman, Greenwood and some other models was proved in the early seventies by Dr. S. Clifford and was also confirmed by our researches. The fact that the outer scale is finite in the atmospheric boundary layer was demonstrated by a number of authors, namely, by Dr. M. Sarazin (experiments were performed in Chili), by Dr. S. McKecknie (Arizona region), and also by measurements at Mauna Kea (Hawaii), and by our own experiments.

Numerous results obtained experimentally allow us to introduce in our model a finite outer scale of atmospheric turbulence. Computing variance of phase fluctuation, for the first time we have compared three the most widely used models of turbulent atmosphere.

Using the models of vertical distribution of turbulence intensity, wind velocity, and outer scale of turbulence, for the vertical atmospheric column we introduced such parameter as an effective outer scale of turbulence, also for the first time.

All in all, materials presented in the two chapters of this report can be viewed as a base for a computer code simulating laser beams propagation in the atmosphere under various conditions. Namely, coherent and partially coherent beams can be described, as well as high-power beams propagating along vertical, slanted, and horizontal paths. Using our models it is possible to compare results of numerical experiments with data of well-known field experiments (for example, with such experiments of US Air Force Phillips Lab as HABE and ARL).

CHAPTER I. A MODEL OF THE ATMOSPHERE

1.1. Altitude profiles of atmospheric parameters

Altitude **profile of turbulence intensity** C_n^2 is an important parameter determining such key parameters as coherence length, size of anisoplanatic patch and some others. In Russia, basing on regular field experiments, semiempirical model of C_n^2 dependence on altitude was developed by Gurvich and Gracheva /15/. The model corresponds to three types of atmospheric conditions:

a) the «best» conditions of propagation (weak turbulence);

$$C_n^2(h[km]) = 5.19 \cdot 10^{-16} \cdot 10^{-0.86 \cdot h} + 10^{-18.34+0.29h-0.0284h^2+0.000743h^3}; \quad (1.1)$$

b) the «worst» conditions of propagation (strong turbulence);

$$C_n^2(h[km]) = 9.5 \cdot 10^{-14} \cdot 10^{-2.09h} + 10^{-14.39+0.17h-0.0348h^2+0.000959h^3}; \quad (1.2)$$

c) «average» conditions of propagation

$$C_n^2(h) = \sqrt{C_n^2(best) \cdot C_n^2(worst)}. \quad (1.3)$$

Graphics of C_n^2 dependence on altitude corresponding to these conditions are presented in Fig. 1.1.

Along with this model we also use well-known models such as the model of Maui Air Force Optical Station /20/ denoted as SLC model /1, 20/.

Daytime model		Nighttime model	
Altitude range	C_n^2 value	Altitude range	C_n^2 value
$h < 18,5m$	1.70×10^{-14}	$h < 18,5m$	8.4×10^{-15}
$18,5 < h < 240m$	$3.13 \times 10^{-13}/h$	$18,5 < h < 110m$	$2.87 \times 10^{-12}/h^2$
$240 < h < 880$	1.3×10^{-15}	$110 < h < 1500$	8.4×10^{-15}
$880 < h < 7200$	$8.87 \times 10^{-7}/h^3$	$1500 < h < 7200$	$8.87 \times 10^{-7}/h^3$
$7200 < h < 20000$	$2.00 \times 10^{-16}/h^{0.5}$	$7200 < h < 20000$	$2.00 \times 10^{-16}/h^{0.5}$

The **outer scale of a turbulence** defines variance of centroid jitter for beams and images. With a laser guide star possibility of correction for turbulent jitter in

an adaptive optics system is principally limited, so in such systems the outer scale influences greatly residual errors.

Also we have analyzed a number of models descriptions of which were published. Namely, the Greenwood good seeing model /21/ and the Hufnagel-Vally model /22/ with an upper atmospheric wind of 54 miles per hour (≈ 24 m/s).

Presently, there exist a lot of models of $L_0(h)$ altitude profiles. Some models are presented below:

$$(A) \quad L_0(h) = \begin{cases} 0,4 & h \leq 1m \\ 0,4h & h > 1m \end{cases} \quad (1.4)$$

$$(B) \quad L_0(h) = \begin{cases} 0,4 & h \leq 1m \\ 0,4h & 1 < h < 25m \\ 2\sqrt{h} & h > 25m \end{cases} \quad (1.5)$$

$$(C) \quad L_0(h) = \begin{cases} 0,4 & h \leq 1m \\ 0,4h & 1 < h < 25m \\ 2\sqrt{h} & 25 < h < 1000m \\ 2\sqrt{1000} & h > 1000m \end{cases} \quad (1.6)$$

$$(D) \quad L_0(h) = \frac{5}{1 + \left[\frac{h - 7500}{2000} \right]^2} \quad (1.7)$$

$$(E) \quad L_0(h) = \frac{4}{1 + \left[\frac{h - 8500}{2500} \right]^2} \quad (1.8)$$

The model (A) is recommended by the authors of Ref. 14 for small heights, (B) is proposed by Fried /1,3/, and (C) is the generalization of models (A) and (B). Shortcomings of the model (A) are well-known so it was not considered in this report. The models (D) and (E) are obtained by generalizing the results of measurements performed in the USA, France, and Chile /1,4,5/.

The vertical profiles corresponding to these models are presented in Fig.1.2. As one can see, the graphs (E) and (D) are similar in character of growth

and in the presence of maximal value at a certain height; so one can consider the first model and obtain the main features of the second.

Wind velocity is a parameter that influence turbulent as well as nonlinear effects which appear at high-power beam propagation in the atmosphere. In the first case wind velocity defines the time of turbulent inhomogeneties transition through a cross section of a beam or an aperture of a telescope that influence temporal spectra of intensity and phase fluctuations of optical waves. So wind speed imposes additional requirements on the temporal bandwidth of adaptive control.

At thermal blooming of high-power beams time of transient processes is also dependent on wind speed. Moreover, wind speed is a parameter that determine intensity of thermal blooming along with a molecular and aerosol absorption because phase aberrations on a path of propagation are inversely proportional to wind velocity.

In our calculation we often use Bufton's model /1/. This model is described by the following equation

$$V(h) = V_g + 30 \exp\left(-\left[\frac{h - 9400}{4800}\right]^2\right), \quad (1.9)$$

where V_g is a parameter of the model corresponding to the wind speed near the surface. We assume that $V_g = 5$ m/s.

Of course, one should keep in mind that the wind velocity changes during a year and even during a day. Moreover, the wind velocity is dependent from geographical position of a site. So for every particular case a particular model should be chosen.

It should also be emphasized that the model of a beam propagating in the atmosphere includes a transverse component of vector sum of the wind velocity and velocity of slewing.

Absorption of optics energy by air is a cause of well-known nonlinear effect referred to as thermal blooming. The coefficient of absorption is a sum of two components: molecular α_m and aerosol α_a . The both components are functions of wavelength:

$$\alpha_{abs} = \alpha_m(\lambda) + \alpha_a(\lambda). \quad (1.10)$$

Atmospheric aerosol absorbs and scatters radiation, so the whole extinction of radiation is the sum of three components: molecular absorption α_m , aerosol absorption α_a , and aerosol scattering α_s :

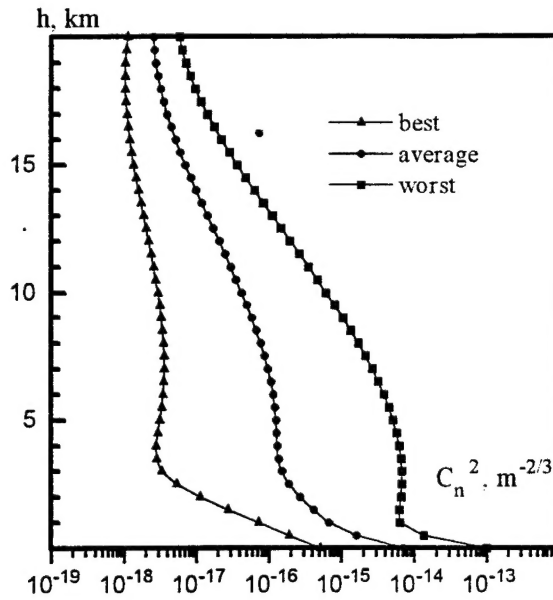


Fig. 1.1 Altitude profiles of turbulence intensity

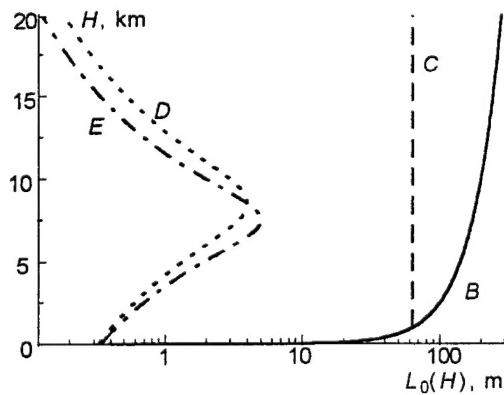


Fig. 1.2 Altitude profiles of the outer scale of turbulence.

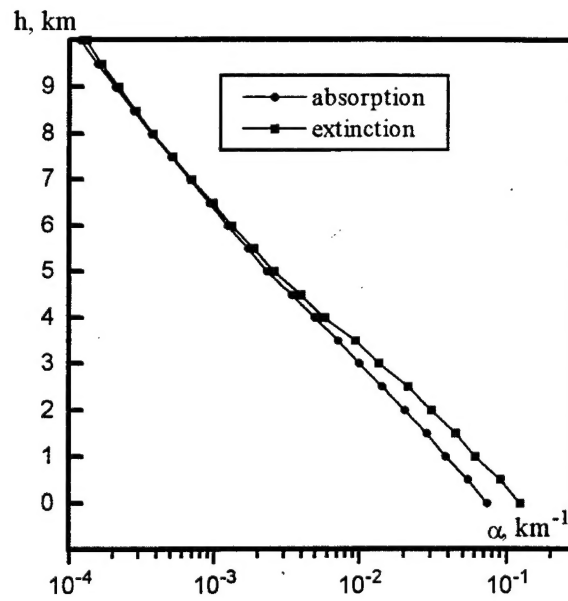


Fig. 1.3. Altitude profiles of absorption and extinction coefficients.

$$\alpha_{ext} = \alpha_m + \alpha_a + \alpha_s. \quad (1.11)$$

All the terms in this equation are functions of wavelength, but the sharpest dependence on wavelength is characteristic for molecular absorption. There are specialized spectroscopic databases and models of altitude profiles of atmosphere gaseous composition using which is possible to compute altitude profiles of molecular absorption. Atmosphere gaseous composition depends upon season and altitude of the site so several altitude profiles correspond to every wavelength. As an example let us consider altitude profiles for the following wavelengths: 0.248, 0.438, 0.514, 0.53, 1.375, and 3.8 μm . For every wavelength the model are presented characteristic to tropics, winter of mid-latitudes, and summed of mid-latitudes (see Tables 1.1 - 1.7). Moreover, for every case we present AGFL model and a model of the Institute of Atmospheric Optics, Siberian Branch of RAS (IAO). The models are shown up to 10 km, but the whole models include profiles up to 60 km.

Let us consider the joint effect of molecular and aerosol absorption for radiation with $\lambda = 1.315 \mu\text{m}$. In Table 1.5 there presented altitude profiles of the summarized absorption and extinction. The index of absorption determines phase distortions for a high-power beams and the index of integral extinction, which takes into account aerosol dispersion, allows for decrease of a beam power along a propagation path. To calculate parameters presented in this Table (and also in the other Tables) we used AFGL model for mid-latitude summer and the mean cycle model for aerosol absorption and extinction. These profiles are shown in Fig. 1.3.

Temperature T and pressure P enter into the model of thermal blooming as parameters which determine a proportionality coefficient between variations of temperature and that of the index of refraction

$$\delta n = \frac{\partial n}{\partial T} \delta T, \quad \frac{\partial n}{\partial T} = -77,6 \frac{P}{T^2} 10^{-6}. \quad (1.12)$$

Into this equation pressure should be substituted in torres and temperature in K^0 . In Table 1.8 and Table 1.9 models of temperature and pressure are presented for different latitudes.

Profiles of absorption change more than profiles of temperature and pressure, so profiles of T and P can be calculated by simple formulas. In particular, for temperature the following model can be used

$$T(h[km]) = \begin{cases} T_0 \cdot (1 - h/60), & h < 15km \\ 0.75 \cdot T_0 & h > 15km \end{cases}; T_0 = 290K$$

Table 1.1. Model of altitude profile of molecular absorption coefficient (in km^{-1}), wavelength $\lambda = 0.248 \mu m$.

Altitude, km	Tropics		Summer of mid-latitudes		Winter of mid-latitudes	
	IAO	AFGL	IAO	AFGL	IAO	AFGL
.0	.5458E+00	.7525E+00	.5668E+00	.8066E+00	.5607E+00	.8065E+00
.5	.5583E+00	.7555E+00	.7092E+00	.8068E+00	.6484E+00	.7642E+00
1.0	.5700E+00	.7521E+00	.8083E+00	.8066E+00	.7091E+00	.7253E+00
1.5	.5847E+00	.7402E+00	.8448E+00	.8022E+00	.7307E+00	.6836E+00
2.0	.5903E+00	.7249E+00	.8738E+00	.8048E+00	.7481E+00	.6583E+00
2.5	.5806E+00	.7060E+00	.8956E+00	.8186E+00	.7658E+00	.6581E+00
3.0	.5733E+00	.6842E+00	.9083E+00	.8323E+00	.7706E+00	.6580E+00
3.5	.5710E+00	.6543E+00	.9089E+00	.8458E+00	.7571E+00	.6438E+00
4.0	.5659E+00	.6310E+00	.9053E+00	.8593E+00	.7402E+00	.6585E+00
4.5	.5574E+00	.6179E+00	.8966E+00	.8709E+00	.7124E+00	.7234E+00
5.0	.5467E+00	.6047E+00	.8848E+00	.8860E+00	.6961E+00	.7789E+00
5.5	.5315E+00	.5912E+00	.8689E+00	.9017E+00	.6969E+00	.8082E+00
6.0	.5187E+00	.5776E+00	.8514E+00	.9268E+00	.6995E+00	.8599E+00
6.5	.5080E+00	.5638E+00	.8292E+00	.9697E+00	.6980E+00	.9467E+00
7.0	.5000E+00	.5502E+00	.8112E+00	.1006E+01	.7104E+00	.1034E+01
7.5	.4950E+00	.5336E+00	.7986E+00	.1029E+01	.7405E+00	.1094E+01
8.0	.4930E+00	.5235E+00	.7880E+00	.1061E+01	.7790E+00	.1209E+01
8.5	.4976E+00	.5236E+00	.7643E+00	.1113E+01	.7895E+00	.1396E+01
9.0	.4986E+00	.5237E+00	.7736E+00	.1154E+01	.8831E+00	.1614E+01
9.5	.4915E+00	.5208E+00	.8169E+00	.1152E+01	.1112E+01	.1862E+01
10.0	.4890E+00	.5241E+00	.8968E+00	.1204E+01	.1329E+01	.2148E+01

Table 1.2. Model of altitude profile of molecular absorption coefficient (in km^{-1}), wavelength $\lambda = 0.438 \mu\text{m}$.

Altitude, km	Tropics		Summer of mid-latitudes		Winter of mid-latitudes	
	IAO	AFGL	IAO	AFGL	IAO	AFGL
.0	.1736E-02	.1070E-04	.1777E-02	.1090E-04	.1917E-02	.1184E-04
.5	.1416E-02	.1022E-04	.1442E-02	.1037E-04	.1543E-02	.1119E-04
1.0	.1143E-02	.9747E-05	.1160E-02	.9860E-05	.1231E-02	.1057E-04
1.5	.9295E-03	.9304E-05	.9432E-03	.9369E-05	.9922E-03	.9989E-05
2.0	.7489E-03	.8861E-05	.7593E-03	.8905E-05	.7924E-03	.9430E-05
2.5	.6081E-03	.8403E-05	.6156E-03	.8469E-05	.6391E-03	.8890E-05
3.0	.4895E-03	.7981E-05	.4948E-03	.8053E-05	.5111E-03	.8395E-05
3.5	.3978E-03	.7602E-05	.4021E-03	.7659E-05	.4138E-03	.7954E-05
4.0	.3202E-03	.7236E-05	.3235E-03	.7279E-05	.3315E-03	.7531E-05
4.5	.2601E-03	.6887E-05	.2626E-03	.6916E-05	.2679E-03	.7126E-05
5.0	.2090E-03	.6549E-05	.2110E-03	.6566E-05	.2145E-03	.6738E-05
5.5	.1690E-03	.6224E-05	.1710E-03	.6228E-05	.1736E-03	.6368E-05
6.0	.1355E-03	.5910E-05	.1373E-03	.5904E-05	.1390E-03	.6012E-05
6.5	.1100E-03	.5611E-05	.1112E-03	.5593E-05	.1124E-03	.5674E-05
7.0	.8839E-04	.5323E-05	.8923E-04	.5296E-05	.8980E-04	.5350E-05
7.5	.7166E-04	.5044E-05	.7229E-04	.5011E-05	.7230E-04	.5037E-05
8.0	.5749E-04	.4782E-05	.5795E-04	.4746E-05	.5762E-04	.4747E-05
8.5	.4225E-04	.4535E-05	.4266E-04	.4503E-05	.4236E-04	.4479E-05
9.0	.3723E-04	.4314E-05	.3758E-04	.4282E-05	.3703E-04	.4236E-05
9.5	.4684E-04	.4101E-05	.4716E-04	.4063E-05	.4607E-04	.4011E-05
10.0	.5959E-04	.3954E-05	.5980E-04	.3913E-05	.5788E-04	.3830E-05

Table 1.3. Model of altitude profile of molecular absorption coefficient (in km^{-1}), wavelength $\lambda = 0.514 \mu\text{m}$.

Altitude, km	Tropics		Summer of mid-latitudes		Winter of mid-latitudes	
	IAO	AFGL	IAO	AFGL	IAO	AFGL
0.0	.1725E-02	.1121E-03	.1768E-02	.1196E-03	.1900E-02	.1184E-04
0.5	.1422E-02	.1121E-03	.1468E-02	.1192E-03	.1556E-02	.1119E-04
1.0	.1164E-02	.1112E-03	.1213E-02	.1187E-03	.1267E-02	.1057E-04
1.5	.9625E-03	.1091E-03	.1011E-02	.1176E-03	.1042E-02	.9989E-05
2.0	.7912E-03	.1066E-03	.8395E-03	.1175E-03	.8539E-03	.9430E-05
2.5	.6558E-03	.1036E-03	.7056E-03	.1190E-03	.7102E-03	.8890E-05
3.0	.5418E-03	.1003E-03	.5923E-03	.1204E-03	.5890E-03	.8395E-05
3.5	.4542E-03	.9588E-04	.5040E-03	.1219E-03	.4945E-03	.7954E-05
4.0	.3795E-03	.9237E-04	.4287E-03	.1234E-03	.4139E-03	.7531E-05
4.5	.3211E-03	.9027E-04	.3694E-03	.1246E-03	.3495E-03	.7126E-05
5.0	.2711E-03	.8816E-04	.3188E-03	.1263E-03	.2965E-03	.6738E-05
5.5	.2311E-03	.8602E-04	.2787E-03	.1281E-03	.2578E-03	.6368E-05
6.0	.1977E-03	.8388E-04	.2444E-03	.1312E-03	.2255E-03	.6012E-05
6.5	.1722E-03	.8172E-04	.2168E-03	.1367E-03	.2001E-03	.5674E-05
7.0	.1507E-03	.7960E-04	.1936E-03	.1414E-03	.1805E-03	.5350E-05
7.5	.1342E-03	.7710E-04	.1759E-03	.1442E-03	.1681E-03	.5037E-05
8.0	.1206E-03	.7549E-04	.1610E-03	.1483E-03	.1595E-03	.4747E-05
8.5	.1069E-03	.7526E-04	.1434E-03	.1550E-03	.1465E-03	.4479E-05
9.0	.1023E-03	.7506E-04	.1399E-03	.1604E-03	.1543E-03	.4236E-05
9.5	.1107E-03	.7447E-04	.1551E-03	.1600E-03	.1940E-03	.4011E-05
10.0	.1226E-03	.7477E-04	.1780E-03	.1669E-03	.2347E-03	.3830E-05

Table 1.4. Model of altitude profile of molecular absorption coefficient (in km^{-1}), wavelength $\lambda = 0.53 \mu\text{m}$.

Altitude, km	Tropics		Summer of mid-latitudes		Winter of mid-latitudes	
	IAO	AFGL	IAO	AFGL	IAO	AFGL
.0	.1467E-02	.1821E-03	.1501E-02	.1919E-03	.1605E-02	.1879E-03
.5	.1220E-02	.1805E-03	.1272E-02	.1901E-03	.1334E-02	.1778E-03
1.0	.1011E-02	.1779E-03	.1075E-02	.1885E-03	.1106E-02	.1685E-03
1.5	.8475E-03	.1741E-03	.9141E-03	.1862E-03	.9253E-03	.1587E-03
2.0	.7081E-03	.1694E-03	.7776E-03	.1857E-03	.7743E-03	.1525E-03
2.5	.5964E-03	.1638E-03	.6708E-03	.1878E-03	.6594E-03	.1519E-03
3.0	.5025E-03	.1579E-03	.5798E-03	.1900E-03	.5614E-03	.1514E-03
3.5	.4307E-03	.1505E-03	.5079E-03	.1924E-03	.4830E-03	.1478E-03
4.0	.3693E-03	.1448E-03	.4461E-03	.1949E-03	.4157E-03	.1506E-03
4.5	.3207E-03	.1415E-03	.3969E-03	.1970E-03	.3603E-03	.1645E-03
5.0	.2788E-03	.1382E-03	.3544E-03	.1999E-03	.3154E-03	.1763E-03
5.5	.2448E-03	.1349E-03	.3202E-03	.2030E-03	.2843E-03	.1825E-03
6.0	.2163E-03	.1316E-03	.2906E-03	.2082E-03	.2584E-03	.1935E-03
6.5	.1945E-03	.1283E-03	.2659E-03	.2174E-03	.2378E-03	.2123E-03
7.0	.1762E-03	.1250E-03	.2452E-03	.2252E-03	.2234E-03	.2312E-03
7.5	.1624E-03	.1211E-03	.2295E-03	.2300E-03	.2168E-03	.2441E-03
8.0	.1512E-03	.1187E-03	.2164E-03	.2367E-03	.2141E-03	.2691E-03
8.5	.1407E-03	.1185E-03	.1996E-03	.2478E-03	.2048E-03	.3101E-03
9.0	.1372E-03	.1184E-03	.1979E-03	.2567E-03	.2215E-03	.3578E-03
9.5	.1433E-03	.1175E-03	.2150E-03	.2562E-03	.2789E-03	.4121E-03
10.0	.1527E-03	.1181E-03	.2425E-03	.2674E-03	.3359E-03	.4747E-03

Table 1.5. Model of altitude profile of molecular absorption coefficient (in km^{-1}), wavelength $\lambda = 1.375 \mu\text{m}$.

Altitude, km	Tropics		Summer of mid-latitudes		Winter of mid-latitudes	
	IAO	AFGL	IAO	AFGL	IAO	AFGL
.0	.6877E+02	.7473E+02	.4685E+02	.5595E+02	.2111E+02	.1541E+02
.5	.5486E+02	.5982E+02	.3748E+02	.4421E+02	.1674E+02	.1256E+02
1.0	.4284E+02	.4780E+02	.2959E+02	.3440E+02	.1300E+02	.1019E+02
1.5	.3261E+02	.4007E+02	.2313E+02	.2663E+02	.9692E+01	.8387E+01
2.0	.2442E+02	.3182E+02	.1781E+02	.2012E+02	.7200E+01	.6783E+01
2.5	.1830E+02	.2194E+02	.1368E+02	.1461E+02	.5663E+01	.5378E+01
3.0	.1357E+02	.1462E+02	.1036E+02	.1041E+02	.4354E+01	.4151E+01
3.5	.1030E+02	.9678E+01	.7865E+01	.7727E+01	.3200E+01	.2997E+01
4.0	.7745E+01	.6345E+01	.5886E+01	.5573E+01	.2308E+01	.2120E+01
4.5	.6019E+01	.5147E+01	.4507E+01	.3928E+01	.1717E+01	.1568E+01
5.0	.4577E+01	.4046E+01	.3347E+01	.2728E+01	.1246E+01	.1132E+01
5.5	.3421E+01	.2971E+01	.2379E+01	.2064E+01	.8983E+00	.8289E+00
6.0	.2512E+01	.2129E+01	.1641E+01	.1539E+01	.6269E+00	.5772E+00
6.5	.1861E+01	.1547E+01	.1140E+01	.1166E+01	.4324E+00	.3524E+00
7.0	.1317E+01	.1093E+01	.7816E+00	.8635E+00	.2971E+00	.2150E+00
7.5	.8335E+00	.7829E+00	.6061E+00	.6322E+00	.1549E+00	.1324E+00
8.0	.5274E+00	.5395E+00	.4580E+00	.4533E+00	.8101E-01	.8147E-01
8.5	.3534E+00	.3593E+00	.3354E+00	.3342E+00	.5258E-01	.5399E-01
9.0	.2367E+00	.2392E+00	.2382E+00	.2394E+00	.3374E-01	.3403E-01
9.5	.1463E+00	.1483E+00	.1671E+00	.1677E+00	.2206E-01	.2245E-01
10.0	.9057E-01	.9195E-01	.1167E+00	.1174E+00	.1397E-01	.1453E-01

Table 1.6. Model of altitude profile of molecular absorption coefficient (in km^{-1}), wavelength $\lambda = 3.8 \mu\text{m}$.

Altitude, km	Tropics		Summer of mid-latitudes		Winter of mid-latitudes	
H, km	IAO	AFGL	IAO	AFGL	IAO	AFGL
.0	.3697E-01	.4008E-01	.2654E-01	.3129E-01	.1408E-01	.1173E-01
.5	.2956E-01	.3218E-01	.2118E-01	.2471E-01	.1129E-01	.9665E-02
1.0	.2271E-01	.2534E-01	.1687E-01	.1944E-01	.9161E-02	.8165E-02
1.5	.1736E-01	.2126E-01	.1288E-01	.1472E-01	.6718E-02	.6987E-02
2.0	.1310E-01	.1691E-01	.1011E-01	.1135E-01	.5356E-02	.5391E-02
2.5	.1000E-01	.1193E-01	.7886E-02	.8558E-02	.4362E-02	.4520E-02
3.0	.7633E-02	.8251E-02	.6179E-02	.6352E-02	.3599E-02	.3766E-02
3.5	.5974E-02	.5835E-02	.4891E-02	.4968E-02	.2935E-02	.3005E-02
4.0	.4675E-02	.4209E-02	.3874E-02	.3869E-02	.2404E-02	.2470E-02
4.5	.3772E-02	.3528E-02	.3136E-02	.3014E-02	.2006E-02	.2081E-02
5.0	.3016E-02	.2919E-02	.2516E-02	.2377E-02	.1682E-02	.1750E-02
5.5	.1801E-02	.2338E-02	.1375E-02	.1966E-02	.1417E-02	.1490E-02
6.0	.1377E-02	.1875E-02	.1030E-02	.1627E-02	.6292E-03	.1259E-02
6.5	.1071E-02	.9497E-03	.7908E-03	.8004E-03	.5087E-03	.4839E-03
7.0	.8155E-03	.7338E-03	.6135E-03	.6424E-03	.4199E-03	.3929E-03
7.5	.5965E-03	.5794E-03	.5085E-03	.5168E-03	.3342E-03	.3272E-03
8.0	.4451E-03	.4522E-03	.4152E-03	.4144E-03	.2749E-03	.2760E-03
8.5	.3526E-03	.3553E-03	.3427E-03	.3410E-03	.2346E-03	.2337E-03
9.0	.2840E-03	.2855E-03	.2813E-03	.2802E-03	.2013E-03	.2001E-03
9.5	.2309E-03	.2323E-03	.2341E-03	.2328E-03	.1726E-03	.1726E-03
10.0	.1916E-03	.1926E-03	.1961E-03	.1951E-03	.1479E-03	.1482E-03

Table 1.7. Model of altitude profile of absorption and extinction coefficients (in km^{-1}), wavelength $\lambda = 3.8 \mu\text{m}$.

H(km)	$\alpha_{\text{abs}}(\text{km}^{-1})$	$\alpha_{\text{ext}}(\text{km}^{-1})$	h(km)	$\alpha_{\text{abs}}(\text{km}^{-1})$	$\alpha_{\text{ext}}(\text{km}^{-1})$
0	7.329E-2	1.2439E-1	10.5	9.6825E-5	2.4872E-4
0.5	5.435E-2	9.097E-2	11	7.343E-5	3.6672E-4
1	3.828E-2	6.054E-2	11.5	5.8165E-5	2.5178E-4
1.5	2.849E-2	4.472E-2	12	4.29E-5	1.3683E-4
2	2.0381E-2	3.069E-2	12.5	3.739E-5	1.2521E-4
2.5	1.4353E-2	2.137E-2	13	3.188E-5	1.1358E-4
3	9.914E-3	1.3609E-2	13.5	2.782E-5	1.0346E-4
3.5	7.136E-3	9.364E-3	14	2.376E-5	9.334E-5
4	4.981E-3	5.739E-3	14.5	2.0775E-5	8.865E-5
4.5	3.4217E-3	3.938E-3	15	1.779E-5	8.396E-5
5	2.3103E-3	2.585E-3	15.5	1.5725E-5	8.024E-5
5.5	1.7122E-3	1.886E-3	16	1.366E-5	7.652E-5
6	1.249E-3	1.3233E-3	16.5	1.2356E-5	8.1125E-5
6.5	9.3248E-4	9.761E-4	17	1.1051E-5	8.5731E-5
7	6.8436E-4	6.974E-4	17.5	1.0095E-5	9.069E-5
7.5	5.0378E-4	5.151E-4	18	9.139E-6	9.5649E-5
8	3.684E-4	3.781E-4	18.5	8.0455E-6	8.4931E-5
8.5	2.7851E-4	2.882E-4	19	6.952E-6	7.4212E-5
9	2.0881E-4	2.185E-4	19.5	6.081E-6	6.3716E-5
9.5	1.5692E-4	1.67E-4	20	5.21E-6	5.322E-5
10	1.2022E-4	1.307E-4			

Table 1.8. Altitude profiles of pressure (in atm)

Altitude, km	Tropics		Summer of mid-latitudes		Winter of mid-latitudes	
	IAO	AFGL	IAO	AFGL	IAO	AFGL
.0	.1013E+01	.1013E+01	.1013E+01	.1013E+01	.1018E+01	.1018E+01
.5	.9573E+00	.9573E+00	.9561E+00	.9561E+00	.9560E+00	.9560E+00
1.0	.9040E+00	.9040E+00	.9020E+00	.9020E+00	.8973E+00	.8973E+00
1.5	.8534E+00	.8534E+00	.8510E+00	.8510E+00	.8420E+00	.8420E+00
2.0	.8050E+00	.8050E+00	.8020E+00	.8020E+00	.7897E+00	.7897E+00
2.5	.7590E+00	.7590E+00	.7548E+00	.7548E+00	.7405E+00	.7405E+00
3.0	.7150E+00	.7150E+00	.7100E+00	.7100E+00	.6938E+00	.6938E+00
3.5	.6730E+00	.6730E+00	.6680E+00	.6680E+00	.6498E+00	.6498E+00
4.0	.6330E+00	.6330E+00	.6280E+00	.6280E+00	.6081E+00	.6081E+00
4.5	.5951E+00	.5951E+00	.5901E+00	.5901E+00	.5687E+00	.5687E+00
5.0	.5590E+00	.5590E+00	.5540E+00	.5540E+00	.5313E+00	.5313E+00
5.5	.5246E+00	.5246E+00	.5197E+00	.5197E+00	.4961E+00	.4961E+00
6.0	.4920E+00	.4920E+00	.4870E+00	.4870E+00	.4627E+00	.4627E+00
6.5	.4613E+00	.4613E+00	.4556E+00	.4556E+00	.4313E+00	.4313E+00
7.0	.4320E+00	.4320E+00	.4260E+00	.4260E+00	.4016E+00	.4016E+00
7.5	.4044E+00	.4044E+00	.3983E+00	.3983E+00	.3737E+00	.3737E+00
8.0	.3780E+00	.3780E+00	.3720E+00	.3720E+00	.3473E+00	.3473E+00
8.5	.3528E+00	.3528E+00	.3474E+00	.3474E+00	.3225E+00	.3226E+00
9.0	.3290E+00	.3290E+00	.3240E+00	.3240E+00	.2992E+00	.2993E+00
9.5	.3070E+00	.3070E+00	.3019E+00	.3019E+00	.2773E+00	.2773E+00
10.0	.2860E+00	.2860E+00	.2810E+00	.2810E+00	.2568E+00	.2568E+00

Table 1.9. Altitude profiles of temperature (in K°)

Altitude, km	Tropics		Summer of mid-latitudes		Winter of mid-latitudes	
H,KM	IAO	AFGL	IAO	AFGL	IAO	AFGL
.0	299.0	299.7	292.0	294.2	272.0	272.2
.5	295.9	296.7	290.1	292.0	271.1	270.5
1.0	293.0	293.7	288.0	289.7	270.0	268.7
1.5	290.5	290.5	285.5	287.6	268.6	267.0
2.0	288.0	287.7	283.0	285.2	267.0	265.2
2.5	285.6	286.0	280.6	282.2	265.3	263.8
3.0	283.0	283.7	278.0	279.2	263.0	261.7
3.5	280.0	280.4	275.0	276.2	260.0	258.7
4.0	277.0	277.0	272.0	273.2	257.0	255.7
4.5	273.9	273.6	269.0	270.2	254.1	252.7
5.0	271.0	270.3	266.0	267.2	251.0	249.7
5.5	268.8	266.9	263.1	264.3	247.5	246.7
6.0	266.0	263.6	260.0	261.2	244.0	243.7
6.5	262.5	260.3	256.5	258.0	240.4	240.7
7.0	259.0	257.0	253.0	254.7	237.0	237.7
7.5	255.5	253.6	249.5	251.4	234.1	234.7
8.0	252.0	250.3	246.0	248.2	231.0	231.7
8.5	248.5	246.9	242.4	244.9	227.1	228.7
9.0	245.0	243.6	239.0	241.7	224.0	225.7
9.5	241.6	240.3	235.9	238.5	221.9	222.0
10.0	238.0	237.0	233.0	235.3	220.0	219.7

1.2. Intercomparison of models of the atmospheric turbulence spectrum

This part deals with the theoretical and experimental studies of optical waves aimed at comparing different models of the atmospheric turbulence spectra. For inhomogeneous optical paths in the atmosphere we introduced the term **turbulence spectrum averaged over the path**

In our Ref. 7 several models of the fluctuations spectral density of refraction index $\Phi_n(k, x)$ of atmosphere were analyzed. It is well known that the following models, describing the behavior of the fluctuations spectral density of the refraction index of the atmosphere in the region adjacent to the energy range, are most widely used:

– von Karman model /1,2/

$$\Phi_n(\kappa, \xi) = 0,033C_n^2(\xi)L_{0K}^{11/3}(1 + \kappa^2 L_{0K}^2)^{-11/6}; \quad (1.13)$$

– exponential model /7/

$$\Phi_n(\kappa, \xi) = 0,033C_n^2(\xi)\kappa^{-11/3}\left\{1 - \exp\left[-\kappa^2 / \kappa_{0R}^2\right]\right\}; \quad (1.14)$$

– Greenwood–Tarazino model /9/

$$\Phi_n(\kappa, \xi) = 0,033C_n^2(\xi)(\kappa^2 L_{0G}^2 + \kappa L_{0G})^{-11/6}. \quad (1.15)$$

Naturally, in these models (1.13)–(1.15) the outer scales L_{0K} , κ_{0R}^{-1} , and L_{0G} are somewhat differ. Here $C_n^2(\xi)$ is the density of turbulent fluctuations.

Let us perform the comparison of models (1.13)–(1.15) on the basis of the calculation of the variance of the phase fluctuations of optical waves, propagating though the atmospheric layer adjacent to the Earth. Let us use the $\bar{\bar{S}}$ equation, describing the phase fluctuations $S(\rho)$ of the optical wave, propagating through the turbulent atmosphere according to the approximation of smooth perturbations /2/:

$$S(\bar{\rho}) = k \int_0^L dx \iint d^2n(\bar{\kappa}, x) \cos \frac{\kappa^2(L-x)\gamma}{2k} \exp(i\bar{\kappa}\bar{\rho}\gamma), \quad (1.16)$$

where k is radiation wave number ($\gamma = 1$ for the plane wave, $\gamma = k/L$ for the spherical wave), L is the length of the optical path. It is not difficult to show that for the fluctuations /2/

$$\begin{aligned} < d^2 n(\vec{\kappa}_1, x_1) d^2 n(\vec{\kappa}_2, x_2) > = \\ = 2\pi \delta(x_1 - x_2) \delta(\vec{\kappa}_1 + \vec{\kappa}_2) \Phi_n(\vec{\kappa}_1, x_1) d^2 \vec{\kappa}_1 d^2 \vec{\kappa}_2 dx_1 dx_2 \end{aligned} \quad (1.17)$$

the variance of phase fluctuations in the plane wave is following /5/

$$< S^2 > = 2\pi^2 k^2 \int_0^L d\xi \int_0^\infty d\kappa \kappa \Phi_n(\kappa, \xi) \left[1 + \cos \frac{\kappa^2 (L - \xi)}{2k} \right]. \quad (1.18)$$

Under the condition $\kappa_0^2 L / k \ll 1$, where κ_0^{-1} is the specific value of outer scale of the turbulence, Eq. (1.18) transforms into

$$< S^2 > \approx 4\pi^2 k^2 \int_0^L d\xi \int_0^\infty d\kappa \kappa \Phi_n(\kappa, \xi). \quad (1.19)$$

Let us compare the variances of phase fluctuations for models (1.13)–(1.15) along the homogeneous path. For the models (1.13), (1.14), and (1.15), respectively, we have

$$< S^2 >_1 \approx (12/5) \pi^2 0,033 k^2 C_n^2 L L_{oK}^{5/3} \quad (1.20)$$

(at $L_{oK}^{-1} \ll \kappa_m$, where κ_m is the wave number for the inner scale of turbulence),

$$< S^2 >_2 \approx (12/5) \pi^2 0,033 \Gamma(1/6) k^2 C_n^2 L \kappa_{oR}^{5/3}, \quad (1.21)$$

$$< S^2 >_3 \approx 4\pi^2 0,033 \frac{\Gamma(1/6) \Gamma(5/3)}{\Gamma(11/6)} k^2 C_n^2 L L_{oG}^{5/3}. \quad (1.22)$$

From the condition of variances equality

$$< S^2 >_1 = < S^2 >_2 = < S^2 >_3$$

for all models (1.13)–(1.15), we obtain the relationships between the scales:

$$L_{oG} \approx 0,27 L_{oK}, \kappa_{oR}^{-1} \approx 0,36 L_{oK}, \kappa_{oR}^{-1} \approx 1,33 L_{oG}. \quad (1.23)$$

Thus, the calculations of the optical characteristics performed using one model of the spectrum can be result in another model by relationship (1.23).

Calculating the variance of star image jitters in the focal plane of telescope, we use the following simplifying assumptions: the amplitude fluctuations in the optical wave are small, the telescope aperture is assumed to be as a Gaussian. Then (see Ref. 8) the variance of image jitter will be

$$\sigma_{\alpha}^2(R) = 16\pi^2 0.033 F^2 \int_0^L d\xi C_n^2(\xi) \times \int_0^{\infty} d\kappa \kappa^{-2/3} \left\{ 1 - \exp(-\kappa^2 / \kappa_{0k}^2) \right\} \exp(-\kappa R^2 / 2) \quad (1.24)$$

for model (1.14). Here R is the effective size of a telescope Gaussian aperture. In Eq. (1.24) the simple calculations lead to

$$\sigma_{\alpha}^2(R) = 8\pi^2 2^{1/6} 0.033 \Gamma(1/6) F^2 R^{-1/3} \int_0^L d\xi C_n^2(\xi) \left\{ 1 - (1 + 2\kappa_{0G}^2 R^2)^{-1/6} \right\}. \quad (1.25)$$

The further calculations require the real profiles of the dependencies of models parameter $C_n^2(\xi)$ and $\kappa_{0R}^{-1}(\xi)$.

For von Karman model (1.13) of turbulence spectrum in Ref. 10 the calculation of the variance of the image jitters for the circular telescope aperture was made

$$\sigma_{\alpha}^2(R) = (\pi k^2 R^2) \int_0^{2R} d\rho \rho \left[D_s''(\rho) + \frac{D_s'(\rho)}{\rho} \right] \times \left\{ \arccos(\rho / 2R) - (\rho / 2R) \sqrt{1 - (\rho / 2R)^2} \right\}, \quad (1.26)$$

where $D_s(\rho)$ is the phase structural function; $2R$ is the diameter of receiving aperture. In the field of applicability of the technique of smooth perturbations the phase structural function were substituted for the structural function of complex phase, therefore

$$D_s''(\rho) + \frac{D_s'(\rho)}{\rho} = 8\pi^2 k^2 \int_0^L d\xi \int_0^{\infty} d\kappa \kappa^3 J_0(\kappa, \rho) \Phi_n(\kappa, \xi). \quad (1.27)$$

Moreover, the function characterizing the averaging effect of the circular aperture in Eq. (1.26), is approximate /11/ using power function

$$(\arccos x - x\sqrt{1-x^2}) \approx (\pi/2) \left[1 - 1,25x + 0,25x^4 \right].$$

The calculation results of arrival angles by (1.26) for homogeneous path are given on Fig. 1.5, curve 1. Here the dependence $R^{-1/3}$, corresponding to Kolmogorov's turbulence spectrum is presented (curve 1)

$$\sigma_{\alpha}^2(2R) \approx 2,84 C_n^2 L(2R)^{-1/3}. \quad (1.28)$$

Comparing curves 1 and 2 one can find, that the finiteness of the value of outer scale of turbulence, taken into account, leads to higher rate of decrease of the image jitters variance with the increase of receiving aperture diameter (at $2R > 0,1\kappa_0^{-1}$). This is compared with the results of Eq. (1.28) as applied to the case $2R\kappa_0 < 1$ (so doing curves 1 and 2 are identical).

Eq. (1.25) can be used to calculate the image jitters variance along inhomogeneous path, if the corresponding altitude profiles $C_n^2(\xi)$ and $\kappa_0^{-1}(\xi)$ are applied.

The experimental test of aperture dependence of star image jitters formed by telescope is carried out /12/ as a part of the complicated measurements of stellar climate in the location of Russian Large Telescope (LTA) in north Caucasus. The image jitter is measured in experiments /12/ using photoelectron provision with diameter of main mirror 605 mm, located in the telescope focal plane. The changing of aperture is realized by superposition of nontrans parent ring diaphragms of different diameters.

On the design features of the used telescope is the shadowing of the central part of the mirror. In practice it should be dealt with the telescope having the aperture in the form of the ring with the diameter of the shadowed part $D_1 = 115$ mm. Earlier /13/ the variance of star image jitters was calculated for telescope having the ring aperture with an external diameter D_1 and internal diameter D_2 . It was shown that in the power region of aperture dependence of image jitters variance we have

$$\sigma_{\alpha}^2(R) \approx 5,69 f(n) D_2^{-1/3} \int_0^{\infty} d\xi C_n^2(\xi), \quad (1.29)$$

where $n = D_1/D_2$,

$$f(n) = (1 - n^2)^{-2} \left\{ 1 + n^{11/3} - 2,15 \frac{n^2}{(1 + n)^{1/3}} {}_2F_1(1/6, 3/2; 3; \frac{4n}{(1 + n)^2}) \right\}. \quad (1.30)$$

Here the function $f(n)$ describes the influence of the shadowing of the central part of the telescope and gives the quantitative overestimation of image jitters variance for the telescope with the ring aperture compared with the circular telescope. Some values of the function $f(n)$ are presented in the Table 1.10. It is not difficult to see, that the function $f(n)$ considerably differs from unity only with noticeable shadowing (more than 50% of the surface).

Table 1.10

n	0	0.5	0.75	0.8	0.9	0.95
$f(n)$	1	1,08	1,37	1,67	4,33	15,17

These results describing the influence of the shadowing of the central part of telescope were used to correct the measured data /7/.

Two sets of experiments (obtained at the different values of atmospheric turbulence) on aperture dependence $\sigma_{\alpha}^2(R)$ at the external diameters of the telescope of 152, 215, 313, 492, and 605 mm. The internal diameter of the ring aperture of telescope was constant and equals to 115 mm. The measured data are presented in relative units, here the power dependence $R^{-1/3}$ was given the comparison. As was shown earlier theoretically the measured data on jitters variance are considerably deviated from the dependence $R^{-1/3}$. This confirms the conclusion (from the comparison Fig. 1.4 and 1.5) about the influence of the finiteness of outer turbulence scale. Seemly it should be profitable to relate the optical measured data with the calculational results on the basis of models.

At present the major quantity of the models of the altitude dependence of the structural parameter of refraction index $C_n^2(h)$ and the altitude dependence of outer scale of turbulence $L_0(h)$ is known. The altitude models of $C_n^2(h)$ are sufficiently numerous /1, 2, 4, 6, 8, 9, 14, 15/, therefore we consider here only two of them. The first is the model proposed in Ref. 10 describing so-called the "best", "average", and "worst" conditions for optical observations. It is of interest the model describing the propagation of visible radiation at the optical range at night /11/.

Thus, the star image jitter is calculated on the basis of this equation for the case of the propagation to the zenth direction. It is seen from the analysis of Eq. (1.25) that all the features of inhomogeneous optical path will be described by the behavior of the function

$$f(R, H_0, H) = \frac{\int_{H_0}^H d\xi C_n^2(\xi) \left[1 + 2\kappa_0^2 R^{-2}\right]^{-1/6}}{\int_{H_0}^H d\xi C_n^2(\xi)} . \quad (1.31)$$

Thus, for inhomogeneous path

$$f(R, H_0, H) = f(R) \equiv \left[1 + 2\kappa_0^2 R^{-2}\right]^{-1/6} . \quad (1.32)$$

If the telescope aperture $R \ll \kappa_0^{-1}$, then

$$f(R, H_0, H) \equiv 1 . \quad (1.33)$$

To introduce the term of the outer scale κ_{0av}^{-1} averaged over optical path, we attempt to approximate the last formula using trial-and-error method:

$$f(R, H_0, H) = f(R) \equiv \left[1 + 2\kappa_{0av}^2 R^{-2}\right]^{-1/6} . \quad (1.33)$$

Our calculations show, that "averaged" over the entire vertical column of the atmosphere from at $H_0 = 0$ to $H = 20000$ m, $\kappa_{0av}^{-1} = 0.5$ m for the «best» conditions in the atmosphere according to Gurvich (Ref. 15), and $\kappa_{0av}^{-1} = 1.0$ m for the "worst" conditions in the atmosphere. Model (1.7) of the outer scale of

turbulence is used. It is of interest to note that the results for model (1.8) are the same.

It should be noted that our results agree with the data in Ref. 6. This demonstrates that the behavior of the turbulence spectrum in the region of low frequencies is well described by models (1.13)–(1.15). The parameters C_n^2 and κ_0^{-1} of these models, in its turn, are described on the basis of empirical altitude dependence. To calculate the characteristics of the optical waves propagating through the atmosphere, one can introduce the average integral spectrum

$$\int_0^\infty d\xi \Phi_n(\kappa, \xi) = 0,025 k^{-2} r_0^{-5/3} \kappa^{-11/3} \left\{ 1 - \exp\left(-\kappa^2 / \kappa_{0av}^2\right) \right\}. \quad (1.35)$$

where r_0 is Fried radius.

Because of the considerable growth /4/ of the inner scale l_0 of the turbulence with increase of the altitude ($l_0 \approx \sqrt[3]{h}$) and the finiteness of the out scale of the turbulence, one can expect the essential decrease of inertial range of sizes of atmospheric turbulent inhomogeneities at high altitudes h ($h > 5000$ m). In its turn, this can change some regularities of description of optical waves fluctuations. In particular, this is of importance for the estimation of the operation efficiency of adaptive systems in atmosphere /16 - 18/.

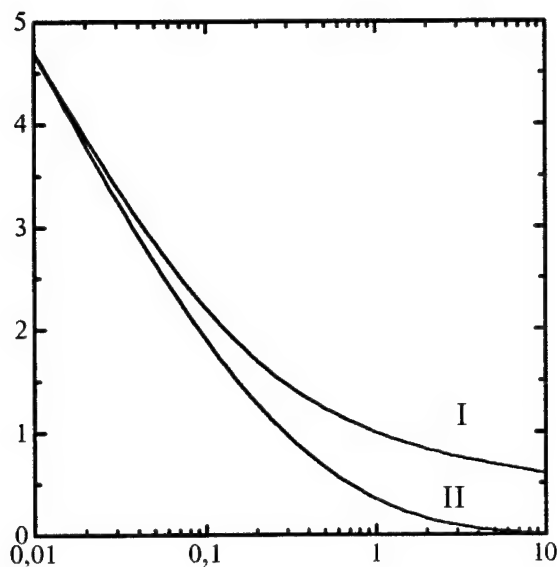


FIG. 1.4. Aperture dependence of fluctuations dispersion of incident angles of optical wave at homogeneous path: calculation for Kolmogorov's turbulence spectrum (I), and calculation for model (1.13) at $\kappa_0 = L_{ok}^{-1}$ (II).

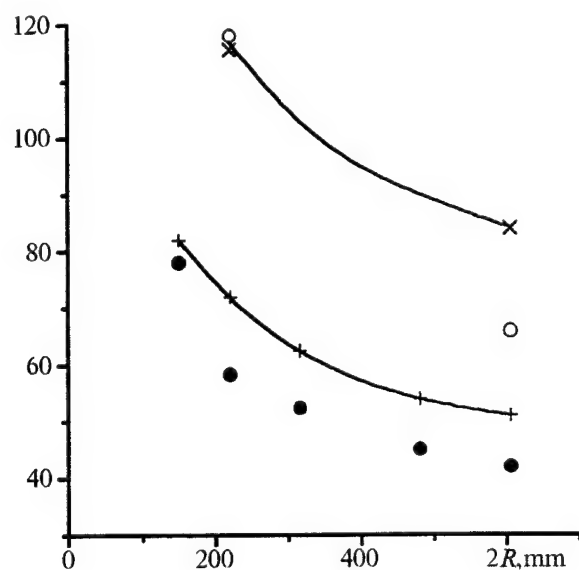


FIG. 1.5. Experimental check of aperture dependence of dispersion of star image tremor in telescope focal plane at diameter of 605 mm: \bullet , \circ — measured data at different values of turbulence, \times — dependence corresponding to turbulence spectrum at infinitive external scale.

1.3. Effective outer scale of atmospheric turbulence

We discuss here some possibilities of introducing the distortions of an optical wave phase, propagating along vertical atmospheric path, as an integral characteristic, describing the turbulence along the path. Several models of the turbulence outer scale profile have been analyzed as well as the structural characteristic of the atmospheric refractive index fluctuations in order to find the value of the efficient outer scale.

The work on design of a large telescope requires the knowledge of its predictable characteristics including the information about parameters of a model /1, 18/ of altitude profiles of atmospheric turbulence such as turbulence intensity and the outer turbulence scale in the planned location of the telescope. These characteristics are the point spread function (PSF) and the efficient angular resolution.

One of the traditional ways to estimate the angular resolution of a designed telescope is to measure the parameters of the image (long-exposition PSF) obtained on a telescope of small diameter. However, the turbulent PSF of a small telescope will correspond to the PSF of a larger telescope if only the outer turbulence scale considerably exceeds the dimension of the telescope diameter in both cases. According to some experimental works /17, 19/ performed in different observatories throughout the world in recent years, this condition is broken for modern projects of telescopes with aperture dimensions of the order of 8–10 m (VLT 4×8 m, Keck 2×10). Saying about the outer scale one should keep in mind that this parameter changes with the height, i.e., it is necessary to use the information about measured parameters of the model of height profiles of atmospheric turbulence.

The possibility to introduce an efficient outer scale as an integral characteristic of turbulence is of great interest as it can permit one to change the height profile for the outer scale. One of the reasons to introduce this parameter is that the applicability of the models of height profiles of atmospheric turbulence is restricted due to their dependence on geographical location. It will also permit

one to simplify mathematical calculations connected with the account for influence of the atmospheric turbulence on the phase of optical waves.

We propose two methods for determining the effective outer scale, namely, by the discrepancy between structure functions of phase fluctuations and by the saturation level.

Determination by the discrepancy

To determine the effective outer scale by this model, minimization of the integral square discrepancy of structure functions of phase fluctuations

$$\Delta(L_0) = \int_0^{\rho_{\max}} [D_\varphi(\rho, L_0) - D_\varphi(\rho, L_0(h))]^2 d\rho \quad (1.36)$$

is used. Here $D_\varphi(r, L_0(h))$ is the structure function corresponding to the height profile of the outer scale $L_0(h)$, $D_\varphi(r, L_0)$ is the function corresponding to the constant value of the outer scale L_0 . The variable ρ_{\max} depends on the studied range (Fig. 1.6) and has a value of either 10 m (what corresponds to the largest diameter of existing telescopes) or $\text{Arg}(90\%)$, i.e., the argument at which the structure function reaches 90% of the saturation level.

The structure function was calculated by modified von Karman spectrum of atmospheric turbulence $\Phi_n(\kappa, \xi) = 0.333 C_n^2(\xi)(\kappa^2 + L_0^{-2}(\xi))^{-11/6}$, where ξ is the current coordinate along the propagation path; for the case of a vertical path, $\xi = h$ where h is the height over the underlying surface.

The discrepancy introduced in such a way defines the divergence degree for two structure functions. The value of the outer scale L_0^* at which the discrepancy $\Delta(L_0)$ is minimal will be called the effective outer scale of atmospheric turbulence.

Determination by the Saturation Level

The name of the method is directly derived from the fact that the value of argument at which the structure function saturates is taken as the upper boundary of the range studied

$$L_0^*(h) = \left[\int_0^\infty L_0^{5/3}(h) C_n^2(h) dh / \int_0^\infty C_n^2(h) dh \right]^{3/5} \quad (1.37)$$

The results presented below indicate that the method is close to the determination by discrepancy [0...Arg(90%)] in its characteristics.

Comparison of the Results

We shall only comment the results of applying the method [0...10 m] to the profile (C) since other methods and profiles have qualitatively similar results.

Figure 1.7 presents the graph of the structure function corresponding to the profile $L_0(h) - C$ together with the family of structure functions calculated using some constant values of the outer scale. One can assume that there exists certain value L_0^* at which the functions $D_\varphi(\rho, L_0^*)$ and $D_\varphi(\rho, L_0(h) - C)$ are most close. Figure 1.8 demonstrates that this assumption is true, namely, the minimum corresponding to the value $L_0^* \approx 32.5$ m is shown by the dashed line. Comparing the curves $D_\varphi(r, L_0(h) - C)$ and $D_\varphi(r, L_0^* = 32.5 \text{ m})$ in Fig. 1.9, we see their similarity indicating the efficiency of the method for the profile $L_0(h) - C$.

The results of calculation of L_0^* (in meters) by the above-mentioned methods for different models of $L_0(h)$ and $C_n^2(h)$ are presented in Tables 1.11 and 1.12.

Comparison of the methods

Analysis of the value L_0^* obtained by different methods for the same height profile $L_0(h)$ demonstrates that its growth (i.e., $L_0^* [0...10 \text{ m}] \ll L_0^* [0...Arg(90\%)] < L_0^* [0...∞]$) is caused by the necessity to compensate for increasing influence of the $D_\varphi(r)$ portions at large argument values with the increase of $\bar{\rho}_{\max}$ (i.e., $\rho_{\max} [0...10 \text{ m}] \ll \rho_{\max} [0...Arg(90\%)] < \rho_{\max} [0...∞]$).

To reduce the increased discrepancy, i.e., to reduce the area between two structure functions, it is necessary "to lift" the structure function $D_\varphi(r, L_{*,0}^*)$ to the structure function $D_\varphi(r, L_0(h))$. And Fig. 1.7 demonstrates that the "lift" of $D_\varphi(\rho, L_0^*)$ occurs with the increase of the value L_0^* .

Comparison by the models of $C_n^2(h)$ used

Studying the dependence of the value L_0^* on the model of $C_n^2(h)$ one can say that lower value of L_0^* for the "best" vision conditions is caused by essential distinctions in the behavior of $C_n^2(h)$. As one can see in Fig. 1.1, that the "best" profile $C_n^2(h)$ rapidly falls off with the growth of height, and the probability of appearance of large-scale fluctuations diminishes. This leads to the decrease of the structure function and L_0^* .

Comparison by the models of $L_0(H)$ used

The considerable difference between the value L_0^* for the models $L_0(h) - C$ and $L_0(h) - D$ can be explained by the following reasoning. The characteristic property of the model $L_0(h) - D$ is the presence of a finite maximal value of L_0 followed by its decrease at heights above 7–8 km (see Fig.1.2), so the appearance of larger scales is impossible. At the same time, the growth of L_0 with the height is inherent in the model $L_0(h) - C$ what increases the influence of large-scale fluctuations and, consequently, one can expect the growth of $D_\phi(\rho)$ what finally leads to the increase of L_0^* .

In the final analysis one can arrive at the following conclusions.

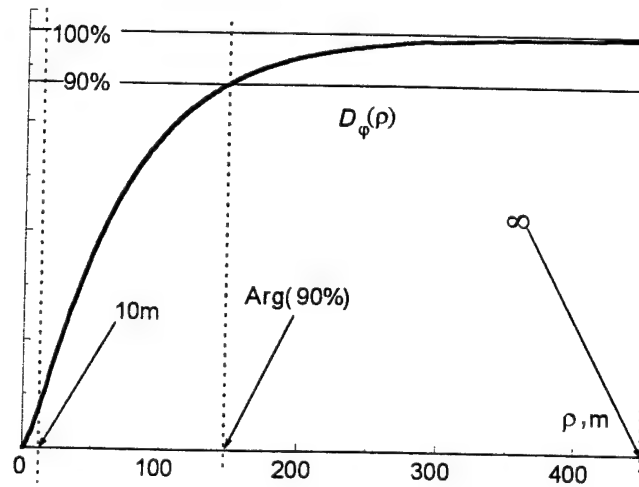
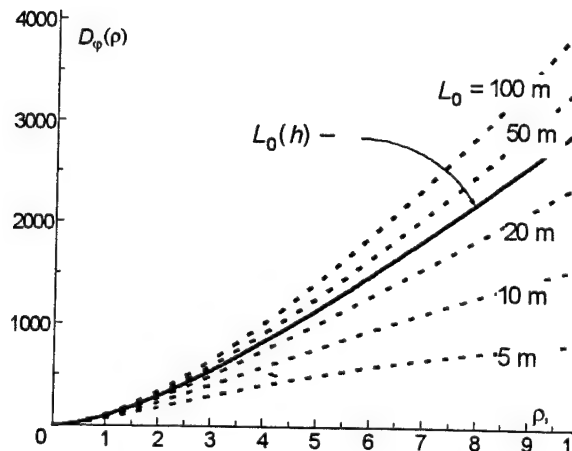
1. One can introduce the effective outer scale of turbulence as an integral parameter describing the character of atmospheric turbulence along the whole propagation path.
2. Introduction of the effective outer scale can considerably simplify mathematical calculations connected with the account for the influence of atmospheric turbulence on the phase of optical wave propagated along vertical atmospheric paths.
3. The description accuracy studied demonstrate that the error caused by the change of the height profile of the outer scale for a constant value, i.e., the effective outer scale, considerably varies depending both on the model of a parameter profile and the method of determination.

Table 1.11

	$C_n^2(h)$ – the worst		
Model	Method		
$L_0(h)$	0...10 m	0...Arg(90%)	0...∞
(B)	34.7	50.6	58.4
(C)	32.5	39.9	42.9
(D)	0.60	0.66	0.71
(E)	0.68	0.75	0.84

Table 1.12

	$C_n^2(h)$ – the worst		
Model	Method		
$L_0(h)$	0...10 m	0...Arg(90%)	0...∞
(B)	55.4	88.5	98.0
(C)	40.6	49.3	52.3
(D)	1.04	1.13	1.78
(E)	1.31	1.46	1.56

FIG. 1.6. Variants of introducing ρ_{\max} .FIG. 1.7 The structure function for the profile (C) and the family of structure functions calculated for fixed values of L_0

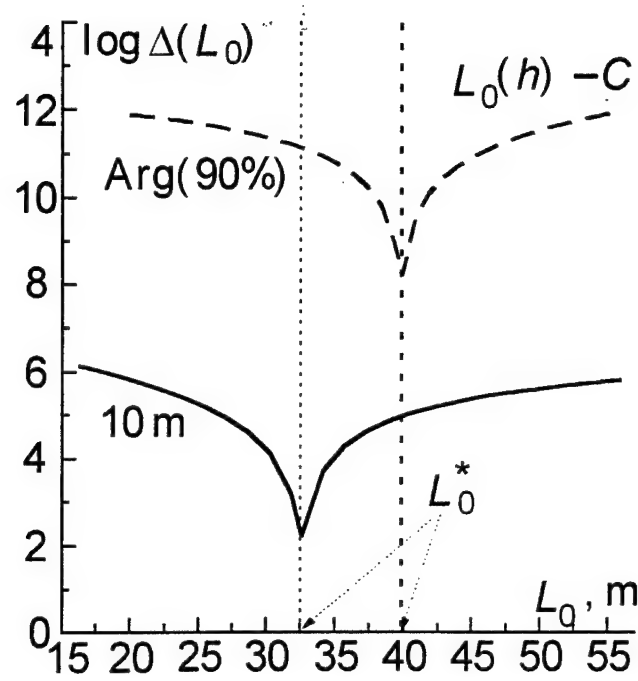


FIG. 1. 8 Discrepancy in the method $[0...10 \text{ m}]$ and the method $[0...Arg(90\%)]$

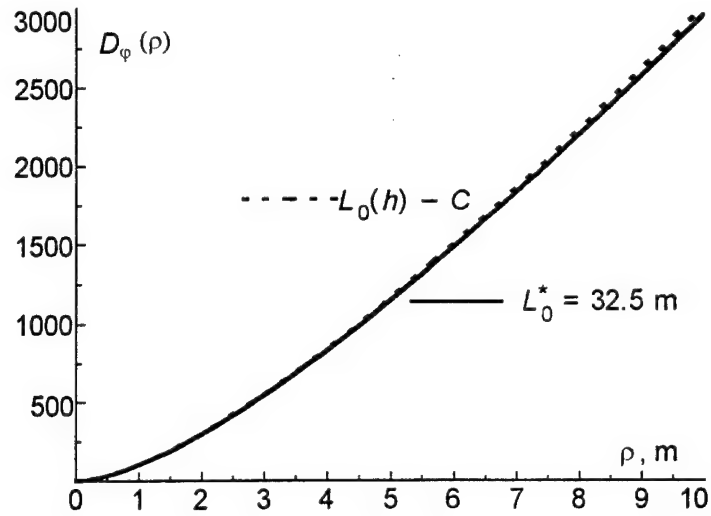


FIG. 1.9. The structure function for the profile $L_0(h) - C$ and for the corresponding effective external scale L_0^* .

References to Chapter I

1. R.E.Good, R.R.Beland, E.A.Murphy, J.H.Brown and E.M.Dewan Atmospheric model of optical turbulence, 1988, Proc.SPIE, Vol. 928, P.165–186.
2. V.I. Tatarskii, *Wave Propagation in the Turbulent Atmosphere* (Nauka, Moscow, 1967).
3. D.L. Fried, Proc. IEEE 55, No. 1 (1967).
4. C.E. Coulman, J. Vernin, Y. Coquegniot, and J.L. Caccia, Appl. Opt. 27, 155–160 (1988).
5. "Site Testing for the VLT. Data Analysis. Part I" European Southern Observatory, 1987, VLT Report, No. 55.
6. T. Stewart McKeckney, J. Opt. Soc. Am. 9, No. 11, 1937–1954 (1992).
7. V.P. Lukin, Atmos. and Oceanic Opt. 5, No. 4, 229–242 (1992).
8. A.S. Gurvich, A.I. Kon, V.L. Mironov, and S.S. Khmelevtsov, *Laser Radiation in Turbulent Atmosphere* (Nauka, Moscow, 1976), 275 pp.
9. D.P. Greenwood and D.O. Tarasino, *A Proposed Form Spectrum in the Input Range*, Proc. SPIE.
10. V.P. Lukin and V.V. Pokasov, *Propagation of Optical Waves through Inhomogeneous Media*, Tomsk, IAO, 1976, pp. 50–53.
11. R.E. Hufnagel, Appl. Opt. 10, 2547–2548 (1970).
12. S.M. Gubkin, O.N. Emaleev, and V.P. Lukin, Astronomical Journal 60, 790–795 (1983).
13. V.P. Lukin, Astronomical circular, No. 1253, 8 (1983).
14. R.E. Hufnagel and N.R. Stanley, J. Opt. Soc. Am. 54, 52–61 (1964).
15. A.S. Gurvich and M.E. Gracheva, Izv. Akad. Nauk. SSSR, Fiz. Atmos. Oceana 10, 1107–1111 (1980).
16. V.P. Lukin and V.V. Pokasov, Appl. Opt. 20, No. 1, 121–135 (1981).
17. V.P. Lukin, Atmos. Oceanic Opt. 5, No. 12, 1294–1304 (1992).
18. V.P. Lukin, *Atmospheric Adaptive Optics* (Nauka, Novosibirsk, 1986), 248 pp.
19. V.P. Lukin, Atmos. and Oceanic Opt. 6, No. 9, 1102–1107 (1993)

20. M. Miller, P. Zieske, D. Hanson, Proc. SPIE, Vol. 75, p. 30. 1976.
21. D.P. Greenwood, J. Opt. Soc. Am., Vol 76, p. 390. 1977.
22. R.E. Hufnagel, OSA Tech. Digest Series, Paper WA 1, 1974.

CHAPTER II. MATHEMATICAL SIMULATION OF LASER BEAM PROPAGATION IN THE ATMOSPHERE

2.1. Problem of coherent radiation propagation

In the problems of coherent beams propagation as well as in the problems of imaging in randomly inhomogeneous medium the wave equation for electromagnetic field of an optics wave is the base for a mathematical model. In the problems considered here polarization effects are negligible and the ratio of a path length to the radius of an aperture is taken so that for a scalar field amplitude it is possible to use small angle approximation (approximation of paraxial beams) [1, 2, 3].

Wave equation

Let us introduce a slow varying component $E(\vec{\rho}, z, t)$ of electromagnetic field complex amplitude in the following way

$$\sqrt{\frac{cn_0}{8\pi}} \vec{E}(\vec{\rho}, z, t) = \vec{e} E(\vec{\rho}, z, t) \exp(ikz - i\omega t), \quad (2.1)$$

so intensity I is related with the component $E(\vec{\rho}, z, t)$ as

$$EE^* = I, \quad (2.2)$$

here c is the speed of light in vacuum, n_0 is the index of refraction for a medium, \vec{e} is vector of polarization, $k = 2\pi / \lambda$ is wave number, ω is frequency of electromagnetic oscillations, $\vec{\rho} = (x, y)$ is vector of coordinates in a beam cross-section (the beam is directed along OZ axis), t is a time variable.

In paraxial approximation propagation of a monochromatic linearly polarized beam in dielectrically inhomogeneous nonmagnetic medium is described by parabolic equation for complex amplitude E

$$2ik \frac{\partial E}{\partial z} = \left(\frac{\partial^2}{\partial x^2} + \frac{\partial^2}{\partial y^2} + 2k^2 \delta n \right) E, \quad (2.3)$$

in assumption that deviations of the index of refraction from unity are small, i.e.,

$$n_0 \approx 1, \delta n = n - 1 \ll 1. \quad (2.4)$$

Algorithms based on finite-difference methods were used to solve the parabolic equation /4/. But nowadays the common method of solution in domain of space frequencies of the complex amplitude E is the splitting algorithm applied together with Discrete Fourier Transform (DFT).

Solution to parabolic equation (2.3) corresponding to propagation of the wave from the plane z_l to plane z_{l+1} can be written in an operator form /5/

$$E(x, y, z_{n+1}) = \exp \left[-\frac{i}{2k} \left(\Delta z \nabla_{\perp}^2 + 2k^2 \int_{z_n}^{z_{n+1}} \delta n dz \right) \right] E(z_n). \quad (2.5)$$

This equation can be approximated by a symmetrized split operator

$$\begin{aligned} E(x, y, z_{l+1}) &= \hat{D}\left(\frac{1}{2} \Delta z\right) \hat{R}(z_l, z_{l+1}) \hat{D}\left(\frac{1}{2} \Delta z\right) E(z_l) + O(\Delta z^2), \\ \hat{D}(\Delta z) &= \exp\left(-i \frac{1}{2k} \Delta z \nabla_{\perp}^2\right), \hat{R}(z_l, z_{l+1}) = \exp\left(-ik \int_{z_l}^{z_{l+1}} \delta n dz\right). \end{aligned} \quad (2.6)$$

Operator \hat{R} describes here refraction on inhomogeneities of the index of refraction and operator \hat{D} corresponds to the solution of the problem of free diffraction. The second order of accuracy for this approximation was proved analytically /5,6/ and confirmed by numerical experiments /7/.

For optical waves the problem of free diffraction on a distance z can be solved using the representation for complex amplitude in the form of a finite Fourier series /3/

$$E(x, y, z) = \sum_{m=-N/2+1}^{N/2} \sum_{n=-N/2+1}^{N/2} E_{mn}(z) \exp \left[\frac{2\pi i}{L} (xm + yn) \right], \quad (2.7)$$

where

$$E_{mn}(z) = \frac{1}{4\pi^2 L^2} \int_0^L \int_0^L dx dy E(x, y, z) \exp \left(-i \frac{2\pi}{L} (xm + yn) \right) \quad (2.8)$$

are coefficients of the series, L is a size of the domain of expansion, N is the number of members in the series. It is also assumed that spectrum of space

frequencies for function $E(x, z, t)$ is finite and the function itself is periodic or can be supplemented to a periodic function. In the case of numerical simulation a continuous field $E(x, z, t)$ is replaced by a discrete field defined in nodes of a calculational grid. Transition from the domain of the original function to the spectral space is performed by the Discrete Fourier Transform. Substituting the spectral representation into the parabolic equation we obtain

$$2ik \frac{\partial E_{mn}}{\partial z} = -\frac{4\pi^2}{L^2} (m^2 + n^2) E_{mn} \quad (2.9)$$

with the following exact solution

$$E_{mn}(z) = E_{mn}(z=0) \exp \left[-\frac{4\pi^2 z}{2ikL^2} (m^2 + n^2) \right]. \quad (2.10)$$

To solve the problem of refraction in a layer Δz we need to obtain the numerical representation for inhomogeneties $\delta n(\vec{\rho}, z)$ of the index of refraction. Refraction is described as beam transition through a phase screen

$$\hat{R}(z_l, z_{l+1}) = e^{i\varphi_l(\vec{\rho})}; \quad \varphi_l(\vec{\rho}) = -k \int_{z_l}^{z_{l+1}} \delta n(\vec{\rho}, z) dz. \quad (2.11)$$

Mathematical model of the index of refraction inhomogeneties depends on the process due to that they appear. Here we consider two effects: random fluctuations induced by the atmosphere and low threshold physical effect known as thermal blooming.

Thermal blooming of high-power laser beams

A scale of variations for induced thermal inhomogeneties in a channel of propagation of a high-power laser beam is comparable with a diffraction length of the beam. In interval Δz an expression for a phase screen can be approximated by the product of a step length and the index of refraction distribution in the middle of interval $[z_l; z_l + \Delta z]$

$$\varphi_l(\vec{\rho}) = k \Delta z \cdot n(\vec{\rho}, z_l + \frac{1}{2} \Delta z) + O(\Delta z^2). \quad (2.12)$$

From the above it follows that we have only to obtain perturbations of the index of refraction in some planes positions of which are determined by the scheme of the splitting algorithm.

Heating of the medium due to absorption of radiation energy induces variations of its density that leads to decrease of the index of refraction related with density by the following law

$$\delta n = K\rho, \quad (2.13)$$

where K is a constant equal to $2/3$ of polarization factor of a molecule or an atom of a gas.

In isobaric approximation density of a medium is explicitly related with temperature by the equation of the gas state so variations of the index of refraction can be expressed through temperature variations

$$\delta n \approx \frac{\partial n}{\partial T}(T - T_0) = n'_T \delta T. \quad (2.14)$$

Isobaric approximation is valid for the normal atmospheric conditions. Exceptions are the following: (1) fast slewing of a cw high-power beam when the speed of the beam relatively to the medium is greater than the speed of sound and (2) when a pulse duration is comparable with acoustic time τ_s

$$\tau_p \approx \tau_s = a/c_s, \quad (2.15)$$

where a is the size of the beam, c_s is the speed of sound.

When the isobaric approximation is valid, distribution of the index of refraction in the beam cross-section is determined by balance of heat which is described by the equation of heat transport for the temperature field $T(x, y, z)$

$$\frac{\partial T}{\partial t} + \vec{V}_\perp \nabla T + \chi \Delta_\perp T = \frac{\alpha}{\rho_0 C_P} I, \quad (2.16)$$

where $\vec{V}_\perp = (V_x, V_y)$ is a transverse component of relative velocity of the beam, χ is heat conductivity, ρ_0 is specific density of the medium, α is an absorption coefficient, and C_P is specific heat at constant pressure.

When the isobaric approximation becomes invalid, variations of the medium density are described by linearized equations of hydrodynamics, which follow from the law of continuity and by the law of impetus and energy conservation [3,8/

$$\frac{d\rho_1}{dt} + \rho_0 \nabla v_1 = 0, \quad \frac{d}{dt} = \frac{\partial}{\partial t} + v \frac{\partial}{\partial x}, \quad (2.17)$$

$$\rho_0 \frac{dv_1}{dt} = -\nabla p_1, \quad (2.18)$$

$$\frac{d}{dt} (p_1 - c_s^2 \rho_1) = (\gamma - 1) \alpha I. \quad (2.19)$$

These equations are valid in the case of small perturbations of density ρ_1 , pressure p_1 , and local speed of the medium flow v_1 relatively to unperturbed values of the corresponding parameters. By eliminating the variables describing perturbation of speed and pressure Eqs. (2.17) - (2.19) can be transformed to the following equation which describes perturbations of density

$$\left[\frac{d^2}{dt^2} - c_s^2 \nabla^2 \right] \frac{d\rho_1}{dt} = (\gamma - 1) \alpha \nabla^2 I. \quad (2.20)$$

For steady-state conditions this equation takes the form

$$\left[\frac{d^2}{dy^2} + (1 - M^2) \frac{\partial^2}{\partial x^2} \right] \frac{\partial \rho_1}{\partial x} = \frac{(\gamma - 1)}{c_s^2 v} \alpha \nabla^2 I, \quad (2.21)$$

where $M = v/c_s$ is Mach's number, $\gamma = C_P / C_V$ is a ratio of specific heat capacities.

When the speed of medium flow is small ($M \ll 1$) equation (2.21) transforms to the equation written in the isobaric approximation

$$\frac{\partial \rho_1}{\partial x} = \frac{(\gamma - 1)}{v c_s^2} \alpha I. \quad (2.22)$$

Solution of this equation yields results equal to that of Eq. (2.16) with $v_y = 0$ and $\chi = 0$.

So the mathematical model of thermal blooming of high-power coherent laser beams in low-absorbing medium includes parabolic equation for a scalar

complex amplitude (2.3) and corresponding material equation describing variations of density and temperature and defining distribution of the index of refraction in the channel of propagation.

$$\begin{cases} 2ik \frac{\partial E}{\partial z} = \left(\frac{\partial^2}{\partial x^2} + \frac{\partial^2}{\partial y^2} + 2k^2 \delta n \right) E \\ \hat{M}(\delta n) = \alpha I, \end{cases} \quad (2.23)$$

where operator \hat{M} describes the relation between induced optical inhomogenities and absorbed energy αI .

As an example of the mathematical model implementation let us consider the results of thermal blooming simulation computed for a Gaussian beam crossing a thin layer L of nonlinear medium (a nonlinear phase screen). In the example under consideration approximation of nonlinear phase screen means that thickness L of the layer is much less than a focus length and diffraction length $L_d = ka_0^2$ of a beam and that attenuation is small ($\alpha L \ll 1$).

In Fig. 2.1 dynamic of thermal blooming under conditions of forced convection is illustrated for speed of convective flow much less than the speed of sound (isobaric approximation, Eq. (2.16)) and for heat conductivity $\chi=0$. In this case the sole parameter of the problem is integer nonlinearity of a layer $P_N = \frac{2\pi}{\lambda} \frac{\alpha}{\rho C_P} \frac{a_0 I_0}{V_\perp} n_T L$, I_0 is initial intensity of the beam. When transient processes end, the phase screen can be described as an integral of normalized beam intensity

$$\varphi(x, y) = P_N \int_{-\infty}^x I(\xi, y) / I_0 d\xi = P_N \int_{-\infty}^x \exp(-\xi^2 - y^2) d\xi. \quad (2.24)$$

As distance x decreases, the value of phase φ at the OX axis approaches $\sqrt{\pi} \times P_N \approx 1,77 P_N$. In calculations the value of P_N parameter was taken equal to 10, that correspond to maximum phase increase at the path (17.7 rad or $2,8\lambda$). For such nonlinear distortions the steady-state maximum value of intensity in the focus decrease more than ten times. In Fig. 2.1 two examples are presented that differ

by direction of wind velocity. For each moment of time 2D distribution of phase distortions in the plane of transmitting aperture is shown as well as distribution of intensity in the focal plane, the beam was Gaussian. In the first case wind was directed along the coordinate axis, in the second case the angle between them was 45° .

Numbers in half-tones pictures show maximum and minimum values of the function. It is seen that the assessment of phase distortions presented above for steady-state regime (17.7 rad) are in good agreement with the results obtained in numerical experiments (16.9 and 16.0 rad). Difference of 5 to 10% can be attributed to errors of numerical model and to the fact that transient process does not end completely.

Calculations were performed by monotonic conservative procedure with approximation of second order, differences were taken against the flow /9/, a model viscosity (heat conductivity) was compensated according to Samarsky algorithm /10/. This method has the advantage to define arbitrary direction of wind velocity in the problem of heat transport. The scheme is stable for small as well as for large intervals of temporal discretization. The problem can also be solved when the wind velocity depends on transverse coordinates (x, y) .

Another situation arises with beam slewing. In this case speed of beam transition relatively to medium can be close or even greater than the speed of sound. In Fig. 2.2 perturbations of density is shown for a regime of forced convection with a speed of the flow close to that of sound (Eq. 2.21). Parameter P_N was taken two times less than in the previous example. In isobaric approximation this corresponds to maximum increment of phase on the path (8.8 rad). It is seen that for $Mach = 0.5 - 0.7$ the results do not differ much, for further increase of M (M approaches unity) phase distortions increase sharply. For M greater than unity we obtain a solution approximately equal to the results of isobaric approximation, but two times greater. It can also be shown analytically that for M approaches infinity this conclusion is fulfilled precisely.

Turbulent distortions of wavefront

Under conditions of turbulent fluctuations longitudinal scale of the index of refraction variations is of the same order as the inner scale of turbulence l_0 which is usually less than the step of discretization Δz . In this case integration of the index of refraction inhomogeneities along coordinate z should be performed analytically. Because of the statistical method employed to define turbulent fluctuations $\delta n(\vec{\rho}, z)$, in result of integration we obtain expressions describing statistical characteristics, for example, a correlation function of phase fluctuations

$$B_\varphi(\rho) = \langle \varphi(\vec{r} + \vec{\rho}) \varphi(\vec{r}) \rangle = k^2 \int_0^{\Delta z} \int_0^{\Delta z} dz' dz'' \langle n(\vec{r} + \vec{\rho}, z_l + z') n(\vec{r}, z_l + z'') \rangle. \quad (2.25)$$

Corresponding spectral density F_φ obtained by the authors of Ref. 5 for von Karman spectrum of turbulence is of the form

$$F_\varphi(\kappa) = 2\pi k^2 \Delta z \Phi_n(\kappa_\perp, \kappa_z = 0, L_0) \cdot K\left(\kappa, \frac{L_0}{\Delta z}\right), \quad (2.26)$$

where Φ_n is 3D spectral density of the index of refraction fluctuations, L_0 is the outer scale, K is a correction function which approaches unity at small values of the second argument, which corresponds to Markov approximation.

In problems where high-power laser beams propagation is considered in a randomly inhomogeneous medium, thermal distortions of beams induced by heating of the medium should be allowed for along with turbulent fluctuations. Within a step of integration over the longitudinal coordinate, turbulent and thermal distortions can be considered as additive, i.e.,

$$\varphi(\vec{\rho}, t) = k \int_{z_l}^{z_{l+1}} \delta n(\vec{\rho}, z, t) dz \approx \varphi_1(\vec{\rho}, t) + \varphi_2(\vec{\rho}, t), \quad (2.27)$$

where φ_1 is nonlinear and φ_2 is turbulent distortions.

Thus simulating numerically by the splitting algorithm a beam propagation in a randomly inhomogeneous medium, realizations of random phase screens should be generated according to the statistics chosen. Simulation of random

processes is a special branch of computational mathematics, application of its methods to the problem of calculation of beam turbulent distortions will be considered further. Here we consider only some problems, such as the choice of a step of discretization over lengthwise coordinate $\Delta\rho$ and choice of the size of a sample.

Whether the technique of numeric experiment is possible to employ is determined mainly by the possibility of representation of an optical wave complex amplitude as a discrete function. According to the laws of computational mathematics this condition limits the spatial width of spectrum κ_{\max} of a function

$$\kappa_{\max} < 1/\Delta\rho. \quad (2.28)$$

A spectrum bandwidth can be estimated using the well-known fact that an angular size of a point object image W seen through the turbulent atmosphere is approximately equal to the ratio of wave length λ to a length of coherence r_0

$$W \approx \lambda/r_0, \quad r_0^{-5/3} = 0.423k^2 \int C_n^2 dz. \quad (2.29)$$

A lens can be viewed as a simple system of image forming that performs Fourier transform of an incident field, so the size W corresponds to the bandwidth of spectrum, i.e., $\kappa_{\max} \sim W/\lambda$. The attention should be paid to the fact that the ratio λ/r_0 correspond to FWHM of an image. A radius of a circle within which falls 95% of energy is three times greater. For a plane wave crossed a layer of atmospheric turbulence a bandwidth of spectrum can be estimated as

$$\kappa_{\max} \approx 3W/\lambda = 3/r_0. \quad (2.30)$$

This leads to the following restrictions of discretization step

$$\Delta\rho < \frac{1}{3}r_0. \quad (2.31)$$

Another restriction appears because small scale turbulent distortions with space frequencies $\kappa > \kappa_{\max}$ can be lost at discretization. Violation of this condition leads to an error approximately equal to the integral over the corresponding spectral interval. Let us impose a limit on this value corresponding to the criterion « $\lambda/10$ »

$$\begin{aligned}
\sigma^2 &= 2\pi \int_{\kappa_{\max}}^{\infty} F_{\varphi}(\kappa) \kappa d\kappa = 2\pi \times 0.489 r_0^{-5/3} \int_{\kappa_{\max}}^{\infty} \kappa^{-8/3} d\kappa \\
&= 0.489 r_0^{-5/3} \frac{3}{5} \kappa_{\max}^{-5/3} = 0.3 (\Delta\rho/r_0)^{5/3} < (2\pi/10)^2 = 0.4
\end{aligned} \tag{2.32}$$

Less strict condition on the step of discretization follows from here, namely, $\Delta\rho < r_0$.

Let us now consider demands to the size N_{smp} of a sample. In the problems considered in the present report we are concerned only in the moment of the first order, i.e., mean intensity. Variance of estimation errors for a mean value is related with variance of fluctuations by the following formula

$$\sigma_{estm\ err}^2 = \frac{\sigma_I^2}{N_{smp}}. \tag{2.33}$$

From this equation we obtain the condition ensuring 10% mean square error of estimation

$$N_{smp} = \frac{\sigma_I^2}{\sigma_{estm\ err}^2} = \frac{\sigma_I^2}{(0.1\langle I \rangle)^2} = 100 \frac{\sigma_I^2}{\langle I \rangle^2} \tag{2.34}$$

Now we can make *a priori* estimation of the sample size using relative variance of intensity fluctuations and taking into account the well known effect of intensity fluctuation saturation. The data obtained experimentally /3/ as well as the results of numeric experiments /5, 12, 13/ manifest that normalized variance of intensity fluctuations almost never exceeds unity. It is true for a plane wave as well as for close-to-axis regions and for an image plane of beams limited in space. So $N_{smp} = 100$ should be taken for estimation of mean intensity with 10% precision on the optical axis of a system. Less strict condition is characteristic to problems of estimation of adaptive systems efficiency because intensity fluctuations are lessened considerably due to correction. In calculations the results of which are presented in the report the size of sample $N_{smp} = 100$ allowed us to assess mean intensity of a beam or image under correction with precision not less than 5%.

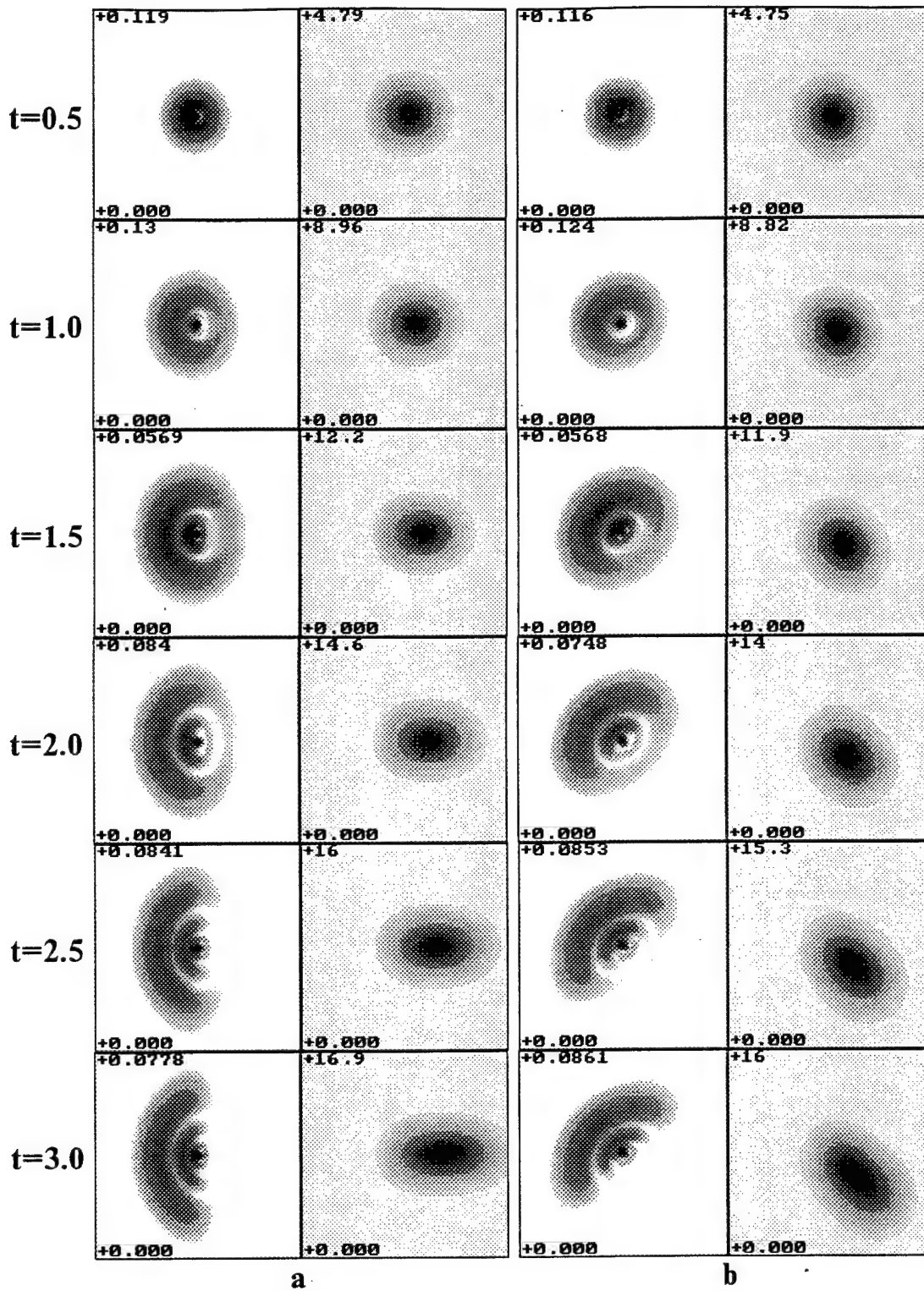


Fig. 2.1. Thermal blooming under condition of forced convection (isobaric approximation). Wind is directed along axis OX (a), an angle between wind and OX axis is 45° (b).

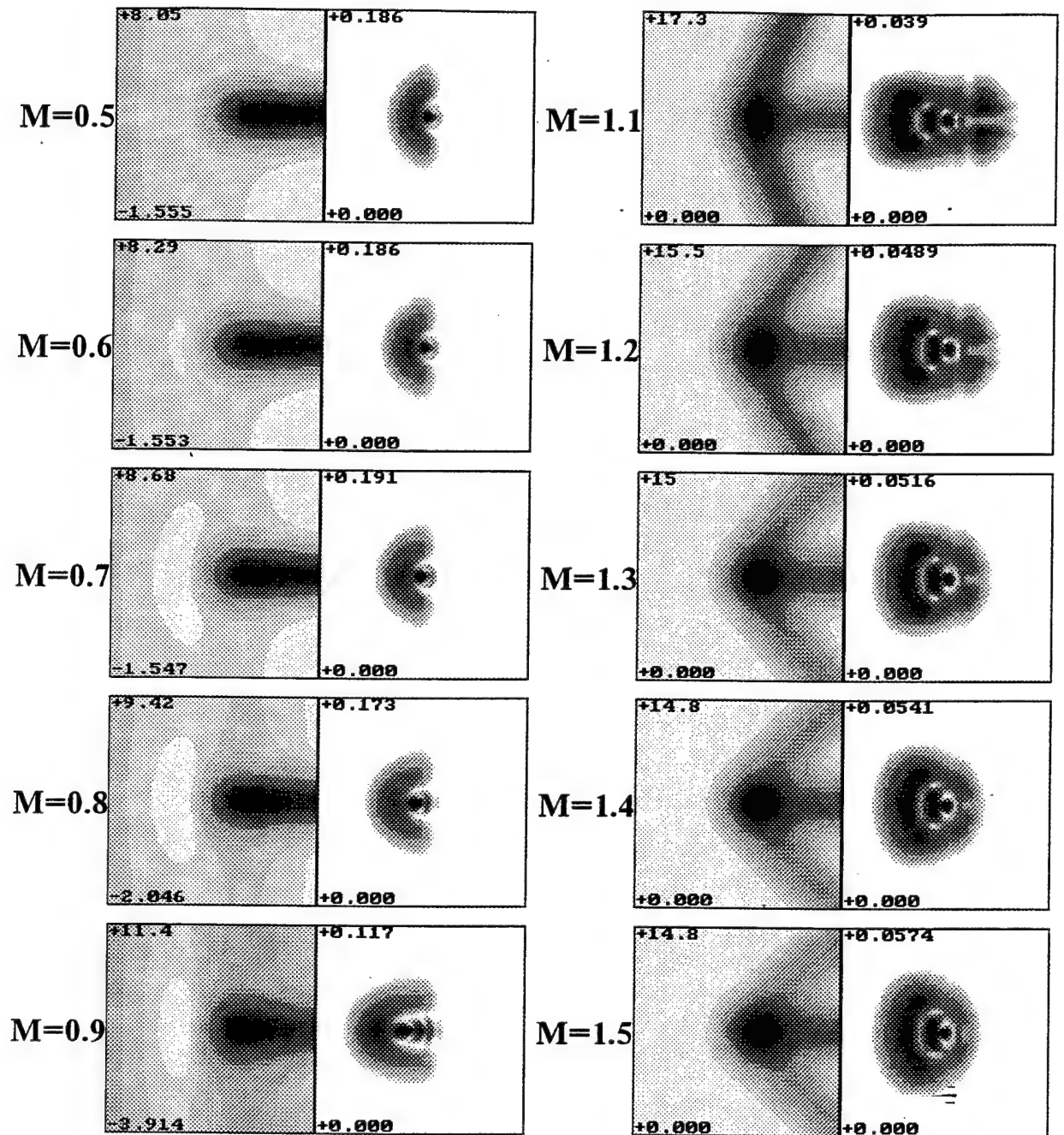


Fig. 2.2. Thermal blooming behind a phase screen under condition of forced convection (steady-state solution of linearized equations of hydrodynamics).

2.2. Generation of random 2D phase screens by Fourier transform

Let us consider simulation of stationary random process with a given spectral density $F(\kappa)$. In the problems where random processes taking part representation is used in the form of stochastic Fourier integral [14]

$$S(\bar{\rho}) = \iint \exp(i\bar{\kappa}\bar{\rho}) d^2 H(\bar{\kappa}) \quad (2.35)$$

In stationary random processes spectral components are delta-correlated and related with spectral density by the following equation

$$\langle d^2 H(\bar{\kappa}) d^2 H^*(\bar{\kappa}') \rangle = F_S(\bar{\kappa}) \delta(\bar{\kappa} - \bar{\kappa}') d^2 \kappa d^2 \kappa' \quad (2.36)$$

Here and further the angular brackets mean averaging over an ensemble and the asterisk signifies complex conjugation.

In numeric experiments with stationary random processes we should to produce samples of field $S(\bar{\rho})$ discrete over space variables such that statistics and correlation properties of discrete random processes correspond to properties of the original continuous process. In accordance with the method of Fourier transformation the simulated process is represented as truncated Fourier series with coefficient which form 2D matrix of spectral counts

$$S(\bar{\rho}) = \sum_{-N/2}^{N/2} \sum_{-N/2}^{N/2} \tilde{S}(\bar{\kappa}_{LM}) \exp(i\bar{\rho}\bar{\kappa}_{LM}). \quad (2.37)$$

Usually in numeric experiments we are interested in values of a function in nodes of an equidistant calculation grid

$$\bar{\rho}_{I,J} = \bar{e}_x I \Delta \rho + \bar{e}_y J \Delta \rho, \quad I, J = 0, 1, 2, \dots, N, \quad (2.38)$$

so the double sum in Eq. 2.37 can be rewritten as

$$S(\bar{\rho}_{I,J}) = S_{I,J} = \sum_{-N/2}^{N/2} \sum_{-N/2}^{N/2} \tilde{S}_{L,M} \exp\{i(I \cdot L + J \cdot M) \Delta \kappa \Delta \rho\}. \quad (2.39)$$

Assuming that

$$\Delta\kappa = \frac{2\pi}{N \cdot \Delta\rho} \quad (2.40)$$

and changing limits of sums we obtain the standard formula of 2D Fourier transform

$$S_{I,J} = \sum_0^{N-1} \sum_0^{N-1} \tilde{S}_{L,M} \exp\left\{\frac{2\pi i}{N}(I \cdot L + J \cdot M)\right\}, \quad (2.41)$$

or an equivalent formula

$$S_{I,J} = \sum_{-N/2}^{N/2} \exp\left(\frac{2\pi i}{N} J \cdot M\right) \sum_{-N/2}^{N/2} \tilde{S}_{L,M} \exp\left(\frac{2\pi i}{N} I \cdot L\right). \quad (2.42)$$

It was shown by the authors of Refs. 15 and 16 that to obtain the given correlation properties in realizations, coefficients of Fourier series should be interrelated with spectral density of the given process by the following equation

$$\langle |\tilde{S}_{L,M}|^2 \rangle = F_S(\kappa_{LM}) \Delta\kappa^2, \kappa_{LM} = \Delta\kappa \sqrt{L^2 + M^2}, \quad (2.43)$$

where $\Delta\kappa$ is an interval of discretization for a spatial frequency. A correlation function of the obtained sequence corresponds to correlation function of a simulated random process if correlation length of the random process and values of correlation function argument taken into consideration are less than the size of a region in space covered by the calculation grid. The last restriction is due to periodicity of the sequence obtained as a result of Fourier transform.

The restrictions in choice of a probability density function of random Fourier coefficients are quite loose. For example, the authors of Ref. 17 showed that for counts in a spectral domain it is possible to use normal distribution as well as uniform distribution. In the last case multidimensional characteristic function of the obtained correlated sequence approaches multidimensional characteristic function of Gaussian process as $O(1/\sqrt{N})$. Other authors use χ^2 distribution of absolute value of complex counts and uniform in interval $[0, 2\pi]$ distribution of its arguments to obtain a random sample of spectral counts that is equivalent to normal distribution of its real and imagine parts.

Indeed, real and imaginary parts of counts obtained as a result of discrete Fourier transform applied to correlated sequence of normal random numbers are also normally distributed random numbers. From this point of view using of a Gaussian function is quite possible.

The main shortcoming that is characteristic to all references quoted above is the absence of arguments on which the choice is based of function describing the distribution of random counts. But usually the problem of obtaining a sequence of correlated numbers is considered and not a problem of a random process simulation. Reasons considered in Ref. 24 clearly justify that to make a procedure more strict from mathematical point of view one should choose a constant value of modulus and uniformly distributed argument in interval $[0; 2\pi]$. Practically, our mathematical manipulations showed that energy in an arbitrary small but finite interval of spectral representation of a random process does not fluctuate disregarding the fact that a spectral amplitude of every harmonic component is a random number as well as its modulus.

The function of phase (argument) distribution for coefficients of Fourier series can be chosen arbitrary because it does not influence the spectral density. But from statistical independence of the real and imaginary part it follows that arguments of Fourier series coefficients are distributed uniformly in interval $[0; 2\pi]$.

Let us consider some peculiarities that arise due to the fact that the considered process is a real one. To obtain two phase screens as a result of Fourier transform it is used often. One screen is in a real and the other is in an imaginary part of a retrieved array. But such approach is possible only for statistically uniform (for example, horizontal) path, because only in this case the both screens have the same statistics. In vertical paths intensity of turbulence, its outer and inner scales as well as speed of phase screen transition (speed of wind) are changed along the path.

It is known that a real component of Fourier transform for 1D real function is a even function of frequency (imagine component is an odd function of frequency), i.e..

$$A(\omega) = A^*(-\omega). \quad (2.44)$$

Fourier transform of 2D field has an analogous property

$$A(\vec{\kappa}) = A^*(-\vec{\kappa}). \quad (2.45)$$

Property of symmetry (2.45) relatively to operation of conjugation for a discrete spectrum of a real function takes the form

$$\tilde{S}_{L,M} = \tilde{S}_{-L,-M}^*. \quad (2.46)$$

After calculation of the inner sum and row-by-row realization of Fourier transform we obtain the matrix of counts

$$\tilde{S}_{I,M}^x = \sum_{-N/2}^{N/2} S_{L,M} \exp\left\{\frac{2\pi i}{N} L \cdot I\right\} \quad (2.47)$$

with a property $\tilde{S}_{I,M}^x = \tilde{S}_{I,-M}^{x*}$. It allows us to calculate the outer sum only for non-negative values of M and in such a way to obtain two fold decrease in number of mathematical operations.

All in all, the developed here modification of the method of spectral samples can be viewed as the following sequence of operations

1. Definition of the first half of rows of 2D array of Fourier coefficients according to the formula for modulus of the spectrum and for phase φ_{rand} uniformly distributed in the interval $[0; 2\pi]$

$$\begin{aligned} \tilde{S}_{L,M} &= F^{1/2} \left(\Delta\kappa \cdot \sqrt{L^2 + M^2} \right) \cdot \Delta\kappa \cdot \exp(i\varphi_{rand}); \\ L &= -N/2, N/2; M = 0, 1, \dots, N/2. \end{aligned} \quad (2.48)$$

2. Calculation of 1D Fourier transforms of these rows

$$\tilde{S}_{I,M}^x = \sum_{-N/2}^{N/2} S_{L,M} \exp\left\{\frac{2\pi i}{N} L \cdot I\right\}, M = 0, 1, \dots, N/2. \quad (2.49)$$

3. Mapping of these transforms onto the second half of rows and their conjugation

$$\tilde{S}_{I,M}^x = \tilde{S}_{I,-M}^{x*}; M = -N/2, \dots, -1. \quad (2.50)$$

4. Column-by-column Fourier transform

$$S_{I,J} = \sum_{-N/2}^{N/2} \tilde{S}_{I,M}^x \exp\left\{\frac{2\pi i}{N} M \cdot J\right\}, J = 0, 1, \dots, N-1 \quad (2.51)$$

In the frame of «frozen turbulence» hypotheses which can be formulated as follows

$$S(\vec{\rho}, t) = S(\vec{\rho} - \vec{V}t, 0) \quad (2.52)$$

the technique described above can readily be generalized to dynamics problems. One property of Fourier transform is that the shift of original function is equivalent to addition of a linear component to a phase of Fourier transform. Taking into account this property Eq. (2.48) can be rewritten as

$$\tilde{S}_{L,M}(t) = F^{1/2} \left(\Delta\kappa \cdot \sqrt{L^2 + M^2} \right) \cdot \Delta\kappa \cdot \exp(i\varphi_{rand}) \exp\left(i\Delta\kappa t [V_x L + V_y M]\right); \quad (2.53)$$

$$L = -N/2, N/2; M = 0, 1, \dots, N/2$$

An example of a phase screen succession representing turbulent aberrations registered with temporal intervals $\Delta t = 2\frac{1}{3}(\Delta\rho/V)$ obtained in this way is shown in Fig. 2.3. An angle between wind velocity and the axis of abscissae is 30° . As it is seen from this example the turbulence moves along vector of wind velocity. Taking the direction which does not coincide with the coordinate axis it is possible to obtain long in the time domain realization of turbulent aberrations that do not coincide. This is possible because at every cycle along X-axis with duration $T_x = (N \times \Delta\rho)/V_x$ a phase screen shifts along y-axis on an interval $D_y = V_y T_x$. The period of exact repetition is determined by the following condition

$$\begin{aligned} nV_y T_x &= nV_y (N \Delta\rho)/V_x = mN \Delta\rho \Rightarrow nV_y = \\ &= mV_x \Rightarrow n = mV_x/V_y = m \cdot \text{ctg}(\vartheta) \end{aligned} \quad (2.54)$$

where n and m are even numbers.

Testing of the technique was performed by comparison of integral from phase variance within a circle after extracting one or several aberrations ($N = 1, \dots, 10$) described by Zernike polynomials Z_l

$$\Delta_N = \frac{1}{\pi R^2} \left\langle \iint_{\rho < R} d^2 \rho \cdot \left(S(\vec{\rho}) - \sum_{l=1}^N a_l Z_l(\vec{\rho}) \right)^2 \right\rangle \quad (2.55)$$

with corresponding parameters obtained theoretically by Fried /18/ and Noll /19/. Calculated values of integral variance of approximation error obtained by averaging over 100 realizations are presented in Fig. 2.3 for 128×128 calculation grid. Three values of the ratio of the domain size L covered by the grid to the aperture diameter D were taken. The values are normalized on corresponding analytically obtained values borrowed from Ref. 19. Results are presented in table 2.1.

Table 2.1. Analytically obtained integral variance of errors for approximation of a turbulent wavefront by a finite number of Zernike polynomials.

Number of polynomials N	$\Delta_N / (D/r_0)^{5/3}$
1	1.03
3	0.134
6	0.0648
8	0.0525

From the curves presented in Fig. 2.3 it is seen that linear and square aberrations are influenced considerably by the loss of space scales greater than the size of the grid. This fact is confirmed by calculations of variance for coefficients of a

Zernike series by which a wavefront is represented. It was assumed that the outer scale of a turbulent spectral density is finite. Parameter Δ_1 characterizing phase aberrations without a phase constant within the aperture (polynomial Z_1) is less considerably than corresponding theoretical value. At the same time for ratio $L/D < 8$ parameters Δ_6 and Δ_{10} differ from theoretically obtained values not more than 5%. For $L/D > 8$ difference increases slowly and approaches theoretical limit. Parameters Δ_3 , Δ_6 and Δ_{10} decrease with approximately the same speed that means bad approximation of high-order polynomials. So using Fourier transform to simulate a turbulent phase screen with power spectrum we obtain excessively low values of tilt fluctuations (tilt corresponds to first-order polynomials Z_2 and Z_3) and somewhat lower values for fluctuations of quadratic aberrations. It can be accounted for by the fact that the method is not suitable for simulation of large scale random inhomogeneities and the grid size L is an analog to the outer scale of turbulence.

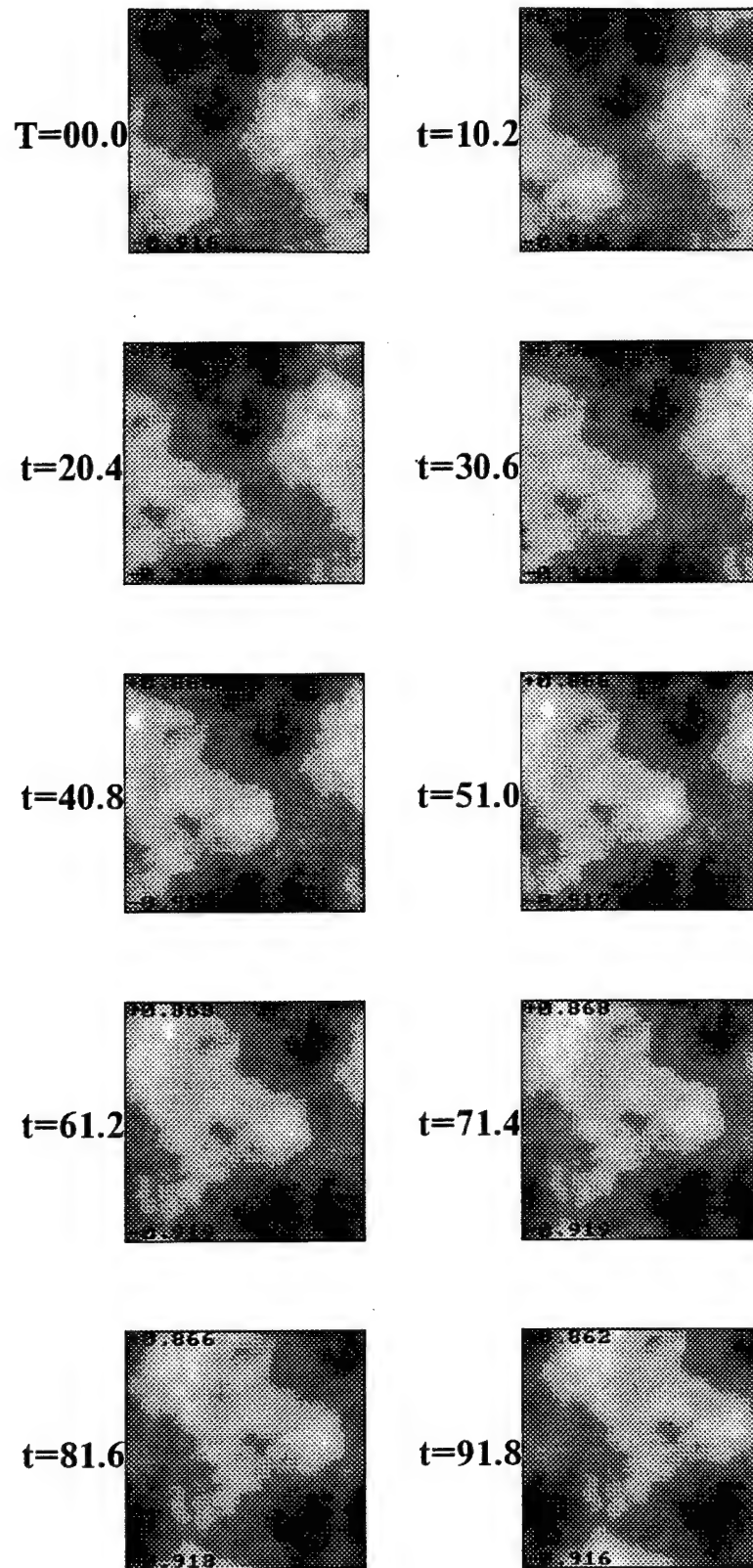


Fig. 2.3. Sequence of phase screens simulating successive turbulent aberrations (interval between nearest screens is $\Delta t = 10 \frac{1}{5} (\Delta \rho / V)$).

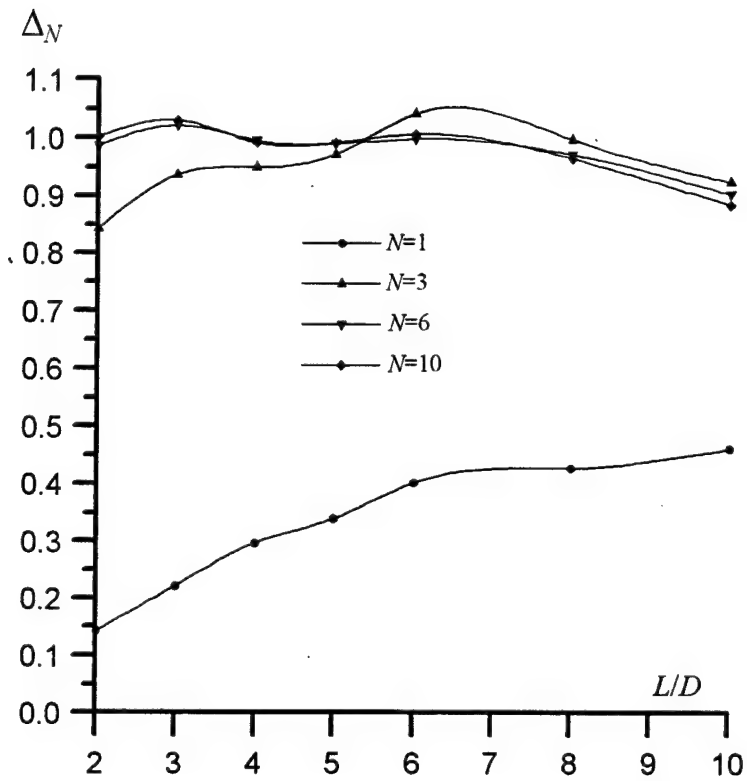


Fig. 2.4. Normalized on theoretical results values of Δ_N parameter calculated for a power spectrum of turbulence.

2.3. Dynamic simulation of large-scale turbulent aberrations of optical phase

As it was pointed out earlier, the method of spectral samples does not allow one to reproduce a scales greater than the size of a calculation grid. As a result the low spatial frequencies of a turbulent spectrum are lost that results in underestimation of atmospheric distortions, mainly, of random refraction and quadratic aberrations of wavefront.

It is natural to try to compensate for underestimation of these aberrations. To do so we need to know statistics of these aberrations, after that we can sum up two phase screens, one obtained by the method of Fourier transform and including high and medium spatial frequencies and other including aberrations induced by low spatial frequencies of the spectrum. This approach was formulated firstly by the authors of Refs. 20 and 21. Here we present detailed description of this approach generalized to the case of time-dependent problem.

Linear and quadratic aberrations coincide with first terms of Zernike series so the theory developed for this series is possible to apply in our case, namely, expressions for statistical characteristics of Zernike coefficients can be used relating these statistical characteristics with a spectrum of a random process.

Let us consider wave front representation as a Zernike series within a circular aperture with radius R

$$S(\vec{r}) = \sum_{l=0}^{\infty} a_l Z_l(\vec{r}) \quad (2.56)$$

A Zernike polynomial Z_l [22] is a product of radial and azimuth components

$$Z_l(\vec{r}) = c_{nm} R_n^m(\vec{r}/R) \cdot V_{ml}(\theta), \quad c_{nm} = 2^{\delta_{m0}/2} \sqrt{n+1} \quad (2.57)$$

$$R_{nm}(\bar{\rho}) = \sum_{s=0}^{(n-m)/2} \frac{(-1)^s (n-s)! \rho^{n-2s}}{s! [(n+m)/2 - s]! [(n-m)/2 - s]!} \quad (2.58)$$

$$V_{m,l} = \cos(m\theta), \quad l = 0, 2, 4, \dots$$

$$V_{m,l} = \sin(m\theta), \quad l = 1, 3, 5, \dots$$

which are characterized by a radial power n and an azimuth frequency m . A difference $n - m$ is an even number and $m \leq n$. Moreover, Zernike polynomials are orthogonal within a circle, i.e.,

$$\iint_{r \leq R} Z_l(\vec{r}) \cdot Z_{l'}(\vec{r}) d^2 r = c_l \delta_{ll'}. \quad (2.59)$$

A method of simulation for a random phase screen using an aberration representation is as follows. Firstly, we generate vector of random expansion coefficients; secondly, this vector we substitute into sum (2.56). So we need to obtain an ensemble of random Zernike coefficients. The simulated process is normal with a zero mean value so coefficients

$$a_l = \frac{1}{\pi R^2} \iint_{r \leq R} S(\vec{r}) Z_l(\vec{r}) d^2 r, \quad (2.60)$$

are also Gaussian with zero mean value. So to define these coefficient we only need to calculate elements of a correlation matrix

$$\begin{aligned} C_{ll''} = \\ = \delta_{m'm''} \cdot 8\pi [(n'+1)(n''+1)]^{1/2} \cdot (-1)^{(n'+n''-m'-m'')} \int_0^\infty F(\kappa) \frac{J_{n'+1}(\kappa R) \cdot J_{n''+1}(\kappa R)}{(\kappa R)^2} \kappa d\kappa \end{aligned} \quad (2.61)$$

This equation define correlation of coefficients for polynomials the azimuth factors of which are equal. In other cases correlation is equal to zero.

For dynamic simulation we need also autocorrelation functions of expansion coefficients

$$\begin{aligned} B_l(\tau) = \\ = 8\pi(n+1) \int_0^\infty \kappa d\kappa \cdot F(\kappa) \frac{J_{n+1}^2(\kappa R)}{(\kappa R)^2} \cdot \left[J_0(\kappa V\tau) + (-1)^{m+l} \cos(2\pi\vartheta) J_{2m}(\kappa V\tau) (1 - \delta_{m0}) \right]. \end{aligned} \quad (2.62)$$

Spectral density of fluctuations of coefficients a_l related with a correlation function by Wiener theorem

$$W_l(\omega) = \frac{1}{\pi} \int_0^\infty B_l(\tau) \cos(\omega\tau) d\tau \quad (2.63)$$

Substituting $B_l(\tau)$ taken in form 2.63 into Eq. 2.62 and calculating the integral with respect to τ we obtain the following equation

$$W_l(\omega) = 8(n+1) \int_{\omega/V}^{\infty} \kappa d\kappa \cdot F(\kappa) \frac{J_{n+1}^2(\kappa R)}{(\kappa R)^2} (\kappa^2 V^2 - \omega^2)^{-1/2} \times \left(1 - (1 - \delta_{m0})(-1)^{l+m} \cos(2m\vartheta) \cos\left(\arcsin\left(\frac{\omega}{\kappa V}\right)\right) \right) \quad (2.64)$$

which can be used to produce random temporal realizations of expansion coefficients.

But some difficulty arises due to correlation of coefficients in Zernike series. The correlation matrix is not diagonal so we cannot generate coefficients as a statistically independent random numbers. To solve this problem we can use expansion into Karhunen-Loeve series, correlation matrix of which is diagonal one by definition.

But straight employment of Karhunen-Loeve expansion is problematic because functions in this basis are lacking explicit analytical form. But where exists a possibility to express Zernike polynomials through Karhunen-Loeve function by orthogonalization procedure of a correlation matrix of Zernike coefficients using general similarity transformation. Detailed description of this procedure is given by N. Roddier in Ref. 23.

More complex problem arises in dynamic simulation. Sometimes orthogonalization procedure of a correlation matrix is impossible here because polynomial coefficients with different angle components are correlated.

Let us note that correlation function for coefficients of two polynomials with equal radial and angular indexes is of the form:

$$B_{l'l''}(\tau) = 8\pi(n+1)(-1)^{n-m} \cdot (-1)^m \cdot 2^{\delta_{m0}-1} \int_0^{\infty} \kappa d\kappa F(\kappa) \frac{J_{n+1}^2(\kappa R)}{(\kappa R)^2} J_{2m}(\kappa V\tau) \sin(2m\vartheta) \quad (2.65)$$

To broke correlation of these polynomials we should direct the axis of abscissae of a basis where polynomials are defined along vector of wind velocity. For such geometry

$$\vartheta = \arctg(V_y/V_x) = 0 \quad (2.66)$$

and correlation is absent. This property allows one to simulate properly dynamic of the first and second order polynomials, i.e., tip and tilt, defocusing, and astigmatism (polynomials Z_2, \dots, Z_6). In this case small-scale aberrations can be simulated by the spectral sample method.

To realize this technique we develop a procedure of calculation of temporal spectrum for coefficients of Zernike expansion, Eq. 2.64. In Fig. 2.5 we represent the results for polynomials of the first, second, and third orders. Temporal samples of Zernike coefficients were obtained according to the technique described in the previous section for 1D case. In Fig. 2.6 examples are presented for coefficients corresponding to tip and tilt, defocusing, and astigmatism. In Fig. 2.7 dynamics of a phase screen is shown which was obtained by summing of liner and quadratic aberrations with small-scale aberrations obtained by the method of spectral samples described in the previous section.

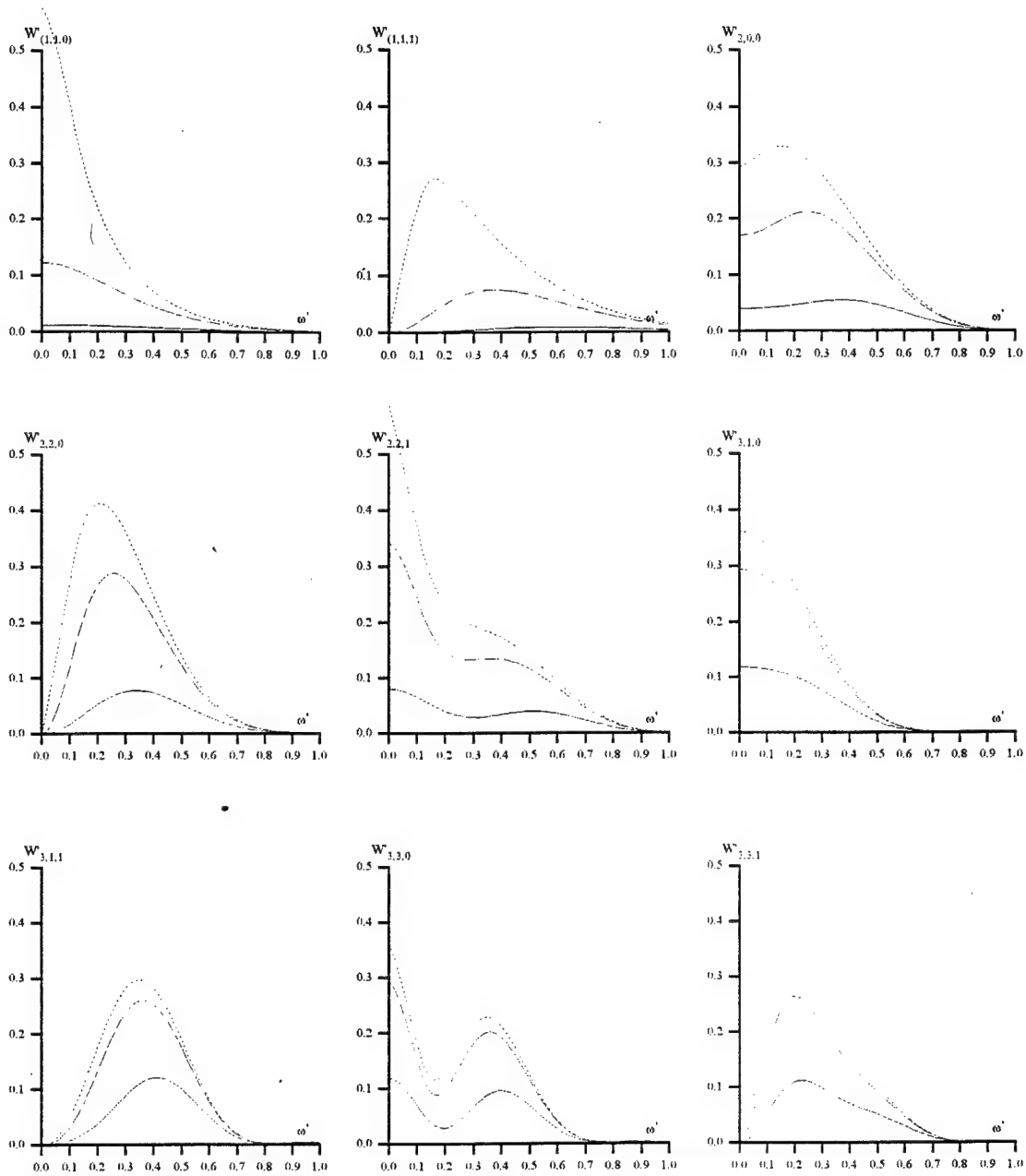


Fig. 2.5. Fluctuation spectra of coefficient of Zernike polynomials of 1, 2, and 3 orders for different values of the outer scale of turbulence. $W' = W / \left(\frac{1}{2} \sigma_n^2 \right)$ is a normalized spectrum, $\omega' = \omega / (3nV/R)$ is a normalized frequency, σ_n^2 is variance of fluctuations corresponding to infinite outer scale, n is a radial power of a polynomial, V is wind velocity (the wind is directed along OX axis), and R is an aperture radius. The three subscripts correspond to the radial power, azimuth frequency, and parameter of parity. The lower curves correspond to $L_0/D=1$, middle curves to $L_0/D=3$, and upper curves to $L_0/D=10$.

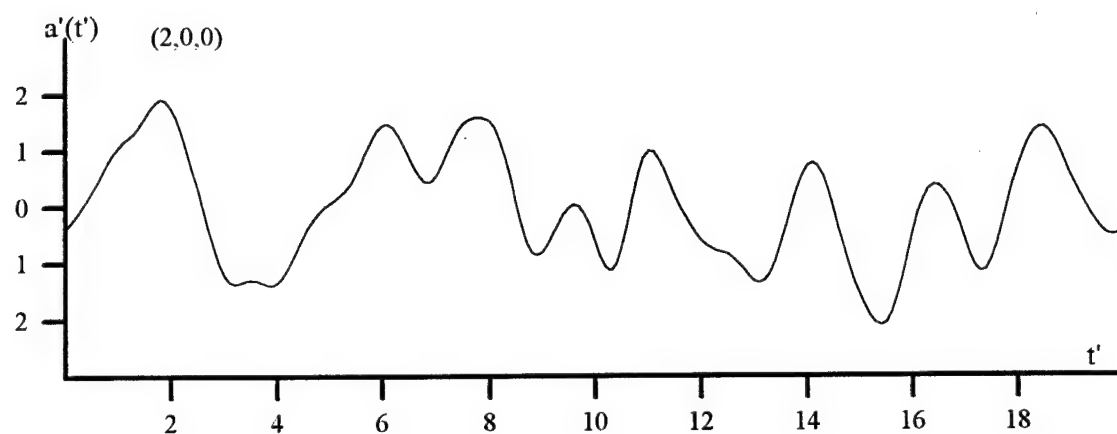
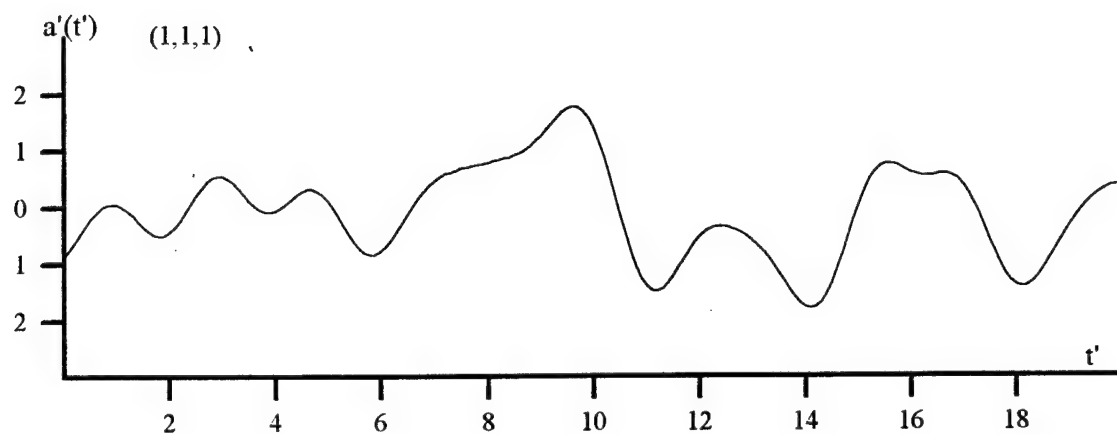
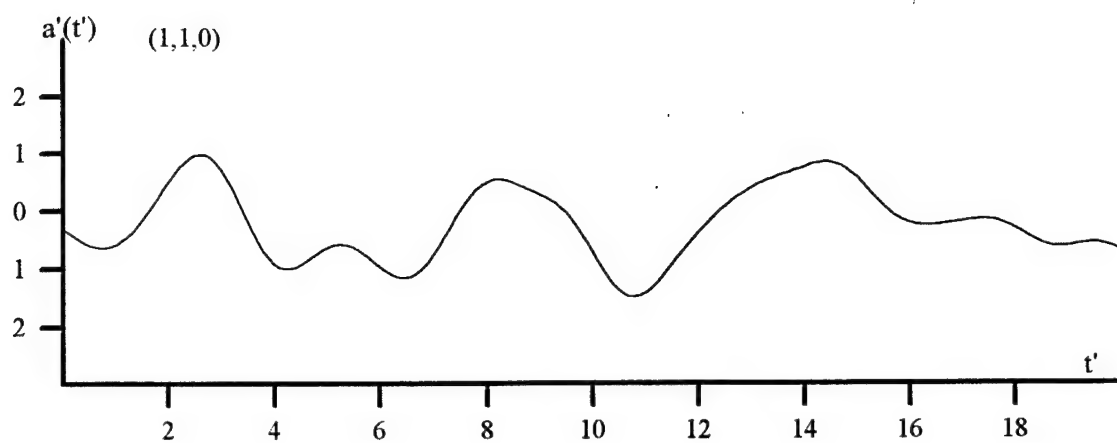


Fig. 2.6. Random temporal samples of coefficients for tip and tilt, defocusing, and astigmatism. $a'_n = a_n/\sigma_n$, $t' = t \cdot V/R$, where σ_n is variance. Calculations performed for $L_0/D = 10$.

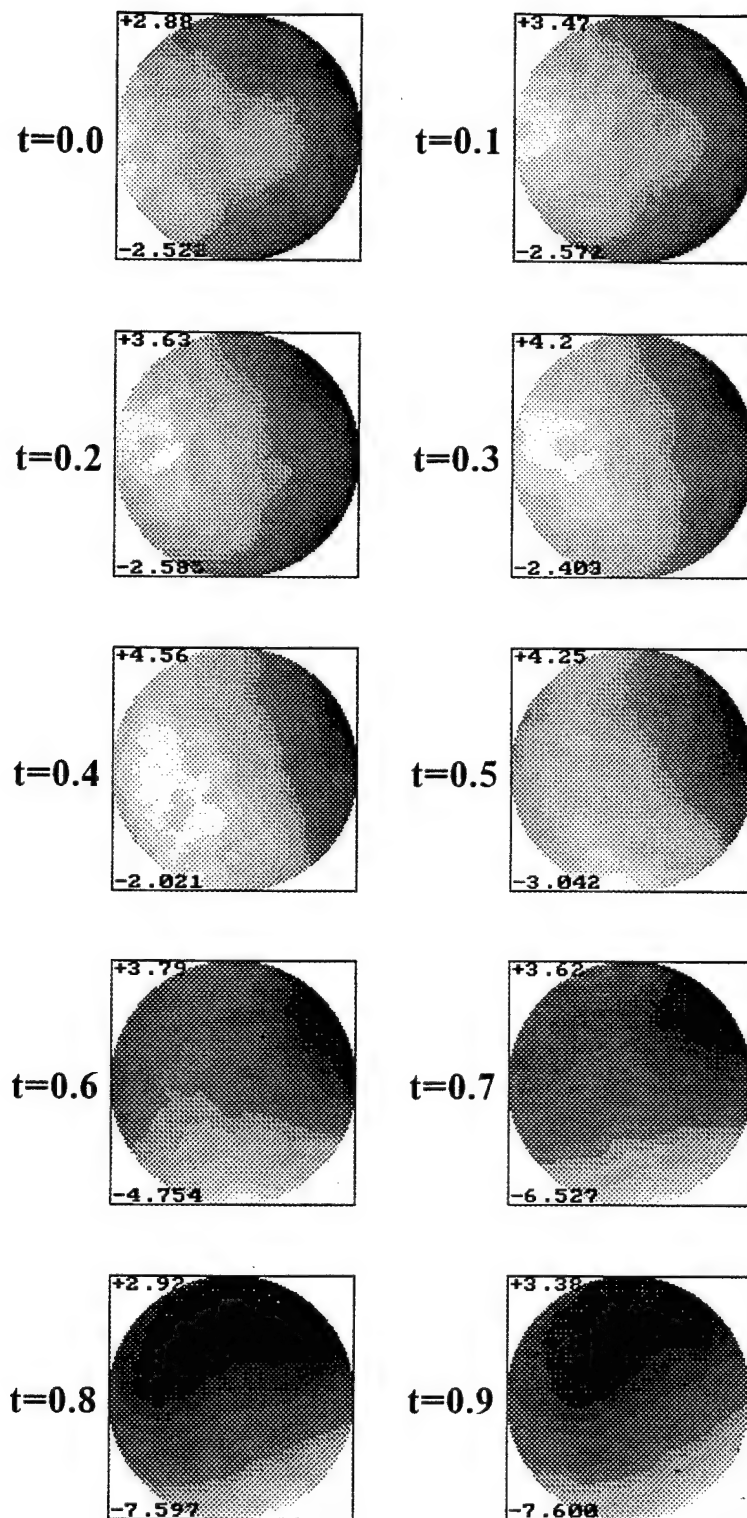


Fig. 2.7. Dynamics of a phase screen obtained by summing of linear and quadratic aberrations with small-scale aberrations obtained by the method of spectral samples. Time is normalized on D/V . Simulation is performed for the outer scale $L_0 = 50 \times D$, $r_0 = D$.

2.4. Modification of the numeric model to the case of partially coherent beams

In the above sections we considered propagation of coherent beams. But radiation divergence for real laser sources is always greater than the diffraction limit. This is due to the processes developed in the active medium of a laser, deformations of a laser cavity, multimode structure of laser radiation and so on.

Formally, in boundary conditions of the wave equation we should allow for phase and amplitude fluctuations within a transmitting aperture. In time-dependent problems this means dependence of phase and amplitude on time

$$E(\vec{\rho}, z = 0) = \sqrt{I_0(\vec{\rho}, t)} \exp(i\varphi(\vec{\rho}, t)). \quad (2.67)$$

In stochastic representation phase and intensity become random function of transverse coordinates

$$E(\vec{\rho}, z = 0) = \sqrt{\tilde{I}_0(\vec{\rho})} \exp(i\tilde{\varphi}(\vec{\rho})). \quad (2.68)$$

Obviously that in the both cases statistic or dynamic description of emitting radiation is unique for every type of laser sources and even for a single laser. But temporal scales of fluctuations of a source intensity and phase are much less than that of the index of refraction in the atmosphere. So in our model we can omit the details of space-time structure of partially coherent beams. Common practice in this case is definition of boundary condition for the second order coherence function

$$\Gamma_2(\vec{\rho}_1, \vec{\rho}_2) = \langle E(\vec{\rho}_1) E^*(\vec{\rho}_2) \rangle. \quad (2.69)$$

If statistics is uniform we can introduce a coherence length in the following manner

$$\Gamma_2(\vec{\rho}_1, \vec{\rho}_2) = \Gamma_{20}(\vec{\rho}_1, \vec{\rho}_2) \exp(-|\vec{\rho}_1 - \vec{\rho}_2|^2 / \rho_c^2), \quad (2.70)$$

where Γ_{20} corresponds to completely coherent radiation ($\rho_c = \infty$)

$$\Gamma_{20}(\vec{\rho}_1, \vec{\rho}_2) = u_0(\vec{\rho}_1) u_0^*(\vec{\rho}_2), \quad (2.71)$$

here u_0 is a regular component of the field.

In the employed mathematical model the wave equation describing a field should be solved. So in the frames of this model we need a method that allows for propagation of a partially coherent radiation.

Let us note that partial coherence is equivalent to additional angular divergence of a beam. Equations for an effective size a of a partially coherent Gaussian beam propagating in the turbulent atmosphere can be written as

$$a^2 = a_g^2 + a_d^2 + a_c^2 + a_t^2. \quad (2.72)$$

Here

$$a_g = a_0(1 - z/F) \quad (2.73)$$

is a size of a beam focused at a distance F in cross-section z , a_0 is the initial effective radius of a Gaussian beam,

$$a_d = \frac{z}{ka_0} = z \cdot \frac{\lambda}{D}; \quad D = 2\pi a_0 \quad (2.74)$$

is cross-section of a cone with base equal to diffraction divergence $1/ka_0$,

$$a_c = \frac{z}{k\rho_c} \quad (2.75)$$

is cross-section of a cone with base equal to divergence of partially coherent beam,

$$a_t = \frac{z}{k\rho_0} \quad (2.76)$$

is cross-section of a cone with base inversely proportional to the coherence length of turbulent phase screen ρ_0 . Let us note that the last formula is written for the problem of beam propagation behind a random phase screen. For a beam propagating in a randomly inhomogeneous medium turbulent divergence is a function of a longitudinal coordinate z .

So to allow for different factors influencing propagation of a beam we should sum corresponding cross-sections. Naturally, the influence of different factors is assumed to be independent.

In that follows we propose modification of numerical model for a coherent beam propagation that allows for initial divergence of a beam. In the case of a random phase screen the result obtained coincides precisely with the written above analytical formula.

Let us consider the proposed modification. As earlier, the wave equation is solved for a coherent beam. But intensity in cross-sections is calculated as convolution of coherent radiation intensity with some function W describing broadening of a beam induced by a partial coherence of a source

$$I(\bar{\rho}, z) = |E(\bar{\rho}, z)|^2 \otimes W(\bar{\rho}, z). \quad (2.77)$$

Assuming that W is Gaussian function with width a_c

$$W(\bar{\rho}, z) = \exp\left(-\frac{\rho^2}{a_c^2}\right) = \exp\left(-\frac{\rho^2}{z^2} k^2 \rho_c^2\right), \quad (2.78)$$

solving the problem of a partially coherent beam diffraction in a vacuum we obtain the results exactly the same as with the use of analytical formula. Indeed, convolution of two Gaussian functions with widths a_1 and a_2 is Gaussian function with square of width equals to the sum of squares of these two functions widths.

$$\exp\left(-\rho^2/a_1^2\right) \otimes \exp\left(-\rho^2/a_2^2\right) = \text{const} \cdot \exp\left(-\rho^2/(a_1^2 + a_2^2)\right). \quad (2.79)$$

This formula can readily be proved by calculating convolution through Fourier transform.

So formula (2.72) of squares summing can be viewed as sequential convolution in the beam cross-section of initial Gaussian intensity distribution obtained in approximation of geometrical optics with functions describing diffraction, partially-coherent, or turbulent divergence.

There is another possible interpretation of the problem. Let us assume that partial coherence of a beam is due to high-frequency fluctuations of beam direction, angle β between beam direction and axis of optical system is a random value. When distribution of mean intensity in a beam cross-section at a distance z from a source is

$$\langle I(\vec{\rho}, z) \rangle = \iint I(\vec{\rho} - \vec{\beta}z, z) f(\vec{\beta}) d^2\beta = I(\vec{\rho}, z) \otimes f(\vec{\rho}/z). \quad (2.80)$$

Here $f(\vec{\beta})$ is 2D function of probability density of the beam random direction, $I(\vec{\rho}, z)$ is intensity distribution in cross-section of unperturbed beam. The second order coherence function is

$$\begin{aligned} \Gamma_2(\vec{\rho}_1, \vec{\rho}_2) &= \Gamma_{20}(\vec{\rho}_1, \vec{\rho}_2) \langle \exp(ik\beta_x(x_1 - x_2)) \rangle \langle \exp(ik\beta_y(y_1 - y_2)) \rangle \\ &= \Gamma_{20}(\vec{\rho}_1, \vec{\rho}_2) \exp(-k^2 \sigma_\beta^2 (\vec{\rho}_1 - \vec{\rho}_2)^2 / 2) \end{aligned} \quad (2.81)$$

in assumption that the beam direction is 2D normally distributed random function with variance σ_β^2 in every realization and correlation between vector components is absent. From the last formula it follows that the relation between coherence length and mean square value of $\vec{\beta}$ is

$$\rho_c = \frac{2}{k\sigma_\beta} \text{ and } \sigma_\beta = \frac{2}{k\rho_c}. \quad (2.82)$$

So considering the case in which partial coherence is induced by jitters of a beam direction we also obtained the formula in which mean intensity of partially coherent beam is defined as convolution of diffraction limited solution of the wave equation with a function describing additional broadening of the beam.

Let us also note that in deriving the convolution formula we did not impose any restrictions on intensity distribution in the beam cross-section and on the function of probability density of beam direction random wandering. So this formula is also valid for non-Gaussian beams. More over, we did not make any assumptions concerning phase of the field regular component, so the equation is also valid for description of beam propagation behind a random or nonlinear phase screen.

All in all, propagation of high-power partially coherent laser beam is described by the following system of equations

$$\left\{ \begin{array}{l} 2ik \frac{\partial E}{\partial z} = \left(\frac{\partial^2}{\partial x^2} + \frac{\partial^2}{\partial y^2} + 2k^2 \delta n \right) E, \\ \hat{M}(\delta n) = \alpha |E^* E| \otimes W(\bar{\rho}, \sigma_\beta, z), \\ W(\bar{\rho}, \sigma_\beta, z) = \exp \left(\frac{-\frac{\rho^2}{\sigma_\beta^2 z^2}}{C_{\text{norm}}} \right), \\ E(\bar{\rho}, z = 0) = u_0(\bar{\rho}). \end{array} \right. \quad (2.82)$$

As earlier, M is an operator describing variations of the index of refraction induced by absorption of beam energy, u_0 is a regular component of the field ($\rho_c = \infty$). Variable σ_β has the meaning of angular divergence due to partial coherence (this divergence is not necessarily induced by random fluctuations of the beam direction). C_{norm} is a constant of normalization.

According to the splitting algorithm convolutions are calculated only in cross-sections which correspond to coordinates of nonlinear phase screen and in the plane of receiving aperture.

We know that to assess properly thermal blooming of a beam in a thick layer of randomly inhomogeneous medium we need further investigation of the proposed model. Possibly, the form of W function is dependent on a mechanism which limits coherence length. But the general features of our approach remain if averaging over fluctuations of the source field is performed more quickly than variation of the index of refraction.

2.5. Modeling the wavefront dislocations

The objective of this part is modeling of phase during wave propagation among atmosphere first under strong scintillation conditions. The complication of the physical reality is manifested when the intensity variations, also called scintillations, develop and phase dislocations or wavefront branch cuts spring up. The wavefront dislocations disturb the processing of wavefront sensors, since the processing is based on the assumed continuity of the phase function. Such disturbances can be due to one dislocation only. In addition, wavefront dislocations cause disintegration of the wavefront into separate beams which might be uncorrelated. Moreover, the amount of energy in the neighborhood of dislocations is limited. As a result the phase at these points is not well characterized.

The appearance of phase dislocations of a light wave propagating through a randomly inhomogeneous medium is studied in quasimonochromatic and parabolic approximations. To this end, the numerical model described in this report is used. The magnitude of the wave fluctuations is characterized by Fried's coherence radius for both weak and strong intensity fluctuations. The order of matrix is equal to 90. Two phase screen are used for modeling both a weak and a strong turbulence. The law of the energy conservation is carry out with computer accuracy. Spectral density of phase fluctuations of the Gaussian beam F_s and other parameters of model is as following.

$$F_s(\kappa) = 0,489 r_o^{-5/3} (\kappa^2 + \kappa_o^2)^{-11/6}, \kappa_o = 2\pi/L_o, L_o = 1\text{m}, L = 6\text{km}, \quad (2.83)$$

$$r_o = \left[0,423 k^2 \int C_n^2(L) dL \right]^{-3/5} = 0,05\text{m}, k = 2\pi/\lambda, \lambda = 0,6328\mu\text{m},$$

here L_o is outer scale of turbulence, L is the path length, κ is spatial frequency, k is wave number, C_n^2 is structural constant of refractive index, r_o is Fried's coherence radius.

As seen from Fig. 2.8.1 the phase dislocations appear at the points where the intensity reaches its maximum. These points correspond to zeros of the

wave function. Near these points, the phase varies spirally. Along the whole length of boundaries between white and black fragments in Fig. 2.8.2, between two points of dislocation formation, the phase surface undergoes discontinuity of $\pm 2\pi$. Such a discontinuity cannot be removed with the use of translations of surface fragments. The dichotomy of maximum and minimum contour lines of the interference pattern, and appearance and disappearance of interference bands occur at points of dislocations (Figs. 2.8.3 and 2.8.4). Contour lines of phase cosine and sine form a radial structure in the vicinity of dislocation points and converge to them (Figs. 2.8.5 and 2.8.6).

We have performed numerical experiment to compare the behavior of wave function scintillations and angular spectrum with the number of phase dislocations appearing with increase in turbulence intensity. The presence of dislocation is determined through calculation of phase different between neighboring points arranged in a closed contour drawn around the point of phase function under analysis. Dislocation occurred if the phase gradient is $\geq 2\pi$ or $\leq -2\pi$. The phase is calculated as inverse tangent of the ratio between imaginary and real components of the wave function. We normalized the number of dislocations to the ratio between the number of counts of calculation grid to the number of counts in a circle where a dislocation is determined. The wave scintillation index is calculated as a normalized variance of wave intensity, while the angular spectrum scintillation index is calculated as a normalized variance of the square of the modules of its Fourier transform. We normalized the variances to the mean square of the corresponding parameter. Estimates of all three parameters under investigation were averaged over nine experiments.

Results of experiment are shown in Fig. 2.9 In the region of large Fried's coherence radii that corresponds to weak turbulence, the wave scintillation index varies linearly, dislocations are absent, and the angular spectrum scintillation index reaches maximum values. Saturation of the wave scintillation index and normalized number of dislocations at unity level takes

place with increase in the turbulence intensity. The angular spectrum scintillation index saturates at unity level as well, but the dependence is reverse as compared with two other plots.

As one would expect, the dislocation number saturates since dislocation density cannot be greater than unity. However, it is interesting that maximum density of dislocations is achieved together with saturation of scintillation indices of a wave and its angular spectrum.

It should be pointed out that the wavefront dislocations and, correspondingly, the zeros of the wave function appear when the wave scintillation index approaches unity, that is at the origin of the region of strong fluctuations.

It have been performed a numerical experiment to compare between each other the behavior of the angular spectrum width and the wavefront dislocation number when the turbulence intensity increases from low to strong fluctuations. Theoretically these functions must be close to one another. The modeling shows that these curves for the Gaussian beam are differed only in an initial values of the dislocation numbers which are not estimate in theory, Fig. 2.10.1. For the plane wave the initial values are coincident but there is not very large distinction in the curve form, Fig. 2.10.2. Probably it is caused the alising. The fact is that a periodically continuation is modeling and there is an interaction between periods in the plane wave case but not in the Gaussian beam case. The addition study of alising is needed.

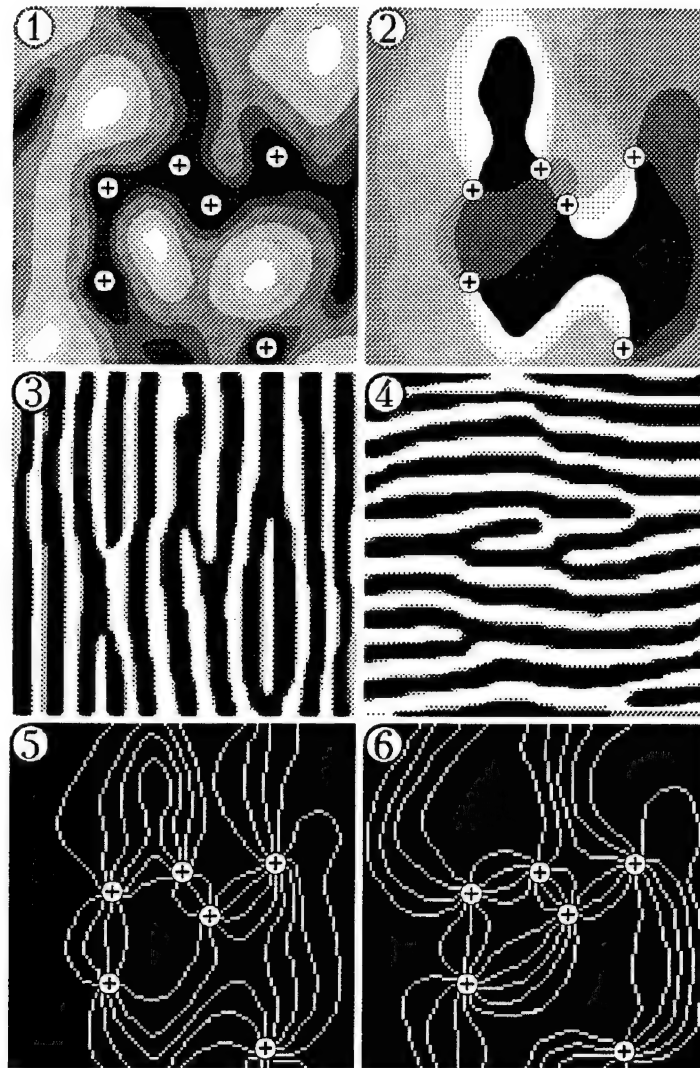


Fig. 2.8. Wave phase dislocations and structures created by them. Crosses denote zeros of the intensity and corresponding points of phase dislocations: wave intensity (1); wave phase (2); interference pattern for unit amplitude and carrier wave perpendicular to horizontal coordinate axis (3); interference pattern for unit amplitude and carrier wave perpendicular to vertical coordinate axis (4); contour lines of phase sine (5); and, contour lines of phase cosine (6).

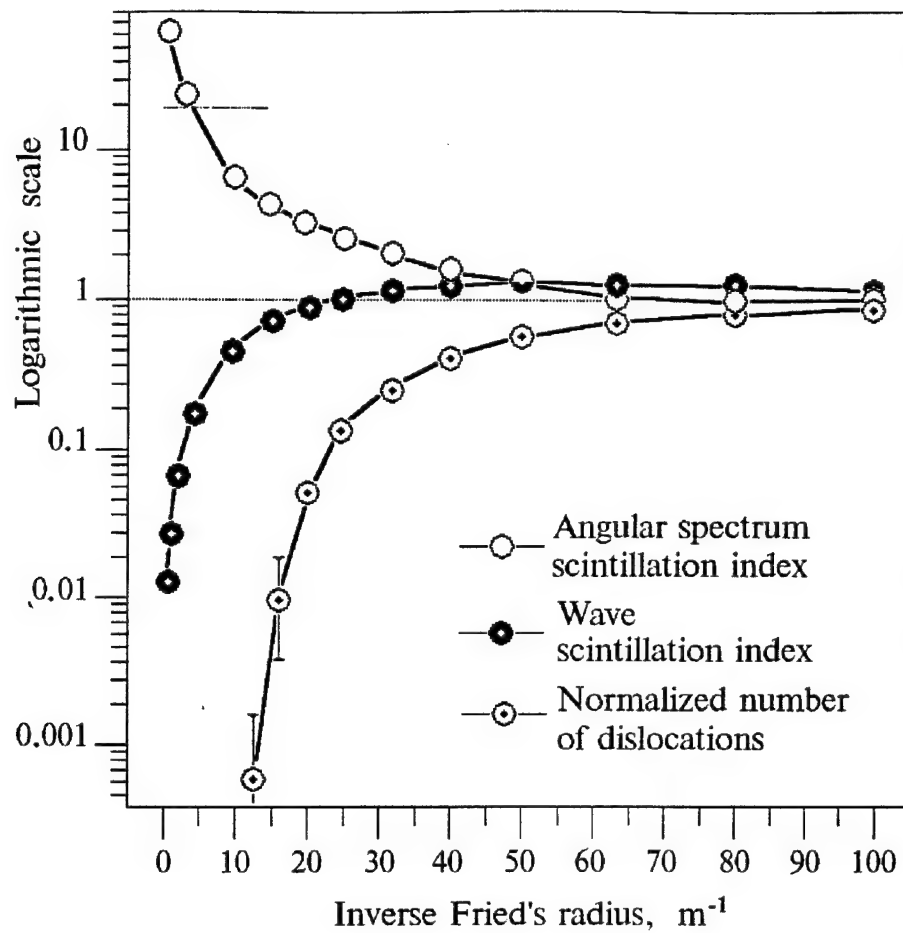


Fig. 2.9. Estimates of scintillation indices of Gaussian beam and its angular spectrum and normalized number of wavefront dislocations. The propagation path is 6 km long, and the wavelength is 0.6328 mm. Standard deviations are indicated as confidence intervals. These deviations are not indicated if their values are less than point size.

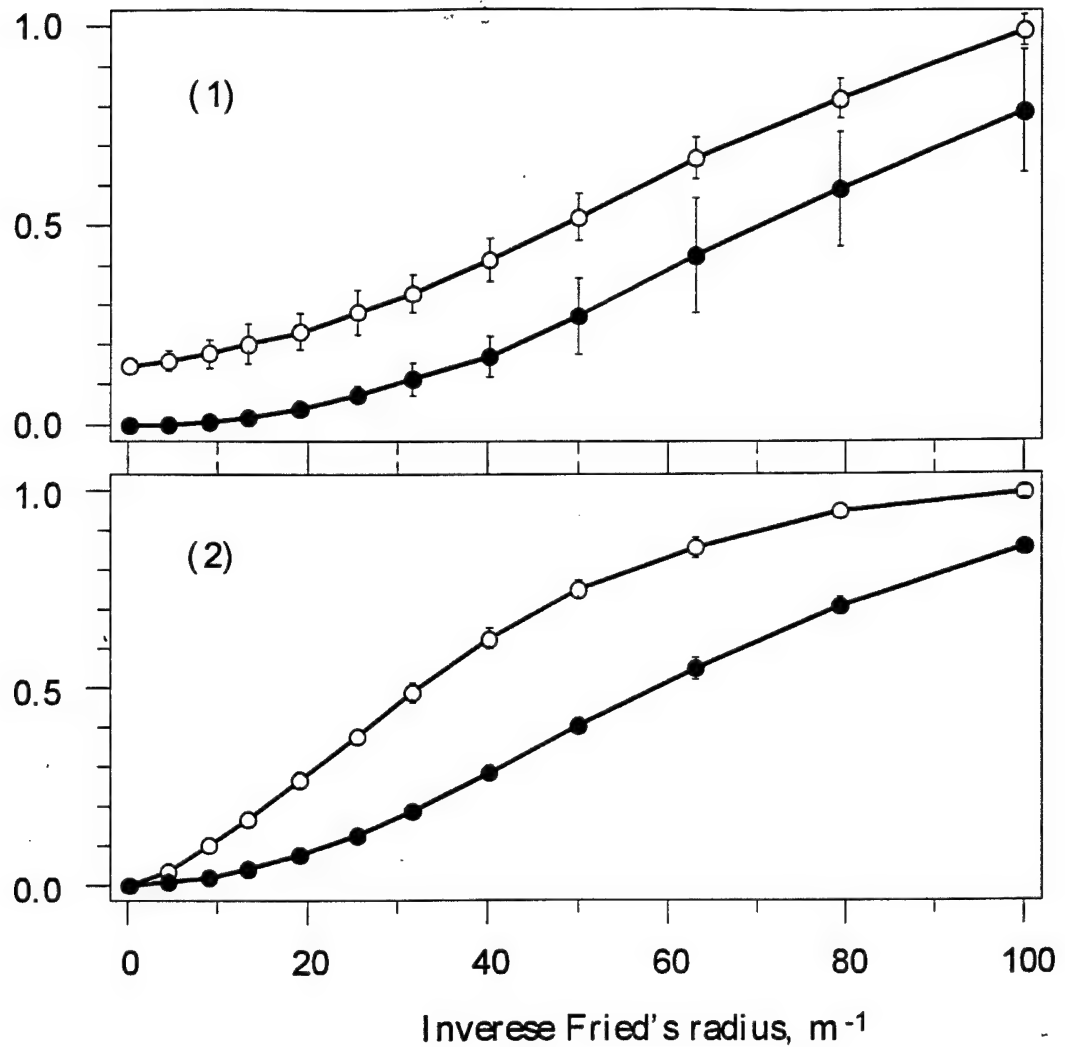


Fig. 2.10. Estimates of normalized number of wavefront dislocations —○— and normalized width of angular spectra —●— : of Gaussian beam (1), plane wave (2) versus the turbulence intensity. Wavelength is equal to $0.6328 \mu\text{m}$. Path length is 16300 m. Effective radius of Gaussian beam in the origin plane is equal to 0.054 m. Fresnel number is equal to 1. Standard deviations are indicated as confidence intervals. These deviations are not indicated if their values are less than point size. Experiment numbers is equal to 25.

References to Chapter II

1. V.I. Tatarskii, *Wave Propagation in the Turbulent Atmosphere* (Nauka, Moscow, 1967).
2. A. Ishimaru, *Wave Propagation and Scattering in Random Media* (Academic Press, New York, 1977).
3. *Laser Beam Propagation in the Atmosphere*, edited by J.W. Strohben (Springer-Verlag, Berlin, Heidelberg, New York, 1978).
4. J.L. Walsh and P.B. Ulrich in: *Laser Beam Propagation in the Atmosphere*, edited by J.W. Strohben (Springer-Verlag, Berlin, Heidelberg, New York, 1978).
5. J.A. Fleck, J.R. Morris, M.D. Feit, Appl. Phys. 1976. V.10. №1, P.129-139
6. G.I. Marchuk, *Methods of Numerical Mathematics* (Nauka, Moscow, 1980).
7. P.A. Konyaev in: *Abstracts of Reports at the VI Conference on Laser Beams Propagation in the Atmosphere*. Tomsk (1981), pp. 195-198.
8. V.V. Vorobiev, *Thermal Blooming of Laser Beams in the Atmosphere: Theory and Model Experiment* (Nauka, Moscow, 1987).
9. B.M. Berkovskii and E.F. Nogotov, *Numerical Experiment in the Problems of Convections* (University Publishsing House, Minsk, 1988).
10. A.A. Samarskii, *Introduction to the Theory of Finite-Difference Schemes*. (Nauka, Moscow, 1971).
11. P.A. Konyaev in: *Abstracts of Reports at the VII Conference on Laser Beams Propagation in the Atmosphere*. Tomsk (1983), pp. 104 - 106.
12. V.P. Kandidov and V.I. Ledenev, Izv. Vyssh. Uchebn. Zaved, Ser. Radiofiz. 1981. V.24, №4, C.438-442.
13. J.M. Martin and S.M. Flatte, Appl. Opt. 1988. V.27, №.11; P.2111-2126
14. S.M. Rytov, *Introduction to Statistical Radiophysics* (Moscow, Nauka, 1966).
15. R. Buckley, Journal of Atmospheric and Terrestrial Phisics. 1975. V.37, №.12, P.1431-1446
16. V.V. Bykov, *Numerical Simulation in Statistical Radiotechnics* (Sov. Radio, Moscow, 1971).

17. L.I. Mirkin, M.A. Rabinovich, and M.A. Yaroslavskii, Zh. Vychisl. Mat. Mat. Fiz. 1972. T.12. №5. C.1353-1357
18. D.L. Fried, J. Opt. Soc. Am. 1965. V.55. №11. P.1426-1435
19. R.J. Noll, J. Opt. Soc. Am. 1976. V.66, №3. P.207-211
20. S.A. Collins [Jr] and D.D. Duncan, J. Opt. Soc. Am. 1975. V.65. №10. P.1218
21. D.D. Duncan and S.A. Collins [Jr], J. Opt. Soc. Am. 1975. V.65. №10, P.1218
22. M. Born and E. Wolf, *Principles of Optics* (Pergamon, New York, 1959).
23. N. Roddier, Opt. Eng. 1990. V.29. №10. P.1174-1180
24. B.V. Fortes and V.P. Lukin, Proc.SPIE. 1992. V.1668. P.477-488



Institute of Atmospheric Optics SB RAS
Laboratory of Coherent and Adaptive Optics

Report on Contract SPC 97 - 4040

(second four month period)

**Principle Investigator
Prof. Lukin V.P.**

Tomsk - 1997

CONTENTS

Introduction	3
Chapter 1. Peculiarities of reflected waves in the turbulent atmosphere	5
1.1. Enhancement of backscattering	5
1.2. Phase fluctuations for mirror reflected wave	6
1.3. Displacement of a sounding volume image in the turbulent atmosphere	7
References to Chapter 1	12
Chapter 2. Efficiency of phase-conjugated adaptive optics systems with reference beacons	14
2.1. Correction of turbulent distortions of optical beams using a point reference source (beacon)	15
2.2. Correction with a plane reference wave	26
References to Chapter 2	32
Chapter 3. Correction of random angular displacements of optical beams	33
3.1. Registration of random angular displacements of optical beams	36
3.2. Correction of random angular displacements of optical beams	40
References to Chapter 3	52
Chapter 4. Correction of random image displacements forming through the turbulent atmosphere	53
4.1. Adaptive correction of the image of an extended object	53
4.2. Improvement of the quality of the image of a star by tracking	68
References to Chapter 4	75
Chapter 5. Modern Concept of an Adaptive Optics System with a Reference Sources	76
References to Chapter 5	79
Appendix A	82
Appendix B	84
Appendix A	93

INTRODUCTION

This report is a summary of the second stage of scientific investigations performed in accordance with contract SPC 97-4040 between Institute of Atmospheric Optics SB RAN (IAO, Tomsk) and European Office of Aerospace Research and Development (EDARD, London).

At the first stage of contract SPC 97-4040 estimating the efficiency of adaptive electro-optics systems we performed an analysis of a model of a turbulent atmosphere and considered a method of solution for the wave equation describing propagation of optical radiation in the atmosphere.

The next problem in creation of the complete model of an adaptive system is simulation of a reference source which is the key element in such systems.

The importance of investigations into the efficiency of adaptive optics systems with an artificial reference source was understood in the end of seventies. In this period (and even earlier) were formulated the main principles upon which the modern concept of adaptive electro-optics systems is based. According to this concept the reference source is the element with the use of which the information is procured concerning the distribution of fluctuations in the channel of radiation propagation. The way in which this channel is formed influences the structure of the whole system.

If the principle of reciprocity is the base for an adaptive system, the most appropriate scheme is the one with an independent source of radiation generating a beam propagating in direction opposite to the corrected beam.

Aiming at the practical realization of the system, the atmosphere should be included into the loop, i.e., the backward scattering should be taken into account with radiation reflected by an object or by inhomogeneities of the atmosphere. In such a way an artificial (virtual) reference source is formed. In the early eighties in adaptive astronomy artificial reference sources were named *laser guide stars*. The realization of such a star is possible using Rayleigh scattering or by scattering on atmospheric aerosol on altitudes from 8 to 20 kilometers or by induced scattering in clouds of atomic metals (such clouds consist mainly of sodium). In the first case a laser guide star is referred to as a Rayleigh guide star, in the second as a sodium guide star.

The requirements to the laser source which forms a Rayleigh star are loose. On the contrary, the requirements to the wavelength, bandwidth, and power of a laser

source forming a sodium star are quite strict. This is due to selectivity and saturation of absorption at induced scattering in sodium vapor at altitudes from 85 to 100 km.

The report on the second stage of contract SPC 97-4040 includes five parts. The first part describes peculiarities of optical radiation reflected from an object, i.e., peculiarities of the sounding signal.

CHAPTER 1. PECULIARITIES OF REFLECTED WAVES IN THE TURBULENT ATMOSPHERE

The interest to problems of this type arose because of demands to generate reference radiation as a result of reflection from some objects in the atmosphere (radiation of a beacon or a guide star). In the atmosphere light can be reflected from inhomogeneities such as clouds or aerosol and from real objects. As an example we have considered radiation mirror-reflected from an object. In such cases one need to take into account peculiarities of optical parameters fluctuations of radiation passed twice through atmospheric inhomogeneities. In adaptive algorithms of phase control most important is the phase of reflected wave so special attention was paid in the report to calculation of phase fluctuations.

Approximately in mid-seventies scientists and engineers working with optical systems of seeing and beam-forming in the atmosphere and also with sounding systems understood that the peculiarities of fluctuations of reflected waves should be allowed for. In contradistinction to transmitting systems, in the systems of optical sounding the effect of two-fold passing of the atmosphere is always present. Sounding radiation passes through the same optical inhomogeneities two times: during the direct and reverse propagation.

1.1. Enhancement of Backscattering

Scientists involved in investigations connected with atmospheric sounding introduces such terms as *effective scattering volume*, *monostatic optical scheme*, *bistatic scheme of laser sounding* and some others.

The following Russian scientists were working in the field: Yu. A. Kravtsov, A. N. Malakhov, A.S. Gurvich, K.S. Gochelashvily, V.I. Shishov, A.I. Saichev, V.A. Banakh, V.A. Mironov, V.U. Zavorotny, V.I. Klyatskin, A.I. Kon, V.I. Tatarskii, Yu.N. Barabanenkov, S.S. Kashkarov, G.Ya. Patrushev, V. P. Aksenov. M.I. Charnotskii, M.L. Belov, V.M. Orlov, I.G. Yakushkin, Z.I. Feizulin, A.G. Vinogradov, A. B. Krupnik, L. Apresyan.

The most complete overview of the problem was presented in Refs. 1 and 2. These papers presents the review of the results of the effect of atmospheric refractive index fluctuations on the propagation of optical wave when the wave traverses the same region of the atmosphere twice. Such situation is realized at reflection of laser beams from a target or at wave backscattering on atmospheric aerosol. In the case

light-wave propagation properties are determined by correlations between incident and wave traversing the same inhomogeneities in a turbulent atmosphere. This may lead to qualitatively new properties of fluctuations as compared with forward propagation, i.e., enhancement of backscattering of intensity fluctuations, long-range correlations in the reflected-wave field and so on.

The priority of Russia in the field was confirmed by the International Meeting for Wave Propagation in Random Media «Scintillation» held in USA (Seattle, August 1992) [3].

When an object is illuminated and viewed through the same turbulence, Prof.J.C.Dainty et al., and Prof.A.S.Gurvich, A.N.Bogaturov, V.A.Myakinin call this "double passage imaging". "The physical basis of double passage imaging lies in the fact that reversible paths of illumination and viewing are coherent with one another, regardless of the phase distortion of the turbulence, and thus double passage imaging is closely linked to the phenomenon of "enhanced backscatter" encountered when dense volume media and highly-sloped rough surfaces are illuminated" [4].

1.2. Phase Fluctuations for Mirror Reflected Wave

In the seventies the Soviet scientists and particularly the scientists working with the Institute of Atmospheric Optics SB RAS were involved into investigation of peculiarities of phase fluctuations in sounding schemes employing mirror reflectors, i.e., fluctuations of optical waves which have passed the atmosphere twice.

The problem of location of mirror objects appeared in some practical investigation, for example, as a part of the project of a laser range-finding with a corner retroreflector, in problems of atmosphere sounding, laser interferometry, registration of wind velocity by Doppler meters and so on. To my mind, the most interesting papers concerning this problem are the publications by Smith et. al. (Refs. 6 and 7). After these papers many other publications devoted to phase fluctuations of mirror-reflected waves had appeared in the period from 1974 to 1980.

In the Institute of Atmospheric Optics the experimental and theoretical investigations of the problem were began in 1976 (Refs. 10-18).

In Ref. 10 the increase (as compared with a direct wave) of phase fluctuations for a wave mirror-reflected from an object in exactly backward direction was demonstrated theoretically. Experimental studies carried out [11] in 1975-1976 confirmed theoretical conclusions. A little early (in 1977) have been considered

efficiency of compensation for phase distortions. Correction of phase fluctuations was assessed using data characterizing a reflected wave. A plane mirror with the radius greater than the radius of a beam was used as a retroreflector. Ref. 12 published in 1977 was devoted to estimation of efficiency of correction for phase fluctuations basing on measurements of the reflected wave phase. It was assumed that the diameter of the retroreflector was greater than that of the beam. But the most detailed investigation was carried out in 1980, when correlation and structure functions were calculated (the results of investigation were published in Ref. 13).

More detailed analysis of phase fluctuations in reflected waves was performed in 1980 and the results were published in Ref. 13. In this paper correlation and structure functions of phase for optical waves were considered for a waves reflected from a mirror.

Special attention was devoted to the phenomenon of *phase fluctuation coupling*. It was pointed out that some peculiarities are specific to statistical characteristics of phase and relevant characteristics for reflected waves [14-18]. These peculiarities should be allowed for in problems of optical radar signal evaluation as well as in adaptive optics systems employing algorithms with a conjugated wave. Several experiments in real atmosphere under random beam angle motion correction have been made in 1976-1980 [14-18].

1.3. Displacement of a Sounding Volume Image in the Turbulent Atmosphere (Ref. 2)

Fluctuations of an image center of gravity were considered in the book by Belov M.L. and Orlov V.M [2]. The image was formed through an inhomogeneous medium in a sounding system with the use of a focused laser beam. Particularly, fluctuations were investigated of the image of a sounding volume. Monostatic and bistatic schemes were considered. For irradiation of the volume focused and collimated laser beams were used. Equations describing the variance of centroid fluctuations were obtained for an image in the photodetector plane without any restrictions on reflection properties of an object (pp. 84 - 95 of Ref. 2).

It was shown that for the case of strong dispersion on a surface (Lambertian approximation) in the bistatic sounding scheme the variance of linear displacements of the image center of gravity can be written as (p. 92 of Ref 2)

$$\langle \rho_{lm}^2 \rangle = \frac{F^2}{x^2} \langle \rho_b^2 \rangle + F^2 \langle (\rho_F^s)^2 \rangle,$$

where $\langle \rho_b^2 \rangle$ is the variance of random displacements of the beam centroid in a sounding plane (it was assumed that the beam propagates upward) and $\langle (\rho_F^s)^2 \rangle$ is the variance of random angular displacements of an image of «secondary» immobile source (downward propagation). So, it was shown that for the bistatic scheme the variance of angular displacements of an image is a sum of angular displacements of the image and of the «secondary» immobile source. If a focused beam is used in strongly scattering medium the secondary source is, practically, a point.

In this period calculations were performed for cases when the «secondary» source can be treated as a point (a small scattering volume) and also for objects with finite volumes. As an example the paper by Kalistratova and Kon can be taken where jitter of image was considered for a thin irradiating string [Ref. 5].

So we can conclude that in the USSR in early eighties scientists understood that in some conditions a volume could be considered as infinite small (a point source or a «laser guide star») and that in other problems its size should be allowed for, i.e., if an object is large enough averaging over its volume is necessary as it was performed by Kalistratova and Kon (Ref. 5).

At the same time the authors of Ref. 2 were not able to calculate correctly mutual correlation between fluctuations of focused beam displacements and displacements of a image of reference sources. It was performed in 1979-1980 [Refs. 8 and 9].

Let us specify the statement of the problem. We wish to examine the mutual correlation between the random displacements of the energy center of gravity of an optical beam that has passed through a layer of turbulent medium and the center of gravity of some image formed by the optical system [8]. This can be an image of a reference source (beacon) or of the optical beam reflected from a flat mirror with infinite radius. Random displacements of the beam centroid are given by the vector

$$\rho_c = \frac{1}{2P_0} \int_0^x d\xi (x - \xi) \iint d^2 R I(\xi, \mathbf{R}) \nabla_{R\varepsilon_1}(\xi, \mathbf{R}),$$

where $\varepsilon_1(\xi, \mathbf{R})$ are fluctuations of permittivity in the point (ξ, \mathbf{R}) , $I(\xi, \mathbf{R})$ is intensity at the point (ξ, \mathbf{R}) generated by the source located in the plane $\xi = 0$; x is the thickness of the turbulent layer, $P_0 = \iint d^2 R I(0, \mathbf{R})$.

The random displacements of the image in the focal plane of the optical system (equivalent to a "thin" lens with focal length F and area $\Sigma = \pi R_0^2$) are given by the expression

$$\rho_{cF} = -\frac{F}{k\Sigma} \iint_{\Sigma} \nabla_{\rho} S(x, \rho) d^2 \rho,$$

where k is the wave number of the radiation, $S(x, \rho)$ are the fluctuations of the phase of the optical wave over the aperture of the optical system (in the $\xi = x$ plane) at the point ρ . The mutual correlation of the random vectors ρ_c and ρ_{cF} is given by

$$K = \langle \rho_c \rho_{cF} \rangle / \left[\langle \rho_c^2 \rangle \langle \rho_{cF}^2 \rangle \right]^{1/2}.$$

Here $\langle \dots \rangle$ denotes averaging over the ensemble of realizations of the random function $\varepsilon_1(\xi, \mathbf{R})$.

To make the situation more clear, let us consider the mutual correlation between random displacements of the center of gravity of a Gaussian beam and the center of gravity of image for a infinite plane wave. The beam and the plane wave propagate along the same optical path.

In that follows we assume that functions $\langle I(x', \mathbf{R}) \rangle$ and $\Phi_{\varepsilon}(x, \kappa)$ are isotropic and average intensity is given in representation

$$\langle I(x', \mathbf{R}) \rangle = \frac{a^2}{a_{\text{Eff}}^2(x')} e^{-R^2 / a_{\text{Eff}}^2(x')},$$

where

$$a_{\text{Eff}}^2(x') = a^2 \left[\left(1 - \frac{x}{f} \xi \right)^2 + \Omega^{-2} + \Omega^{-2} \left(\frac{1}{2} D_s(2a) \right)^{6/5} \right],$$

$\Omega = \frac{ka^2}{x'}$, a and f are initial parameters of the Gaussian beam $D_s(2a)$ are phase structure function, $x' = x\xi$. All in all we obtain

$$K = \int_0^1 d\xi (1-\xi) \int_0^\infty d\kappa \kappa^3 \Phi_n(\kappa) \exp\left(-\frac{\kappa^2(R_0^2 + a_{eff}^2)}{4}\right) \cos\left(\frac{\kappa^2 x(1-\xi)}{2\kappa}\right) /$$

$$\left/ \left(\int_0^1 d\xi (1-\xi)^2 \int_0^\infty d\kappa \kappa^3 \Phi_n(\kappa) \exp\left(-\frac{\kappa^2 a^2 q^2}{2}\right) \right)^{1/2} \left(\int_0^1 d\xi \int_0^\infty d\kappa \kappa^3 \Phi_n(\kappa) \times \right. \right.$$

$$\left. \times \exp\left(-\frac{\kappa^2 R_0^2}{2}\right) \cos^2\left(\frac{\kappa^2 x(1-\xi)}{2\kappa}\right) \right)^{1/2},$$

The form of K is similar in the case of spherical wave and also in the case when these waves or Gaussian beam are reflected from a flat reflector with infinite radius.

In calculations we use the following spectrum

$$\Phi_n(\kappa) = 0.033 C_n^2 (\kappa^2 + \kappa_0^2)^{-11/6},$$

which accounts for deviation from a power series in a vicinity of the outer scale $L_0 = 2\pi\kappa_0^{-1}$.

As an example, let us estimate correlation between displacement of image for a plane wave in the focus of a telescope and random displacement of a beam with initial diameter equal to the diameter of the input pupil of the telescope. Estimation is performed for a homogeneous path, the parameters of the problem are the following:

$$\kappa_0^{-1} \gg R_0, a_{eff}, \sqrt{x/k}; kR_0^2 \gg x, \Omega^{-2} \left(\frac{1}{2} D_s(2a) \right)^{6/5} \ll 1.$$

We obtained the value of K approximately equals to 0.84.

Thus, the high positive correlation was shown between displacements of a Gaussian beam and displacements of the plane wave centroid assuming that beam propagation and image forming are on the same path and in the same direction.

Due to relatively high correlation, an algorithm of control for correction of random angular displacements of beam $\bar{\rho}_c/x$ can be performed, according to the formula $\alpha(a/2R_0)^{1/3} \rho_{cF}/F$, where α is coefficient of the loop which chosen to ensure the minimum of residual angular displacements of the beam

$$\min \left\langle \left(\frac{\rho_c}{x} - \frac{\alpha(a/2R_0)^{-1/3} \rho_{cF}}{F} \right)^2 \right\rangle.$$

So, passing from linear measurements to angular it is possible to control a laser beam position using data of measurements of the reference source image [8].

Later (Ref. 9) these results were generalized for the case of beam and image forming when propagation is realized in opposite directions. It was also assumed that forming of the image in the focal plane of a telescope performed for the following scenarios:

- plane wave, spherical wave, Gaussian beam,
- radiation reflected from a plane mirror.

For a plane wave propagating over a homogeneous path and for a broad beam it was obtained that

- $K = -0.87$ (collimated beam),
- $K = -0.82$ (focused beam).

For spherical waves and any others the results could be obtained from the data published in Ref. 9. So as early as in 1979 the sign of mutual correlation was determined and its value estimated. In Ref. 9 (1980) have been made mention of the fundamental possibility of using radiation backscattered by the atmospheric aerosol.

In more details these problems are considered in the third chapter of the report.

Summing up, we can conclude that Soviet scientists in 1976 - 1980 obtained all functions necessary to analyze random displacements of the image of a sounding object for bistatic as well as for monostatic schemes.

But when we encounter with some particular problem, we still need to answer a question about model of scattering (or reflecting) medium, which, in its turn, defines a model of a secondary source (see Eq. 1). It is possible to introduce the model of this source directly as well as to solve the problem of backscattering [2].

References to Chapter 1

1. V.A.Banakh, V.L.Mironov, *Propagation of laser sounding radiation in the atmosphere*. (Novosibirsk, Nauka, 1986).
2. V.M. Orlov, I.V. Samokhvalov, G.G. Matvienko, M.L. Belov, A.N. Kozhemyakov, *The elements of theory of wave scattering and optical ranging*. (Novosibirsk, Nauka, 1982).
3. Meeting Digest of "Scintillation" International Meeting for Wave Propagation in Random Media, Conference Chairs V.I. Tatarskii, A.Ishimaru, University of Washington Seattle, USA, August 1992.
4. J.C.Dainty, C.J.Solomon, N.J.Wooder, A.N.Bogaturov, A.S.Gurvich, V.A.Myakinin, "Double Passage Imaging", Meeting Digest of "Scintillation" International Meeting for Wave Propagation in Random Media, Conference Chairs V.I. Tatarskii, A.Ishimaru, University of Washington, Seattle, USA, August (1992).
5. M.A. Kalistratova, A.I. Kon, "Fluctuations of arrival angle of light waves from extended source in turbulent atmosphere", *Izv.VUZov. Radiofizika* 9, No.6, 1100-1107(1966).
6. I. Smith, T.Pries, K.I.Skipka, M.A.Hinuitier, "High-frequency plane-wave filter function for folded paths", *Journ.Opt.Soc.Am.* 62, No.9, 1183-1187(1972).
7. I. Smith, T.Pries, "Temporal-frequency spectra for waves propagating over straight and folded paths", *Applied Optics* 14, No.5 (1975).
8. V.P.Lukin, "Tracking of random angular displacements of optical beams", *Proc.V All-Union Symposium, Tomsk, part II*, p.33-36, 1979.
9. Lukin V.P., Correction for Random Angular Displacement of Optical Beams, *Kvantovaya Elektronika*, V.7, No.6, pp.1270-1279, 1980 [Sov.J.Quantum Electron., 10, No.6, pp.727-732, 1980].
10. V.P. Lukin, "The fluctuation of wave beam in turbulent atmosphere under reflection", I All-Union Meeting on "Atmospheric Optics", Tomsk, Proc. Part I, 129-133(1976).
11. V.P. Lukin, V.V. Pokasov, "The experimental measurements of fluctuations in backscattering wave in turbulent atmosphere", I All-Union Meeting on "Atmospheric Optics", Tomsk, Proc. Part I, 134-137(1976).

12. V.P. Lukin, "Efficiency of the compensation of phase distortions of optical waves", Sov.J.Quantum.Electron.7, No.4, 522-524(1977).
13. V.P.Lukin, "Phase fluctuations of specularly reflected optical waves", Optika i Spectroscopy, V.48, No.3, pp.594-599, 1980.
14. V.P. Lukin, V.V. Pokasov, S.M. Slobodjan, "The correction of random angular displacements of wave beams", I All-Union Meeting on "Atmospheric Optics", Tomsk, Proc. Part I, 259-262(1976).
15. V.P. Lukin, V.M. Sazanovich, S.M. Slobodjan, "Random displacements of images at sounding in the atmosphere", V All-Union Symposium on Atmospheric Laser Ranging, Tomsk, Proc. Part II, 43-48 (1978).
16. V.P. Lukin, "Registration of random angular displacements of optical beams", V All-Union Symposium on Laser Beam Propagation, Tomsk, Proc. Part II, 33-36(1979).
17. V.P. Lukin, "Improvement of an image quality formed through the turbulent atmosphere", II All-Union Meeting on "Atmospheric Optics", Tomsk, Proc. Part II, 93-96 (1980).
18. O.N. Emaleev, V.V. Pokasov, S.F. Potanin, V.P. Lukin, V.M. Sazanovich, O.L. Tuzov, "Fluctuation of images in the close-to-earth layer of the atmosphere", II All-Union Meeting on "Atmospheric Optics", Tomsk, Proc. Part II, 97-100(1980).

CHAPTER 2. EFFICIENCY OF PHASE-CONJUGATED ADAPTIVE OPTICS SYSTEMS WITH REFERENCE BEACONS

In this chapter an overview is presented of papers which deal with systems forming a laser beam in a turbulent atmosphere.

One of first paper on the subject was published in 1979 [1]. In this paper the possibility is analyzed to use two-color adaptive optics system. In such a system wavelength of a reference beam was taken different from that of the direct beam. The possibility to use a reflected beam as a reference source was also considered in the paper. It was assumed that reflected beam travels through the atmosphere two times, firstly, along a direct path, and secondly, along a backward path. It was pointed out that the efficiency of correction is higher for a point retroreflector (a point retroreflector forms a spherical wave) if phase fluctuations in the direct beam are reciprocal to fluctuations in the reverse beam.

In 1981 the paper (Ref. 2) was published where phase conjugation algorithm was compared with algorithm of wave front reversal (full field phase conjugation). An analysis was performed for an adaptive optics system with a point retroreflector. It was shown that phase conjugation with point retroreflector insures high enough efficiency of correction. The algorithm is possible to realize with a wave reflected from an object on which the radiation is focused. In particular it is possible to use a wave backward scattered by atmospheric aerosol. Correcting distortions in a small-radius laser beam by phase conjugation algorithm we can use a plane wave or a laser beam with large radius counter propagating to the direct beam as a reference source.

Later in the book [3] written in 1986 the main theses of Ref. 2 were illustrated for two limits: correction with a plane wave as a reference one and correction with a spherical wave. In 1996 this book was translated into English and published by SPIE

(Ref.4). The problems considered here were put into the first chapter of this book (paragraphs 1.1 and 1.2) and partially into the second (paragraphs 2.1 and 2.2) and third (paragraph 3.2) chapters.

In the present chapter we will analyze the possibilities of correction of turbulent distortions of optical beams. Under consideration we are going to base on the past papers what were published in Russia from 1978 until 1983.

We will examine two limiting cases: the one in which correction is based on a point reference source (beacon), and the case of a wide reference beam $\Omega_0 \rightarrow \infty$ in the limit of a plane wave [2].

The first of these is realized when both sources (corrected and reference) and are located in the random inhomogeneous medium and their angular dimensions differ strongly $ka^2 \gg (x_1 - x_0)$, $ka^2 \ll (x_1 - x_0)$, and the second, when the reference source (of any geometry) is far enough removed from the layer of random inhomogeneous medium, and for which the reference wave is already a plane wave by the time it reaches the layer.

2.1. Correction of Turbulent Distortions of Optical Beams Using a Point Reference Source (Beacon)

We will examine the case in which the wavelength of the input radiation differs from that of the reference radiation. We will use the phase approximation in the Huygens-Kirchhoff method to calculate the moments of the corrected field.

The corrected field is given by formula

$$U_c^{PC}(x_1, \rho) = \iint d^2 \rho_1 U_0(\rho_1) G(x_1, \rho; x_0, \rho_1) \frac{G^*(x_0, \rho_1; x_1, \rho_b)}{G_0^*(x_0, \rho_1; x_1, \rho_b)}$$

for the phase conjugation (PC) algorithm and formula

$$U_c^{WFR}(x_1, \rho) = \iint d^2 \rho_1 U_0(\rho_1) G(x_1, \rho; x_0, \rho_1) G^*(x_0, \rho; x_1, \rho_b)$$

for the wave front reversal (WFR) algorithm. It follows that the moments of the corrected fields can be expressed in terms of the moments of the product:

$$B(x_1, \rho, \tau; x_0, \rho_1, \rho_2) = G(x_1, \rho; x_0, \rho_1) G^*(x_1, \rho; x_0, \rho_1). \quad (1)$$

First, let us consider the behavior of the average corrected field $\langle U_k(x_1, \rho) \rangle$. Here the angular brackets denote the ensemble average over all possible realizations of the random inhomogeneous medium. It is well known that the average field in the absence of correction is of no practical interest since

$$\begin{aligned} \langle U(x_1, \rho) \rangle &= \iint d^2 \rho_1 U_0(\rho_1) \langle G(x_1, \rho; x_0, \rho_1) \rangle = \\ &= \frac{k}{2\pi i |x_1 - x_0|} \exp\left\{-\frac{1}{2} \sigma_s^2\right\} \iint d^2 \rho_1 U_0(\rho_1) \exp\left\{ik \frac{(\rho - \rho_1)^2}{2(x_1 - x_0)}\right\} \end{aligned} \quad (2)$$

since σ^2 - the variance of the phase fluctuations - becomes significant already at short distances under conditions of real atmospheric turbulence. At the same time, the average corrected field is given by

$$\begin{aligned} \langle U_k(x_1, \rho) \rangle &= i\Omega \frac{1 + i\Omega}{(1 + \Omega^2)} \times \\ &\times \exp\left\{-\frac{1}{2} D_s(x_1, \rho_b - \rho; x_0, 0) - \Omega \frac{k\rho^2}{2(x_1 - x_0)} \cdot \frac{1 + i\Omega}{(1 + \Omega^2)} + i \frac{k\rho^2}{2(x_1 - x_0)}\right\} \end{aligned} \quad (3)$$

for the PC algorithm, and

$$\begin{aligned} \langle U_k(x_1, \rho) \rangle &= \frac{k}{2\pi i |x_1 - x_0|} \exp \left\{ -\frac{1}{2} D_s(x_1, \rho - \rho_b; x_0, 0) + i \frac{k(\rho^2 - \rho_b^2)}{2(x_1 - x_0)} \right\} \times \\ &\times \iint d^2 \rho_1 U_0(\rho_1) \exp \left\{ i k \rho_1 \frac{(\rho - \rho_b)}{(x_1 - x_0)} \right\} \end{aligned} \quad (4)$$

for the WFR algorithm. We find that for a wide enough ($\Omega \gg 1$) beam the average field for the PC algorithm

$$\begin{aligned} \langle U_k(x_1, \rho) \rangle &= \exp \left\{ i \frac{k\rho^2}{2\Omega^2(x_1 - x_0)} - \frac{k\rho^2}{2\Omega(x_1 - x_0)} - \frac{1}{2} D_s(x_1, \rho; x_0, 0) \right\}, \\ \rho_b &= 0, \end{aligned}$$

diffraction practically the same as the field in vacuum

$$U_{vac}(x_1, \rho) = \exp \left\{ \frac{k\rho^2}{2(x_1 - x_0)} \left(\frac{i}{\Omega^2} - \frac{1}{\Omega} \right) \right\}$$

for points $\rho < r_0$, where r_0 is the coherence radius. For $\rho > r_0$ the mean field falls off faster than the diffraction field. In contrast with phase conjugation, wavefront reversal reconstructs the mean field (4) in such a way that the input plane wave ($U_0(\rho) = 1$) in fact forms the point reference source (by a process of focusing):

$$\langle U_k(x, \rho) \rangle = \delta(\rho - \rho_b) \frac{k}{2\pi i |x_1 - x_0|} \exp \left\{ -\frac{1}{2} D_s(x_1, \rho - \rho_b; x_0, 0) + i \frac{k(\rho^2 - \rho_b^2)}{2(x_1 - x_0)} \right\}, \quad (6)$$

Average intensity distribution. Let us turn now to an analysis of the higher moments of the corrected field: the average intensity distribution and the variance of the relative intensity fluctuations. For PC correction the average intensity distribution in the phase approximation is given by

$$\begin{aligned}
\langle I_k(x_1, \rho) \rangle &= \left(\frac{k}{2\pi(x_1 - x_0)} \right)^2 \iint d^4 \rho_{1,2} U_0(\rho_1) U_0^*(\rho_2) \times \\
&\times \exp \left\{ i k \frac{(\rho_1^2 - \rho_2^2)}{2(x_1 - x_0)} - i k \rho \frac{(\rho_1 - \rho_2)}{(x_1 - x_0)} + [-D_s(x_1, \rho; x_0, 0) - \right. \\
&- D_s(x_1, 0; x_0, \rho_1 - \rho_2) + \frac{1}{2} D_s(x_1, -\rho; x_0, \rho_1 - \rho_2) + \\
&\left. + \frac{1}{2} D_s(x_1, \rho; x_0, \rho_1 - \rho_2) \right\}
\end{aligned} \tag{7}$$

Here and below we will assume that the point reference source is located at the origin.

Transforming now to new variables: $\rho_1 - \rho_2 = \rho r_0$, $\rho_1 + \rho_2 = 2Rr_0$, $\rho = r r_0$, and

introducing the notation $q = k r_0^2 / (x_1 - x_0)$, and $q_F = k r_0^2 / F$, we have

$$\begin{aligned}
\langle I_k(x_1, \mathbf{r}) \rangle &= \frac{q^2}{4\pi^2} \iint d^2 \rho d^2 R \exp \left\{ -\frac{q}{\Omega} \left(R^2 + \frac{\rho^2}{4} \right) + i(q_F - q) \mathbf{R} \rho + \right. \\
&+ i q \mathbf{r} \rho - \int_0^1 d\eta [|\eta \mathbf{r}|^{5/3} + |(1 - \eta) \rho|^{5/3} - \\
&\left. - \frac{1}{2} |(1 - \eta) \rho + \eta \mathbf{r}|^{5/3} - \frac{1}{2} |(1 - \eta) \rho - \eta \mathbf{r}|^{5/3} \right\}.
\end{aligned} \tag{8}$$

The integration over $d^2 R$ in expression (8) can be done analytically, whence we obtain

$$\begin{aligned}
\langle I_k(x_1, \mathbf{r}) \rangle &= \frac{q\Omega}{4\pi} \iint d^2 \rho \exp \left\{ -\left(\frac{q}{4\Omega} + \frac{\Omega(q_F - q)^2}{4q} \right) \rho^2 + \right. \\
&+ i q \mathbf{r} \rho - \int_0^1 d\eta [|\eta \mathbf{r}|^{5/3} + |(1 - \eta) \rho|^{5/3} - \frac{1}{2} |(1 - \eta) \rho + \eta \mathbf{r}|^{5/3} - \\
&\left. - \frac{1}{2} |(1 - \eta) \rho - \eta \mathbf{r}|^{5/3} \right\}.
\end{aligned} \tag{9}$$

It should be borne in mind that for the same notation in vacuum

$$I_0(x_1, \mathbf{r}) = \frac{\Omega^2}{[1 + \Omega^2 (q_F - q)^2 / q^2]} \exp \left\{ -\frac{q^3 \Omega r^2}{[q^2 + \Omega^2 (q_F - q)]^2} \right\}. \tag{10}$$

Let us consider the behavior of the average intensity (9) of the corrected field for various turbulence intensity regimes. As our input radiation we will use wide ($\Omega \gg 1$)

optical beams. The average intensity distribution varies substantially, depending on the focusing of the input beam:

$$\begin{aligned} \langle I_k(x_1, \mathbf{r}) \rangle = & \frac{q\Omega}{4\pi} \iint d^2\rho \exp\left\{-\frac{q}{4\Omega}(1+\Omega^2)\rho^2 + iq\rho\mathbf{r} - \right. \\ & - \int_0^1 d\eta [|\eta\mathbf{r}|^{5/3} + |(1-\eta)\rho|^{5/3} - \frac{1}{2} |(1-\eta)\rho + \eta\mathbf{r}|^{5/3} - \\ & \left. - \frac{1}{2} |(1-\eta)\rho - \eta\mathbf{r}|^{5/3}] \right\} \end{aligned} \quad (11)$$

for a collimated beam ($q_F = 0$), and

$$\begin{aligned} \langle I_k(x_1, \mathbf{r}) \rangle = & \frac{q\Omega}{4\pi} \iint d^2\rho \exp\left\{-\frac{q}{4\Omega}\rho^2 + iq\rho\mathbf{r} - \right. \\ & - \int_0^1 d\eta [|\eta\mathbf{r}|^{5/3} + |(1-\eta)\rho|^{5/3} - \frac{1}{2} |(1-\eta)\rho + \eta\mathbf{r}|^{5/3} - \\ & \left. - \frac{1}{2} |(1-\eta)\rho - \eta\mathbf{r}|^{5/3}] \right\} \end{aligned} \quad (12)$$

for an input beam focused in the receiver plane ($q_F = +q$). In the case of a divergent beam ($q_F = -q$) the average intensity distribution is given by an expression practically identical with expression (11) except for the absence of the term $\exp\left\{-\frac{q}{4\pi}(1+4\Omega^2)\rho^2\right\}$. For "weak" fluctuations ($q \gg 1$) the region of substantial integration over ρ for the collimated and divergent beams (11) is given by $|\bar{\rho}| \leq (q\Omega)^{-1/2} \ll 1$, from which it follows that it is possible to expand the last term in the exponential in expression (11) in a power series in ρ :

$$\langle I_k(x_1, \mathbf{r}) \rangle = \frac{q\Omega}{4\pi} \iint d^2\rho \exp\left\{-\frac{q\Omega}{4}\rho^2 + iq\rho\mathbf{r} - \frac{3}{8}\rho^{5/3}\right\}. \quad (13)$$

We find that for $q\Omega \gg 1$ the average intensity distribution (13) is practically indistinguishable from the vacuum distribution (10), and for a wide enough beam ($\Omega \gg 1$) the condition $q\Omega \gg 1$ can be realized even in the region of "strong"

fluctuations ($q \ll 1$). If we apply the quadratic approximation of the phase structure function to expression (13), we obtain

$$\langle I_k(x_1, r) \rangle \cong \frac{\Omega}{(\Omega + 4\gamma/q)} \exp\left\{-\frac{q^2 r^2}{(\Omega + 4\gamma/q)}\right\}, \quad (14)$$

where $\gamma \approx 1$. For the case of "very strong" fluctuations ($q \ll 1$), even for $q\Omega < 1$, the region of substantial integration over ρ in expression (11) is given by $|\rho| \geq (q\Omega)^{1/2} > 1$, from which it follows that

$$\langle I_k(x_1, r) \rangle / I_0(x_1, r) \approx \exp\left(-\frac{3}{8} r^{5/3}\right), \text{ for } r < 1, \quad (15)$$

$$\text{for } r \gg 1, \langle I_k(x_1, r) \rangle / I_0(x_1, r) \approx \frac{q\Omega}{4\gamma} \exp\left(\frac{q}{\Omega} r^2\right), \quad (16)$$

and the difference from the vacuum distribution (10) is substantial.

Thus, for wide collimated and divergent beams, all the way to the region of "strong" fluctuations ($q \ll 1$), the average intensity distribution of the PC-corrected field is diffraction-limited. In the region of "very strong" fluctuations ($q\Omega < 1$) it remains essentially diffraction-limited only for $r < 1$ ($|\rho| < r_0$), but for $r > 1$ the distribution is greatly changed, specifically, it is broadened.

For a focused beam ($q_F = q$) the average intensity (12) has a somewhat different character: already for $q < \Omega$ (even if, as before, $q \gg 1$) for $r < 1$ expression (15) is valid, and, for $r \gg 1$, expression (16). Consequently, correction of a focused beam by the PC algorithm is much poorer than for a collimated or divergent beam.

At the same time, the WFR algorithm, which corrects the field according to the scheme (1.2.2), forms the average intensity in the phase approximation according to the formula

$$\begin{aligned}
\langle I_k(x_1, \rho) \rangle &= \frac{k^2}{4\pi^2(x_1 - x_0)^2} \iint d^4 \rho_{1,2} U_0(\rho_1) U_0^*(\rho_2) \times \\
&\times \exp\{ik\bar{\rho} \frac{(\rho_1 - \rho_2)}{(x_1 - x_0)} + [-D_s(x_1, \rho; x_0, 0) - D_s(x_1, 0; x_0, \rho_1 - \rho_2) + \\
&+ \frac{1}{2} D_s(x_1 - \rho; x_0, \rho_1 - \rho_2) + \frac{1}{2} D_s(x_1, \rho; x_0, \rho_1 - \rho_2)]\}.
\end{aligned} \tag{17}$$

What distinguishes the integrand in expression (17) from the integrand in expression (7), which applies for the PC algorithm, is the absence of the term $\exp[ik(\rho_1^2 - \rho_2^2)/2(x_1 - x_0)]$. Making a change of variables and carrying out the integration in Eq.(17), we obtain

$$\begin{aligned}
\langle I_k(x_1, \mathbf{r}) \rangle &= \frac{q\Omega k^2}{16\pi^3(x_1 - x_0)^2} \iint d^2 \rho \exp\left\{-\left(\frac{q}{4\Omega} + \frac{q_F^2 \Omega}{4q}\right) \rho^2 \right. \\
&+ i q \mathbf{r} \rho - \int_0^1 d\eta [|\eta \mathbf{r}|^{5/3} + |(1-\eta)\rho|^{5/3} - \frac{1}{2} |(1-\eta)\rho + \eta \mathbf{r}|^{5/3} - \\
&\left. - \frac{1}{2} |(1-\eta)\rho - \eta \mathbf{r}|^{5/3}]\right\}.
\end{aligned} \tag{18}$$

For a collimated beam this gives

$$\begin{aligned}
\langle I_k(x_1, \mathbf{r}) \rangle &= \frac{q\Omega k^2}{16\pi^3(x_1 - x_0)^2} \iint d^2 \rho \exp\left\{-\frac{q}{4\Omega} \rho^2 + i q \mathbf{r} \rho - \right. \\
&- \int_0^1 d\eta [|\eta \mathbf{r}|^{5/3} + |(1-\eta)\rho|^{5/3} - \frac{1}{2} |(1-\eta)\rho + \eta \mathbf{r}|^{5/3} - \\
&\left. - \frac{1}{2} |(1-\eta)\rho - \eta \mathbf{r}|^{5/3}]\right\},
\end{aligned} \tag{19}$$

and for a divergent or focused beam ($\delta^2 = \Omega^2$)

$$\begin{aligned}
\langle I_k(x_1, \mathbf{r}) \rangle &= \frac{q\Omega k^2}{16\pi^3(x_1 - x_0)^2} \iint d^2 \rho \exp\left\{-\frac{q}{4\Omega} (1 + \Omega^2) \rho^2 + i q \rho \mathbf{r} - \right. \\
&- \int_0^1 d\eta [|\eta \mathbf{r}|^{5/3} + |(1-\eta)\bar{\rho}|^{5/3} - \frac{1}{2} |(1-\eta)\bar{\rho} + \eta \mathbf{r}|^{5/3} - \\
&\left. - \frac{1}{2} |(1-\eta)\bar{\rho} - \eta \mathbf{r}|^{5/3}]\right\},
\end{aligned} \tag{20}$$

If we compare expressions (19), (20) with (11), (12), we find that the WFR algorithm gives practically the same dependence on the turbulent intensity for a collimated input beam as the PC algorithm gives for a focused beam, and vice versa, while for a divergent or focused beam, to within a constant factor, WFR correction gives the same average intensity as the PC algorithm gives for a collimated beam.

In the PC algorithm, correction is directed at compensating for the action of turbulence and providing diffraction-limited characteristics of the radiation at the receiver. The radiation distribution formed is almost the same as in vacuum, the only errors present being the result of incompleteness of correction. The PC algorithm is most effective for collimated and divergent beams: an almost diffraction-limited average intensity distribution (as in vacuum) is realized as long as $q\Omega > 1$, i.e., even in the region of "strong" intensity fluctuations a focused beam is well corrected only in the region of "weak" fluctuations $q \gg \Omega$. At the same time, the WFR algorithm compensates not only the fluctuational phase shift, but also the diffractive phase shift, focuses an initially collimated beam (with good reproduction of the average intensity only for $q > \Omega$), and collimates divergent and focused beams with good reproduction of the average intensity distribution for $q\Omega > 1$.

Residual intensity fluctuations. Let us dwell now on the intensity fluctuations of the corrected field. We will consider the phase approximation for $\langle I_k^2(x_1, \mathbf{r}) \rangle$ and σ_k^2 in the case of PC correction:

$$\begin{aligned}
\langle I_k^2(x_1, \mathbf{r}) \rangle &= \left(\frac{k}{2\pi(x_1 - x_0)} \right)^4 \iint d^8 \rho_{1,2,3,4} U_0(\rho_1) U_0^*(\rho_2) U_0(\rho_3) U_0^*(\rho_4) \times \\
&\times \exp \left\{ ik \frac{\rho_1^2 - \rho_2^2 + \rho_3^2 - \rho_4^2}{2(x_1 - x_0)} - ik\bar{\rho} \frac{(\rho_1 - \rho_2) + (\rho_3 - \rho_4)}{(x_1 - x_0)} + \right. \\
&+ [-D_s(x_1, \rho; x_0, 0) - D_s(x_1, 0; x_0, \rho_1 - \rho_2) + \frac{1}{2} D_s(x_1, -\rho; x_0, \rho_1 - \rho_2) + \\
&+ \frac{1}{2} D_s(x_1, \rho; x_0, \rho_1 - \rho_2) - D_s(x_1, \rho; x_0, 0) - D_s(x_1, 0; x_0, \rho_3 - \rho_4) + \\
&+ \frac{1}{2} D_s(x_1, -\rho; x_0, \rho_3 - \rho_4) + \frac{1}{2} D_s(x_1, \rho; x_0, \rho_3 - \rho_4) + \\
&+ \frac{1}{2} [2D_s(x_1, 0; x_0, \rho_1 - \rho_3) - D_s(x_1, -\rho; x_0, \rho_1 - \rho_3) - D_s(x_1, \rho; x_0, \rho_1 - \rho_3) + \\
&+ 2D_s(x_1, 0; x_0, \rho_2 - \rho_4) - D_s(x_1, -\rho; x_0, \rho_2 - \rho_4) - D_s(x_1, \rho; x_0, \rho_2 - \rho_4)] - \\
&- \frac{1}{2} [2D_s(x_1, 0; x_0, \rho_1 - \rho_4) - D_s(x_1, -\rho; x_0, \rho_1 - \rho_4) - D_s(x_1, \rho; x_0, \rho_1 - \rho_4) + \\
&+ 2D_s(x_1, 0; x_0, \rho_2 - \rho_3) - D_s(x_1, -\rho; x_0, \rho_2 - \rho_3) - D_s(x_1, \rho; x_0, \rho_2 - \rho_3)] \}.
\end{aligned} \tag{21}$$

The quantity $\langle I_k(x_1, \rho) \rangle^2$ is written out analogously. The residual intensity fluctuations of the corrected field can be characterized by the quantity

$$\sigma_k^2(\rho) = \langle I_k^2(x_1, \rho) \rangle / \langle I_k(x_1, \rho) \rangle^2 - 1.$$

Let us transform in expression (21) to new variables:

$$2\mathbf{r}_1 \mathbf{r}_0 = \rho_1 + \rho_2 + \rho_3 - \rho_4, \quad 2\mathbf{r}_3 \mathbf{r}_0 = \rho_1 - \rho_2 - \rho_3 - \rho_4,$$

$$2\mathbf{r}_2 \mathbf{r}_0 = \rho_1 - \rho_2 - \rho_3 + \rho_4, \quad 2\mathbf{r}_4 \mathbf{r}_0 = \rho_1 + \rho_2 + \rho_3 + \rho_4.$$

From these calculations, we find that for the case of weak fluctuations ($q \gg 1$, $q \gg \Omega$)

the region of substantial integration in $\langle I_k^2 \rangle$ and $\langle I_k \rangle^2$ is $|\mathbf{r}_1, \mathbf{r}_2, \mathbf{r}_3| \ll 1$, wherefore the corresponding exponentials in Eq.(21) can be expanded in their respective series since $|\mathbf{r}| \gg |\mathbf{r}_1, \mathbf{r}_2, \mathbf{r}_3|$, which gives

$$\begin{aligned}
\sigma_k^2(\vec{r}) = & \frac{3}{4} \iint d^6 r_{1,2,3} \exp\left\{-\frac{q}{2\Omega} \left[r_1^2 + r_2^2 + r_3^2 \left(1 + \frac{\Omega^2 (q - q_F)^2}{q^2} \right) \right]\right\} + \\
& i(q - q_F) \mathbf{r}_2 \mathbf{r}_1 - i q \mathbf{r}_3 \mathbf{r} \{ |\mathbf{r}_1 + \mathbf{r}_2|^{5/3} + |\mathbf{r}_1 - \mathbf{r}_2|^{5/3} - |\mathbf{r}_1 + \mathbf{r}_3|^{5/3} - \\
& - |\mathbf{r}_1 - \mathbf{r}_3|^{5/3} \} / \iint d^6 r_{1,2,3} \exp\left\{-\frac{q}{2\Omega} \left[r_1^2 + r_2^2 + r_3^2 \left(1 + \frac{\Omega^2 (q - q_F)^2}{q^2} \right) \right]\right\} + \\
& i(q - q_F) \mathbf{r}_2 \mathbf{r}_1 - i q \mathbf{r}_3 \mathbf{r} \approx 0 \left[(q/\Omega)^{-5/6} \right] \ll 1.
\end{aligned} \tag{22}$$

Consequently, in this region ($q \gg \Omega$) for arbitrary parameters of the input beam the intensity fluctuations are completely suppressed by PC correction. Note that the dependence of the diffraction part of $\langle I_k^2(\mathbf{x}_1, \mathbf{r}) \rangle$ on \mathbf{r}_3 is such that the region of integration over \mathbf{r}_3 is $\left[1 + \Omega^2 (q - q_F)^2 / q^2 \right]$ times narrower than over \mathbf{r}_1 and \mathbf{r}_2 . Therefore, for collimated ($q_F = 0$) and divergent ($q_F = -q$) beams, for $q \Omega \gg 1$, even in the region of "strong" fluctuations ($q \ll 1$), the \mathbf{r}_3 -dependence of the integrands in $\langle I_k^2(\mathbf{x}_1, \mathbf{r}) \rangle$ and $\langle I_k(\mathbf{x}_1, \mathbf{r}) \rangle^2$ is the same. Therefore it is possible to calculate

$$\iint d^2 r_3 \exp\left\{-\frac{q}{2\Omega} \left[1 + \frac{\Omega^2 (q - q_F)^2}{q^2} \right] r_3^2 - i q \mathbf{r}_3 \mathbf{r} \right\},$$

by setting $\mathbf{r}_3 = 0$ in the rest of the integrand. Let us consider the region in which $q < \Omega$, but $q \Omega \gg 1$. Here

$$\sigma_k^2(r) \approx 0.13 (q \Omega)^{1/6} r^2, \tag{23}$$

and we have efficient correction for $r \leq 2.8 (q \Omega)^{-1/6}$. If the fluctuations are so "strong" that $q \Omega < 1$, then here as before the region of permissible values of $|\mathbf{r}_1|$ and $|\mathbf{r}_2|$ is Ω times wider than in \mathbf{r}_3 , wherefore the exponential in Eq. (21) can be expanded in a series in the small quantities \mathbf{r}_3 (small in comparison with \mathbf{r}_2 and \mathbf{r}_1). We then have

$$\sigma_k^2(r) \approx 1.13(q/\Omega)^{1/6} r^2, \quad r < 1$$

and there is no correction in the region $r \gg 1$.

The intensity fluctuations in a focused beam possess the property

$$q \gg \Omega, \quad \sigma_k^2 \approx (q/\Omega)^{-5/6},$$

$$q \gg 1, \quad q/\Omega \approx 1, \quad \begin{cases} \sigma_k^2(r) \approx 1.13(q/\Omega)^{1/6} r^2, & r \ll 1 \\ \sigma_k^2(r) \approx 1, & r \gg 1 \end{cases}$$

$$q \leq 1, \quad q/\Omega \ll 1 \quad \sigma_k^2(r) \approx 1.13(q/\Omega)^{1/6} r^2$$

in the very narrow region ($r \ll (\Omega/q)^{1/12}$).

The PC algorithm suppresses fluctuations quite efficiently

- for a collimated or divergent input beam under the condition $q\Omega > 1$ for weak r , and under the condition $q\Omega < 1$ for $r < 1$,
- for a focused input beam under the condition $q/\Omega \gg 1$ for any r , under the condition $1 < q < \Omega$ for $r \ll 1$, and under the condition $q < 1$ for $r \ll (\Omega/q)^{1/12}$.

At the same time, the WFR algorithm leads to an expression for $\langle I_k^2(x_1, \rho) \rangle$ that practically coincides with expression (21) with the only difference being the absence in the integrand of the phase term $\exp\{ik(\rho_1^2 - \rho_2^2 + \rho_3^2 - \rho_4^2)/2(x_1 - x_0)\}$. Analysis shows that this circumstance turns out to be quite important: the WFR algorithm is most efficient at suppressing fluctuations for a focused input beam (just as PC correction is for a collimated or divergent beam) and is substantially worse for a collimated or divergent beam.

2.2. Correction with a Plane Reference Wave

In the preceding sections we showed that the algorithms of adaptive correction, based on the reciprocity of fluctuations, can be used effectively for the correction of turbulent fluctuations in optical waves of various geometry. Of course, the ratio of the dimensions of the input and reference sources determines the efficiency of this correction. For a wide optical beam ($\Omega \gg 1$) the most suitable reference source is a point reference source: for a plane wave a good reference wave is spherical, and conversely, by virtue of reciprocity. For a narrow input beam ($\Omega \ll 1$), the reference source should be wide ($\Omega_0 \gg 1$), in the limit - a plane wave.

This is realized in practice when we use a reference source which is quite far from the turbulent layer, as a result of which by the time the reference wave arrives at the layer it is already a plane wave. In this case the PC-corrected field is written as

$$U_k(x_1, \rho) = \iint d^2 \rho_1 d^2 \kappa_1 U_0(\rho_1) \exp(i \kappa_1 \rho) \frac{v(x_1, \kappa_1; x_0, \rho_1) v^*(x_1, \kappa_0; x_0, \rho_1)}{v_0^*(x_1, \kappa_0; x_0, \rho)}$$

Here the reference plane wave propagates at an angle κ_0 to the X axis. Let $\kappa_0 = 0$.

Now let us consider the corrected field for a collimated beam:

$$U_k(x_1, \rho) \approx \frac{\exp\left\{-\rho^2 / [2a^2(1 + A/q\Omega) + i 2a^2/\Omega]\right\}}{[(1 + A/\Omega q) + i/\Omega]}, \quad A \approx 1. \quad (24)$$

In a narrow beam the mean field

- for "very weak" fluctuations ($q\Omega \gg 1$, although $\Omega \ll 1$)

$$U_k(x_1, \bar{\rho}) \approx \frac{\exp\left\{-\rho^2 / [2a^2(1 + i/\Omega)]\right\}}{(1 + i/\Omega)},$$

is reconstructed to its vacuum value,

- for $\Omega q \approx 1$ the result is practically the same,
- for "moderate" fluctuations ($\Omega \ll 1$, $q \approx 1$) the mean field

$$U_k(x_1, \rho) \approx \frac{q\Omega}{2} (1 - i) \exp\left\{-\frac{\Omega}{2a^2} \rho^2 + i \frac{\Omega}{2a^2} \rho^2\right\},$$

differs strongly from the diffraction-limited field. Thus, the mean field is reconstructed to its vacuum value only as long as $q\Omega > 1$.

Let us consider the behavior of the average intensity

$$\begin{aligned} \langle I_k(x_1, \mathbf{r}) \rangle = \frac{\Omega}{16\pi^3 q} \iint d^2\rho d^4 v_{1,2} \exp\left\{-\frac{q}{4\Omega} \rho^2 + i\mathbf{r}(v_1 - v_2) - i\rho \frac{(v_1 + v_2)}{2} - \right. \\ \left. i \frac{(v_1^2 - v_2^2)}{2q} - \frac{[(v_1 - v_2) + q_F \rho]^2 \Omega}{4q}\right\} \end{aligned} \quad (25)$$

Here a reference plane wave normally incident on the entrance pupil has been used; here $q_F = 0$ for a collimated input beam, and $q_F = \pm q$ for a divergent (focused) input beam.

Let us consider different fluctuation regions. In the region of "weak" fluctuations ($q \gg 0$ even for $q\Omega \gg 1$) for \mathbf{r} the region of permissible values is given by the condition $|\rho| \leq (\Omega/q)^{1/2} \ll 0$, and for $v_1 - v_2$, by the condition $|v_1 - v_2|/q \leq (\Omega q)^{1/2}$, whence expression (25) simplifies somewhat:

$$\begin{aligned} \langle I_k(x_1, \mathbf{r}) \rangle \cong \frac{\Omega}{16\pi^3 q} \iint d^2\rho d^4 v_{1,2} \exp\left\{-\frac{q}{4\Omega} \rho^2 + i\mathbf{r}(v_1 - v_2) - i\rho \frac{(v_1 + v_2)}{2} - \right. \\ \left. - i \frac{(v_1^2 - v_2^2)}{2q} - \frac{[(v_1 - v_2) + q_F \rho]^2 \Omega}{4q} - \int_0^1 d\eta \left| \eta \frac{v_1 - v_2}{q} \right|^{5/3}\right\}, \end{aligned} \quad (26)$$

i.e., in the second exponential in expression (25) we have set $\rho = 0$. Making use of the equality

$$\begin{aligned} \iint d^2\rho \exp\left\{-\frac{q}{4\Omega}\rho^2 + i\rho(v_1 - v_2) - \frac{q_F^2\Omega\rho^2}{4q} + \frac{q_F\Omega}{4q}\rho(v_1 + v_2)\right\} = \\ = \frac{4\pi q\Omega}{(q^2 + q_F^2\Omega^2)} \exp\left\{-\frac{q\Omega\left[(v_1 + v_2) - iq_F\frac{\Omega}{q}(v_1 - v_2)\right]^2}{4(q_F^2 + q_F^2\Omega)}\right\}, \end{aligned} \quad (27)$$

we arrive (in the case of a collimated input beam) at the expression

$$\begin{aligned} \langle I_k(x_1, \mathbf{r}) \rangle = \frac{\Omega^2}{4\pi^2 q^2} \iint d^4 v_{1,2} \exp\left\{i\mathbf{r}(v_1 - v_2) - i\frac{(v_1^2 - v_2^2)}{2q} + \right. \\ \left. + \frac{(v_1 - v_2)\Omega}{4q} - \Omega\frac{(v_1 + v_2)^2}{4q}\right\} \exp\left\{-\frac{3|v_1 - v_2|^{5/3}}{8q^{5/3}}\right\}, \end{aligned} \quad (28)$$

We can simplify this expression further by introducing the notation $v_1 - v_2 = v$,

$v_1 + v_2 = 2\bar{v}$, as a result of which we arrive at the following expression:

$$\langle I_k(x_1, \mathbf{r}) \rangle = \frac{\Omega}{4\pi q} \iint d^4 v \exp\left\{i\mathbf{r}v - \frac{(1 + \Omega)}{2q\Omega}v^2 - \frac{3v^{5/3}}{8q^{5/3}}\right\}. \quad (29)$$

If we use the quadratic approximation, we obtain, taking into account the conditions $q \gg 1$ and $\Omega \ll 1$,

$$\langle I_k(x_1, \mathbf{r}) \rangle \cong \frac{\Omega}{4q(\beta + 1/4 q\Omega)} \exp\left\{-\frac{k\rho^2}{4(x_1 - x_0)q(\beta + 1/4 q\Omega)}\right\}, \quad (30)$$

where β satisfies the relation

$$\exp\left(-\frac{3}{8}(v/q)^{5/3}\right) = \exp(-\beta v^2).$$

If q is very large ($\beta \ll 1/4q\Omega$ since $\beta \sim q^{5/3}$), the average intensity distribution is practically the same as in vacuum:

$$I_0(x_1, \mathbf{r}) = \Omega^2 \exp\left(-\Omega \frac{k\rho^2}{(x_1 - x_0)}\right).$$

Note that expression (30) for the average intensity distribution remains valid as long as $q \gg \Omega$, i.e., even for $q < 1$. If the fluctuations are so "strong" that $q < \Omega \ll 1$, then, resorting to asymptotic analysis, we obtain

$$\langle I_k(x_1, \mathbf{r}) \rangle \cong \frac{q\Omega}{(4 + \beta q^2)} \exp\left\{-\frac{q}{4(4 + \beta q^2)} \cdot \frac{k\rho^2}{(x_1 - x_0)}\right\}. \quad (31)$$

From expression (31) it can be seen that not only does the axial intensity increase by a factor of $q/[\Omega(4 + \beta q^2)]$ in comparison with the vacuum distribution, but its distribution is also broadened.

For a focused beam ($q_F = q$) expression (2) transforms as follows:

$$\begin{aligned} \langle I_k(x_1, \mathbf{r}) \rangle &= \frac{\Omega}{16\pi^3 q} \iint d^2\rho d^4 v_{1,2} \cdot \\ &\exp\left\{-\frac{q}{4\Omega}\rho^2 + i\mathbf{r}(\mathbf{v}_1 - \mathbf{v}_2) - i\bar{\rho} \frac{(\mathbf{v}_1 + \mathbf{v}_2)}{2} - i \frac{(\mathbf{v}_1^2 - \mathbf{v}_2^2)}{2q} - \frac{[(\mathbf{v}_1 - \mathbf{v}_2) + q\bar{\rho}]^2 \Omega}{4q}\right\} \\ &\exp\left\{-\int_0^1 d\eta \left[|\rho|^{5/3} + \left|\rho + \eta \frac{\mathbf{v}_1 - \mathbf{v}_2}{q}\right|^{5/3} + \left|\eta \frac{\mathbf{v}_1}{q}\right|^{5/3} + \left|\eta \frac{\mathbf{v}_2}{q}\right|^{5/3} - \left|\rho - \eta \frac{\mathbf{v}_2}{q}\right|^{5/3} - \left|\rho + \eta \frac{\mathbf{v}_1}{q}\right|^{5/3} \right] \right\} \end{aligned} \quad (32)$$

For "weak" fluctuations ($q_F \gg 1$, $q\Omega \geq 1$) the regions of permissible values of the integration variables in Eq. (32) are

$$|\rho| \leq \sqrt{\frac{\Omega}{q}} \ll 1, |\bar{\mathbf{v}}_1 - \bar{\mathbf{v}}_2| \leq (q/\Omega)^{1/2} \gg 1, \frac{|\bar{\mathbf{v}}_1 - \bar{\mathbf{v}}_2|}{q} \leq (q\Omega)^{-1/2} \leq 1.$$

Therefore, in the second exponential in expression (32) we can set $\rho = 0$ in comparison with $|v|/q$. This makes it possible to perform the integration in Eq. (32) over $d^2\rho$ analytically. Then, making the substitutions $v_1 - v_2 = v$ and $v_1 + v_2 = 2\mu$, we have

$$\begin{aligned} \langle I_k(x_1, \mathbf{r}) \rangle &\cong \frac{\Omega^2}{4\pi^2 q^2 (1 + \Omega^2)} \iint d^2 v d^2 \mu = \\ &\exp \left\{ i\mathbf{r}v - i \frac{\bar{\mu}\bar{r}}{q(1 + \Omega^2)} - \frac{\Omega v^2}{4q(1 + \Omega^2)} - \frac{\mu^2 \Omega}{q(1 + \Omega^2)} - \frac{3v^{5/3}}{8q^{5/3}} \right\} \\ &= \frac{\Omega}{4\pi q} \iint d^2 v \exp \left\{ i\mathbf{r}v - v^2/4q\Omega - \frac{3}{8} (v/q)^{5/3} \right\}. \end{aligned} \quad (33)$$

The average intensity distribution in a focused beam after PC correction is written as

$$\langle I_k(x_1, \rho) \rangle = \frac{\Omega^2}{(1 + 4q\Omega\beta)} \exp \left\{ - \frac{\Omega}{(1 + 4\beta q\Omega)} \cdot \frac{k\rho^2}{(x_1 - x_0)} \right\}. \quad (33)$$

If $4\beta q\Omega \ll 1$, we obtain the vacuum distribution of the average intensity. The condition $4\beta q\Omega \ll 1$ is realized even for "very strong" fluctuations.

Thus, for a narrow beam the PC algorithm using a plane reference wave focuses the input wave even when the condition of "very strong" intensity fluctuations is realized. The WFR algorithm (recall expression (13) for correction in narrow beams using a plane reference wave ($\Omega_0 \gg \Omega$, $\Omega \ll 1$)) forms such a distribution in vacuum:

- for $\delta_0 = \delta = 0$ $I_0(x_1, \bar{\rho}) \sim \Omega^2 \exp \left(- \Omega \frac{k\rho^2}{(x_1 - x_0)} \right)$,
- for $\delta_0 = \Omega_0$, $\delta = \Omega$ $I_0(x_1, \bar{\rho}) \sim 1$, for arbitrary $|\rho|$,
- for $\delta_0 = \Omega_0$, $\delta = 0$ $I_0(x_1, \bar{\rho}) \sim 1$, for arbitrary $|\rho|$,
- for $\delta_0 = 0$, $\delta = \Omega$ $I_0(x_1, \bar{\rho}) \sim \Omega^2 \exp \left(- \Omega \frac{k\rho^2}{(x_1 - x_0)} \right)$.

Consequently, the WFR algorithm can be used to form not only a narrow beam, but also a plane wave. In this case, if the reference plane wave is focused, then the corrected field forms a plane wave; if the reference plane wave is collimated, correction via WFR provides a narrow input beam with diffraction-limited characteristics.

It is not difficult to show that for correction using a plane reference wave normally incident on the entrance pupil, the expressions for the corrected field in the WFR algorithm coincide to within a constant factor with the corresponding expression using the PC algorithm. An important distinction between the corrected field in the case of a plane reference wave and the corrected field for a point reference source is that suppression of the fluctuations in the corrected field is not ideal even on the optical axis ($\rho = 0$).

Finally, let us dwell on the intensity fluctuations of the corrected field (8) in the case of correction by a reference plane wave. In particular, for "weak" fluctuations ($q \gg 1$), after some not too complicated, but cumbersome calculations we find that the variance of the intensity fluctuations $\sigma_k^2 \cong \pi/2q\Omega$. This means that when using a plane wave as the reference wave it is possible to suppress the intensity fluctuations (in optical beams of arbitrary geometry) if $q\Omega \gg 1$.

Along with correction in narrow beams, a plane wave can be used as the reference wave when correcting so-called diffraction-limited beams ($\Omega \approx 1$).

References to Chapter 2.

1. V.P.Lukin, "Efficiency of some correction systems", *Optics Letters*, **4**, No.1, p.15-17 (1979).
2. Lukin V.P., "Comparative characteristics of some correction algorithms", *Kvantovaia Elektronika*, **11**, pp.1311-1315(1981)[*Sov.J.Quantum Electron.*11, pp.1311-1315, 1981].
3. V.P.Lukin, *Atmosferaia adaptivnaia optika* (Novosibirsk: Nauka, 1986, 248p.).
4. V.P.Lukin, *Atmospheric Adaptive Optics* (SPIE Press Volume PM 23, 1996).

CHAPTER 3. CORRECTION FOR RANDOM ANGULAR DISPLACEMENTS OF OPTICAL BEAMS

In problems of optical location, communication, and energy transmission one frequently runs up against the problem of transporting radiant energy in the form of a light beam to an object located in a random inhomogeneous medium. Here, as a rule, it is necessary to maximize the amount of energy delivered to the object. As is well known, scattering of radiation by refractive index inhomogeneities of the medium leads to a decrease of the average intensity in the near-axial region of the light beam and to the appearance of intensity fluctuations, which taken together substantially degrade the energetic characteristics of the indicated systems.

A radical means of dealing with these undesirable effects is to use various adaptive methods which allow one at least in principle to almost completely eliminate the influence of the inhomogeneities of the medium. The essence of these methods reduces to controlling the initial distribution of the beam field on the basis of information about the instantaneous distribution of inhomogeneities of the medium in which the beam is propagating.

In light of the difficulty of controlling multi-element adaptive correctors operating in the turbulent atmosphere, correction algorithms of the simplest type, correcting, for example, the total wavefront tilt, acquire special importance.

Since the type of correction under discussion is quite simple to use, it is worth our various characteristics of the optical radiation that has passed through the layer of turbulent medium. To control the direction of an optical beam with the aim of decreasing its effective diameter, we can make use of the existence of a statistical connection between the random displacements of the energy centroid of the optical beam and the centroid of the image of the given beam (or an auxiliary beam) in the optical system.

It should be noted that the method of solution of equations describing statistics of a laser beam centroid random shifts can be used successfully in analysis of an image forming in adaptive telescopes employing a *laser guide star*.

So in Ref. 1 (1979) the results were presented of investigations into characteristics of a mutual correlation function and variance of the centroid random shifts of a Gaussian beams and random angular wandering of a plane wave image. (To my regret Ref. 1 never has been published into English.).

This approach was further developed in Ref. 2 published in 1980. In contradistinction to Ref. 1 in this paper were considered several scenarios of an optical experiment. In the each scenario the mutual correlation function was estimated for shifts of a Gaussian beam centroid and shifts of a reference source image. The schemes were considered

- with a beacon in the geometry of experiment (direct and reference beams are coaxial and propagating in opposite directions);
- with a reference wave reflected from a plane mirror.

Mutual correlation for beam shifts and plane (spherical) wave image wandering was calculated. A possibility was analyzed to stabilize position of a laser beam centroid by registering the position of a plane wave image. Also the fact was stressed that the backward scattering of atmospheric aerosol is possible to use (experimental setup is shown in Fig. 35 of Ref. 3 and in Fig. 1 of the present report). An analysis was also performed of spatial and temporal change of mutual correlation for Gaussian beam shifts and wanderings of an image of a reference source. It was found out, that from the point of view of tip and tilt control, the direct and reverse path are reciprocal if a difference between a telescope axis and direction of the beam is greater than the outer scale of turbulence.

In 1981 the results obtained up to date were summarized in Ref. 3 which was published in *Applied Optics*. In 1982 a new experiment was described and data were supplied [4] on using a mutual correlation of random shifts of a laser beam and shifts of image of a reference source for adaptive correction of angular displacements. The optical setup of the experiment (see Fig. 2) allowed one to use some reference sources as well as to employ radiation reflected from an object.

The materials presented in Chapter 3 were published in Refs. 1-4 and also in my book *Atmospheric Adaptive Optics* (Ref. 5).

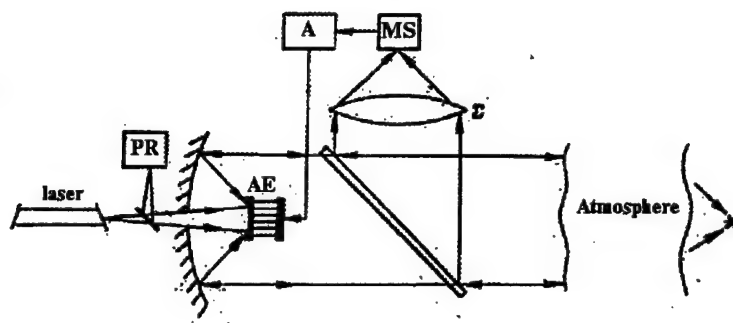


Fig.1. Scheme of the telescope. Σ – additional imaging aperture, MS - image moment sensor, A - amplifier, AE - adaptive element, PR - photo-registrator.

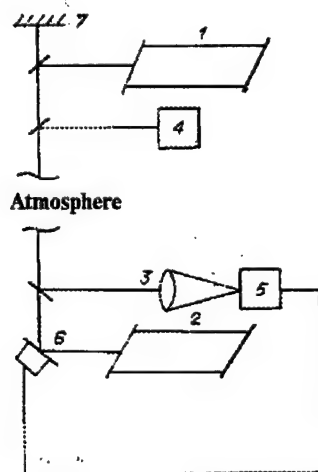


Fig. 2 The optical setup of the experiment. 1, 2 - lasers, 3 - lens, 4 - photodetector, 5 - image motion meter, 6 - tip-tilt mirror, 7 - flat mirror.

3.1. Registration of Random Angular Displacements of Optical Beams

Due to development and improvement of adaptive optics systems and algorithms modern scientists and engineers investigate attentively correlation links between parameters of optical radiation traveling in a random medium. For example, to decrease the effective size of the beam it is possible to use the correlation between random displacements of the center of gravity of this beam and the center of gravity of its image in some optical system. References sources (beacons) are possible to use as well as beams reflected from a target [1].

Let us specify the statement of the problem. We wish to examine the mutual correlation between the random displacements of the energy center of gravity of an optical beam that has passed through a layer of turbulent medium and the center of gravity of some image formed by the optical system [1-5]. This can be an image of a reference source (beacon) or of the optical beam reflected from a flat mirror with infinite radius. Random displacements of the beam centroid are given [6] by the vector

$$\rho_c = \frac{1}{2P_0} \int_0^x d\xi (x - \xi) \iint d^2 R I(\xi, \mathbf{R}) \nabla_R \varepsilon_1(\xi, \mathbf{R}), \quad (1)$$

where $\varepsilon_1(\xi, \mathbf{R})$ are fluctuations of permittivity in the point (ξ, \mathbf{R}) , $I(\xi, \mathbf{R})$ is intensity at the point (ξ, \mathbf{R}) generated by the source located in the plane $\xi = 0$; x is the thickness of the turbulent layer, $P_0 = \iint d^2 R I(0, \mathbf{R})$.

The random displacements of the image in the focal plane of the optical system (equivalent to a "thin" lens with focal length F and area $\Sigma = \pi R_0^2$) are given by the expression [7]:

$$\rho_{cF} = -\frac{F}{k\Sigma} \iint_{\Sigma} \nabla_{\rho} S(x, \rho) d^2 \rho, \quad (2)$$

where k is the wave number of the radiation, $S(x, \rho)$ are the fluctuations of the phase of the optical wave over the aperture of the optical system (in the $\xi = x$ plane) at the point ρ . The mutual correlation of the random vectors ρ_c and ρ_{cF} is given by

$$K = \langle \rho_c \rho_{cF} \rangle / \left[\langle \rho_c^2 \rangle \langle \rho_{cF}^2 \rangle \right]^{1/2}. \quad (3)$$

Here $\langle \dots \rangle$ denotes averaging over the ensemble of realizations of the random function $\varepsilon_1(\xi, \mathbf{R})$.

To make the situation more clear, let us consider the mutual correlation between random displacements of the center of gravity of Gaussian beam and the center of gravity of image for a infinite plane wave. The beam and plane wave propagate along the same optical path. The phase gradients are calculated in the first approximation of the smooth perturbation method [8]:

$$\nabla_{\rho} S(x, \rho) = \frac{k^3}{4\pi} \int_0^x \frac{dx'}{(x - x')^2} \iint d^2 \rho' (\rho - \rho') \varepsilon_1(x', \rho') \cos \frac{k(\rho - \rho')^2}{2(x - x')}$$

Introducing this formula into Eq. 3 we obtain

$$\begin{aligned} \langle \rho_c \rho_{cF} \rangle = & -\frac{k^2 F}{8\pi P_0 \Sigma} \int_0^x d\xi (x - \xi) \int_0^x \frac{dx'}{(x - x')^2} \iint d^2 \rho' \iint d^2 \rho d^2 R (\rho - \rho') \times \\ & \times \cos \frac{k(\rho - \rho')^2}{2(x - x')} \langle I(\xi, \mathbf{R}) \rangle \nabla_R \langle \varepsilon_1(\xi, \mathbf{R}) \varepsilon_1(x', \rho') \rangle. \end{aligned} \quad (4)$$

The absence of correlation between local and integer quantities is used in the procedure of averaging.

In the assumption that fluctuations are delta-correlated we obtain

$$\nabla_R \langle \varepsilon_1(\xi, \mathbf{R}) \varepsilon_1(x', \rho) \rangle = -4\pi \delta(x' - \xi) \iint d^2 \kappa \kappa \Phi_{\varepsilon}(0, \kappa) \sin \kappa(\mathbf{R} - \rho')$$

Let us also introduce a pupil function of the following form

$$\iint_{\Sigma} d^2 \rho \rightarrow \int_{-\infty}^{+\infty} \int_{-\infty}^{+\infty} d^2 \rho e^{-\rho^2/R_0^2},$$

where $\Sigma = \pi R_0^2$. After these mathematical manipulations integration is possible to perform for the following formulae [2]:

$$\begin{aligned} & \iint_{\Sigma} d^2 \rho d^2 \rho' e^{-\rho^2/R_0^2} \kappa(\rho - \rho') \cos \frac{\kappa(\rho - \rho')^2}{2(x - x')} \sin \kappa(\mathbf{R} - \rho') = \\ & = \frac{2\pi R_0^2 (x - x')^2}{\kappa^2} \cos(\kappa \mathbf{R}) e^{-\rho^2 R_0^2/4} \cos \frac{\kappa^2 (x - x')}{2\kappa} \end{aligned}$$

from the above it is follows that

$$\langle \rho_c \rho_{cF} \rangle = \frac{\pi^2 R_0^2}{P_0 \Sigma} \int_0^x dx' (x - x') \iint d^2 R \langle I(x', \mathbf{R}) \rangle \iint d^2 \kappa \Phi_\varepsilon(0, \kappa) \kappa^2 \times \\ \times \cos \kappa \mathbf{R} \cos \frac{\kappa^2 (x - x')}{2k} e^{-\kappa^2 R_0^2 / 4}.$$

In that follows we assume that functions $\langle I(x', \mathbf{R}) \rangle$ and $\Phi_\varepsilon(\xi, \kappa)$ are isotropic and average intensity is given in [7,9] representation

$$\langle I(x', \mathbf{R}) \rangle = \frac{a^2}{a_{Eff}^2(x')} e^{-R^2 / a_{Eff}^2(x')}, \quad (5)$$

where

$$a_{Eff}^2(x') = a^2 \left[\left(1 - \frac{x}{f} \xi \right)^2 + \Omega^{-2} + \Omega^{-2} \left(\frac{1}{2} D_s(2a) \right)^{6/5} \right],$$

$\Omega = \frac{ka^2}{x'}$, a and f are initial parameters of the Gaussian beam $D_s(2a)$ are phase structure function, $x' = x\xi$.

As a result we obtain

$$\langle \rho_c \rho_{cF} \rangle = 2\pi^2 x^2 F \int_0^1 d\xi (1 - \xi) \int_0^\infty d\kappa \kappa^3 \Phi_\varepsilon(\kappa) \exp\left(-\frac{\kappa^2 (R_0^2 + a_{Eff}^2)}{4}\right) \cos \frac{2\kappa^2 x(1 - \xi)}{2k}$$

To perform normalization of Eq. 3 let us calculate functions $\langle \rho_c^2 \rangle$ and $\langle \rho_{cF}^2 \rangle$. In diffraction approximation

$$\langle \rho_c^2 \rangle = \pi^2 x^3 \int_0^1 d\xi (1 - \xi)^2 \int_0^\infty d\kappa \kappa^3 \Phi_\varepsilon(\kappa) \exp\left(-\frac{\kappa^2 a^2 q^2(\xi)}{2}\right)$$

and

$$\langle \rho_{cF}^2 \rangle = 4\pi^2 x F^2 \int_0^1 d\xi \int_0^\infty d\kappa \kappa^5 \Phi_\varepsilon(\kappa) \exp\left(-\frac{\kappa^2 R_0^2}{2}\right) \cos \frac{2\kappa x(1 - \xi)}{2k},$$

where

$$q(\xi) = \left[\xi^2 \Omega^{-2} + \left(1 - \frac{x}{f} \xi \right)^2 \right]^{1/2},$$

All in all we obtain

$$\begin{aligned}
K = & \int_0^1 d\xi (1 - \xi) \int_0^\infty d\kappa \kappa^3 \Phi_n(\kappa) \exp\left(-\frac{\kappa^2(R_0^2 + a_{\text{eff}}^2)}{4}\right) \times \\
& \times \cos\left(\frac{\kappa^2 x(1 - \xi)}{2\kappa}\right) \left/ \left(\int_0^1 d\xi (1 - \xi)^2 \times \right. \right. \\
& \times \int_0^\infty d\kappa \kappa^3 \Phi_n(\kappa) \exp\left(-\frac{\kappa^2 a^2 q^2}{2}\right) \left. \right)^{1/2} \left(\int_0^1 d\xi \int_0^\infty d\kappa \kappa^3 \Phi_n(\kappa) \times \right. \\
& \times \exp\left(-\frac{\kappa^2 R_0^2}{2}\right) \cos^2\left(\frac{\kappa^2 x(1 - \xi)}{2\kappa}\right) \left. \right)^{1/2}, \tag{7}
\end{aligned}$$

The form of K is similar in the case of spherical wave and also in the case when these waves or Gaussian beam are reflected from a flat reflector with infinite radius.

In calculations we use the following spectrum

$$\Phi_n(\kappa) = 0.033 C_n^2 (\kappa^2 + \kappa_0^2)^{-11/6},$$

which accounts for deviation from a power series in a vicinity of the outer scale $L_0 = 2\pi\kappa_0^{-1}$. As an example, let us estimate correlation between displacement of image for a plane wave in the focus of a telescope and random displacement of a beam with initial diameter equal to the diameter of the input pupil of the telescope. Estimation is performed for a homogeneous path, the parameters of the problem are the following:

$$\kappa_0^{-1} \gg R_0, \quad a_{\text{eff}}, \quad \sqrt{x/k}; \quad kR_0^2 \gg x, \quad \Omega^{-2} \left(\frac{1}{2} D_s(2a) \right)^{6/5} \ll 1.$$

We obtain the value of K approximately equals to 0.84.

Due to relatively high correlation, an algorithm of control for correction of random angular displacements of beam $\bar{\rho}_c/x$ can be performed, according to the formula $\alpha(a/2R_0)^{1/3} \rho_{cF}/F$, where α is coefficient of the loop which chosen to ensure the minimum of residual angular displacements of the beam

$$\min \left\langle \left(\frac{\rho_c}{x} - \frac{\alpha(a/2R_0)^{-1/3} \rho_{cF}}{F} \right)^2 \right\rangle.$$

3.2. Correction of Random Angular Displacements of Optical Beams

According to the existing classification [10, 11, 5] one of the simplest ways of correcting the distorted wavefront of an optical beam that has passed through a layer of turbulent atmosphere is to compensate for the fluctuations of the angle of incidence associated with the wavefront tilt. A decrease in the mean diameter of the beam in the observation plane due to such correction leads to a relative increase in the intensity of the incident field. In a number of cases this lowest form of correction in the class of possible phase distortions can be effectively used in place of an adaptive phase corrector, e.g., in systems in which it is necessary to minimize the random wandering of the beam as a whole, all the way to low-frequency random refraction. It is clear that this type of correction is most effective for distances traversed in a medium in which the optical beam does not break up into separated luminous points, but fluctuates on the average as a whole.

Since the type of correction under discussion is quite simple to use, it is worth our while to estimate its efficiency. Let us consider this question for systems using both reference sources (beacons) and reflected optical beams (those which have traversed their paths twice) [5, 10, 11].

In connection with this, we will pay close attention to the correlations between the various characteristics of the optical radiation that has passed through the layer of turbulent medium. To control the direction of an optical beam with the aim of decreasing its effective diameter, we can make use of the existence of feedback between the random displacements of the energy center of gravity of the optical beam and the center of gravity of the image of the given beam (or an auxiliary beam) in the optical system [2].

Let us specify the statement of the problem. We wish to examine the mutual correlation between the random displacements of the energy center of gravity of an optical beam that has passed through a layer of turbulent medium and the center of gravity of some image formed by the optical system [5]. This can be an image of a reference source (beacon) or of the optical beam reflected from the object. The random displacements of the energy center of gravity of the optical beam are given by the vector [6, 7]

$$\rho_c = \frac{1}{P_0} \int_0^x (x - \xi) d\xi \iint d^2 R I(\xi, \mathbf{R}) \nabla_R n_1(\xi, \mathbf{R}), \quad (1)$$

where $n_1(\xi, \mathbf{R})$ are the refractive index fluctuations at the point (ξ, \mathbf{R}) , $I(\xi, \mathbf{R})$ is the field intensity at the point (ξ, \mathbf{R}) due to a source located at the origin in the $\xi = 0$ plane, x is the thickness of the turbulent layer, and

$$P_0 = \iint d^2 R I(0, \mathbf{R}). \quad (2)$$

At the same time, the random displacements of the image in the focal plane of the optical system (equivalent to a "thin" lens with focal length F and area $\Sigma = \pi R_0^2$) in the phase approximation are given by the expression [6, 7]:

$$\rho_{cF} = -\frac{F}{k\Sigma} \iint_{\Sigma} \nabla_{\rho} S(x, \rho) d^2 \rho, \quad (3)$$

where k is the wave number of the radiation, $S(x, \rho)$ are the fluctuations of the phase of the optical wave over the aperture of the optical system (in the $\xi = x$ plane) at the point ρ . The mutual correlation of the random vectors ρ_c and ρ_{cF} is given by

$$K = \langle \rho_c \rho_{cF} \rangle / [\langle \rho_c^2 \rangle \langle \rho_{cF}^2 \rangle]^{1/2}. \quad (4)$$

Here $\langle \dots \rangle$ denotes averaging over the ensemble of realizations of the random function $n_1(\xi, \mathbf{R})$. Let us consider some optical scenarios for which K can be calculated analytically, namely:

- a correction scheme based on a beacon (the beam which is to be corrected and the reference beam are coaxial and propagate in opposite directions),
- a scheme which uses the wave reflected by a flat mirror as the reference radiation,
- a scheme which uses a point reflector.

The specific feature common to all these optical scenarios consists in the choice of the reference source on the displacements of whose image center of gravity the correction is based.

From the point of view of calculating K , these scenarios differ only in the analytic expression for $S(x, \rho)$. It is presently generally taken for granted that the phase fluctuations in the optical wave are described with sufficient accuracy by the approximation of smooth perturbations [8]. At present this is practically the only way of obtaining an analytic form suitable for calculation. For a Gaussian beam reflected

from an unbounded flat mirror located a distance X from the transmitter, in the approximation of smooth perturbations we have [14]

$$\begin{aligned} \nabla_{\rho} S(x \longleftrightarrow x, \rho) = & i \frac{k}{2} \int_0^x dx' \iint \left\{ \kappa_1 \gamma \exp[i\kappa_1 \rho - \right. \\ & \left. - i\gamma \frac{\kappa_1^2 (2x - x')}{2k}] + \kappa_1 \hat{\gamma} \exp\left[i\kappa_1 \rho \hat{\gamma} - i\hat{\gamma} \frac{\kappa_1^2 x'}{2k}\right] + \right. \\ & \left. + \kappa_1 \gamma^* \exp\left[i\kappa_1 \rho \gamma^* + i\gamma^* \frac{\kappa_1^2 (2x - x')}{2k}\right] + \kappa_1 \gamma^* \exp\left[i\kappa_1 \rho \hat{\gamma}^* + i\hat{\gamma}^* \frac{\kappa_1^2 x'}{2k}\right] \right\} dn(\kappa_1, x'), \end{aligned} \quad (5)$$

where

$$\gamma = \frac{1 + i\alpha x'}{1 + i2\alpha x}, \quad \hat{\gamma} = \frac{1 + i(2x - x')}{1 + i2\alpha x}, \quad \alpha = \frac{2}{ka^2} + i/f,$$

a and f are the parameters of the Gaussian beam, $dn(\mathbf{k}, x')$ is the spectral density of the refractive index fluctuations $n_1(\mathbf{r})$, where

$$\begin{aligned} n_1(\mathbf{r}) = & \iint dn(\kappa, x') \exp(i\kappa \rho), \\ \mathbf{r} = & \{x', \rho\}, \quad \kappa \rho = \kappa_2 y + \kappa_3 z. \end{aligned}$$

In the present notation we can rewrite expression (1) for ρ_c in the form

$$\rho_c = \frac{1}{P_0} \int_0^x d\xi (x - \xi) \iint d^2 R I(\mathbf{R}, \xi) \iint dn(\kappa_2, \xi) \kappa_2 \exp(i\kappa_2 \mathbf{R}) \quad (6)$$

then from (5) and (6) we have

$$\begin{aligned} \langle \rho_c \rho_{cf} \rangle = & \frac{F}{2P_0 \Sigma} \int_0^x d\xi (x - \xi) \int_0^x dx' \iint_{\Sigma} d^2 \rho \iint d^2 R \langle I(\mathbf{R}, \xi) \rangle \times \\ & \times \iint \langle dn(\kappa_1, x') dn(\kappa_2, \xi) \rangle \kappa_2 \exp(i\kappa_2 \mathbf{R}) \left\{ \kappa_1 \gamma \exp\left[i\kappa_1 \rho \gamma - i\gamma \frac{\kappa_1^2 (2x - x')}{2k}\right] + \right. \\ & \left. + \kappa_1 \hat{\gamma} \exp\left[i\kappa_1 \rho \hat{\gamma} - i\hat{\gamma} \frac{\kappa_1^2 x'}{2k}\right] + \kappa_1 \gamma^* \exp\left[i\kappa_1 \rho \gamma^* + i\gamma^* \frac{\kappa_1^2 (2x - x')}{2k}\right] + \right. \\ & \left. + \kappa_1 \hat{\gamma}^* \exp\left[i\kappa_1 \rho \hat{\gamma}^* + i\hat{\gamma}^* \frac{\kappa_1^2 x' - x'}{2k}\right] \right\}. \end{aligned} \quad (7)$$

In the averaging over the ensemble of realizations of the refractive index fluctuations in expression (7), we have made use of the absence of correlations between the local and integrated random quantities⁶. Next we make use of the relation

$$\langle dn(\kappa_1, x') dn(\kappa_2, \xi') \rangle = 2\pi\delta(x' - \xi)\delta(\kappa_1 + \kappa_2)\Phi_n(\xi, \kappa_1)d^2\kappa_1d^2\kappa_2,$$

and to simplify the calculations we replace the physical aperture by an untruncated Gaussian aperture [9]:

$$\iint_{\Sigma} d^2\rho \Rightarrow \iint_{-\infty}^{+\infty} d^2\rho \exp(-\rho^2 / 2R_0^2),$$

where $\Sigma = \pi R_0^2$. This last step allows us to carry out the integration $(\iint d^2\rho)$, which leads to the expression

$$\begin{aligned} \langle \rho_c \rho_{cF} \rangle = & \frac{\pi F}{R_0} \int_0^{x''} d\xi (x - \xi) \iint d^2R \langle I(R, \xi) \rangle \iint d^2\kappa \kappa^2 \Phi_n(\kappa, \xi) \exp(-i\kappa R) \times \\ & \times \left\{ \gamma \exp\left[-\frac{\kappa^2 \gamma^2 R_0^2}{2} - i\gamma \frac{\kappa^2 (2x - \xi)}{2k}\right] + \hat{\gamma} \exp\left[-\frac{\kappa^2 \hat{\gamma}^2 R_0^2}{2} - i\hat{\gamma} \frac{\kappa^2 \xi}{2k}\right] + \right. \\ & \left. + \hat{\gamma} \exp\left[-\frac{\kappa^2 \gamma^{*2} R_0^2}{2} + i\gamma^* \frac{\kappa^2 (2x - \xi)}{2k}\right] + \hat{\gamma}^* \exp\left[-\frac{\kappa^2 \hat{\gamma}^{*2} R_0^2}{2} + i\hat{\gamma}^* \frac{\kappa^2 \xi}{2k}\right] \right\}. \end{aligned} \quad (8)$$

In the calculations that are to follow we assume isotropy of $\langle I(R, \xi) \rangle$ and $\Phi_n(\kappa, \xi)$ and make use of the following representation for the average intensity [6]:

$$\langle I(R, \xi) \rangle = \frac{a^2}{a_{eff}^2(\xi)} = \exp(-R^2 / a_{eff}^2(\xi)), \quad (9)$$

where $a_{eff}^2(\xi) = a^2 \left[(1 - \xi / f)^2 + \Omega^{-2} + \Omega^{-2} \left(\frac{1}{2} D_s(2a) \right)^{6/5} \right]$, $\Omega = ka^2 / \xi$, and $D_s(2a)$ is

the phase structure function. In this case

$$\iint d^2R \langle I(R, \xi) \rangle \exp(-i\kappa R) = \pi a^2 \exp\left(-\frac{\kappa^2 a_{eff}^2}{4}\right).$$

Further simplifications of $\langle \rho_c \rho_{cF} \rangle$ are possible only for specific forms of γ and $\hat{\gamma}$.

To estimate K in addition to $\langle \rho_c \rho_{cF} \rangle$, the corresponding variances $\langle \rho_c^2 \rangle$ and $\langle \rho_{cF}^2 \rangle$ are needed. Thus, for the diffraction approximation [15], we have

$$\langle \rho_c^2 \rangle = \pi^2 x^3 \int_0^1 d\xi (1 - \xi)^2 \int_0^\infty d\kappa \kappa^3 \Phi_n(\kappa, x\xi) \exp(-\kappa^2 a^2 q^2(\xi) / 2), \quad (10)$$

where $q(\xi) = [\xi^2 \Omega^{-2} + (1 - x\xi / f)^2]^{1/2}$. The quantity $\langle \rho_{cF}^2 \rangle$ can be calculated with the help of (3) and (5), in analogy with $\langle \rho_c \rho_{cF} \rangle$:

$$\begin{aligned} \langle \rho_{cF}^2 \rangle = & \pi^2 F^2 \int_0^x d\xi (1 - \xi / x)^2 \int_0^\infty d^2 \kappa \kappa^3 \Phi_n(\kappa, \xi) \left\{ \exp \left[-\frac{\kappa^2 \gamma^2 R_0^2}{2} - i\gamma \frac{\kappa^2 (2x - \xi)}{2k} \right] + \right. \\ & + \exp \left[-\frac{\kappa^2 \gamma^2 R_0^2}{2} - i\gamma \frac{\kappa^2 \xi}{2k} \right] + \exp \left[-\frac{\kappa^2 \gamma^{*2} R_0^2}{2} + i\gamma^* \frac{\kappa^2 (2x - \xi)}{2k} \right] + \\ & \left. + \exp \left[-\frac{\kappa^2 \gamma^{*2} R_0^2}{2} + i\gamma^* \frac{\kappa^2 \xi}{2k} \right] \right\}. \end{aligned} \quad (11)$$

Expression (11) is the variance of the jitter of the center of gravity of the image of a Gaussian beam reflected by an unbounded flat mirror. We now finally have all the components needed to calculate K .

Expressions (8) and (11) substantially simplify for those cases in which an unbounded plane or spherical wave is used as the reference wave [2,5]. Thus, for a plane wave ($\gamma = \gamma^* = 1$) [2, 5]

$$\begin{aligned} \langle \rho_c \rho_{cF} \rangle = & -4\pi^2 F \int_0^x d\xi (x - \xi) \int_0^\infty d\kappa \kappa^3 \Phi_n(\kappa, \xi) \times \\ & \times \cos \frac{\kappa^2 x}{2k} \cos \frac{\kappa^2 (x - \xi)}{2k} \exp \left[-\frac{\kappa^2}{4} (a_{\text{eff}}^2 + 2R_0^2) \right], \end{aligned} \quad (12)$$

$$\langle \rho_{cF}^2 \rangle = 4\pi^2 F^2 \int_0^x d\xi \int_0^\infty d\kappa \kappa^3 \Phi_n(\kappa, \xi) \cos^2 \frac{\kappa^2 x}{2k} \cos^2 \frac{\kappa^2 (x - \xi)}{2k} \exp(-\kappa^2 R_0^2), \quad (13)$$

and for a spherical wave, ($\gamma = \xi / x$)

$$\begin{aligned} \langle \rho_c \rho_{cF} \rangle = & -4\pi^2 a^2 F \int_0^x d\xi (x - \xi) \int_0^\infty d\kappa \kappa^3 \Phi_n(\kappa, \xi) \times \\ & \times \exp(-\frac{\kappa^2 a_{\text{eff}}^2}{4}) \cos \frac{\kappa^2 \gamma \hat{\gamma} x}{2k} \gamma \exp(-\frac{\kappa^2 R_0^2 \hat{\gamma}^2}{2}), \end{aligned} \quad (14)$$

$$\langle \rho_{cF}^2 \rangle = 4\pi^2 F^2 \int_0^x d\xi (x - \xi)^2 \int_0^\infty d\kappa \kappa^3 \Phi_n(\kappa, \xi) \cos^2 \frac{\kappa^2 x}{2k} \gamma \hat{\gamma} \exp(-\kappa^2 R_0^2 \hat{\gamma}^2). \quad (15)$$

Using these and analogous expressions, it can be shown, for example, that for a plane wave (i.e., investigating the mutual correlation of the random displacements of

the center of gravity of a plane wave, and the random displacements of the energy center of gravity of a Gaussian beam):

$$\begin{aligned}
 K = & -\int_0^1 d\xi (1-\xi) \int_0^\infty d\kappa \kappa^3 \Phi_n(\kappa, x\xi) \cos \frac{\kappa^2 x}{2k} (1-\xi) \times \\
 & \times \cos \frac{\kappa^2 x}{2k} \exp \left[-\frac{\kappa^2}{4} (2R_0^2 + a_{\text{eff}}^2) \right] / \left\{ \left[\int_0^1 d\xi \int_0^\infty d\kappa \kappa^3 \Phi_n(\kappa, x\xi) \times \right. \right. \\
 & \times \cos^2 \frac{\kappa^2 x}{2k} \cos^2 \frac{\kappa^2 (1-\xi)}{2k} x \exp(-\kappa^2 R_0^2) \left. \right] \times \\
 & \times \left[\int_0^1 d\xi (1-\xi)^2 \int_0^\infty d\kappa \kappa^3 \Phi_n(\kappa, x\xi) \exp(-\kappa^2 a^2 q^2 / 2) \right] \left. \right\}^{1/2}. \quad (16)
 \end{aligned}$$

Other cases: reflection of a Gaussian beam from a flat mirror, reflection from a point scatterer, and direct propagation (use of a beacon) are described in analogous fashion.

We calculate the integrals in expression (16) using the spectrum

$$\Phi_n(\kappa, x\xi) = 0.033 C_n^2 \kappa^{-11/3} [1 - \exp(-\kappa^2 / \kappa_0^2)], \quad (17)$$

which takes account of the deviation from a power law in the outer scale κ_0^{-1} region.

For convenience, we denote the integrals in (16) as follows:

$$K = A_1 / \{A_2 A_3\}^{1/2}.$$

Analysis shows that under the condition

$$\kappa_0^{-1} \gg R_0, \quad a, \quad \sqrt{x/k} \quad (18)$$

integrals A and A_1 or their analogs can be calculated using the Kolmogorov spectrum ($\kappa_0 = 0$). In this case

$$\begin{aligned}
 A_1 = & -0.033 \int_0^1 d\xi (1-\xi) C_n^2(x\xi) \frac{\Gamma(1/6)}{4} \left\{ \left(d_{\text{eff}}^2 + \frac{ix(2-\xi)}{2k} \right) + \right. \\
 & + \left(d_{\text{eff}}^2 - \frac{ix(2-\xi)}{2k} \right)^{-1/6} + \left(d_{\text{eff}}^2 + \frac{ix\xi}{2k} \right)^{-1/6} + \left(d_{\text{eff}}^2 - \frac{ix\xi}{2k} \right)^{-1/6} \left. \right\}, \\
 A_2 = & -0.033 \int_0^1 d\xi C_n^2(x\xi) \frac{\Gamma(1/6)}{8} \left\{ R_0^{-1/3} + \left(R_0^2 + \frac{ix}{k} \right)^{-1/6} + \right. \\
 & + \left(R_0^2 - \frac{ix}{k} \right)^{-1/6} + \left(R_0^2 - \frac{ix(1-\xi)}{k} \right)^{-1/6} + \left(R_0^2 + \frac{ix(2-\xi)}{k} \right)^{-1/6} + \\
 & \left. \frac{1}{2} \left(R_0^2 - \frac{ix(2-\xi)}{k} \right)^{-1/6} + \frac{1}{2} \left(R_0^2 + \frac{ix(2-\xi)}{k} \right)^{-1/6} + \frac{1}{2} \left(R_0^2 - \frac{ix\xi}{k} \right)^{-1/6} \right\}.
 \end{aligned}$$

Here $d_{eff}^2 = \frac{2R_0^2 + a_{eff}^2}{4}$. As for A_3 , its dependence on κ_0 must be kept since

$$A_3 = 0.033 \int_0^1 d\xi (1-\xi)^2 C_n^2(x-\xi) \frac{\Gamma(1/6)}{2} \times \\ \times \left[(a^2 q^2(\xi) / 2)^{-1/6} - (a^2 q^2(\xi) / 2 + \kappa_0^{-2})^{-1/6} \right]$$

and given condition (18), we can only realize the condition $aq \geq \kappa_0^{-1}$. Indeed, since

$$q(\xi) = \left[\xi^2 \Omega^{-2} + (1 - x\xi / f)^2 \right]^{1/2},$$

in a quasispherical wave ($\Omega \ll 1$), for example, $q(\xi) = \xi^2 \Omega^{-1} \gg 1$, and for this case condition (18) does not contradict the condition $aq(\xi) \cong \kappa_0^{-1}$. Let us consider the more interesting case $x / (kR_0^2) \ll 1$, i.e., that of a large receiver aperture. Then, on a path with homogeneous turbulence ($C_n^2(x\xi) = C_n^2$) we have

$$K = - \int_0^1 d\xi (1-\xi) \left[(2R_0^2 + a_{eff}^2) / 4 \right]^{-1/6} R_0^{1/3} \left/ \left[\int_0^1 d\xi (1-\xi)^2 \times \right. \right. \\ \left. \left. \times \left\{ (a^2 q^2 / 2)^{-1/6} - (a^2 q^2 / 2 + \kappa_0^{-2})^{-1/6} \right\} \right]^{1/2} \right. \quad (19)$$

Next, omitting simple calculations of the integrals entering into (19), we present in the Table which is a summary of calculated values of K for various scenarios.

	Wide beam $\Omega \gg 1, \Omega^{-2} \left(\frac{1}{2} D_s(2a) \right)^{6/5} \ll 1$	
	$x/f = 0$	$x/f = +1$
$R_0 \gg a$	$K = -0.87 \left(\frac{2R_0^2}{a^2} \right)^{-1/12}$	$K = -0.82 \left(\frac{2R_0^2}{a^2} \right)^{-1/12}$
$2R_0^2 = a^2$	$K = -0.87$	$K = -0.82$
$R_0 \ll a$	$K = -0.7 \left(\frac{a^2}{2R_0^2} \right)^{-1/12} \Omega^{-1/6}$	$K = -0.62 \left(\frac{a^2}{2R_0^2} \right)^{-1/12} \Omega^{-1/6}$

Not repeating all the calculations, we next give an expression for the correlation coefficient K for propagation along one and the same path (or out and back for reciprocity of the outbound and return paths) of a spherical reference wave and an

arbitrary wave beam. From the point of view of realization, this corresponds to correction using either a point reference source (a beacon) or a field reflected from a point "spike" on the target. We obtain from Eqs.(10), (11), (14):

$$\begin{aligned}
 K = & - \int_0^1 d\xi (1-\xi)^2 \int_0^\infty d\kappa \kappa^3 \Phi_n(\kappa, x\xi) \cos\left[\frac{\kappa^2 x}{2k} (1-\xi)\xi\right] \times \\
 & \times \exp\left[-\frac{\kappa^2}{4} (a_{\text{Eff}}^2 + 2R_0^2(1-\xi)^2)\right] / \left[\int_0^1 d\xi (1-\xi)^2 \int_0^\infty d\kappa \kappa^3 \Phi_n(\kappa, x\xi) \times \right. \\
 & \times \cos^2\left[\frac{\kappa^2 x}{2k} (1-\xi)\xi\right] \exp(-\kappa^2 R_0^2(1-\xi)^2) \left. \right]^{1/2} \times \\
 & \times \left[\int_0^1 d\xi (1-\xi)^2 \int_0^\infty d\kappa \kappa^3 \Phi_n(\kappa, x\xi) \cos^2\left[\frac{\kappa^2 x}{2k} (1-\xi)\xi\right] \exp(-\kappa^2 a^2 q^2 / 2) \right]^{1/2}.
 \end{aligned} \tag{20}$$

Let us now consider in more detail in (19) the case of large apertures¹⁹: R_0 commensurate with κ_0^{-1} . For practically any geometry of the reference wave, the condition $R_0 \gg \sqrt{\frac{\kappa}{k}}$ using the model (17) leads to the following expression for K :

$$\begin{aligned}
 K = & -R_0^{1/6} \int_0^1 d\xi (1-\xi) \left[d_{\text{Eff}}^{-1/3} - (d_e^2 + \kappa_0^{-2})^{-1/6} \right] \times \\
 & \times \left[\int_0^1 d\xi (1-\xi)^2 \left\{ (a^2 q^2 / 2)^{-1/6} - (a^2 q^2 / 2 + \kappa_0^{-2})^{-1/6} \right\} \right],
 \end{aligned} \tag{21}$$

where $d_{\text{Eff}}^2 = (a_{\text{Eff}}^2 + 2R_0^2) / 4$. If the initial Gaussian beam is wide enough

$$\left(\Omega \gg 1, \quad \bar{x} / f = 0, \quad q(\xi) = 1, \quad \Omega^{-2} \left(\frac{1}{2} D_s(2a) \right)^{6/5} \ll 1, \quad a_{\text{Eff}} = a \right),$$

then we arrive at the form

$$\begin{aligned}
 K = & -\frac{\sqrt{3}}{2} R_0^{1/6} \left[\left(\frac{2R_0^2 + a^2}{4} \right)^{-1/6} - \left(\frac{2R_0^2 + a^2}{4} + \kappa_0^{-2} \right)^{-1/6} \right] / \\
 & / \left[\left(\frac{a^2}{2} \right)^{-1/6} - \left(\frac{a^2}{2} + \kappa_0^{-2} \right)^{-1/6} \right]^{1/2}.
 \end{aligned} \tag{22}$$

For $2R_0^2 = a^2$

$$K = -\frac{\sqrt{3}}{2} R_0^{1/6} \left[1 - (1 - \beta^{-2})^{-1/6} \right]^{1/2},$$

where $\beta = \kappa_0 R_0$. In summary, we can draw the following conclusions:

- for small apertures ($\beta \ll 1$)

$$K = -\frac{\sqrt{3}}{2},$$

and the largest possible correlation is realized;

- for $\beta \approx 0.5$

$$K = -\frac{\sqrt{3}}{2} (1 - 0.76)^{1/2} \approx -0.49 \frac{\sqrt{3}}{2},$$

and the correlation falls to half-maximum;

- for $\beta \gg 1$

$$K = \frac{1}{2^{3/2} \beta},$$

and correlation is almost completely absent. Finally, it should be noted that a high level of correlation remains only for apertures $R \leq 0.5 \kappa_0^{-1}$.

Thus, for all cases of practical interest it is possible to estimate the mutual correlation K . Let us consider the control algorithm for correction of ρ_c , the random displacements of the center of gravity of the beam, on the basis of measurements of ρ_{cF} , the displacements of the center of gravity of the image in the focal plane of the optical system. One can easily convince oneself that the control algorithm can be driven by the signal $\alpha \frac{x}{F} \rho_{cF} (a^2 / 2R_0^2)^{-1/6}$, where α is the feedback coupling coefficient, chosen from the condition of minimization of the functional

$$\left\langle \left[\rho_c - \alpha \frac{x}{F} \rho_{cF} (a^2 / 2R_0^2)^{-1/6} \right]^2 \right\rangle. \quad (23)$$

The magnitude of the functional (23) for fixed a characterizes the residual distortions associated with the random displacements of the optical beam. As is clear, for example, from the Table, for such correction the variance of the residual distortions associated

with the random displacements of the beam center of gravity stands at roughly 25% of its value in the absence of correction.

In light of the above calculations, it is safe to recommend the following optical system (see Fig.1) working in the atmosphere, which tracks the random wander of the beam center of gravity. A spherical mirror with its central part removed and replaced by a long-focal-length lens serves as the transmitting mirror that forms the optical beam. The displacements of the image center of gravity are registered in the focal plane of this lens using some kind of measuring device. The signal from this device, which is proportional to the components of the random displacement of the focal spot $\rho_{cF} = \{y_{cF}, z_{cF}\}$, is fed to a signal processing system for processing the angular displacements $y_{cF} / F, z_{cF} / F$. This information is then used to vary the instantaneous direction of the beam axis.

In this approach the system can process both displacements of the image of some reference source and radiation reflected by an illuminated object. Here mention should be made of the fundamental possibility of using radiation backscattered by the atmospheric aerosol.

Such an adaptive correction system does not require a phase distortion analyzer; instead, it requires an intensity distribution analyzer, but one with sufficient dynamic range and sufficient frequency range.

The above analysis assumes that the transmitting and measuring channels are coaxial, while a more realistic approach would be to treat the transmitting and measuring channels as having different apertures with the axes of the transmitted and received beams separated in space or tilted one with respect to the other by some angle. For parallel offset of the two beam axes, the correlation falls substantially at distances^{6,10} of the order of κ_0^{-1} . If image quality is what matters, then the relative tilt of the beam axes in the transmitting and measuring channels should not exceed the isoplanatism angle [16], which is defined as the maximum angular separation of two point objects which can be (simultaneously) clearly distinguished when looking through the turbulent medium.

Thus, the given approach allows one to minimize broadening of an optical beam due to random wander of its center of gravity. It should also be noted that because of

the weak selectivity of $K, \langle \rho_{cf}^2 \rangle$ and $\langle \rho_c^2 \rangle$, the transmitting and measuring channels can operate in different wavelength ranges.

Since any system processing random mirror tilts possesses a finite response time (the time constant τ), the degree of correlation K will differ from the value calculated according to formula (4). In general, the degree of correlation K is a function of the response time τ :

$$K(\tau) = \langle \rho_c, \rho_{cf}(\tau) \rangle / [\langle \rho_c^2 \rangle \langle \rho_{cf}^2(\tau) \rangle]^{1/2}, \quad (24)$$

Not repeating the calculations, which are analogous to the foregoing, we obtain the following expression for $K(\tau)$ under the conditions:

$$R_0^2 \gg \frac{x}{k}, \quad \max(aq(\xi), R_0, a) \ll \kappa_0^{-1}, \quad C_n^2(x\xi) = C_n^2, \\ \kappa_0(x\xi) = \kappa_0, \quad v(x\xi) = v$$

$$K(\tau) = -\frac{\sqrt{3}}{2} R_0^{1/6} \left(\frac{a^2}{2} \right)^{1/12} \left(\frac{R_0^2}{2} + \frac{a^2}{4} \right)^{-1/6} {}_1F_1^{1/2} \left(\frac{1}{6}, 1; -\frac{v^2 \tau^2}{2(R_0^2 + a^2/1)} \right). \quad (25)$$

in a wide ($\Omega \gg 1, x/f = 0$) collimated beam. $|K|$ attains its maximum value at $2R_0^2 = a^2$, where

$$K(\tau) = -0.87 {}_1F_1^{1/2} \left(\frac{1}{6}, 1; -\frac{v^2 \tau^2}{2a^2} \right). \quad (26)$$

and for $\tau = 0$ (instantaneous processing) $K(0) = -0.87$, while for larger τ ($v\tau/a \gg 1$)

$$K(\tau) = -0.94 \left(\frac{v\tau}{a} \right)^{-1/6}. \quad (26)$$

As can be seen from (25), a sufficiently high correction efficiency is achieved under the condition

$$\tau < a/v,$$

where a is the initial beam diameter and v is the mean wind speed. Thus, for aperture $a \leq 1$ m and mean wind speed $v = 3 - 5$ m/s, sufficient efficiency of processing requires that the time constant of the system not exceed 0.02s.

The relative decrease of the mean diameter of the image formed by the beam with and without correction can serve as a criterion of the quality of correction for the correction algorithm developed here.

References to Chapter 3.

1. V.P. Lukin, Abstracts of Papers Presented at Fifth All-Union Symposium on Propagation of Laser Radiation in the Atmosphere [in Russian], Part 1, Institute of Atmospheric Optics, Siberian Division, Academy of Sciences of USSR, Tomsk (1979).
2. V.P. Lukin, Correction of random angular displacements of optical beams, *Kvantovaya Elektron.* (Moscow) 7, 1270 - 1279 (June 1980).
3. V.P.Lukin, V.V.Pokasov, Optical wave phase fluctuations, *Applied Optics*, V.20, No.1, p.121-135, 1981,.
4. Lukin V.P., Emaleev O.N., Correction for Angular Displacement of Optical Beams, *Kvantovaya Elektronika*, V.9, No.11, pp.2264-2271, 1982 [*Sov.J.Quantum Electron.*, V.12, No.11, p.144-147, 1982].
5. V.P.Lukin, *Atmosferaia adaptivnaia optika*. (Novosibirsk: Nauka, 1986, 248p.) (V.P.Lukin, *Atmospheric Adaptive Optics*, SPIE Press Volume PM 23, 1996).
6. Klyatskin V.I., Kon A.I., *Izv.VUZov. Radiofizika*, V.15, No.9, 1381(1972).
7. A.S. Gurvich, A.I. Kon, V.L. Mironov, and S.S. Khmelevtsov, *Laser Radiation in Turbulent Atmosphere* [in Russian] (Nauka, Moscow, 1976).
8. V.I. Tatarskii, *Wave Propagation in a Turbulent Medium* (McGraw-Hill, New York (1961); reprint Dover, New York, 1968).
9. Kon A.I., *Izv.VUZov. Radiofizika*, V.13, No.1, 61(1970).
10. J.W. Hardy, *Proc. IEEE* 66, 651 (1978).
11. *J. Opt. Soc. Am.* 67, No. 3 (1977).
12. S. Lawrence, *Appl. Opt.* 14, 2750 (1975).
13. R.F. Lutomorski, W.L. Woodie, and R.G. Buser, *Appl. Opt.* 16, 665 (1977).
14. V.P. Lukin, in: *Propagation of Optical waves in Inhomogeneous Media* [in Russian], Institute of Atmospheric Optics, Siberian Division, Academy of Sciences of USSR, Tomsk (1976), pp. 137-142.
15. A.I. Kon, V.L. Mironov, and V.V. Nosov, *Izv. Vyssh. Uchebn. Zaved Radiofiz.* 17, 1501 (1974).
16. S. Pollaine, A. Buffington, and F.S. Crawford, *J. Opt. Soc. Am.* 69, 84 (1979).

CHAPTER 4. IMPROVEMENT OF THE QUALITY OF AN IMAGE FORMED THROUGH THE ATMOSPHERE BY METHODS OF ADAPTIVE OPTICS

Here we describe the possibilities of improving the quality of images formed by an adaptive optical system through the atmosphere. To correct the image of a star formed by a telescope, mainly two approaches are used: one based on measurements of reference source fields and one based on maximization of the sharpness functional.

In this chapter we will consider correction realized by an adaptive optical system functioning as a system with feedback utilizing information about the instantaneous distribution of the inhomogeneities of the medium in which the propagation takes place. We will make use of algorithms of adaptive control based on the reciprocity principle.

4.1. Adaptive Correction of the Image of an Extended Object

This part of our consideration is based on the paper [Ref.1, 1983]. The quality of the image of an extended object, formed by an optical system through the turbulent atmosphere, can be improved with the help of adaptive correction. To do this, information about the distribution of the turbulent inhomogeneities of the medium along the propagation path is extracted from measurements of reference source fields.

A reference source, as an object with a known amplitude-phase distribution, located at a known distance from the receiver, can be formed directly on the surface of the object being imaged, or it can be located at infinity (a reference star), or, finally, it can be located between the object and the objective.

Let the extended object lie in the plane x_{obj} , the point reference source in the plane x_{ref} , and let the entrance aperture of the telescope be located in the plane x_o . The distribution of the field U_{obj} of the extended object, formed in the x_o plane, is given by

$$U(x_o, \rho) = \iint d^2 \rho_1 U_{obj}(\rho_1) G(x_o, \rho; x_{obj}, \rho_1). \quad (1)$$

$G(x_o, \rho; x_{obj}, \rho_1)$ is the Green's function of the turbulent atmosphere between the planes x_o and x_{obj} . We will denote the entrance aperture of the telescope as $W(\rho)$, and we

will replace the action of the telescope by an equivalent lens introducing the phase term $\exp(-ik\rho^2 / 2f)$, where f is the equivalent focal length of the telescope.

We assume that the correction is based on the phase conjugation algorithm using measurements of the phase of the wave from the reference source. In this regard, if the reference source is so small or so far away that it is not resolved by the optical system of the telescope, it can be treated as a point source. The phase of the wave (with wave number $k = 2\pi / \lambda$) from the reference source in the entrance aperture plane x_0 can be written as

$$S_{ref}(x_0, \rho) = \frac{k\rho^2}{2(x_{ref} - x_0)} + S(x_0, \rho; x_{ref}, 0), \quad (2)$$

where $S(x_0, \rho; x_{ref}, 0)$ is the random phase due to turbulence of a spherical wave as it propagates from the x_{ref} plane to the x_0 plane. We assume that the point source is located on the optical axis of the telescope. This means that the conditions of the experiment allow us to form the reference source on the same optical axis as that on which the object is located. Here we are not discussing techniques for forming reference sources.

There are a great number of techniques for separating out the diffraction phase $k\rho^2 / 2(x_{ref} - x_0)$ from $S(x_0, \rho; x_{ref}, 0)$ in expression (2). With the purely turbulent contribution to the phase of the reference source (2) thus available to us, we can solve the correction problem using either the phase conjugation (PC) algorithm or the total phase conjugation (TPC) algorithm.

The TPC algorithm uses the total phase (2) to correct the wave front and because of this forms a beam of arbitrary geometry only in the plane of the reference source. If we succeed in whatever way in separating the diffraction phase from the turbulent phase in (2), we can apply the PC algorithm for the purpose of beam formation in an arbitrary plane (different from the plane of the reference source), or for image correction. Here, however, it is necessary that the turbulence-induced phase of the reference source measured in the x_0 plane practically coincide with the phase of the object field over the entire path to the object.

This can be realized, for example, along slant paths, where the turbulent intensity $C_n^2(h)$ decreases with height h . The reference source upon which the experimental

scheme in question is based should be located somewhat higher than the effective layer of atmospheric turbulence H_{eff} , and the choice of its location is governed by the condition

$$\frac{\int_{H_0}^{\infty} dh C_n^2(h) - \int_{H_0}^{H_{eff}} dh C_n^2(h)}{\int_{H_0}^{\infty} dh C_n^2(h)} \leq \varepsilon,$$

where ε is determined by the admissible level of residual distortions in the optical wave in which the aberration-free image is being formed. Here it is assumed that the object is located practically at infinity, i.e., outside the atmosphere. H_0 is the height of the entrance aperture of the telescope.

Let us consider the phase-conjugation algorithm (PC) in detail, employing it only within the limits of the aperture $W(\rho)$. Then the corrected field is written as

$$U_c(x_0, \rho) = W(\rho) \frac{G^*(x_0, \rho; x_{ref}, 0)}{G_0^*(x_0, \rho; x_{ref}, 0)} \iint d^2 \rho_1 U_{obj}(\rho_1) G(x_0, \rho; x_{obj}, \rho_1). \quad (3)$$

The ratio $G^*(x_0, \rho; x_{ref}, 0) / G_0^*(x_0, \rho; x_{ref}, 0)$ is called the correction function. The corrected field in the image plane of the object x'_{obj} is formed in the same way as in a "thin lens":

$$U_{im}(x'_{obj}, \rho) = \iint d^2 \rho_2 U_c(x_0, \rho_2) \exp(-ik\rho_2^2 / 2f) G(x'_{obj}, \rho; x_0, \rho_2). \quad (4)$$

Here it is assumed that the image is formed in vacuum in the optical system of the telescope. Adding quantities (3) and (4), we

$$U_{im}(x'_{obj}, \rho) = \iint d^2 \rho_1 d^2 r_2 W(\rho_1) \exp(-ik\rho_1^2 / 2f) G_0(x'_{obj}, \rho; x_0, \rho_1) \times \\ \times U_{obj}(r_1) G^*(x_0, \rho_1; x_{ref}, 0) G(x_0, \rho_1; x_{obj}, r_1) / G_0^*(x_0, \rho_1; x_{ref}, 0) \quad (5)$$

As a result, if the ratio

$$G^*(x_0, \rho_1; x_{ref}, 0) / G_0^*(x_0, \rho_1; x_{ref}, 0) = \exp(-iS(x_0, \rho_1; x_{ref}, 0)),$$

then the average intensity distribution in the image plane x' is equal to

$$\begin{aligned}
\langle I_{im}(x'_{obj}, \rho) \rangle = & \iint d^4 \rho_{1,2} d^4 r_{1,2} \exp(-ik(\rho_1^2 - \rho_2^2) / 2f) W(\rho_1) \\
& \times W(\rho_2) G_0(x_0, \rho_1; x'_{obj}, \rho) G_0^*(x_0, \rho_2; x'_{obj}, \rho) U_{obj}(\mathbf{r}_1) U_{obj}^*(\mathbf{r}_2) \\
& \times G_0^*(x_0, \rho_2; x_{obj}, \mathbf{r}_2) G_0(x_0, \rho_1; x_{obj}, \mathbf{r}_1) \langle \exp\{i([S(x_0, \rho_1; x_{ref}, 0) \\
& - S(x_0, \rho_2; x_{ref}, 0)] - [S(x_0, \rho_1; x_{obj}, \mathbf{r}_1) - S(x_0, \rho_2; x_{obj}, \mathbf{r}_2)])\} \rangle.
\end{aligned} \tag{6}$$

Here we have used the phase approximation for the Green's function expressed as $G = G_0 \exp(iS)$, where S is the random phase due to turbulence, calculated in the geometric-optics approximation, and the angular brackets $\langle \dots \rangle$ indicate averaging over the ensemble of turbulent fluctuations.

Below, for convenience, we will denote the expression standing inside the angular brackets in expression (6) simply as $\langle \dots \rangle$. In the calculation of $\langle \dots \rangle$ we will assume that the fluctuations of the phase S are Gaussian, whence it follows that

$$\begin{aligned}
\langle \dots \rangle = & \exp \left\{ -\frac{1}{2} D_S(x_0, \rho_1 - \rho_2; x_{ref}, 0) - \frac{1}{2} D_S(x_0, \rho_1 - \rho_2; x_{obj}, \mathbf{r}_1 - \mathbf{r}_2) \right. \\
& + \langle S(x_0, \rho_1; x_{ref}, 0) S(x_0, \rho_1; x_{obj}, \mathbf{r}_1) \rangle \\
& - \langle S(x_0, \rho_2; x_{ref}, 0) S(x_0, \rho_2; x_{obj}, \mathbf{r}_2) \rangle \\
& - \langle S(x_0, \rho_1; x_{ref}, 0) S(x_0, \rho_2; x_{obj}, \mathbf{r}_2) \rangle \\
& \left. + \langle S(x_0, \rho_2; x_{ref}, 0) S(x_0, \rho_1; x_{obj}, \mathbf{r}_1) \rangle \right\},
\end{aligned} \tag{7}$$

where $D_S(x_0, \rho_1 - \rho_2; x_{obj}, \mathbf{r}_1 - \mathbf{r}_2)$ is the phase structure function of two spherical waves whose sources are separated by the displacement $\mathbf{r}_1 - \mathbf{r}_2$, and whose observation points, by the vector $\rho_1 - \rho_2$. Let us consider correlation functions of the type $\langle S(x_0, \rho_1; x_{ref}, 0) S(x_0, \rho_1; x_{obj}, \mathbf{r}_1) \rangle$ in more detail. Since the random phase in the geometric-optics approximation can be represented in the form of an expansion

$$S(x_0, \rho; x_{ref}, 0) = k \int_{x_0}^{x_{ref}} d\xi \iint dn(\kappa, \xi) \exp \left(i k \rho \frac{\xi}{(x_{ref} - x_0)} \right), \tag{8}$$

the given correlation can be written as

$$\begin{aligned}
\langle S(x_{ref}, \rho_1) S(x_{obj}, \rho_2) \rangle &= k^2 \int_{x_0}^{x_{ref}} d\xi_2 \iint \langle dn(\kappa_1, \xi_1) dn(\kappa_2, \xi_2) \rangle \\
&\times \exp \left\{ i \left(\kappa_1 \rho_1 \frac{\xi_1}{(x_{ref} - x_0)} + \kappa_2 \rho_2 \frac{\xi_2}{(x_{ref} - x_0)} \right) \right\}.
\end{aligned} \tag{9}$$

Using the representation

$$\langle dn(\kappa_1, \xi_1) dn(\kappa_2, \xi_2) \rangle = 2\pi \delta(\xi_1 - \xi_2) \delta(\kappa_1 + \kappa_2) \Phi_n(\kappa_1, \xi_1) d^2 \kappa_1 d^2 \kappa_2,$$

we can transform expression (9) into the following form:

$$\begin{aligned}
\langle S(x_{ref}, \rho_1) S(x_{obj}, \rho_2) \rangle &= 2\pi k^2 \int_{x_0}^{x_{ref} \leq x_{obj}} d\xi \iint d^2 \kappa \Phi_n(\kappa, \xi) \\
&\times \exp \left\{ i \kappa \xi / (x_{ref} - x_0) \left[\rho_1 - \rho_2 \left(\frac{x_{ref} - x_0}{x_{obj} - x_0} \right) \right] \right\},
\end{aligned}$$

where $\Phi_n(\kappa, \xi)$ is the spectral density of the refractive index fluctuations.

Thus, in the geometric-optics approximation

$$\begin{aligned}
&S(x_0, \rho_1; x_{ref}, 0) S(x_0, \rho_2; x_{obj}, \mathbf{r}_1) > \\
&= B_s \left(x_0, \rho_1 - \rho_2; x_{ref}, \mathbf{r}_1 \left(\frac{x_{ref} - x_0}{x_{obj} - x_0} \right) \right).
\end{aligned} \tag{10}$$

Now, taking (10) into account, we bring (7) into the form

$$\begin{aligned}
\langle \dots \rangle &= \exp \left\{ -\frac{1}{2} D_s(x_0, \rho_1 - \rho_2; x_{ref}, 0) - \frac{1}{2} D_s(x_0, \rho_1 - \rho_2; x_{obj}, \mathbf{r}_1 - \mathbf{r}_2) \right. \\
&\quad - \frac{1}{2} D_s \left(x_0, 0; x_{ref}, \mathbf{r}_1 \left(\frac{x_{ref} - x_0}{x_{obj} - x_0} \right) \right) \\
&\quad + \frac{1}{2} D_s \left(x_0, \rho_1 - \rho_2; x_{ref}, \mathbf{r}_1 \left(\frac{x_{ref} - x_0}{x_{obj} - x_0} \right) \right) \\
&\quad + \frac{1}{2} D_s \left(x_0, \rho_1 - \rho_2; x_{ref}, \mathbf{r}_2 \left(\frac{x_{ref} - x_0}{x_{obj} - x_0} \right) \right) \\
&\quad \left. - \frac{1}{2} D_s \left(x_0, 0; x_{ref}, \mathbf{r}_2 \left(\frac{x_{ref} - x_0}{x_{obj} - x_0} \right) \right) \right\}.
\end{aligned} \tag{11}$$

Making use of the representation of the Green's function in free space, we can rewrite expression (6) as

$$\begin{aligned} \langle I_{lm}(x'_{obj}, \rho) \rangle = & \frac{k^4}{16\pi^2(x_0 - x'_{obj})^2(x_{obj} - x_0)^2} \iint d^4\rho_{1,2} d^4r_{1,2} W(\rho_1) W^*(\rho_2) \\ & \times U_{obj}(r_2) \exp \left\{ -ik \frac{(\rho_1^2 - \rho_2^2)}{2f} + ik \frac{(\rho_1 - \rho)^2}{2(x_0 - x'_{obj})} \right. \\ & \left. - ik \frac{(\rho_2 - \rho)^2}{2(x_0 - x'_{obj})} + ik \frac{(r_1 - \rho_1)^2}{(x_{obj} - x_0)} - ik \frac{(r_2 - \rho_2)^2}{2(x_{obj} - x_0)} \right\} \langle \dots \rangle. \end{aligned} \quad (12)$$

Let us first consider the diffraction terms in expression (12), which condition the formation of the image in vacuum. We choose as the image plane the x' plane, which is the plane conjugate to the x plane. From the condition for conjugate planes we have

$$1/(x_0 - x'_{obj}) - 1/(x_{obj} - x_0) = 1/f \quad (13)$$

and since $(x_{obj} - x_0) \gg f, x_0 - x'_{obj}$, we arrive at the conclusion that

$$1/(x_0 - x'_{obj}) = 1/f.$$

Consequently, remote objects are practically always imaged at the focus. On the basis of this result it is possible to simplify the diffraction terms in expression (12). It then follows that in vacuum the intensity distribution in the focal plane has the following form:

$$\begin{aligned} I(f, \rho) = & \frac{k^4}{16\pi^2 f^2 (x_{obj} - x_0)^2} \iint d^4\rho_{1,2} d^4r_{1,2} W(\rho_1) W^*(\rho_2) U_{obj}(r_1) \\ & \times U_{obj}^*(r_2) \exp \left\{ -ik \frac{\rho(\rho_1 - \rho_2)}{f} + ik \frac{[(r_1 - \rho_1)^2 - (r_2 + \rho_2)^2]}{2(x_{obj} - x_0)} \right\}. \end{aligned} \quad (14)$$

If we assume a Gaussian object $U_{obj}(r) = \exp(-r^2/2a_{obj}^2)$ (a_{obj} is the effective radius of the object), we have

$$\begin{aligned} I(f, \rho) = & \frac{k^2 \Omega_{obj}^2}{4\pi^2 f^2 (1 + \Omega_{obj}^2)} \iint d^4\rho_{1,2} W(\rho_1) W^*(\rho_2) \exp \left\{ -ik \frac{\rho(\rho_1 - \rho_2)}{f} \right. \\ & \left. + i \frac{k}{2(x_{obj} - x_0)} (\rho_1^2/(1 - i\Omega_{obj}) - \rho_2^2/(1 + i\Omega_{obj})) \right\} \end{aligned} \quad (15)$$

where $\Omega_{obj} = k a_{obj}^2 / (x_{obj} - x_0)$.

Let us turn to the case of image correction. Here it should be noted that there is one term (the second) in the exponent in expression (11) that determines the fluctuations in a system without correction, which depends on the integration over the entire path from the object to the telescope; the remaining terms are associated with correction. In the calculations we use the following expression for the phase structure function:

$$D_s(x, \rho_1 - \rho_2; \mathbf{r}_1 - \mathbf{r}_2) = 2.91k^2 \int_{x'}^x d\xi C_n(\xi) \left| \frac{(\xi - x')}{(x - x')} (\rho_1 - \rho_2) + \frac{(x - \xi)}{(x - x')} (\mathbf{r}_1 - \mathbf{r}_2) \right|^{5/3}. \quad (16)$$

The refractive index structure characteristic in the integrand in (16) depends on the integration variable, namely the distance covered along the propagation path.

Let us consider the case of vertical propagation (telescope pointed at zenith). In the calculations we allow for the altitude dependence of C_n^2 . This dependence is realized in practice in the form of various models.

Let us carry out an estimate based on the following model:

$$C_n^2(x) = \begin{cases} C_{n_0}^2 (x/x_0)^{-2/3}, & x_0 \leq x \leq x_t, \\ C_{n_t}^2 (x/x_t)^{-4/3}, & x > x_t, \end{cases} \quad (17)$$

where $C_{n_0}^2$ is the value of the structure characteristic at the initial altitude, x_t is the altitude at which the 2/3-power dependence goes over to the 4/3-power dependence, and $C_{n_t}^2 = C_{n_0}^2 (x_t/x_0)^{-2/3}$. Thus, this model is defined by the parameters x_t and $C_{n_0}^2$.

In the calculations connected with formula (11) we require that $x_{obj}, x_{ref} > x_t$.

Substituting expression (16) into formula (11), after combining like terms we have

$$\begin{aligned}
\langle \dots \rangle = \exp \left\{ -1.46k^2 |\mathbf{r}_1 - \mathbf{r}_2|^{5/3} (x_{obj} - x_0)^{-5/3} \int_{x_0}^{x_{obj}} (\xi - x_0)^{5/3} C_n^2(\xi) d\xi \right. \\
- 1.46k^2 |\rho_1 - \rho_2|^{5/3} (x_{obj} - x_0)^{-5/3} \int_{x_{ref}}^{x_{obj}} (x_{obj} - \xi)^{5/3} C_n^2(\xi) d\xi \\
\left. - 1.46k^2 |\rho_1 - \rho_2|^{5/3} \int_{x_0}^{x_{ref}} \left[\left(\frac{x_{obj} - \xi}{x_{obj} - x_0} \right)^{5/3} - \left(\frac{x_{ref} - \xi}{x_{ref} - x_0} \right)^{5/3} \right] C_n^2(\xi) d\xi \right\}.
\end{aligned} \quad (18)$$

Here note that \mathbf{r}_1 and \mathbf{r}_2 are the integration variables over the object, and ρ_1 and ρ_2 , over the aperture of the telescope. Analysis of expression (18) reveals that the term containing $|\mathbf{r}_1 - \mathbf{r}_2|^{5/3}$ (the object variables) is the same as in the absence of correction. It is just this term that is determined by the action of the so-called non-isoplanatism of the atmosphere.

This parameter is connected with the problem of constructing the image of an extended object. There are two terms in expression (18) containing $|\rho_1 - \rho_2|^{5/3}$ (the variables of the entrance aperture of the telescope), one of which is determined by inhomogeneities in the region between the reference source and the object (this part remains uncompensated since the reference source is located closer than the object to the objective), and the other, by the inhomogeneities between the objective and the reference source (its presence is due to the inequality of the curvature of the spherical waves arriving from the reference source and from the object plane).

It is clear that for model (17) the altitude region corresponding to the 2/3 power gives the greatest contribution, and for this reason it is always necessary to choose $x_{ref} > x_i$. In this regard, all the integrals in expression (18) can be divided into two parts:

$$\int_{x_0}^{x_{obj}} d\xi(\dots) = \int_{x_0}^{x_i} d\xi(\dots) + \int_{x_i}^{x_{obj}} d\xi(\dots) \quad (19)$$

If the 2/3-power region of spectrum (17) is absent, then the first term in (19) is equal to zero. Substituting model (17) into (18), we arrive at the formula

$$\begin{aligned}
\langle \dots \rangle = & \exp \left\{ -1.46k^2 |\mathbf{r}_1 - \mathbf{r}_2|^{5/3} \left[\frac{11}{6} C_{n_0}^2 \frac{x_0^{2/3} (x_t - x_0)^2}{x_{obj}^{5/3}} \right. \right. \\
& + \frac{3}{4} C_{n_1}^2 \left(\frac{x_t^{4/3}}{x_0^{1/3}} - \frac{x_t^{4/3} (x_t - x_0)^{4/3}}{x_{obj}^{5/3}} \right) \left. \right] - 1.46k^2 |\rho_1 - \rho_2|^{5/3} \frac{5}{4} C_{n_0}^2 x_0^{2/3} \\
& \times \left(\frac{x_t^{4/3}}{x_{ref}} - \frac{x_0^{4/3}}{x_{ref}} \right) - 1.46k^2 |\rho_1 - \rho_2|^{5/3} 3C_{n_1}^2 \left[x_t^{4/3} (x_t^{-1/3} - x_{ref}^{-1/3}) \right. \\
& \left. \left. - x_t (1 - x_t/x_{ref})^{5/3} \right] \right\}.
\end{aligned} \tag{20}$$

Now let us consider each of the terms in (20) separately. First, let us turn our attention to the term containing $|\mathbf{r}_1 - \mathbf{r}_2|^{5/3}$. It determines what objects can be seen clearly and in their entirety in the objective at a given level of turbulence along the path, and does not undergo any change upon correction. Consequently, correction with one reference source does not remove the problem of non-isoplanatism, and for correction of the image of a large object it is necessary to form several reference sources. In order to be able to calculate further, we introduce the quantity r_a , the radius of the isoplanar region, as follows:

$$\begin{aligned}
1.46k^2 |\mathbf{r}_1 - \mathbf{r}_2|^{5/3} \left[\frac{11}{6} C_{n_0}^2 \frac{x_0^{2/3} (x_t - x_0)^2}{x_{obj}^{5/3}} + \frac{3}{4} C_{n_1}^2 (x_t^{4/3} / x_{obj}^{1/3} \right. \\
\left. - x_t^{4/3} (x_t - x_0)^{4/3} / x_{obj}^{5/3} \right] = |\mathbf{r}_1 - \mathbf{r}_2|^{5/3} / r_a^{5/3}.
\end{aligned} \tag{21}$$

In this context, we say that the object is located in the isoplanar region if $a_{obj} < r_a$. The quantity r_a has a simple physical meaning. From formula (21), taking into account only the first (and main) term, we have

$$r_a = \frac{x_{obj}}{(x_t - x_0)} \left(2.68k^2 C_{n_0}^2 x_0^{2/3} (x_t - x_0)^{1/3} \right)^{-3/5},$$

or

$$\frac{r_a}{x_{obj}} = \frac{\left(2.68k^2 C_{n_0}^2 x_0^{2/3} (x_t - x_0)^{1/3} \right)^{-3/5}}{(x_t - x_0)}.$$

Thus it turns out that the region of isoplanatism in the object plane is discernible from a distance equal to the range of the object at the same angle at which the coherence radius of the layer of atmosphere is discernible through this layer. Let us consider the term containing $|\rho_1 - \rho_2|^{5/3}$:

$$1.46k^2|\rho_1 - \rho_2|^{5/3} \left\{ \frac{5}{4} C_{n_0}^2 x_0^{2/3} (x_t^{4/3} - x_0^{4/3}) / x_{ref} + C_{n_1}^2 [x_t \times (1 - x_t^{1/3} / x_{ref}^{1/3}) - x_t (1 - x_t / x_{ref})^{5/3}] \right\}. \quad (22)$$

Note that for $x_t \gg x_0$ this term reduces to

$$1.46 \cdot \frac{5}{4} k^2 |\rho_1 - \rho_2|^{5/3} C_{n_0}^2 x_0^{2/3} x_t^{4/3} / x_{ref}.$$

Let us compare it with the same term in the case of no correction:

$$7 \cdot 1.46k^2 |\rho_1 - \rho_2|^{5/3} C_{n_0}^2 x_0^{2/3} x_t^{1/3}.$$

The action of correction is characterized by a relative decrease of the fluctuations proportional to x_t / x_{ref} . Term (22) can be represented in analogy with the phase structure function in the absence of correction as $|\rho_1 - \rho_2|^{5/3} / r_{eff}^{5/3}$, where r_{eff} is the effective coherence radius.

Summing up all these results, we obtain the following expression for an object having Gaussian shape:

$$\begin{aligned} \langle I(f, \bar{\rho}) \rangle = & \frac{k^4}{16\pi^4 f^2 (x_{obj} - x_0)^2} \iint d^4 \rho_{1,2} W(\rho_1) W^*(\rho_2) \times \\ & \times \exp \left\{ -ik \frac{\rho(\rho_1 - \rho_2)}{f} + ik \frac{(\rho_1^2 - \rho_2^2)}{2(x_{obj} - x_0)} \right\} \iint d^4 r_{1,2} \exp \left\{ -\frac{r_1^2}{2a_{obj}^2} \times \right. \\ & \times (1 - i\Omega_{obj}) - ik \frac{r_1 \rho_1}{(x_{obj} - x_0)} - \frac{r_2^2}{2a_{obj}^2} (1 + i\Omega_{obj}) + \\ & \left. + ik \frac{r_2 \rho_2}{(x_{obj} - x_0)} - |r_1 - r_2|^{5/3} / r_a^{5/3} - |\rho_1 - \rho_2|^{5/3} / r_{eff}^{5/3} \right\}. \end{aligned} \quad (23)$$

which can be compared with the diffraction-limited result (12). Calculating out the diffraction integral gives the following results:

$$\iint d^2 r_1(\dots) = 2\pi a_{obj}^2 / (1 - i\Omega_{obj}) \exp\left\{-k\rho_1^2 \Omega_{obj} / [2(x_{obj} - x_0)(1 - i\Omega_{obj})]\right\},$$

for a circular aperture

$$W(\rho) = \begin{cases} 1, & \rho \leq R, \\ 0, & \rho > R, \end{cases}$$

$$\begin{aligned} \iint d^2 \rho_1 W(\rho_1) \exp\left\{-\rho_1^2 \left[\frac{k}{2(x_{obj} - x_0)} \cdot \frac{\Omega_{obj}}{(1 - i\Omega_{obj})} - i \frac{k}{2(x_{obj} - x_0)} \right] - \right. \\ \left. - ik \frac{\rho \rho_1}{f} \right\} = \pi R^2 \frac{J_1\left(\frac{k\rho R}{f}\right)}{\left(\frac{k\rho R}{2f}\right)} - \pi R^2 \frac{\Omega_R}{4} \left(\frac{\Omega_{obj} - i}{1 + \Omega_{obj}^2} \right) \times \\ \times {}_1F_2\left(2; 1, 3; \frac{k^2 \rho^2 R^2}{4f^2}\right); \Omega_R = \frac{kR^2}{(x_{obj} - x_0)}. \end{aligned}$$

Finally we arrive at following expression for $\Omega_R < \Omega_{obj}$:

$$\begin{aligned} I_0(\rho) = \frac{k^2 R^4 \Omega_{obj}^2}{\pi^2 f^2 (1 + \Omega_{obj}^2)} \left\{ \frac{J_1^2\left(\frac{k\rho R}{f}\right)}{\left(\frac{k\rho R}{f}\right)^2} - \frac{\Omega_R \Omega_{obj}}{4(1 + \Omega_{obj}^2)} \cdot \frac{J_1\left(\frac{k\rho R}{f}\right)}{\left(\frac{k\rho R}{f}\right)} \times \right. \\ \left. \times {}_1F_2\left(2; 1, 3; \frac{k^2 \rho^2 R^2}{4f^2}\right) + \frac{\Omega_R^2}{64(1 + \Omega_{obj}^2)} {}_1F_2\left(2; 1, 3; \frac{k^2 \rho^2 R^2}{4f^2}\right) \right\} \end{aligned} \quad (24)$$

for the case when the image of a Gaussian object is formed in the telescope in the absence of turbulence.

In order to carry out the corresponding calculations in (23) without using a computer, we use the quadratic approximation. We introduce the optical transfer function $\langle \tau(\vec{r}) \rangle$ for the system atmosphere-telescope :

$$\langle I(f, \rho) \rangle = \frac{k^2}{4\pi^2 f^2} \iint d^2 r \langle \tau(\vec{r}) \rangle \exp(-ik\vec{r} \cdot \vec{\rho}/f). \quad (25)$$

After some simple calculations we arrive at the formula

$$\begin{aligned}
\langle \tau(\mathbf{r}) \rangle = & \frac{\Omega_{obj}^2}{(1 + \Omega_{obj}^2 + 4\Omega_{obj}/\Omega_a)} \exp\left\{-\frac{r^2}{r_{eff}^2} - \frac{kr^2}{4(x_{obj} - x_0)}\right\} \times \\
& \times \frac{\Omega_{obj}(1 + 4\Omega_{obj}/\Omega_a)}{(1 + 4\Omega_{obj}/\Omega_a + \Omega_{obj}^2)} \left\{ \iint d^2x W(\mathbf{x} + \mathbf{r}/2) W(\mathbf{x} - \mathbf{r}/2) \times \right. \\
& \times \exp\left\{-\frac{kx^2}{(x_{obj} - x_0)} \cdot \frac{\Omega_{obj}}{(1 + 4\Omega_{obj}/\Omega_a + \Omega_{obj}^2)} + ik \frac{\mathbf{x}\mathbf{r}}{4(x_{obj} - x_0)} \times \right. \\
& \left. \left. \times \frac{(1 + 4\Omega_{obj}/\Omega_a)}{(1 + 4\Omega_{obj}/\Omega_a + \Omega_{obj}^2)} \right\}, \quad \Omega_a = kr_a^2/(x_{obj} - x_0).
\end{aligned}$$

Calculating further for the optical transfer function $\langle \tau(\mathbf{r}) \rangle$ for a Gaussian aperture $W(x) = \exp(-x^2/2R^2)$, we obtain

$$\begin{aligned}
\langle \tau(\mathbf{r}) \rangle = & \frac{\pi R^2 \Omega_{obj}^2}{(1 + 4\Omega_{obj}/\Omega_a + \Omega_R \Omega_{obj} + \Omega_{obj}^2)} \exp\left\{-\frac{r^2}{4R^2} \left[1 + \right. \right. \\
& + 4 \frac{\Omega_R}{\Omega_{eff}} + \frac{\Omega_R \Omega_{obj}(1 + 4\Omega_{obj}/\Omega_a)}{(1 + 4\Omega_{obj}/\Omega_a + \Omega_{obj}^2)} + \\
& \left. \left. + \frac{\Omega_R^2(1 + 4\Omega_{obj}/\Omega_a)^2}{(1 + 4\Omega_{obj}/\Omega_a + \Omega_{obj}^2)(1 + 4\Omega_{obj}/\Omega_a + \Omega_{obj}^2 + \Omega_R \Omega_{obj})} \right] \right\}.
\end{aligned} \tag{26}$$

If the beam is propagating through vacuum, we have the following expression:

$$\begin{aligned}
\tau_0(r) = & \frac{\pi R^2 \Omega_{obj}^2}{(1 + \Omega_R \Omega_{obj} + \Omega_{obj}^2)} \exp\left\{-\frac{r^2}{4R^2} \left[1 + \frac{\Omega_R \Omega_{obj}}{(1 + \Omega_{obj}^2)} + \right. \right. \\
& \left. \left. + \frac{\Omega_R^2}{(1 + \Omega_{obj}^2) + (1 + \Omega_R \Omega_{obj} + \Omega_{obj}^2)} \right] \right\}
\end{aligned} \tag{27}$$

for the optical transfer function of a telescope imaging a Gaussian beam. Let us analyze the case $(\Omega_{obj}^2 \gg \Omega_{obj}/\Omega_a, \Omega_{obj} \gg 1, \Omega_{obj} > \Omega_R)$ in detail. From (26) and (27) we have

$$\begin{aligned} \langle \tau_0(r) \rangle = \tau_0(r) \exp \left\{ -\frac{r^2}{4R^2} \left[\frac{4\Omega_R}{\Omega_{eff}} + \frac{4\Omega_R}{\Omega_a} + \right. \right. \\ \left. \left. + \Omega_R^2 \left(\frac{(1 + 4\Omega_{obj}/\Omega_a)^2}{\Omega_{obj}^4} - \Omega_{obj}^{-4} \right) \right] \right\}. \end{aligned} \quad (28)$$

Thus, the optical transfer function (28) depends substantially on the ratio of the entrance radius of the telescope to the effective coherence radius ($\Omega_R/\Omega_{eff} = R^2/r_{eff}^2$), and of the radius of the object to the radius of the isoplanatism zone ($\Omega_{obj}/\Omega_a = a_{obj}^2/r_a^2$), and also on combinations of these parameters. If the conditions $\Omega_R < \Omega_{eff}$, $\Omega_{obj} < \Omega_a$, and $\Omega_R < \Omega_{obj}$ are fulfilled, i.e.: if the object occupies one isoplanar zone, then the effective coherence radius exceeds the radius of the entrance aperture and the falloff scale of $\langle \tau(r) \rangle$ coincides with the falloff scale of $\tau_0(r)$. It is easy to see that for a plane wave ($\Omega_{obj} \rightarrow \infty$) the Fourier transform of (27), analogous to (25), is written as

$$I_0(\rho) = \frac{k^2 R^4}{f^2} \exp(-k^2 \rho^2 R^2 / f^2). \quad (29)$$

Both for a Gaussian and a circular aperture (26) in vacuum the intensity distribution of the image is substantially decreased at distances $\rho \approx f/kR$. Correspondingly, the scale of the optical transfer function $\tau_0(r)$ is equal to the radius of the entrance aperture of the telescope R . Transforming (28), we have

$$\begin{aligned} \langle \tau(r) \rangle = \tau_0(r) \exp \left\{ -\frac{r^2}{4R^2} \left[4 \frac{\Omega_R}{\Omega_{eff}} + 4 \frac{\Omega_R}{\Omega_a} + 8 \frac{\Omega_R^2}{\Omega_{obj}^2} \left(\frac{2}{\Omega_{obj}\Omega_a} + \frac{4}{\Omega_{obj}^2} \right) \right] \right\} \\ \approx \tau_0(r) \exp \left\{ -r^2 (1/r_{eff}^2 + 1/r_a^2) \right\}, \end{aligned} \quad (30)$$

where

$$\begin{aligned} \tau_0(r) \cong \pi R^2 \exp \left\{ -\frac{r^2}{4R^2} \left[1 + \frac{\Omega_R}{\Omega_{obj}} + \frac{\Omega_R^2}{\Omega_{obj}^4} \right] \right\} \approx \\ \approx \pi R^2 \exp \left\{ -\frac{r^2}{4R^2} (1 + \Omega_R/\Omega_{obj}) \right\}. \end{aligned} \quad (31)$$

We renormalize $\tau_0(r)$ as in Ref. 287 [$\tau_0(0) = 1$].

Employing the optical transfer function introduced in this way, we can calculate one of the functions which determine the quality of the combined optical system atmosphere-telescope, namely the resolution

$$\mathfrak{R} = \iint d^2\kappa < \tau(\kappa) >, \quad (32)$$

where $\kappa = kr/f$ is the spatial frequency. Integrating over the spatial frequencies directly in expression (26), we obtain

$$\mathfrak{R} = \frac{2\pi k^2 \Omega_{obj}^2 R^2 f^{-2}}{(1 + 4\Omega_{obj}/\Omega_a + \Omega_{obj}^2 + \Omega_R \Omega_{obj})} \left[1 + 4 \frac{\Omega_R}{\Omega_{eff}} + \frac{\Omega_R \Omega_{obj} (1 + 4\Omega_{obj}/\Omega_a)}{(1 + 4\Omega_{obj}/\Omega_a + \Omega_{obj}^2)} \right. \\ \left. + \Omega_R^2 (1 + 4\Omega_{obj}/\Omega_a)^2 / [(1 + 4\Omega_{obj}/\Omega_a + \Omega_{obj}^2) \times (1 + 4\Omega_{obj}/\Omega_a + \Omega_R \Omega_{obj} + \Omega_{obj}^2)] \right]$$

(33)

The resolution \mathfrak{R} , as a measure of the optical quality of the system, determines the magnitude of the minimal resolvable distance $\delta l \approx \frac{1}{2\sqrt{\mathfrak{R}}}$. The optical system has its maximum resolution in vacuum, and it is determined by the parameters R, λ , and f for a planar wavefront:

$$\delta l_0 = \frac{f}{2\sqrt{2\pi k R}}.$$

In a turbulent medium the limiting resolution (the minimum value of δl) for an arbitrarily large telescope (the limit $R \rightarrow \infty$) is determined by the coherence radius r_0 :

$$\delta l_{\min} \approx \frac{f}{2\sqrt{2\pi k r_0}}, \quad r_0 \ll R. \quad (34)$$

It is just this circumstance that lowers the efficiency of large telescopes. Practically speaking, $R = 2r_0$ represents the limit of resolution for large telescopes. Application of adaptive correction to a telescope increases its limiting resolution. Applying (33) to the case $\Omega_{obj} \gg \Omega_R, \Omega_{obj} \gg 1$, we obtain

$$\mathfrak{R} \cong 2\pi k^2 \left[f^2 \left(\frac{1}{R^2} + \frac{4}{r_{eff}^2} + \frac{4}{r_a^2} \right) \right]. \quad (35)$$

Consequently, the resolution is determined by the minimal value of the radius of the telescope R , the effective coherence radius r_{eff} , and the radius of isoplanatism r_a . For

given telescope radius and height of the object -- and it is the latter which determines the isoplanatism angle (and the isoplanatism radius r_a), it is possible, by appropriate choice of the location of the reference source x_{ref} , to increase r_{eff} . If we locate the reference source on the object itself (in practice this means $r_{eff} = \infty$), we have

$$\mathfrak{R} \cong 2\pi k^2 \left/ \left[f^2 \left(\frac{1}{R^2} + \frac{4}{r_a^2} \right) \right] \right. \quad (36)$$

In this case the resolution of the system in the object plane is limited by the radius of the isoplanatism region r_a . From (35) we have

$$\delta l = \frac{f}{2\sqrt{2\pi kR}} \left(1 + \frac{4R^2}{r_{eff}^2} + \frac{4R^2}{r_a^2} \right)^{1/2},$$

i.e., the objective of the telescope becomes diffraction-limited under the condition that $R < r_a$, $R < r_{eff}$. If one of these conditions is not met, the quality of the optical system is decreased. For all intents, in this case, the radius of an objective having limiting efficiency

$$R \geq 2 \left/ \left[\frac{1}{r_{eff}^2} + \frac{1}{r_a^2} \right] \right.^{1/2}, \quad (37)$$

and for the reference source on the object ($r_{eff} = \infty$)

$$R_{lim} \geq 2r_a. \quad (38)$$

We find that by choosing the position of the reference source we can change the radius of the aperture that gives maximum efficiency (37) all the way to the limit R_{lim} (38).

In conclusion we can state that an adaptive optical system working in the atmosphere using a reference source can achieve a substantially increased efficiency. The choice of the height of the reference source is determined both by the form of the profile C_n^2 along the propagation path and by the level of permissible residual distortions. The optical system forms an aberration-free image only of one isoplanar region. If the angular dimensions of the object exceed this region, then using only one reference source it is not possible to obtain a diffraction-limited image. The dimension of this isoplanar region depends linearly on the distance, and the isoplanatism angle (the ratio of the radius of the object to the distance from the observation plane to the object) coincides with the angle at which the coherence radius of the atmosphere is

discernible within the limits of the effective layer from a distance equal to the thickness of this layer. The efficiency of the optical device from the point of view of its resolution can by the appropriate choice of the location of the reference source be brought up to its limiting level, determined by the radius of the isoplanar region, and, consequently, starting at heights for which $r_a > R$, we have diffraction-limited resolution.

By virtue of reciprocity [2-4] (of the fluctuations) these results carry over to the problem of focusing an optical beam through the atmosphere with the help of a reference source. If the problem is one of focusing optical radiation in the plane of the reference source, the total phase conjugation (TPC) algorithm can be brought to bear, making use of the entire phase (2), and the initial beam must be collimated. The interesting situation arises in which the wavelengths of the formed beam and the reference source do not coincide (let λ_1 be the wavelength of the reference beam and λ_2 be that of the beam formed through the atmosphere). Then the plane of optimal focusing (for an initial collimated beam) x_{foc} is related to the position of the plane of the reference source as follows:

$$\frac{k_1}{x_{ref} - x_0} = \frac{k_2}{x_{foc} - x_0}.$$

And in order to focus the beam in the plane of the reference source, additional focusing is necessary, with radius of curvature

$$f_{add} = \frac{\lambda_1(x_{ref} - x_0)}{\lambda_1 - \lambda_2}.$$

4.2. Improvement of the Quality of the Image of a Star by Tracking

In this section we investigate some characteristics of a telescope whose aperture tracks the random angular displacements of the optical radiation impinging upon it. Here it should be noted [3,4] that because of the complexity of control of multi-element adaptive correctors under actual conditions of the turbulent atmosphere, realization in practice of adaptive systems in observational astronomy runs up against serious technical difficulties. For this reason, correction algorithms of the simplest

type, correcting, for example, the total tilt of the wavefront impinging upon the aperture of the telescope, are of special importance.

From experience it is well known that the image of a star in a small telescope (resolution 3-4") presents an almost undistorted picture, but which jitters strongly with frequencies from (1-2) to (10-20)Hz over its entire extent. At the telescope objective diameters of 100-150cm, the image of the star looks like an immobile, smeared out disk. Consequently, only in small telescopes, in which -- in contrast to large ones -- the main distorting factor is image jitter, not smearing as in the latter, improvement of the quality of the image can be achieved by tracking the slopes of the impinging wave front.

We will estimate the improvement in image quality for such correction on the basis of transfer functions of the system atmosphere-telescope. By definition, the transfer function of such a system is

$$\tau(\mathbf{f}) = B \iint d^2x U(\mathbf{x}) U^*(\mathbf{x}) \exp(i2\pi \mathbf{f} \mathbf{x}), \quad (1)$$

where B is chosen such that $\tau(0) = 1$, \mathbf{f} is the spatial frequency vector, the amplitude of the image in the focal plane of a "thin" lens is equal to

$$U(\mathbf{x}) = A \iint d^2v U(\mathbf{v}) \exp\left(-i \frac{2\pi}{\lambda F} \mathbf{v} \mathbf{x}\right), \quad (2)$$

A is a normalization constant, λ is the wavelength of the radiation, F is the focal length of the lens, and $U(\mathbf{v})$ is the wave field incident upon the lens. When estimating the quality of the image, one often uses the averaged transfer function $\langle \tau(\mathbf{f}) \rangle$ for which the averaging time (or ensemble), as was shown in Ref.5, is of fundamental importance. In general, it is necessary to consider the averaging time as a parameter; however, for practical purposes one distinguishes two limiting cases: short and long exposure. In the latter case, the averaging of $\tau(\mathbf{f})$ is carried out over the entire ensemble of fluctuations of the field $U(\mathbf{v})$. An exposure is considered to be short if the averaging time is such that of the phase fluctuations taking place in the field $U(\mathbf{v})$ incident on the receiver aperture of the telescope, random tilts of the wave front as a whole are excluded.

In this case, in place of the function $\Phi(\mathbf{v})$ characterizing the phase fluctuations of the field $U(\mathbf{v})$, one uses the function $\tilde{\Phi}(\mathbf{v}) = \Phi(\mathbf{v}) - \mathbf{a}\mathbf{v}$, where \mathbf{a} is a random vector connected with $\Phi(\mathbf{v})$ in such a way that $\mathbf{a}\mathbf{v}$ optimally coincides with $\Phi(\mathbf{v})$ in the sense of the mean square difference over the aperture, i.e.,

$$\frac{\partial}{\partial a_i} \iint d^2\mathbf{v} W(\mathbf{v}) [\Phi(\mathbf{v}) - \mathbf{a}\mathbf{v}]^2 = 0,$$

where a_i are the components of \mathbf{a} . As was shown in Ref. 6, for symmetric apertures $[W(\mathbf{v}) = W(v)]$ we have

$$\mathbf{a} = \iint d^2\mathbf{v} W(v) \Phi(\mathbf{v}) \mathbf{v} / \left(\pi \int_0^\infty dv v^3 W(v) \right).$$

In the notation of Ref. 5 we have for long exposure

$$\langle \tau(\mathbf{f}) \rangle_1 = \tau_0(\mathbf{f}) \exp(-3.44 (\lambda F f / r_0)^{5/3}), \quad (3)$$

and for short exposure in the near zone ($D \gg \sqrt{\lambda L}$)

$$\langle \tau(\mathbf{f}) \rangle_{sh} \approx \tau_0(\mathbf{f}) \exp[-3.44 (\lambda F f / r_0)^{5/3}] \left\{ 1 - (\lambda F f / D)^{1/3} \right\}. \quad (4)$$

Here f is the spatial frequency, D is the diameter of the objective, r_0 is the coherence radius, defined by the relation

$$D_\phi(r) = 6.88 (r/r_0)^{5/3},$$

where $D_\phi(r)$ is the structure function of the complex phase and L is the distance traversed in the medium. It can be shown that since the radiation from the star arriving at the turbulent layer is a plane wave, the parameter r_0 is given by

$$r_0 \approx 2.1 \left(1.45 k^2 \int_0^\infty dh C_n^2(h) \right)^{-3/5}, \quad (5)$$

where $k = 2\pi/\lambda$ and $\int dh C_n^2(h)$ is the integrated turbulence profile.

Using $\langle \tau(\vec{f}) \rangle$, we can write out the overall resolution of the optical system atmosphere-telescope

$$\mathfrak{R} = \iint d^2 f \langle \tau(\mathbf{f}) \rangle \quad (6)$$

In Ref. 5, by analyzing the behavior of the function \mathfrak{R} , calculated using formulas (3) and (4), it was found that one obtains a higher-quality image with a short exposure than with a long exposure. On the basis of the data of Ref. 5, one can calculate this relative improvement (under tip-tilt correction) of the image quality Δ , as a function of the dimensionless parameter D/r_0 (Fig. 3).

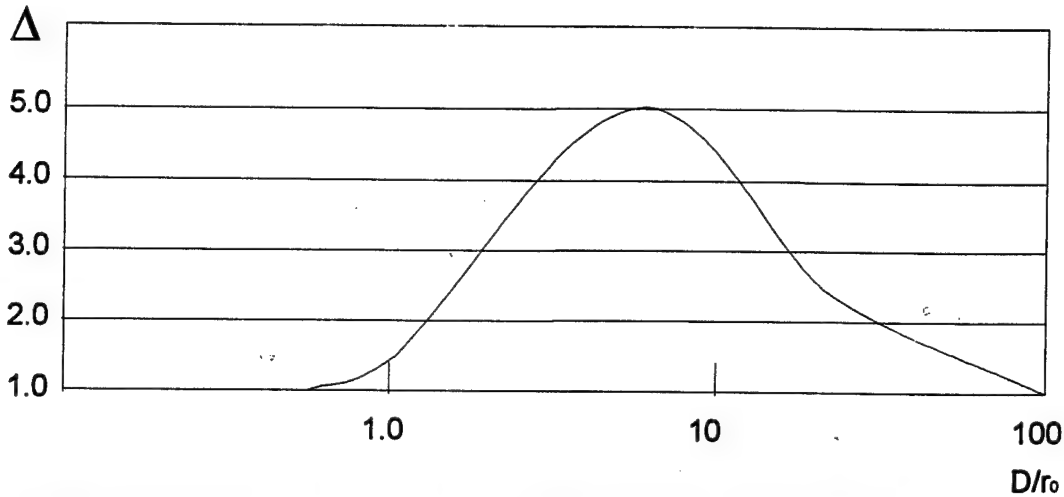


Fig. 3. Image quality Δ , as a function of the dimensionless parameter D/r_0 .

From the figure it can be seen that the so-called "limiting resolution" $\mathfrak{R}_{\max} = \frac{\pi}{4} (r_0/\lambda F)^2$, obtaining for long exposure, can be exceeded by a factor of more than 4.3 by going from a long exposure to a short one.

However, when observing faint stars one cannot use short exposures, and, consequently, improvement of image quality can be achieved only by tracking the random tilts of the arriving wave front. In this case, as can be easily seen, improvement of image quality is also characterized by the curve in Fig. 3.

In connection with the above, the parameter r_0 , which characterizes the degree of atmospheric turbulence, acquires special importance for estimating "seeing" through the atmosphere. There are a significant number of publications dedicated to measuring the magnitude of the coherence radius r_0 by astronomical methods. It is of interest to analyze the results of these efforts.

Thus, in Ref. 7 on the basis of nighttime astronomical measurements for $\lambda = 0.55 \mu m$ observing at zenith, a median value of r_0 was obtained equal to 11.4cm with standard deviation 36%. From the results of 24 nights of viewing, the authors of Ref.8 obtained values of r_0 within the range 5.3 to 17.8cm with mean value 9.6cm for $\lambda = 0.5 \mu m$. Ref.9 gives values of r_0 in the interval 4-15cm. The authors of Ref.10 obtained $r_0 = 10cm$ from measurements of the Polar Star. The most consistent measurements of r_0 were carried out by the authors of Ref.11, who carried out measurements on three mountain tops in New Mexico simultaneously. They obtained a nighttime value of $r_0 = 9.0 \pm 4.0 cm$ and a daytime value of $r_0 = 4.5 \pm 1.8 cm$.

Summarizing these results, we conclude that the coherence radius r_0 at $\lambda = 0.5 \mu m$ for the vertical column of atmosphere reaches 10cm in the nighttime and two times less under daytime conditions. Consequently, the optimal diameter of the aperture, i.e., the value for which correction of random tilts of the wave front over the entire aperture is effective, is about 40cm during the nighttime and around 20cm during the day.

At the same time, the magnitude of r_0 is closely connected with the model of the altitude profile of the refractive index structure parameter. Therefore, measurements of r_0 (Refs. 7, 10, 8, 11, 9) can serve as valuable material for checking the utility of various models of the altitude profile of the structure characteristic C_n^2 . Thus, in Ref.13 on the basis of the model of Ref.14 it was found that typical nighttime values of r_0 should exceed 10cm ($\lambda = 0.5 \mu m$). For the conditions of the Mount Palomar observatory from the same model the authors of Ref.15 obtained a mean value of $r_0 = 13 cm$. These values of r_0 are somewhat higher than those reached experimentally. Reference16 generalizes extensive material describing the behavior of the altitude profile of the temperature structure parameter C_T^2 over the steppe. The results of this study are approximated by the dependence

$$\Psi_{C_T^2}(\xi) = 4.64 \cdot 10^{-2} \xi^{-4/3} + 0.6 \exp[-12(\xi - 1.1)^2], \quad (7)$$

where $\xi = h/h\xi$, h is the altitude above the underlying surface, $h\xi$ is the thickness of the boundary layer, and $\Psi_{C_T^2}(\xi) = C_T^2(\xi)/C_T^2(0.1)$. Thus, the model of Ref.16 is prescribed by two parameters: $h\xi$ and $C_T^2(0.1)$. To estimate the parameter r_0 at

zenith ($\Theta = 0^\circ$), it is necessary to calculate $\int_{h_0}^{\infty} dh C_n^2(h)$, where h_0 is the height of the entrance aperture of the telescope above the underlying surface. At the wavelength $\lambda = 0.5 \mu m$, under average meteorological conditions, $C_n^2 \approx 0.69 \cdot 10^{-12} C_T^2$. If we take $h_0 = 0.01 h \xi$, we obtain

$$\int_{h_0}^{\infty} C_n^2(h) dh \approx 0.51 \cdot 10^{-12} C_T^2(0.1) h \xi,$$

in which case

$$r_0 \approx 2.1 (1.1 \cdot 10^{-12} C_T^2(0.1) h \xi)^{-3/5}.$$

If we use the characteristic values of $h \xi$ and C_T^2 , we find that r_0 varies within the range from 3.4 to 10.4 cm for daytime conditions, with an average value of ~ 6.8 cm. This is somewhat higher than the median values of r_0 from the direct measurements; however, it should be noted that the model of Ref.16 was based on measurements over the steppe, while the measurements of Refs.12, 7, and 11 were carried out atop high mountain peaks.

For telescopes correcting random wave front tilts, the parameter r_0 can be taken as the radius of the isoplanar region. By isoplanar region here we mean that portion of the atmosphere over which the optical transfer function is constant. The radius of this region is inversely proportional to the height of the turbulent layers causing the atmospheric phase distortions. The isoplanatism angle associated with the dimension of this region determines the maximum angular separation of two stars which can be observed with identical sharpness through a telescope. This same angle determines that portion of the sky which the tracking system can service while processing random tilts and working with one star.

A number of measurements of the isoplanatism angle have been carried out. Thus, the authors of Ref.10 obtained an isoplanatism angle of $4.7''$ from measurements made with a telescope with a 1.57m-diameter objective. The authors of Ref.17 obtained an isoplanatism angle of $4''$ - $10''$ from measurements made with the Mount Wilson telescope. If we assume that all of the turbulence is concentrated within a narrow layer at some altitude, then these latter measurements correspond to the presence of a turbulent layer in the altitude range 1.1-1.7 km. In the model of Ref.16, the turbulent inhomogeneities are distributed continuously; however, within the limits of the altitude

$h\xi$ there are local maxima. We will attempt to estimate the isoplanatism angle Θ_a from the formula $\Theta_a = r_0/h\xi$. The data of Ref.16 give $\Theta_a \approx 4''-17''$. Disregard of the distributedness of the turbulent inhomogeneities naturally leads to exaggerated values of Θ_a ; however, they are quite near to the experimental values.

Finally, let us consider some characteristics of a telescope with random tilt correction. The effective diameter of the objective of such a telescope exceeds the effective diameter of a telescope without correction by roughly a factor of 3.5. In this case, the resolution is improved by a factor of 4.3.

It is well known that the characteristics of a telescope viewing through the atmosphere enjoy reciprocity whether we use it to construct an image or use it as a transmitter. Therefore it is possible to decrease the distortions of the transmitted signal by measuring the fluctuations in the image of some auxiliary source. In this case, the random displacements of the center of gravity of the image of a point object -- a star -- are tracked in the focal plane of the telescope, and this signal is then used to control the transmitted radiation, and in this way one can decrease the average diameter of the transmitted wave beam. As was shown in Refs.4, 5 the variance of the random displacements of the energetic center of gravity of the optical beam can be decreased by a factor of four in this way. It is necessary only that the angle between the line of sight to the reference star and the average direction of the transmitted radiation not exceed the isoplanatism angle (around $10''-15''$) in the visible range.

In conclusion, it is necessary to emphasize the importance of measurements of the parameters r_0 and Θ_a , and also the need to confirm the applicability of various models of the altitude profile of atmospheric turbulence.

References to Chapter 4.

1. Lukin V.P., Matyuchin V.F., An Adaptive Image Correction, *Kvantovaia Elektronika*, V.10, No.12, pp.2465-2473, 1983 [*Sov.J.Quantum Electron.*, V.13, No.12, pp.1604-1610, 1983].
2. Lukin V.P., Charnotskii M.I., The Reciprocity Principle and Adaptive Control of Optical Radiation Parameters, *Kvantovaia Elektronika*, 9, No.5, pp.952-958, 1982 [*Sov.J.Quantum Electron.* 12, No.5 , pp.602-606, 1982].
3. V.P.Lukin, *Atmosferaia adaptivnaia optika*. Novosibirsk: Nauka, 1986, 248p.
4. V.P.Lukin, *Atmospheric Adaptive Optics*, SPIE Press Volume PM 23, 1996.
5. D.L.Fried, *J.Opt.Soc.Am.*67, No.3, 370-375(1977).
6. R.F.Lutomirski, W.L.Woodie, and R.G.Buser, *Applied Optics* 16, No.3, 665(1977).
7. D.L.Fried, G.E.Mevers, *Applied Optics* 13, No.11, 2620(1984).
8. M.G.Miller and Zieske, *J.Opt.Soc.Am.*67, No.12, 1680-1685(1980).
9. D.L.Walter and K.E.Kunkel, *J.Opt.Soc.Am.*71, No.4, 397-405(1981).
10. D.L.Walter, *J.Opt.Soc.Am.*71, No.4, 406-409(1981).
11. D.L.Walter, D.L.Favier, and I.R.Hanis, *J.Opt.Soc.Am.*69, No.6, 828-837(1979).
12. B.Widrow, P.E.Mantey, L.J.Griffiths, and B.Goode, *Proc.IEEE* 55, No.12, 2143-2159(1967).
13. D.L.Fried, *J.Opt.Soc.Am.*56, No.10, 1380-1385(1966).
14. R.E.Hufnagel and N.R.Stanley, *J.Opt.Soc.Am.*54, No.4, 52(1964).
15. D.Korff, *J.Opt.Soc.Am.*63, No.1, 8-13(1973).
16. S.L.Zubkovskii, V.p.Kukharetz, L.R.Tsvang, *Akad.Nauk SSSR, Fiz.Atmos.Okeana* 15, No.1, 44(1979).
17. S.Pollaine, A.Buffington, and F.S.Crawford, *J.Opt.Soc.Am.*69, No.1, 84-89(1979).
18. V.S.Komarov, A.A.Mittsel', I.I.Ippolitov, and T.V.Blakhovskaya, in: *Seventh All-Union Symposium on Laser and Acoustic Sounding of the Atmosphere*, Part 2, Abstracts, IAO, Tomsk, 1982, 248-251.

CHAPTER 5. MODERN CONCEPT OF AN ADAPTIVE OPTICS SYSTEM WITH A REFERENCE SOURCES

In the world community of scientists and engineers working in the field of adaptive optics the interest to development of optical schemes with an artificial reference source rose again in 1985 due to great amount of papers appeared in this period which was devoted to the problem of employing a signal scattered by atmospheric inhomogeneities as a reference one. This signal, for example, can be used for image correction in a ground-based telescope [1,2].

One of the most promising trends in the modern astronomy is a creation of ground-based adaptive telescopes which employ a signal of a laser guide star (LGS) [1-3]. The importance of investigations into the efficiency of adaptive optics systems with an artificial reference source was understood in the end of seventies. In this period were formulated the main principles upon which the modern concept of adaptive systems is based [4, 11, 12, 13]. According to this concept the reference source is the element with the use of which the information is procured concerning the distribution of fluctuations in the channel of radiation propagation. The way in which this channel is formed influences the structure of the whole system. If the principle of reciprocity is the base for an adaptive system, the most appropriate scheme is the one with an independent source of radiation generating a beam propagating in direction opposite to the corrected beam [4, 11].

Aiming at the practical realization of the system, the atmosphere should be included into the loop, i.e., the backward scattering should be taken into account with radiation reflected by an object or by inhomogeneities of the atmosphere. In such a way an artificial (virtual) reference source is formed. In the early eighties in adaptive astronomy artificial reference sources were named *laser guide stars* [1].

There are two main schemes of LGS generation: monostatic and bistatic. The laser used for this purposes is ground-based so the optical radiation travels two times through atmospheric inhomogeneities. First, upward, to form the LGS itself. Second, downward, in result of backscattering (secondary emission, or elastic aerosol scattering) by atmospheric inhomogeneities. In monostatic scheme it is assumed that correlation of fluctuations for the upward and downward propagation (for direct and secondary beams) are maximum. Quite different conditions are characteristic for the bistatic scheme (in some papers the term "bistatic" means the LGS scheme formation, where there is no correlation between upward and downward

propagation). In the both schemes one need to take into account peculiarities of optical parameters fluctuations of radiation passed twice through atmosphere.

The LGS is aimed at providing a reference source bright enough for adaptive optics. This concept recently begun to be widely discussed, but in fact it is not so new. I would like to declare that two scientific terms: *effective scattering volume* and *laser guide star* are scientific synonyms. The first term had been introduced earlier by specialists in atmospheric optics and laser sounding [5, 6]. The second term - *laser guide star* - had been introduced in astronomy for application with adaptive optical image correction. In this connection the great benefit for the tasks of adaptive optics for astronomy possible to obtain with application earlier theoretical investigations which have been developed in the atmospheric optics and laser sounding [5].

In the this part of report are presenting some results and formulae concerning fluctuations of waves reflected from an object and waves passed twice atmospheric inhomogeneities. In particular, the corresponding mathematical apparatus allows one to estimate correlation characteristics of a LGS [5-10].

In Ref.9 (1980) author have made mention of the fundamental possibility of using radiation backscattered by the atmospheric aerosol. Summing up we can conclude that Soviet scientists in eighties obtained all functions necessary to analyze random displacements of the image of a sounding object for bistatic as well as for monostatic schemes [4-10]. But in any cases under to solve some principal problem, the question about the model of scattering or refracting media still is always arise. The solution of this problem have been determined the model of "secondary" source. Possible as to interaction of model of similar source, as a solution of problem for backscattering.

Here should be noted the importance of the Summer NATO School *Adaptive Optics in Astronomy* held in 1993 for development of researches concerning application of laser guide stars. Since when this problem has been discussed on the conferences held by SPIE and OSA, namely, Munich'93, Kona'94, Photonics West'95, Denver'96, Hawaii'96, Orlando'97, San Diego'97 and on the conferences held in Russia (Tomsk'94, Tomsk'95, Shatura'97).

The two main problems: focus isoplanarity and full-aperture tip-tilt correction for LGS application for ground-based telescope were arose in the new papers [2, 15].

A series of papers on the subject have also been written, among them I would like to pay a special attention to Refs. 13 and 14. Thus Refs. 13, 14 describes the possibility of obtaining the partially-corrected image was described with resolution close to diffraction limited one for adaptation by the Rayleigh (10 km altitude) and sodium beacons (100 km). The angular position of the artificial guide star is assumed to be fixed. It was shown that in the both cases the Strehl ratio decreases with the telescope diameter. Paper [14] presented here in Appendix A.

The second problem - tip-tilt full aperture correction were developed firstly in papers [16, 18, 19, 20]. To my mind, the most complete literature review of the modern state of LGS was made by R. Ragazzoni [16]. The two techniques for measuring with a LGS is proposed in [18]. The first technique exploits a laser beam transmitting through the main telescope and two auxiliary telescope, which are separated from the transmitter, are used to measure a LGS image motion, averaging over its angular extent. In his paper [18] author mentioned that monostatic LGS can not be used for tip-tilt correction for main telescope, but bistatic scheme (without correlation between upward and downward propagation) permits to single out the tilt component corresponding to the transmitting beam which is highly correlated with the tilt for natural star. Unfortunately, author of [18] did not make adequately references [8, 9]. The new approach [19] same author exploits a small beam transmitted from main telescope, and signal for tilt correction is determined by subtracting the LGS motion measured simultaneously with the main and auxiliary telescopes. There are not necessary references [6-10] in paper [19] too.

In my order, I would like to declare that in my papers [21, 22], where I have made the analysis of R. Ragazzoni scheme [16], I did not present full list of references and missed citation of papers [16, 18, 19].

Papers [21, 22] are connecting with "optimal" algorithm, here these papers are presented in Appendix B and Appendix C. The "optimal" algorithm in some cases give increasing of efficiency for tip-tilt correction with LGS application. This algorithm is based on the model of turbulence of atmosphere for site of ground-based telescope. Among other papers reviewing the methods of a laser guide star forming I would like to list the following [22-25].

References to Chapter 5.

1. R. Foy, A. Labeyrie, "Feasibility of adaptive telescope with laser probe", *Astron. Astrophys.* **152**, p. L29 - L31, 1985.
2. R. Fugare, "Laser beacon adaptive optics", *Optics & Photonics News*, 14-19, June 1993.
3. V.P. Linnik, "On the possibility of reducing the influence of atmospheric seeing on the image quality of stars", *Optics and Spectroscopy*, No.4, 401-402 (1957).
4. Lukin V.P., Charn. tskii I., The Reciprocity Principle and Adaptive Control of Optical Radiation Parameters, *Kvantovaya Elektronika*, 9, No.5, pp.952-958, 1982 [*Sov.J.Quantum Electron.*, 12, No.5, pp.602-606, 1982].
5. Meeting Digest of "*Scintillation*" International Meeting for Wave Propagation in Random Media, Conference Chairs V.I. Tatarskii, A. Ishimaru, University of Washington, Seattle, USA, August 1992.
6. V.M. Orlov, I.V. Samokhvalov, G.G. Matvienko, M.L. Belov, A.N. Kozhemyakov, *The elements of theory of wave scattering and optical ranging* (Novosibirsk, Nauka, 1982).
7. M.A. Kalistratova, A.I. Kon, "Fluctuations of arrival angle of light waves from extended source in turbulent atmosphere", *Izv.VUZov. Radiofizika* **9**, No.6, 1100-1107 (1966).
8. V.P. Lukin, "Tracking of random angular displacements of optical beams", V All-Union Symposium on Laser Beam Propagation, Tomsk, Proc. Part II, 33-36, 1979.
9. V.P. Lukin, "Correction for Random Angular Displacements of Optical Beams", *Kvant. Elektron.* **7**, 1270-1279 (1980) [*Sov.J.Quantum Electron.* **10**, 727-732 (1980)].
10. V.L. Mironov, V.V. Nosov, B.N. Chen, "Correlation of shifting of laser source optical images in the turbulent atmosphere", *Izv.VUZov. Radiofizika* **25**, No.12, 1467-1471 (1982).
11. V.P. Lukin, *Atmosfernaia adaptivnaia optika*. Novosibirsk: Nauka, 1986, 248p. [V.P. Lukin, *Atmospheric Adaptive Optics*, SPIE Press Volume PM 23, 1996].
12. Lukin V.P., Pokasov V.V., "Quasimode" correction of an image passing through a randomly inhomogeneous medium", *Sov.J.Quantum Electron.*, V.13, No.5, p.626-629, 1983.

13. Lukin V.P., Matyuchin V.F., "An Adaptive Image Correction", *Kvantovaya Elektronika*, V.10, No.12, pp.2465-2473, 1983 [*Sov.J.Quantum Electron.*, V.13, No.12, pp.1604-1610, 1983].
14. Lukin V.P., "Limiting resolution of adaptive telescope operating with the use of artificial star", *Proc.of ICO-16 "Active and Adaptive Optics"*, 1993, Munich, pp.521-524.
15. D. L. Fried, J. Belshev, "Analysis of fundamental limits of artificial-guide-star adaptive optics-system performance for astronomical imaging", *J. Opt. Soc. Am. A*, 11, No. 1, p. 277 - 287, 1994.
16. R. Raggazzoni, S. Esposito, E. Marchetti, "Auxiliary telescopes for the absolute tip-tilt determination of a laser guide star", *Mon. Not. R. Astr. Soc.*, 276, p. L76 - L78, 1995.
17. V.P.Lukin, B.V.Fortes, "Efficiency of adaptive correction of images in a telescope using an artificial guide star", in *Adaptive Optics*, OSA/ESO Technical Digest Series, 23, 91-93(1995).
18. M.S.Belen'kii, "Full aperture tilt measurement technique with a laser guide star", in *Atmospheric Propagation and Remote Sensing IV*, editor J.C. Dainty, *Proc.SPIE* 2471, 289-296 (1995).
19. M.S.Belen'kii, "Tilt angular correlation and tilt sensing techniques with a laser guide star" in *Optics in Atmospheric Propagation, Adaptive Systems, and Lidar Technique for Remote Sensing*, editor J.C. Dainty, *Proc.SPIE*, 2956, 206-217 (1996).
20. R.Raggazzoni, "Absolute tip-tilt determination with laser beacons", *Astron.Astrophys.* 305, L13-L16 (1996).
21. V.P.Lukin, "Laser beacon and full aperture tilt measurement", in *Adaptive Optics* Vol.13 of OSA Technical Digest Series (Optical Society of America, Washington, D.C., 1996) Addendum AMB-35, pp.1-5.
22. V.P.Lukin, B.V.Fortes, "Comparison of Limit Efficiencies for Various Schemes of Laser Reference Star Formation", *Atm.Oceanic Optics* 10, 34-41 (1997).
23. Lukin V.P., "Computer modeling of adaptive optics & sites for telescope design", *ESO Conference Workshop Proceeding*, No.54, 1996, pp.373-378.
24. Lukin V.P., Fortes B., "Efficiency of adaptive correction of images in a telescope using an artificial guide star", *ESO Conference Workshop Proceeding*, No.54, 1996, pp.191-194.

25. Lukin V.P., "Hybrid scheme of forming a laser reference star", Atmos.Oceancic Opt., V.10, No.8, p.609-611, 1997.

EFFICIENCY OF ADAPTIVE CORRECTION OF IMAGES IN A TELESCOPE USING AN ARTIFICIAL GUIDE STAR

Vladimir P. Lukin, Boris V. Fortes

*Institute of Atmospheric Optics,
Siberian Branch of the Russian Academy of Sciences,
av. Akademicheskii 1, Tomsk, 634055, Russia*

It is well known that the use of a bright natural star as a reference source is limited by the angle of isoplanarity^{1,2,3}, which usually does not exceed 10 angular seconds, while the sufficiency bright stars are located less closely. In this connection in recent years the formation technique of artificial guide stars is gathering force, based on the effect of laser backscattering in the atmosphere^{4,5}.

However, phase distortions of the scattered radiation diverging wave does not coincide with the distortions of the initially plane corrected wave⁶. In this case this difference increases with the decrease of height on scattering volume and with the increase of size of the telescope entrance pupil. Formation of laser guide stars at large altitude is limited by small scattering coefficient.

The present paper describes the possibility of obtaining of partially-corrected image with resolution close to diffraction limited for adaptation by the Rayleigh and sodium beacons. For making the calculations the numerical model of the adaptive telescope⁷ was supplemented by the artificial star simulator. The details of atmospheric scattering were not taken into account.

The upward propagation of a laser beam is simulated as the propagation of a convergent cone of rays intersecting in a focal plane. In this case the initial size of the cone is equal to the telescope diameter. The shift of the beacon (cone top) can be written as

$$\vec{\rho}_b = \int_0^L \vec{s}(z) dz, \quad (1)$$

where L is the path length, $\vec{s}(z)$ is the vector determining the direction of beam axis. In numerical simulation due to a discrete representation of random-inhomogeneous medium this integral is expressed as

$$\vec{\rho}_b = \sum_{K=1}^{N_z} \vec{s}(z_K) \cdot (z_{K+1} - z_K), \quad (2)$$

where Z is the K -phase screen position. The beam axis tilt is defined by its refraction at all preceding phase screens, including a running one, that is,

$$\vec{s}(z_K) = \sum_{K'=1}^K \vec{s}_{K'}, \quad (3)$$

where \vec{s}_K is the K -screens contribution to be determined as an approximation of wave front distortions $S_K(\vec{\rho})$ by the liner functions, i.e., as solution of problem:

$$\iint_{|\vec{\rho}-\vec{\rho}_K| < R_K} [S_K(\vec{\rho}) - (\vec{\rho} - \vec{\rho}_K) \cdot \vec{s}_K - C]^2 d^2\rho \rightarrow \min \quad (4)$$

where

$$\vec{\rho}_K = \sum_{K'=1}^K \vec{s}(z_{K'}) \cdot (z_{K'+1} - z_{K'}) \text{ and } R_K = R_0 \cdot (1 - z_K/L) \quad (5)$$

is the current position of the beam center and its radius, respectively.

The subsequent part of the problem is the simulation of "downward" propagation of a scattering wave. Considering a reference source as a point one and neglecting by the ray deformation when propagating through the turbulent medium, the optical path length for the ray at the point $(\bar{\rho}, 0)$ can be expressed as an integral

$$l(\bar{\rho}) = \int_0^P n(p) dp = P \cdot n_0 + \int_0^L \kappa(\bar{\rho} + (\bar{\rho}_b - \bar{\rho}) \cdot z/L, z) \cdot p'_z \cdot dz, \quad (6)$$

where

$$P = \sqrt{(\bar{\rho} - \bar{\rho}_b)^2 + L^2} \quad \text{and} \quad p'_z = z \cdot \sqrt{1 + \frac{(\bar{\rho}_b - \bar{\rho})^2}{L^2}} \quad (7)$$

is the beam length and the coordinate along it, real from the receiving aperture, $\tilde{n} = n - n_0$ is the refractive index fluctuations. In the paraxial approximation, i.e., at $(\bar{\rho} - \bar{\rho}_b)^2 / L^2 \ll 1$ we have

$$P \approx L + \frac{\rho_b^2}{2L} + \frac{\rho^2}{2L} - \bar{\rho} \frac{\bar{\rho}_b}{L} \quad \text{and} \quad p'_z = \sqrt{1 + \frac{(\bar{\rho}_b - \bar{\rho})^2}{L^2}} \approx 1. \quad (8)$$

Assuming $n_0 \approx 1$ for the optical path length we obtain the following expression:

$$l(\bar{\rho}) \approx L + \frac{\rho_b^2}{2L} + \frac{\rho^2}{2L} - \bar{\rho} \frac{\bar{\rho}_b}{L} + \int_0^L \kappa(\bar{\rho} + (\bar{\rho}_b - \bar{\rho}) \cdot z/L, z) dz. \quad (9)$$

The first two components do not depend on ρ and are the same for all the rays. The third component corresponds to the divergent spherical wave (in paraxial approximation). If the reference wave passes through the same optics, by means of which the laser beam was focused, this component is compensated. The fourth component describes the total tilt of the reference wave occurring as a result of the fact that because of random refraction the reference wave source is shifted from the telescope axis. The last component represents the turbulent distortions of the reference wave. Random fluctuations of the optical path length are written as

$$T(\bar{\rho}) = -\bar{\rho} \frac{\bar{\rho}_b}{L} + \int_0^L \kappa(\bar{\rho} + (\bar{\rho}_b - \bar{\rho}) \cdot z/L, z) dz. \quad (10)$$

The random-inhomogeneous field of the refractive index in accordance with the splitting technique^{8,9} is represented as a sequence of thin phase screens that is equivalent to the following expression

$$\kappa(\bar{\rho}, z) = \sum_{K=1}^{N_z} S_K(\bar{\rho}) \cdot \delta(z_K) \quad (11)$$

Substituting this expression to Eq. (10) we obtain:

$$T(\bar{\rho}) = -\bar{\rho} \frac{\bar{\rho}_b}{L} + \sum_{K=1}^{N_z} S_K(\bar{\rho} + (\bar{\rho}_b - \bar{\rho}) \cdot z_K/L) \quad (12)$$

At numerical simulation the transverse coordinates are also presented as discrete ones, i.e., the values of phase distortions are known only in the nodes of the grid

$$S_{I,J,K} = S(x_I, y_J, z_K). \quad (13)$$

Traditionally it is sufficient, however, in this case it is necessary to interpolate these values to an arbitrary point. In the software developed for this purpose we use the two-dimensional linear interpolation that is quite sufficient for the problem being studied.

For calculations we have used the following semiempirical model of the altitude profile of turbulence intensity:

$$C_n^2(h[km]) = 5.19 \cdot 10^{-16} \cdot 10^{-0.86h} + 10^{-18.34+0.29h-0.0284h^2+0.000743h^3} \quad (14)$$

The calculations were performed for the visible range. The coherence radius for this altitude profile (14) is approximately equal to 18 cm at $\lambda=0.55\mu\text{m}$. The angular position of the artificial guide star is assumed to be fixed, i.e., $\vec{r}_p = 0$

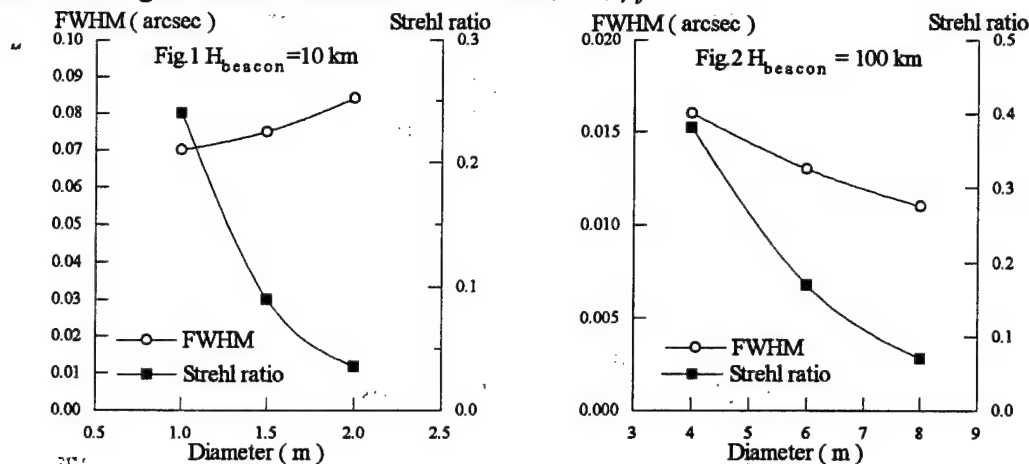


Figure 1 gives the results of calculations for the height of the reference source $H_{\text{beacon}} = L = 10 \text{ km}$ (Rayleigh scattering), Fig.2 gives the results of calculations for the height $H_{\text{beacon}} = L = 100 \text{ km}$. It is assumed that the adaptive system has an infinite spatial-temporal resolution. In both cases the Strehl ratio decreases with the telescope diameter increase. At the same time the angular resolution (FWHM) varies slightly ($L = 10 \text{ km}$) and even is improved ($L = 100 \text{ km}$) remaining close to a diffraction one.

REFERENCES

1. D. Korff, G. Dryden, R. P. Leavitt, "Isoplanicity: the translation invariance of the atmospheric Green's function", J. Opt. Soc. Am., 1975, Vol. 65, No. 11, P. 1321-1330.
2. D. L. Fried, "Anisoplanatism in adaptive optics", J. Opt. Soc. Am., 1982, Vol. 72, No. 1, P. 52-61.
3. R. J. Sasiela, "Strehl ratios with various types of anisoplanatism", J. Opt. Soc. Am. A, 1992, Vol. 9, No. 8, P. 1398-1405.
4. L. A. Thompson, C. S. Gardner, "Experiments on laser guide stars at Mauna Kea observatory for adaptive imaging in astronomy", Nature (London), 1987, Vol. 328, No. 16 July, P. 229-231.
5. L. C. Bradley, "Pulse-train excitation of sodium for use as a synthetic beacon", J. Opt. Soc. Am. B, 1992, Vol. 9, No. 10, P. 1931-1944.
6. B. M. Welsh, C. S. Gardner, "Effects of turbulence-induced anisoplanatism on the imaging performance of adaptive-astronomical telescopes using laser guide stars", J. Opt. Soc. Am. A, 1991, Vol. 8, No. 1, P. 69-80.
7. B. V. Fortes, V. P. Lukin, "Modeling of the image observed through the turbulent atmosphere", Proc. SPIE, 1992, Vol. 1668, P. 477-488.
8. J. A. Fleck, J. R. Morris, M. D. Feit, "Time-dependent propagation of high-energy laser beam through the atmosphere", Appl. Phys., 1976, Vol. 10, No. 1, P. 129-139.
9. P. A. Konyaev, V. P. Lukin, "Thermal distortions of focused laser beams in the atmosphere", Appl. Opt., 1985, Vol. 24, No. 3, P. 415-421.

LIMITING EFFICIENCIES AND APPLICABILITY OF DIFFERENT WAYS TO FORM REFERENCE LASER STARS

APPENDIX B

V.P. Lukin and B.V. Fortes

*Institute of Atmospheric Optics,
Siberian Branch of the Russian Academy of Sciences, Tomsk
Received September 30, 1996*

We describe here three possible schemes of the laser reference star formation, namely, monostatic, bistatic, and intermediate. We also determine here limiting potentialities of methods of correction for random tilts of a wavefront from natural star using a signal from a laser star. The monostatic scheme of the laser reference star formation is shown to be totally inapplicable for these purposes. The capabilities of the bistatic correction scheme are estimated. Then we show the possibility of using an intermediate scheme.

Among the problems that seriously challenge the investigators of adaptive optical telescopes is the need for use of reasonably bright stars as reference sources, since the telescope wavefront sensor, as a rule, needs for a large amount of energy of star radiation to provide its proper functioning. The requirement to the reference source energy as well as the necessity of simultaneous staying in one isoplanar area with the image of a star being studied (or any other space object) and of a reasonably bright reference star, provided allowing for the fact that the atmospheric isoplanatism angle is very small (in the visible range along the direction to zenith this angle is 10"-15") essentially decreases the percentage of sky coverage with this telescope.

The investigators of adaptive optics solved this problem when using the focused laser radiation guided from the Earth and backscattered by the atmospheric inhomogeneities,¹⁻³ namely, elastic aerosol scattering at 8-20 km altitude or a re-emission at 80-100 m altitude from the atomic sodium clouds.

The problem of forming of a laser reference star is in fact a combination of many scientific and technical problems to be solved, such as design of a specialized laser system, choice of an optimal altitude for the laser reference star, measurement of the phase of laser radiation reflected by the atmosphere and, finally, the selection of the control algorithm.

In this connection, of particular interest is the publication by Dr. Robert Fugate, a well-known in the U.S. specialist in laser systems, in which the author states that by the time of his publication⁴ (February 1996) no laser reference stars, using the scattering from the atomic sodium clouds were operating successfully, were unknown to him. Here it should be noted that it is just sodium layer reference stars which can provide obtaining the best characteristics of the adaptive telescopes.

In addition to the above problems, the use of laser reference stars meets an obstacle, namely, the problem of impossibility of full correction for the random wavefront tilts from a natural star based on

measurements of tilts of a wavefront from a laser reference star.

No doubts that the use of the laser reference stars, due to the light backscatter, is connected with the problem on selecting an optimal algorithm for making use of optical measurement data to correct for random jitter of a star image. It is just this problem we deal with in this paper.

Let us consider the following scheme of the optical experiment: formation of the natural star image in the focal plane of a ground-based telescope takes place (F is the focal length of the optical system, Σ is the size of the optical system aperture). As was already noted, the star image jitter formed in the focal plane occurs due to the influence of atmospheric turbulence over the telescope. We define this image jitter as a random shift of the position of the center of gravity (provided that these fluctuations are small) of the star image intensity using the vector

$$\rho_F^{\text{pl}} = -\frac{F}{k\Sigma} \iint_{\Sigma} d^2\rho \nabla_{\rho} S^{\text{pl}}(0, \rho), \quad (1)$$

where k is the radiation wave number; $S^{\text{pl}}(0, \rho)$ are the phase fluctuations in the plane wave from the star formed.

In its turn, the measured random vector of the laser reference star image jitter, formed on the basis of the focused laser radiation, using a ground-based laser system, is given by the expression

$$\rho_m = \rho_c F/x + \rho_F^{\text{sph}}, \quad (2)$$

where

$$\rho_c = \frac{1}{\rho_0} \int_0^x d\xi (x - \xi) \iint d^2R l(\xi, R) \nabla_R n_1(\xi, R) \quad (3)$$

is the position of the center of gravity, focused at a distance x from the source of the Gaussian laser beam; $l(\xi, R)$ is the current value of the optical field intensity; $\nabla_R n_1(\xi, R)$ is the gradient of fluctuations of the

atmospheric refractive index. We consider that the laser radiation is focused onto a sufficiently small spot, not resolved by a telescope through the atmosphere. The second term in (2) is of the form

$$\rho_F^{\text{sph}} = -\frac{F}{k\Sigma} \iint_{\Sigma} d^2\rho \nabla_{\rho} S^{\text{sph}}(\rho, 0) \quad (4)$$

and represents the point source image jitter in the telescope focal plane.

We construct the correction algorithm of a star image jitter^{5,6} ρ_F^{pl} in the form:

$$\rho_F^{\text{pl}} - \rho_k, \quad (5)$$

where $\rho_k = A\rho_m$, and the coefficient A is chosen to provide the minimal variance of the residual distortions

$$\langle (\rho_F^{\text{pl}} - A\rho_m)^2 \rangle_{\min} = \langle \epsilon^2 \rangle. \quad (6)$$

Having found the minimum for variance in the form of Eq. (6), we obtain

$$\langle \epsilon^2 \rangle_{\min} = \langle (\rho_F^{\text{pl}})^2 \rangle - \frac{\langle \rho_F^{\text{pl}} \rho_m \rangle^2}{\langle (\rho_m)^2 \rangle}, \quad (7)$$

where the correcting coefficient A is expressed only in terms of the determinant functions as

$$A = \langle \rho_F^{\text{pl}} \rho_m \rangle / \langle (\rho_m)^2 \rangle. \quad (8)$$

It should be noted that the traditional correction algorithm in the form of Eq. (5), where $A \equiv -1$, does not provide minimum (6) to the variance and therefore cannot be considered as any serious alternative.

In a real experiment we have only the measurement data ρ_m , since the vector ρ_F^{pl} , characterizing the real star jitter, whose image should be corrected, cannot be measured, since the real star emits only little light for the measurements with the wavefront sensor to be feasible.

At the same time, the coefficient A can be calculated using a model description of the altitude behavior of the turbulence intensity $C_n^2(\xi)$. Taking into account Eqs. (2) and (8), the variance and correlation, as components of Eq. (7) can be written in the form (using normalization and changing the characteristics for angular ones)

$$\langle (\varphi_m)^2 \rangle = \langle (\varphi_c)^2 \rangle + \langle (\varphi_F^{\text{sph}})^2 \rangle + 2 \langle \varphi_F^{\text{sph}} \varphi_c \rangle, \quad (9)$$

$$\langle \varphi_F^{\text{pl}} \rho_m \rangle = \langle \varphi_F^{\text{pl}} \varphi_c \rangle + \langle \varphi_F^{\text{pl}} \varphi_F^{\text{sph}} \rangle. \quad (10)$$

Now the question arises on how can the algorithm (5) be useful for correction? First of all, based on the knowledge of a model of the altitude turbulence profile one can:

1) estimate the limiting level of correction of the general wavefront tilt, φ_F^{pl} by the following expression:

$$\langle \beta^2 \rangle_{\min} = \langle (\varphi_F^{\text{pl}})^2 \rangle \left\{ 1 - \frac{\langle \varphi_F^{\text{pl}} \varphi_m \rangle^2}{\langle (\varphi_F^{\text{pl}})^2 \rangle \langle (\varphi_m)^2 \rangle} \right\},$$

where the second term is estimated using the models of turbulent atmosphere.

2) calculate the scaling factor A of measured values of ρ_m in the control algorithm, expressed in terms of the average values

$$A = \langle \varphi_F^{\text{pl}} \varphi_m \rangle / \langle \varphi_m^2 \rangle.$$

There are several schemes of laser reference star formation. From the viewpoint of calculation of variance and correlation from Eqs. (9) and (10) only two schemes can be mentioned as limiting ones, namely the monostatic and bistatic schemes. In the monostatic scheme the star image formation in the telescope and the formation of the laser reference star image take place through one and the same atmospheric inhomogeneities. In the bistatic scheme the reference star is formed in the region isoplanar with the image of a natural star, but the propagation of a focused laser beam itself, forming the reference star, occurs through turbulent inhomogeneities, uncorrelated with those on the way from the natural star.

MONOSTATIC SCHEME

Thus, for the monostatic scheme the correction coefficient $A = A_M$ in Eq. (8) and its components are calculated by formulas (9) and (10), respectively⁵.

$$\begin{aligned} \langle \varphi_m^2 \rangle &= (2^{7/6} \pi^2 0.033 \Gamma(1/6)) \times \\ &\times [R_0^{-1/3} + a_0^{-1/3} - 2^{7/6} (R_0^2 + a_0^2)^{-1/6}] \times \\ &\times \int_0^x d\xi (1 - \xi/x)^{5/3} C_n^2(\xi), \end{aligned} \quad (11)$$

provided that the focused ($x=f$) laser beam is sufficiently wide ($(ka_0^2)/x \gg 1$) and the turbulent laser beam broadening does not exceed focusing (i.e., $\Omega^{-2} (1/2 D_S(2a_0))^{6/5} \ll 1$);

$$\begin{aligned} \langle \varphi_F^{\text{pl}} \varphi_c \rangle &= (-2^{4/3} \pi^2 0.033 \Gamma(1/6)) \times \\ &\times \int_0^x d\xi C_n^2(\xi) (1 - \xi/x) [(R_0^2 + a_0^2 (1 - \xi/x)^2)^{-1/6}]. \end{aligned} \quad (12)$$

When making these calculations we consider the radiation from a natural star as an infinite plane wave, propagating from zenith, and a laser beam is formed coaxially with the main telescope, forming the image, then

$$\begin{aligned} \langle \varphi_F^{\text{pl}} \varphi_F^{\text{sph}} \rangle &= (2^{4/3} \pi^2 0.033 \Gamma(1/6)) R_0^{-1/3} \times \\ &\times \int_0^x d\xi C_n^2(\xi) (1 - \xi/x) [1 + (1 - \xi/x)^2]^{-1/6}. \end{aligned} \quad (13)$$

The latter expression represents the correlation between the plane wave image jitter and the point source image jitter (measured in the telescope focal plane), with the source being at a distance x from the telescope.

The variance of the star image jitter is calculated by the following formula:

$$\langle \phi_F^2 \rangle = (2^{7/6} \pi^2 0.033 \Gamma(1/6)) R_0^{-1/3} \int_0^\infty d\xi C_n^2(\xi). \quad (14)$$

Since the star is far out of the atmosphere, the upper integration limit in Eq. (14) tends to ∞ . Using these designations the minimal variance of residual fluctuations of angular shifts of the star image for a monostatic scheme is given in the form

$$\frac{\langle \phi^2 \rangle_{\min}}{F^2} = \langle \beta^2 \rangle_{\min} = \langle \phi_F^2 \rangle \left\{ 1 - \frac{2^{1/3} f_M(x, C_n^2)}{[1 + b^{-1/3} - 2^{1/6}(1 + b^2)^{-1/6}]} \right\}, \quad (15)$$

where $b = a_0/R_0$,

$$f_M(x, C_n^2) = \frac{\left\{ \int_0^x d\xi C_n^2(\xi) \left[(1 + b^2(1 - \xi/x)^2)^{-1/6} - [1 + (1 - \xi/x)^2]^{-1/6} \right] \right\}^2}{\int_0^x d\xi C_n^2(\xi) (1 - \xi/x)^{5/3} \int_0^\infty d\xi C_n^2(\xi)} \quad (16)$$

From Eqs. (11), (15), and (16) it is clear that $b = 1$ ($a_0 = R_0$) the signal ϕ_m becomes noninformative because $\langle \phi_m(R_0 = a_0) \rangle = 0$. At the same time, the function $f_M(x, C_n^2)$ vanishes. Therefore, for the monostatic scheme of the laser reference star formation, from the standpoint of information content of ϕ_m as well as from the power standpoint, the domain of admissible values of $b = a_0/R_0$ is the interval (0, 1), i.e., $b < 1$. For very small values of the parameter b the estimate of minimal value of the variance of the residual star image jitter is expressed as

$$\langle \beta^2 \rangle_{\min} = \langle \phi_F^2 \rangle \left\{ 1 - \frac{2^{1/3} f_M(x, C_n^2)}{[1 + b^{-1/3} - 2^{1/6}(1 + b^2)^{-1/6}]} \right\}, \quad (17)$$

where the function

$$f_M(x, C_n^2) = \frac{\left\{ \int_0^x d\xi C_n^2(\xi) (1 - \xi/x) (1 - [1 + (1 - \xi/x)^2]^{-1/6}) \right\}^2}{\int_0^x d\xi C_n^2(\xi) (1 - \xi/x)^{5/3} \int_0^\infty d\xi C_n^2(\xi)} \quad (18)$$

is the limit for the function $f_M(x, C_n^2)$ from Eq. (16) at the parameter $b \rightarrow 0$.

Table I gives the calculated values of all the parameter of a monostatic scheme interesting for us. The calculations have been done for different values of the parameter b ($b = 0; 0.75; 0.80; 0.85; 0.90; 0.95$) with the use of the model of $C_n^2(\xi)$ from Ref. 7 for the mean conditions of vision through the turbulent atmosphere and the altitudes of location of a reference source x from 5 to 100 km. Table I shows that the value of the function

$f_M(x, C_n^2)$ varies from 6.48 to 11.2. In the same table the values of the quantity

$$A_m = \langle \rho_F^2 \rho_m \rangle / \langle \rho_m \rangle^2,$$

are given, calculated by the formula (8) for the monostatic scheme of the laser reference star formation. Thus, for the parameter $b = 0.95$ the values of A_m vary from -15 to -16.1. Here the value of $C_M = \langle \beta^2 \rangle / \langle \phi_F^2 \rangle$ is given, characterizing the ratio of the value of variance of residual fluctuations to the value of variance of the natural star jitter signal. The calculational data show that the values of C_M vary from 0.9197 to 0.87. These results clearly demonstrate that because of small value of $f_M(x, C_n^2)$ and owing to the fact that C_M only slightly differs from 1, no efficient correction of random tilts with the use of the monostatic scheme of the laser reference star formation can be expected. It should be noted that this result has been obtained for the case of optimal correction, therefore the use of "direct" correction algorithm and the optical measurement data (at $A \equiv 1$) the correction (6) is much less effective.

Owing to the fact that $f_M(x, C_n^2)$ is small, the optimal value of the ratio b , minimizing the variance $\langle \beta^2 \rangle_{\min}$, given by Eq. (17), turns out to be comparable with the dimension of the telescope aperture R_0 . It is known that in this case (when $a_0 \rightarrow R_0$) the measured signal ϕ_m decreases, and its variance $\langle \phi_m^2 \rangle$ vanishes. Therefore, a compromise should exist in the choice of such a ratio $b = a_0/R_0$, which, on the one hand, minimizes the variance (17), and, on the other hand, provides the measurement a measurable signal ϕ_m , i.e., ensures a reasonable level of the variance (11). For example, one can select the value $b = a_0/R_0$, such that

$$1 + b^{-1/3} - 2^{1/6}(1 + b^2)^{-1/6} \leq 0.01,$$

i.e., the signal of the reference star jitter proved to be ten times smaller than real star jitter (although this

TABLE I.

x_i km	$f_M \cdot 10^3$							A_M							C_M						
	0	0.75	0.80	0.85	0.90	0.95		0.75	0.80	0.85	0.90	0.95		0.75	0.80	0.85	0.90	0.95			
5	6.48	0.8096	0.522	0.295	0.1314	0.03286		-2.4	-3.22	-4.59	-7.33	-15.6		0.9387	0.934	0.9292	0.9245	0.9197			
10	7.82	0.9644	0.6211	0.3506	0.156	0.03896		-2.42	-3.24	-4.62	-7.38	-15.7		0.927	0.9214	0.9159	0.9103	0.9048			
15	8.58	1.05	0.6784	0.3828	0.1703	0.04251		-2.43	-3.26	-4.64	-7.41	-15.7		0.9202	0.9142	0.9082	0.9022	0.8961			
20	9.14	1.12	0.7199	0.406	0.1805	0.04505		-2.44	-3.28	-4.67	-7.45	-15.8		0.9153	0.9089	0.9026	0.8963	0.8899			
85	11.1	1.32	0.8494	0.4779	0.212	0.05277		-2.5	-3.35	-4.77	-7.61	-16.1		0.8998	0.8926	0.8853	0.8782	0.8711			
90	11.1	1.33	0.8522	0.4795	0.2126	0.05293		-2.5	-3.35	-4.77	-7.61	-16.1		0.8995	0.8922	0.885	0.8778	0.8707			
95	11.2	1.33	0.8548	0.4809	0.2133	0.05308		-2.51	-3.35	-4.77	-7.61	-16.1		0.8992	0.8919	0.8846	0.8774	0.8703			
100	11.2	1.34	0.8572	0.4822	0.2138	0.05322		-2.51	-3.35	-4.77	-7.61	-16.1		0.8989	0.8916	0.8843	0.8771	0.87			

TABLE II.

x_i km	f_b	A_b					C_b				
		0.1	0.5	1.0	3.0		0.1	0.5	1.0	3.0	
5	0.6284	0.3524	0.4918	0.5557	0.6564		0.749	0.6497	0.6041	0.5324	
10	0.7127	0.3465	0.4837	0.5465	0.6455		0.7153	0.6027	0.551	0.4697	
15	0.7523	0.3424	0.4779	0.54	0.6378		0.6995	0.5806	0.5261	0.4403	
20	0.77	0.3383	0.4722	0.5335	0.6301		0.6925	0.5707	0.5149	0.4271	
85	0.7919	0.3231	0.451	0.5096	0.6018		0.6837	0.5585	0.5011	0.4108	
90	0.7922	0.3228	0.4505	0.5091	0.6012		0.6836	0.5583	0.5009	0.4106	
95	0.7926	0.3225	0.4501	0.5086	0.6007		0.6834	0.5581	0.5007	0.4103	
100	0.7929	0.3222	0.4497	0.5082	0.6002		0.6833	0.558	0.5005	0.4101	

opinion is too optimistic), then the optimal ratio b should be equal to $b_{\text{opt}} \geq 0.86$. However, it is known that it is very difficult to perform accurate measurements of small signals under conditions of noise and background fluctuations. This shows once more that the correction of wavefront tilts in the monostatic scheme is ineffective since any effective correction should be expected for the parameter value $b \rightarrow 1$, i.e., for the case when the measured value itself becomes small and, hence, it is measured with larger error.

BISTATIC SCHEME

According to the bistatic scheme the laser star formation is performed through the turbulent inhomogeneities uncorrelated with those inhomogeneities, through which the natural star image is formed with the telescope. This can be done using lateral irradiation (at a sufficiently large spacing between the optical axes of the laser beam propagation and the telescope). Using the same procedure of search for minimum of variance of residual fluctuations of image jitter, we obtain for the residual level of fluctuations from Eq. (7), respectively,

$$\langle \beta^2 \rangle_{\min} = \langle (\Phi_F)^2 \rangle - \frac{\langle \Phi_F^{\text{pl}} \Phi_F^{\text{sph}} \rangle^2}{\langle (\Phi_b)^2 \rangle}, \quad (19)$$

where

$$\langle \phi_b \rangle^2 = \langle \phi_c \rangle^2 + \langle \phi_F \rangle^2 : \quad (20)$$

Having made the same calculations as for the monostatic scheme, we obtain the following expressions for the correcting coefficient $A = A_b$ and for the residual level of corrected variance (7), where

$$A_b = \frac{\langle \phi_F \rangle^2}{\langle \phi_c \rangle^2 + \langle \phi_F \rangle^2} = \frac{2^{1/6} \int_0^x d\xi C_n^2(\xi) (1 - \xi/x) [1 + (1 - \xi/x)^2]^{-1/6}}{(1 + b^{-1/3}) \int_0^x d\xi C_n^2(\xi) (1 - \xi/x)^{5/3}}, \quad (21)$$

$$\frac{\langle e^2 \rangle_{\min}}{F^2} = \langle \beta^2 \rangle_{\min} = \langle \phi_F \rangle^2 \left\{ 1 - \frac{2^{1/3} f_b(x, C_n^2)}{(1 + b^{-1/3})} \right\}, \quad (22)$$

$$f_b(x, C_n^2) = \frac{\left(\int_0^x d\xi C_n^2(\xi) (1 - \xi/x) [1 + (1 - \xi/x)^2]^{-1/6} \right)^2}{\int_0^x d\xi C_n^2(\xi) (1 - \xi/x)^{5/3} \int_0^x d\xi C_n^2(\xi)} \quad (23)$$

As the analysis of the latter expressions has shown, the effective correction with the bistatic scheme of the reference star formation ensures the minimum variance of residual image jitter (22) with the correction in the form

$$\phi_F - A_b \phi_b,$$

where ϕ_b is the signal of the reference bistatic star image jitter, A_b is given by formula (21). It is clear that in contrast to the monostatic scheme the correction within the bistatic scheme is possible at any ratio $b = a_0/R_0$, it is evident that the correction is the better the larger is the value b (see (22)). If $b = 1$, from Eq. (22) we find that

$$\langle \beta^2 \rangle_{\min} = \langle \phi_F \rangle^2 \{ 1 - 2^{-2/3} f_b(x, C_n^2) \}.$$

The functions $f_b(x, C_n^2)$, A_b , $C_b = 1 - \frac{2^{1/3} f_b(x, C_n^2)}{1 + b^{-1/3}}$ are represented in Table II for the model of the turbulent atmosphere⁷ at different altitudes of the reference source formation $x \in [1, 100]$ km, and for the values of the parameter $b = a_0/R_0$, 0.1; 0.5; 1.0; 3.0, respectively. The values of the function $f_b(x, C_n^2)$ vary from 0.628 to 0.7930. Therefore a more effective correction should be expected from the bistatic scheme as compared with the monostatic one. Besides, in the bistatic scheme we do not face the situation when the measured signal or its variance $\langle \phi_b \rangle^2$ vanishes. Of course, the bistatic scheme has a limiting correction level, and the variance of residual distortions (for example, for $b = 1$) as a result of such correction proved to be equal to

$$\langle \beta^2 \rangle_{\min} \approx \langle \phi_F \rangle^2 \{ 1 - 2^{-2/3} f_b(x, C_n^2) \}.$$

The two limiting schemes of laser reference star formation can be compared only by means of concrete estimates. It should be noted that it is necessary to make the estimation not for a separate telescope (with adaptive optics) but for the whole observatory, for example, the Mauna Kiya observatory on Hawaiian Islands, where the three largest telescopes (Keck I, Keck II, and CHFT) are located, operating with the adaptive correction of turbulent distortions. The first two telescopes are with the 10 m aperture, and the CHFT telescope (Canada, Hawaiian Islands, France) has the 3.6 m aperture.

Thus, when investigating, with the use of the monostatic scheme, equals the variance of residual distortions for every telescope

$$\langle \beta^2 \rangle_{\min} = \langle \phi_F \rangle^2 \left\{ 1 - \frac{2^{1/3} f_b(x, C_n^2)}{[1 + b^{-1/3} - 2^{1/6} (1 + b^{-2})^{-1/6}]} \right\}.$$

If the Keck I telescope produces the bistatic star for the Keck II telescope (the distance between the telescopes is 85 m), then we have

$$\langle \beta^2 \rangle_{\min} = \langle \phi_F \rangle^2 \{ 1 - 2^{-2/3} f_b(x, C_n^2) \},$$

if the Keck I telescope produces the star for the CHFT telescope, then

$$\langle \beta^2 \rangle_{\min} = \langle \phi_F \rangle^2 \left\{ 1 - \frac{2^{1/3} f_b(x, C_n^2)}{1 + (10/3.6)^{-1/3}} \right\}.$$

If CHFT produces the star for the pair of Keck I and Keck II telescopes, then

$$\langle \beta^2 \rangle_{\min} = \langle \phi_F \rangle^2 \left\{ 1 - \frac{2^{1/3} f_b(x, C_n^2)}{1 + (3.6/10)^{-1/3}} \right\}.$$

Before making the final conclusions we consider the so-called intermediate scheme of the laser reference star formation.

INTERMEDIATE SCHEME OF THE LASER REFERENCE STAR FORMATION

Let us consider the bistatic scheme of laser reference star formation in detail as is stated below. Let we have got two telescopes whose axes are spaced by the distance (vector) ρ_0 . For simplicity we consider that one of these telescopes is focused to zenith and forms a natural star image, and the second telescope, forming the laser reference star, is inclined at an elevation angle θ relative to the first telescope so that the elevation angle equals numerically $\theta = \pi/2 - \rho_0/x$, where x is the altitude at which the laser reference star is formed.

Let us first consider cross-correlations of random shifts of the center of gravity $\rho_c(\rho_0)$ of the laser beam formed with the second telescope whose directional pattern axis is shifted by the vector ρ_0 and is inclined at an angle $\theta = \pi/2 - \rho_0/x$ to the horizon, as well as the shifts of the center of gravity of the plane wave image ρ_F

and the spherical wave image ρ_F^{sph} formed by the first telescope, i.e., the correlations

$$\langle \rho_F^{\text{pl}} \rho_c(\rho_0) \rangle, \quad \langle \rho_F^{\text{sph}} \rho_c(\rho_0) \rangle.$$

It is important to understand that the first correlation, $\langle \rho_F^{\text{pl}} \rho_c(\rho_0) \rangle$ for the plane wave, decreases faster with the increase of the value of spacing between the telescope optical axes ρ_0 than the second one, $\langle \rho_F^{\text{sph}} \rho_c(\rho_0) \rangle$, for the spherical wave. We try to prove this on the basis of analytical and numerical calculations. Let us write the expression for the vector of energy center of gravity of a laser beam, formed with the second telescope from the ground surface, in the form

$$\rho_c(\rho_0) = \frac{1}{\rho_0} \int_0^x d\xi (x-\xi) \iint d^2R \langle I(\xi, \mathbf{R}) \rangle \nabla_R n_1(\xi, \mathbf{R}), \quad (24)$$

where

$$\nabla_R n_1(\xi, \mathbf{R}) = i \iint d^2n(\xi, \mathbf{\kappa}) \exp(i \mathbf{\kappa} \cdot \mathbf{R}), \quad (25)$$

and the mean intensity distribution of a laser beam, shifted to the vector ρ_0 and tilted at an angle θ to the Earth ($\theta = \pi/2 - \rho_0/x$), is given by the expression

$$\langle I(\xi, \mathbf{R}) \rangle = \frac{a_0^2}{a_{\text{eff}}^2(\xi)} \exp\{-(\mathbf{R} - \rho_0(1-\xi/x))^2/a_{\text{eff}}^2(\xi)\}. \quad (26)$$

Having made the calculations, we obtain

$$\begin{aligned} \rho_c(\rho_0) &= i \int_0^x d\xi (x-\xi) \iint d^2n(\xi, \mathbf{\kappa}) \times \\ &\times \exp\{-\kappa^2 a_{\text{eff}}^2(\xi)/4\} \exp[i\kappa \rho_0(1-\xi/x)]. \end{aligned} \quad (27)$$

As a result we have the following expressions for the variance $\rho_c(\rho_0)$ and cross-correlations $\langle \rho_F^{\text{pl}} \rho_c(\rho_0) \rangle$, $\langle \rho_F^{\text{sph}} \rho_c(\rho_0) \rangle$:

$$\begin{aligned} \langle \rho_c(\rho_0) \rangle^2 &= \frac{\langle \rho_c(\rho_0) \rangle^2}{x^2} = \\ &= (2\pi^2 0.033 \Gamma(1/6)) 2^{1/6} a_0^{-1/3} \times \\ &\times \int_0^x d\xi C_n^2(\xi) (1-\xi/x)^{5/3}, \end{aligned} \quad (28)$$

$$\begin{aligned} \langle \rho_c(\rho_0) \rho_F^{\text{sph}} \rangle &= \frac{\langle \rho_c(\rho_0) \rho_F^{\text{sph}} \rangle}{x F} = \\ &= (-2\pi^2 0.033 \Gamma(1/6)) 2^{1/3} (R_0^2 + a_0^2)^{-1/6} \times \\ &\times {}_1F_1\left(1/6; 1; -\frac{\rho_0^2}{R_0^2 + a_0^2}\right) \int_0^x d\xi C_n^2(\xi) (1-\xi/x)^{5/3}, \end{aligned} \quad (29)$$

$$\langle \rho_c(\rho_0) \rho_F^{\text{pl}} \rangle = \frac{\langle \rho_c(\rho_0) \rho_F^{\text{pl}} \rangle}{x F} =$$

$$\begin{aligned} &= [-2\pi^2 0.033 \Gamma(1/6)] 2^{1/3} \int_0^x d\xi C_n^2(\xi) (1-\xi/x) \times \\ &\times \{R_0^2 + a_0^2(1-\xi/x)^2\}^{-1/6} \times \\ &\times {}_1F_1\left(1/6; 1; -\frac{\rho_0^2(1-\xi/x)^2}{(R_0^2 + a_0^2(1-\xi/x)^2)}\right). \end{aligned} \quad (30)$$

Having analyzed the latter expressions we can state that the correlation between the slant beam and a spherical wave decreases slower than the correlation between this beam and a plane wave.

All the values calculated for this intermediate case are marked by the subscript "i". Besides, together with the parameter $b = a_0/R_0$ the parameter $d = \rho_0/R_0$ is introduced, characterizing the spacing between the laser beam axis, forming the star and the axis of the main telescope. In the general case (for arbitrary values of the parameters $b = a_0/R_0$ and $d = \rho_0/R_0$) we have, using Eqs. (28), (29), and (30) for a correcting factor $A = A_i$ and the values C_i , $\langle \beta^2 \rangle_i$, characterizing the variance of residual distortions, the following expressions:

$$\begin{aligned} A_i &= 2^{1/6} \left[\int_0^x d\xi C_n^2(\xi) (1-\xi/x) \left\{ (1+(1-\xi/x)^2)^{-1/6} - \right. \right. \\ &- (1+b^2(1-\xi/x)^2)^{-1/6} \times \\ &\times {}_1F_1\left(1/6; 1; -\frac{\rho_0^2(1-\xi/x)^2}{(1+b^2(1-\xi/x)^2)}\right) \left. \right\} \times \\ &\times \left[1 + b^{-1/3} - 2^{-7/6} (1+b^2)^{-1/6} \times \right. \\ &\times {}_1F_1\left(1/6; 1; -\frac{d^2}{(1+b^2)}\right) \left. \right] \int_0^x d\xi C_n^2(\xi) (1-\xi/x)^{5/3} \Big]^{-1}, \end{aligned}$$

$$\langle \beta^2 \rangle_i = \langle \rho_F^{\text{pl}} \rangle^2 C_i,$$

$$\begin{aligned} C_i &= 1 - 2^{1/3} \left[\int_0^x d\xi C_n^2(\xi) (1-\xi/x) \times \right. \\ &\times \left\{ (1+(1-\xi/x)^2)^{-1/6} - (1+b^2(1-\xi/x)^2)^{-1/6} \times \right. \\ &\times {}_1F_1\left(1/6; 1; -\frac{\rho_0^2(1-\xi/x)^2}{(1+b^2(1-\xi/x)^2)}\right) \left. \right\} \times \\ &\times \left[1 + b^{-1/3} - 2^{-7/6} (1+b^2)^{-1/6} \times \right. \\ &\times {}_1F_1\left(1/6; 1; -\frac{d^2}{(1+b^2)}\right) \left. \right] \times \\ &\times \int_0^x d\xi C_n^2(\xi) (1-\xi/x)^{5/3} \int_0^\infty d\xi C_n^2(\xi) \Big]^{-1}. \end{aligned}$$

It can easily be seen that at $d \rightarrow 0$ we obtain the expressions for the monostatic scheme, and at $d \rightarrow \infty$ we obtain the expressions for a bistatic scheme. For an

arbitrary parameter $d = \rho_0/R_0$ the values of A_i , C_i , $\langle \beta^2 \rangle_i$ exist even at $b = 1$ ($a_0 = R_0$) in contrast to the monostatic scheme. At $b = 1$ we obtain

$$\langle \beta^2 \rangle_i = \langle (\varphi_F)^2 \rangle = \frac{\left(\int_0^x d\xi C_n^2 \left(1 - \frac{\xi}{x}\right) \left[1 + \left(1 - \frac{\xi}{x}\right)^2 \right]^{-1/6} \left[1 - {}_1F_1 \left(\frac{1}{6}; 1; -\frac{d^2 \left(1 - \frac{\xi}{x}\right)^2}{\left(1 + b^2 \left(1 - \frac{\xi}{x}\right)^2}\right)} \right] \right)^2}{\left[1 - {}_1F_1 \left(\frac{1}{6}; 1; 1 - \frac{d^2}{2} \right) \right] \int_0^x d\xi C_n^2 \left(1 - \frac{\xi}{x}\right)^{5/3} \int_0^x d\xi C_n^2(\xi)} \quad (31)$$

Let us consider the asymptotic behavior of the expression for the correcting factor $A = A_i$ and the values of C_i , $\langle \beta^2 \rangle_i$ at the parameter $d \rightarrow \infty$. In this case we use the analytical continuation for a hypergeometric function

$${}_1F_1(1/6; 1; z) = \frac{(-z)^{-1/6}}{\Gamma(5/6)} \left(1 + \frac{1}{36(-z)} + \dots \right).$$

As a result, the denominator in A_i equals

$$\left[1 + b^{-1/3} - \frac{2^{7/6} d^{-1/3}}{\Gamma(5/6)} \right] \int_0^x d\xi C_n^2(\xi) (1 - \xi/x)^{5/3}$$

and the numerator equals

$$1 - {}_1F_1 \left(\frac{1}{6}; 1; -d^2 \frac{(1 - \xi/x)^2}{1 + b^2(1 - \xi/x)^2} \right) = \frac{(1 - \xi/x)^{-1/3}}{\Gamma(5/6)} (1 + (1 - \xi/x))^{1/6}.$$

We obtain that

$$\langle \beta^2 \rangle = \langle (\varphi_F)^2 \rangle = C_i = \langle (\varphi_F)^2 \rangle = \left\{ 1 - \frac{2^{1/3} F^2}{\left[1 + b^{-1/3} - \frac{2^{7/6} F^2}{\Gamma(5/6)} \right] \int_0^x d\xi C_n^2(\xi) (1 - \xi/x)^{5/3} \int_0^x d\xi C_n^2(\xi)} \right\} \quad (32)$$

and the function

$$F = \int_0^x d\xi C_n^2(\xi) \left\{ \frac{(1 - \xi/x)^2}{\left[1 + (1 - \xi/x)^2 \right]^{1/6}} - \frac{(1 - \xi/x)^{2/3}}{\Gamma(5/6) d^{1/3}} \right\}. \quad (33)$$

It turns out that the numerator of the function C_i (see Eq. (32)) at $d \rightarrow \infty$ does not depend on the parameter $b = a_0/R_0$, whereas the denominator depends on $b = a_0/R_0$ as follows:

$$\left[1 + b^{-1/3} - \frac{2^{7/6} d^{-1/3}}{\Gamma(5/6)} \right] \int_0^x d\xi C_n^2(\xi) (1 - \xi/x)^{5/3}.$$

Thus, one can decrease the variance (32) of residual fluctuations of the random star position by increasing $b = a_0/R_0$.

Tables III and IV give the results of calculations of the functions A_i and C_i by formula (31) at $b = 1$, the altitude of beacon from 5 to 100 km, the spacing between the first and second telescopes $d = 2^3, 3^3, \dots, 10^3$. When comparing the data of these two tables with the column (at $b = 1$) from Table II one can see that the values of A_i and C_i approach the values of A_b and C_b when $d \rightarrow \infty$.

TABLE III.

x, km	$d^{1/3}$								
1	2	3	4	5	6	7	8	9	10
5	0.5372	0.5465	0.5496	0.5511	0.552	0.5526	0.5531	0.5534	0.5537
10	0.5299	0.5382	0.541	0.5423	0.5432	0.5437	0.5441	0.5444	0.5447
15	0.5271	0.5335	0.5357	0.5368	0.5374	0.5378	0.5381	0.5384	0.5386
20	0.5237	0.5286	0.5302	0.5311	0.5316	0.5319	0.5321	0.5323	0.5324
85	0.5075	0.5085	0.5089	0.509	0.5092	0.5092	0.5093	0.5093	0.5093
90	0.5071	0.5081	0.5084	0.5086	0.5087	0.5087	0.5088	0.5088	0.5088
95	0.5067	0.5077	0.508	0.5081	0.5082	0.5083	0.5083	0.5084	0.5084
100	0.5064	0.5073	0.5076	0.5077	0.5078	0.5079	0.5079	0.508	0.508

TABLE IV.

$x, \text{ km}$	$d^{1/3}$								
1	2	3	4	5	6	7	8	9	10
5	0.814	0.7441	0.7091	0.6881	0.6741	0.6641	0.6566	0.6508	0.6461
10	0.7877	0.7089	0.6695	0.6458	0.63	0.6187	0.6102	0.6037	0.5984
15	0.7729	0.6907	0.6496	0.6249	0.6084	0.5966	0.5878	0.581	0.5755
20	0.765	0.6817	0.64	0.615	0.5983	0.5864	0.5775	0.5705	0.565
85	0.7512	0.6679	0.6262	0.6012	0.5845	0.5726	0.5637	0.5567	0.5512
90	0.751	0.6676	0.626	0.601	0.5843	0.5724	0.5634	0.5565	0.5509
95	0.7508	0.6674	0.6257	0.6007	0.5841	0.5722	0.5632	0.5563	0.5507
100	0.7506	0.6672	0.6255	0.6005	0.5839	0.572	0.563	0.5561	0.5505

As a practical outcome of the above considerations we can state that one can, based on the results obtained, quantitatively characterize the spacing between the optical axes of the main and star forming telescopes characteristic of the so-called bistatic scheme.

Thus, the following conclusions can be drawn:

1. Monostatic scheme does not remove the wavefront tilts.

2. Bistatic and intermediate schemes (at spacing between the axes of the two telescopes $d > 40$) are practically identical.

3. Bistatic scheme, where the two telescopes are used for correction of random tilts is more efficient at larger values of the parameter b .

REFERENCES

1. C. Primmerman, D. Murphy, et al., *Nature* (London) **353**, 141–143 (1991).
2. R. Fugate, J. Ellerbroek, et al., *J. Opt. Soc. Am.* **A11**, 310–324 (1994).
3. D. Fried and J. Belsher, *J. Opt. Soc. Am.* **A11**, 277–286 (1994).
4. R. Fugate, *Optics and Photonics News* **4**, No. 6, 14–19 (1993).
5. V.P. Lukin, *Atmospheric Adaptive Optics* (Nauka, Novosibirsk, 1986), 275 pp.
6. V.P. Lukin, *Laser Beacons and Full Aperture Tilt Measurements*. Proc. "Adaptive Optics", OSA, 1996, p. AMB35-1–AMB35-5.
7. M.E. Gracheva and A.S. Gurvich, *Izv. Akad. Nauk SSSR, Fiz. Atmos. Okeana* **16**, No. 10, 1107–1111 (1980).

HYBRID SCHEME OF FORMING A LASER REFERENCE STAR

APPENDIX C

V.P. Lukin

*Institute of Atmospheric Optics,
Siberian Branch of the Russian Academy of Sciences, Tomsk
Received May 19, 1997*

The results are presented connected with the construction of an algorithm for total wave-front tilt correction of a real star image based on the data of measuring the angular position of a laser reference star. A hybrid scheme of formation of the laser reference star is used, because to measure the position of this star, three telescopes are used: one of them operates in the regime of monostatic star and two others in the regime of bistatic star.

This article is logical continuation of a number of publications.¹⁻⁵ In addition, there exists a definite connection of the main idea of this paper and publications of Ragazzoni⁶ and especially Belen'kii.⁷ However, in spite of its similarity, especially to the results of Ref. 7, there are significant differences which are discussed at the end of the paper. For correct comparison of our results with the data obtained in Ref. 7, the same designations are used, where possible.

To implement the proposed correction algorithm based on the hybrid scheme of forming a laser reference star, three telescopes should be used: principal and two auxiliary telescopes placed so that their configuration forms an isosceles rectangular triangle. The following scheme of forming the laser reference star is realized: a wide Gaussian laser beam is focused with the principal telescope at the distance X . The star is formed solely by the central part of the principal telescope (it is assumed that the initial laser beam diameter $a_0 < a_b$, where a_0 is the aperture diameter of the principal telescope).

In the focal plane of the principal telescope, the angular jitter in the image center of gravity of the laser reference star is measured along the OY and OZ axes. Simultaneously, in the focal planes of two auxiliary telescopes the angular shifts of the image along one of the two axes are measured in the direction transverse to the corresponding direction of separation of the axes of principal and auxiliary telescopes.

The laser reference star formed by focusing of the laser radiation represents a long cylinder with diameter a_m and length a_b , that is, $a_b \gg a_m$. Suppose that the separations of principal and auxiliary telescopes are such that for the auxiliary telescopes the laser reference star is formed by the bistatic scheme.^{2,6,7} In this case, the size of a laser beacon \hat{a}_b (connected with a_b , altitude of star formation X , and separations between the axes of auxiliary telescopes and the principal telescope), seen from the points of location of the auxiliary telescopes is much greater than the beacon size seen from the point of the principal telescope location ($\hat{a}_b \gg a_m$).

Thus, we obtain that for the principal telescope, the formed star can be considered as monostatic. Then instantaneous position of its image (on the OY and OZ axes) is

$$\begin{aligned}\varphi_{m,y} &= \varphi_{lb,y} + \varphi_{ps,y}, \\ \varphi_{m,z} &= \varphi_{lb,z} + \varphi_{ps,z},\end{aligned}\quad (1)$$

where $(\varphi_{lb,y}, \varphi_{lb,z})$ specify the instantaneous angular positions (on the axes) of the gravity center of the laser beam focused at the distance X into the turbulent atmosphere; $(\varphi_{ps,y}, \varphi_{ps,z})$ specify the instantaneous angular positions of the image of the focused laser beacon considered as a point source. The auxiliary telescopes measure only one component of the image jitter of the laser reference star, that is, finally we have the following pair of measurable angles:

$$\begin{aligned}\varphi_{b,y} &= \varphi_{lb,y} + \varphi_{ss,y}, \\ \varphi_{b,z} &= \varphi_{lb,z} + \varphi_{ss,z},\end{aligned}\quad (2)$$

where $(\varphi_{ss,y}, \varphi_{ss,z})$ characterize the instantaneous angular positions of the image formed by an extended incoherent source, most correctly calculated in Ref. 7. Further, we calculate the corresponding differences:

$$\begin{aligned}\varphi_{m,y} - \varphi_{b,y} &= \varphi_{ps,y} - \varphi_{ss,y}, \\ \varphi_{m,z} - \varphi_{b,z} &= \varphi_{ps,z} - \varphi_{ss,z}.\end{aligned}\quad (3)$$

Because the auxiliary telescopes operate in the regime of the bistatic reference star, corresponding variances of differences (3) are expressed as

$$\begin{aligned}\langle (\varphi_{ps,y} - \varphi_{ss,y})^2 \rangle &= \langle (\varphi_{ps,y})^2 \rangle + \langle (\varphi_{ss,y})^2 \rangle = \\ &= \langle (\varphi_{ps,y})^2 \rangle \{ 1 + (\hat{a}_b/a_{a0})^{-1/3} \},\end{aligned}\quad (4)$$

where \hat{a}_{a0} is the size of the auxiliary telescope.

Now let us formulate the problem on optimal correction (decrease) for the angular jitter in the real star $\vec{\varphi}_{ns}(\varphi_{ns,y}, \varphi_{ns,z})$ on the basis of measured angles (1)–(3) and necessary calculations. In fact, we should minimize the variance of the residual angular shifts of the real star through the correction based on the measurements, namely:

$$\begin{aligned}\beta_y^2 &= \langle [\varphi_{ns,y} - A(\varphi_{m,y} - \varphi_{b,y})]^2 \rangle, \\ \beta_z^2 &= \langle [\varphi_{ns,z} - A(\varphi_{m,z} - \varphi_{b,z})]^2 \rangle.\end{aligned}\quad (5)$$

Taking the advantage of the results obtained in Refs. 2-5, we have (for the isotropic spectrum of turbulence)

$$\beta_y^2 = \beta_z^2 = \langle (\varphi_{ns,y})^2 \rangle = \left\{ 1 - \frac{2^{1/3} f(X, C_n^2)}{[1 + (\hat{a}_b/a_{ab})^{-1/3}]} \right\} \quad (6)$$

where

$$f(X, C_n^2) = \frac{\int_0^X d\xi C_n^2(\xi) (1 - \xi/X) [1 + b^2 (1 - \xi/X)^{-1/6}]^2}{\int_0^\infty d\xi C_n^2(\xi) (1 - \xi/X)^{5/3}}, \quad (7)$$

$\langle (\varphi_{ns,y})^2 \rangle$ is the variance of the angular shift of the real star image (along one axis); $b = a_0/a_{ab}$. Optimal value of the correcting coefficient \hat{A} , minimizing functionals (5), is calculated for the average model vertical profiles of the structure parameter for the refractive index in the atmosphere $\bar{N}_n^2(\xi)$, characterizing the turbulent intensity

$$A_{opt} = \frac{2^{1/6} \int_0^X d\xi C_n^2(\xi) (1 - \xi/X) [1 + b^2 (1 - \xi/X)^{-1/6}]}{(1 + (\hat{a}_b/a_{ab})^{-1/3}) \int_0^\infty d\xi C_n^2(\xi) (1 - \xi/X)^{5/3}} \quad (8)$$

Let us estimate numerically the efficiency of this correction for the real parameters of the experiment.

Let the principal telescope have the diameter varying between 3 and 10 m. The auxiliary telescopes we select from one-meter telescopes. Let the diameter of the laser beam forming the star be $\hat{a}_0 = 1$ m. The wave parameter for the focused laser beam Ω ($\Omega = ka_0^2/X$) is in the interval 10-100 for altitudes X varying from 10 to 100 km. Hence, in the focal waist the laser beacon size is $a_m = 1-10$ cm. Thus, the laser star cross section is seen by the principal telescope at angles $\theta \leq 0.1''$, which practically can be considered as a point source. At the same time, the length of the laser star is a_b and hence for proper separation of the auxiliary telescope axes, the visible size of the star \hat{a}_b may be several minutes of arc, that is, the laser star can be considered as an extended incoherent source in the image planes of the auxiliary telescopes. The real ratio is $\hat{a}_b/a_{ab} \approx 10^3$, $b = 1$. In calculations, we used the average model $\bar{N}_n^2(\xi)$ suggested in Ref. 8.

Summarizing these data and making calculations, we obtain for Eqs. (6)-(8)

$$\Delta = \frac{\beta_y^2}{\langle (\varphi_{ns,y})^2 \rangle} = \frac{\beta_z^2}{\langle (\varphi_{ns,z})^2 \rangle} = \left(1 - \frac{2^{1/3} f(X, C_n^2)}{(1 + 0.1)} \right) \quad (9)$$

$$A_{opt} = \frac{2^{1/6} \int_0^X d\xi C_n^2(\xi) (1 - \xi/X) [1 + (1 - \xi/X)^{-1/6}]}{1.1 \int_0^\infty d\xi C_n^2(\xi) (1 - \xi/X)^{5/3}} \quad (10)$$

Results of numerical calculations are tabulated. The data for the case of nonoptimal correction (that is, for $\hat{A} = 1$) are also given in Table I. In this case,

$$\Delta = \frac{\beta_y^2}{\langle (\varphi_{ns,y})^2 \rangle} = 1 + [1 + (\hat{a}_b/a_{ab})^{-1/3}] \frac{\int_0^X d\xi C_n^2(\xi) (1 - \xi/X)^{5/3}}{\int_0^\infty d\xi C_n^2(\xi)} - 2^{7/6} \frac{\int_0^X d\xi C_n^2(\xi) (1 - \xi/X) [1 + b^2 (1 - \xi/X)^{-1/6}]^2}{\int_0^\infty d\xi C_n^2(\xi)} \quad (11)$$

Thus, from the table it can be seen that already for the altitude of laser reference star formation higher than 10 km, this algorithm effectively corrects for the jitter in the real star image on the basis of measuring

components of the jitter in two perpendicular separated telescopes.

TABLE I.

X, km	A_{opt}	Δ from Eq. (9)	Δ from Eq. (11)
1	1.22	0.509	0.5139

(two components) of the jitter in the monostatic star image in the principal telescope and individual

10	1.096	0.1799	0.1802
100	1.019	0.0866	0.0927

It should be noted that in practice there is no need to optimize the correction by this scheme (that is, specially calculate the parameter \bar{A}); nonoptimal correction (for $\bar{A} = 1$) also highly efficiently corrects for the angular shift of the real star within the limits of isoplanatic angles with the use of the laser reference star.

Apparently, our results should be compared with the data of Ref. 7. First of all, we note that the final result is that the control signal so obtained, in contrast with the results of Belen'kii,⁷ is completely independent of the laser beam characteristics. In Ref. 7, the useful signal for the correction is φ_{fa} , that is, the wave-front tilt on the entire aperture. At the same time, the total tilt of the beam φ_{lb} (in the beacon plane) is

$$\varphi_{lb} = \varphi_{fa} + \varphi_{lt}, \quad (12)$$

where φ_{lt} is the local tilt of the beam.

In this treatment, φ_{fa} is determined by integration over the path in the upward direction (although from Ref. 7 it is not clear, what wave: plane? laser beam? spherical wave?). However, on the backpath (in formulation of Belen'kii) this term is compensated in Eq. (12); therefore, in the principal telescope we measure

$$\varphi_m = \varphi_{lb} - \varphi_{fa} = \varphi_{lt}.$$

It is well known that in the monostatic scheme the variance of the angular jitter

$$\langle \varphi_m^2 \rangle = \text{const} (a_0^{-1/3} + a_0^{-1/3} - 2^{7/6} (a_0^2 + a_0^2)^{-1/6}) \times$$

$$\times \int_0^X d\xi C_n^2(\xi) \left(1 - \frac{\xi}{X}\right)^{5/3},$$

therefore, the complete correction can be realized only for the case $a_0 = \bar{a}_0$. In this case, jitter in the beam of diameter \bar{a}_0 is compensated by the point source jitter on the aperture \bar{a}_0 (when $a_0 = \bar{a}_0$). Thus, the useful signal for the correction is the angle φ_{fa} (in Belen'kii's

opinion, this is a portion of the jitter in the beam propagating upward caused by the entire aperture of the telescope). However, this is not the case. Most probably, separation of the term φ_{fa} from sum (12) is a far-fetched maneuver in the chain of explanation.

In my reasoning, the useful signal (for the correction) is the difference $\varphi_{ps} - \varphi_{ss}$, representing the image jitter of the point source without the average jitter of the secondary incoherent sources, being the difference of two measurements $\varphi_m - \varphi_b$; in this case, the useful correction signal represents the results of integration (practically for the point source) over the downward propagation path, whereas the signal obtained by Belen'kii (φ_{fa}) is the portion (see formula (12)) of the beam jitter φ_{lb} , connected with the integration of the turbulence over the upward propagation path.

I would say that the method suggested by Belen'kii is true in the essence of its operations, but was explained incorrectly; as a result, this complicates the understanding of actual operation of this algorithm.

And finally, the main point is that the angle φ_{lb} from (12) does not comprise the term, which would be useful for efficient correction for the tilt angle of the real star φ_{ns} . In my opinion, Belen'kii offers very strange explanation for each term of sum (12). According to his treatment, the total tilt of the laser beam φ_{lb} (in the plane X) does not depend on the size of the principal mirror, but each term of sum (12) depends on this size. I am convinced this is not the case: the total tilt of the beam φ_{lb} cannot comprise any components that depend on the characteristics of foreign objects, namely, of the principal telescope in this case, rather than on the characteristics of the beam itself (beam diameter and distance of focusing) and the propagation medium.

REFERENCES

1. V.P. Lukin and B.V. Fortes, ESO Conference and Workshop Proceeding, No. 54, 101-194 (1993).
2. V.P. Lukin, Atmos. Oceanic Opt. **9**, No. 11, 948-956 (1996).
3. V.P. Lukin and B.V. Fortes, Atmos. Oceanic Opt. **10**, No. 1, 34-41 (1997).
4. V.P. Lukin and E.V. Nosov, Pure and Applied Optics, 1997. (in print).
5. V.P. Lukin, OSA Proc. Adaptive Optics, MB35-1-MB35-5 (1996).
6. R. Ragazzoni, Astrophys. J. **465**, L73-L75 (1996).
7. M.S. Belen'kii, Proc. SPIE **2956**, 206-217 (1996).
8. M.A. Gracheva and A.S. Gurvuch, Fiz. Atmos. Okeana, No. 10, 1107-1111 (1980).



Institute of Atmospheric Optics SB RAS
Laboratory of Coherent and Adaptive Optics

Report on Contract SPC 97 - 4040
(third four month period)

Principle Investigator
Prof. Lukin V.P.

Tomsk - 1998

CONTENTS

Intoduction	3
Chapter 1. The main elements of an adaptive system model: a reference source, wave front sensor, and adaptive mirror	4
1.1. A reference wave	4
1.2 Wave front sensor	12
1.3. Wave front correctors	22
1.4. Computer codes	32
References to Chapter 1	40
Chapter 2. Partial correction for turbulent distortions in telescope	42
2.1 Wave front correctors and partial correction of the PSF	44
2.2 Hartmann sensor and partial correction	56
2.3 Cone anisoplanatism and partial correction	59
References to Chapter 2	63

INTRODUCTION

The first report on Contract SPC 97-4040 was devoted to the methods of numeric simulation of waves propagating in randomly inhomogeneous medium. It was shown that with the use of the developed models it is possible to describe correctly turbulent and thermal distortions of coherent beams.

To describe a whole adaptive optics system it is also necessary to take into account limits of its spatio-temporal resolution, or, in other words, its ability to form a given wave front with high speed and in some spatial interval. Temporal resolution of the system is defined by an algorithm of control and by characteristic frequency of its optics and electronics components and its mechanical parts. Spatial resolution is defined mainly by geometry of such key elements as a wave front sensor and corrector.

In Chapter 1 we consider mathematical and numerical simulation of a sensor and corrector allowing for their geometry, number of elements, and mechanical properties. Simulation of a reference sources is also considered in Chapter 1 including simulation of anisoplanarity cone of a laser guide star.

In Chapter II we apply the model and developed on its base computer codes in the problem of adaptive forming of images in a telescope. Here the main attention is devoted to the analysis of the structure of a point spread function under the condition of partial correction.

CHAPTER 1. THE MAIN ELEMENTS OF AN ADAPTIVE SYSTEM MODEL: A REFERENCE SOURCE, WAVE FRONT SENSOR, AND ADAPTIVE MIRROR

In the present Chapter of the report we consider three main elements of an adaptive loop:

- ♦ reference source;
- ♦ wave front sensor;
- ♦ corrector of a wave front.

We have investigated the following modifications of these elements: a reference source, natural guide star, artificial guide star; an ideal quadratic sensor, an ideal sensor of phase differences, Hartmann-Shack sensor, modal corrector, segmented mirror with hexagonal elements, mirror with given response functions, and deformable mirror with continuous surface. The results of simulation of these elements are presented partly in this report and will also be included in next reports.

1.1. A reference wave

A typical adaptive optics system employs a reference wave to obtain information about atmospheric inhomogeneities. In phase conjugated adaptive systems /1, 2, 3/ as a reference wave can be used a wave reflected from an object, or an additional laser, or radiation scattered by the atmosphere /4/. In adaptive systems of an image correction for correction of distortions is used a portion of incident wave /5, 6/.

Let us consider a reference wave as a coherent monochromatic radiation with a complex amplitude $U(\vec{\rho}, z, t)$

$$\vec{E}_{ref}(\vec{\rho}, z, t) = \vec{u} \cdot U(\vec{\rho}, z, t) \cdot \exp(i\omega t + ikz). \quad (1.1)$$

Here and hereafter all the notations used are the same as in the first report on Contract SPC 97-4040.

Propagation of this wave in direction opposite to Z-axis is described by the parabolic equation:

$$-2ik \frac{\partial U}{\partial z} = \left(\frac{\partial^2}{\partial x^2} + \frac{\partial^2}{\partial y^2} + k^2(n^2/n_0^2 - 1) \right) U. \quad (1.2)$$

In imaging systems the wave with aberrations that should be corrected propagates in the same direction as a reference wave and so it is described in the same way. In the systems of beam focusing waves propagate in opposite directions. In this case the complex amplitude of corrected beam $E(\vec{\rho}, z, t)$

$$\bar{E}(\vec{\rho}, z, t) = \bar{e} \cdot E(\vec{\rho}, z, t) \cdot \exp(i\omega t - ikz) \quad (1.3)$$

is described by the equation

$$2ik \frac{\partial E}{\partial z} = \left(\frac{\partial^2}{\partial x^2} + \frac{\partial^2}{\partial y^2} + k^2(n^2/n_0^2 - 1) \right) E. \quad (1.4)$$

A reference beam in a phase conjugated system

Let us consider an adaptive system in which distortions compensated according *phase conjugation algorithm*. To estimate the characteristics of this algorithm the reference wave should be defined in such a way that in the absence of aberrations the conditions of propagation would be same as in the absence of adaptive control. So the boundary conditions for the corrected beam should be written using the difference ΔS of wave front of the reference wave from the diffraction limited phase distribution S_D :

$$E_0(\vec{\rho}) = E(0, \vec{\rho}) = A_0(\vec{\rho}) \cdot \exp(i\Delta S) \quad \Delta S = S(\vec{\rho}) - S_D(\vec{\rho}), \quad (1.5)$$

or

$$E_0(\vec{\rho}) = A_0(\vec{\rho}) \exp(i \arg(U(\vec{\rho}) \cdot U_D(\vec{\rho}))). \quad (1.6)$$

Here A_0 is a complex amplitude of the initial beam in the plane of transmitting aperture. If the reference and corrected beams have different wavelengths, the procedure of adaptive correction should be formulated in terms of wave fronts

$$E_0(\vec{\rho}) = A_0(\vec{\rho}) \cdot \exp(ik(\theta(\vec{\rho}) - \theta_{\pi}(\vec{\rho}))), \quad (1.1.7)$$

where θ is eikonal of the reference wave. Eqs. (1.1.7) and (1.1.8) do not impose any additional conditions on the reference wave, but it is assumed that the phase of the wave in vacuum is known.

Phase conjugation (PC) we will consider as a full field phase conjugation (FFPC), but without the amplitude control, i.e.,

$$E_0(\vec{\rho}) = U_0^*(\vec{\rho}) \quad (\text{FFPC}), \quad (1.1.8)$$

$$E_0(\vec{\rho}) = |A_0(\vec{\rho})| \cdot \exp[-i \arg(U_0(\vec{\rho}))] \quad (\text{PC}). \quad (1.1.9)$$

To obtain with Eq. (1.1.9) in vacuum the same results as for beams without correction the following condition should be imposed on the field of the reference beam:

$$U_0^D(\vec{\rho}) = \text{const} \cdot A_0(\vec{\rho}), \text{ i.e., } \arg(U_0^D(\vec{\rho})) = \arg(A_0(\vec{\rho})), \quad (1.1.10)$$

here U_0^D - is diffraction limited wave front. The wave equation can be conjugated so this condition is satisfied if the boundary condition for a reference wave is expressed through diffraction limited wave front U_0^D of a beam without correction

$$U(\vec{\rho}, L) = \text{const} \cdot E^D(\vec{\rho}, L). \quad (1.1.11)$$

In the problem with boundary conditions formulated in this way the phase conjugation of the reference wave approaches the full field phase conjugation when optical distortions on the path of propagation decrease.

The conditions stated above insure the results of correction almost the same as the results obtained in vacuum, at least under the small distortions. So the estimations of this kind can be considered as estimations of limits of adaptive system efficiency.

An artificial star used in an adaptive telescope

Let us consider a problem of reference source simulation in adaptive imaging systems. In this case reference and corrected wave propagate in the same direction. If a portion of corrected beam energy transferred to the wave sensor, this wave is a reference and corrected at once.

In a ground-based adaptive telescope the reference source is a natural or artificial star. In such systems there are different causes of residual errors. For

example, angular anisoplanarity /7, 8, 9, 10/ and quantum noise in the case of a natural star. If an artificial star is taken as a beacon, the residual errors associated, first of all, with the fact that reference wave is divergent and travels through inhomogeneities different from that for a plane wave irradiated by a star.

Boundary conditions for a reference wave irradiated by a natural star can readily be written. The wave is plane, the axis of propagation is slanted on some angle γ to Z - axis of coordinate system:

$$U_0(\vec{\rho}, \vec{\gamma}) = A \cdot \exp(ik\vec{\gamma}\vec{\rho}). \quad (1.1.12)$$

Numerical simulation becomes difficult if this angle is greater than $1''$. Really, the spatial spectrum of complex amplitude for this radiation is the following

$$\tilde{U}(\vec{\kappa}) = \int_{-\infty-\infty}^{\infty} \int_{-\infty-\infty}^{\infty} A \cdot \exp(ik\vec{\gamma}\vec{\rho}) \exp(i\vec{\kappa}\vec{\rho}) d^2\rho = A \cdot \delta(k\vec{\gamma}). \quad (1.1.13)$$

This spectrum corresponds to the spatial frequency $\kappa = k\gamma$, but according to Kotelnikov theorem the maximum frequency that can be reproduced on the grid with a step of discretization $\Delta\rho$ is

$$\kappa_{\max} = \frac{\pi}{\Delta\rho}. \quad (1.1.14)$$

Using the condition $k\gamma < \kappa_{\max}$ we obtain

$$\gamma < \frac{\pi}{k\Delta\rho} = \frac{\lambda}{2\Delta\rho}. \quad (1.1.15)$$

With typical wavelength $\lambda=10^{-6}$ m and $\Delta\rho=10^{-1}$ m

$$\gamma < 5 \cdot 10^{-6} \approx 1''. \quad (1.1.16)$$

At the same time the angles of most interest are of order of $10''$, that means that the step of discretization on the grid should be taken 10^{-2} m. If we consider the problem of 10-m telescope the computational grid is 1000×1000 , that is too much.

To decrease the dimension of the problem we propose the following technique. The boundary condition for the complex amplitude is written in the same way as for a wave propagating along the axis of the optical system ($\gamma = 0$) and each phase screen is shifted on the interval $\bar{\Delta} = \vec{\gamma} \cdot \vec{z}$ which is equal to the distance between the axis of optical system and the «central» beam of the plane

wave. In other words we make the change

$$U_0(\vec{\rho}, \vec{\gamma}), S(\vec{\rho}) \rightarrow U_0(\vec{\rho}, \vec{\gamma} = 0), S(\vec{\rho} - \vec{\gamma}z). \quad (1.1.17)$$

With $\gamma = 10''$ on the upper boundary of the atmosphere ($z = 20$ km) the shift is equal approximately to 1 meter. When the direction vector γ coincide with wind velocity V , the shift of a screen in a space can be substituted by equivalent temporal interval, i.e.,

$$U_0(\vec{\rho}, \vec{\gamma}), S(\vec{\rho}, t) \rightarrow U_0(\vec{\rho}, \vec{\gamma} = 0), S(\vec{\rho}, \vec{\gamma}z/\vec{V}). \quad (1.1.18)$$

Let us consider the problem of **simulation of an artificial star**. The idea to change a natural star for an artificial beacon appeared due to difficulty associated with correction of residual errors induced by angular anisoplanarity. So such a beacon is usually placed on the axis of the optics system.

A laser guide star is formed by backscattering of radiation. So the propagation of a laser beam should be simulated from the ground to the upper layers of the atmosphere and in the opposite direction. In the both cases we encounter difficulty, and the method of numerical simulation should be modified.

One of the problems is that computations should be made for a focused beam with large Fresnel number. In a case of 3m telescope with an artificial star generated by a laser beam of a wavelength $0.5 \cdot 10^{-6}$ focused at 10 kilometers Fresnel number is

$$N_F = \frac{D}{\sqrt{\lambda L}} = \frac{3}{\sqrt{0.5 \cdot 10^{-6} \cdot 10^4}} \approx 42, \quad (1.1.19)$$

and wavenumber (Gaussian beam) is

$$\Omega^{-1} = \frac{L}{kR^2} = \frac{\lambda L}{2\pi(D/4)^2} = \frac{0.5 \cdot 10^{-6} \cdot 10^4}{6.28 \cdot 0.75^2} \approx 1.5 \cdot 10^{-3} \quad (1.1.20)$$

With such wavenumbers the lens transform of initial wave front should be performed but this type of transformation is not always possible. But at the same time we should understand that the main cause of residual errors is purely geometrical. A large Fresnel number and relatively short path allows one to conclude that the approximation of geometric optics is possible in the problem.

We propose the following method of solution

The upward propagation is considered as a convergent cone of rays intersecting in the lens focal plane, the base of the cone is equal to the diameter of transmitting aperture. Simulating upward propagation it is necessary to define shifting of the focal spot in transverse direction due to random refraction. Broadening of the spot due to refraction and turbulence can be taken out of consideration because beacon is seen through a subaperture of Hartmann-Shack sensor as an object that cannot be resolved.

The shift of a focal spot (the top of a cone) can be written as

$$\Delta \vec{\rho} = \int_0^L \vec{s}(z) dz \quad (1.1.21)$$

where L is path length, $\vec{s}(z)$ is a vector defining the direction of the axis in a cross section z . In numeric experiments the randomly inhomogeneous medium is represented by a set of discrete layers so the integral in Eq. (1.1.21) is substituted by a sum

$$\Delta \vec{\rho} = \sum_{j=1}^{N_z} \vec{s}(z_j) \cdot (z_{j+1} - z_j), \quad (1.1.22)$$

where z_j is coordinate of j th phase screen. The tilt of the beam axis is defined by refraction on the whole set of screens (from the ground to j th phase screen including also this screen), i.e.,

$$\vec{s}(z_j) = \sum_{j'=1}^j \vec{s}_{j'}, \quad (1.1.23)$$

where \vec{s}_j is contribution of j th screen. This contribution should be defined as a mean gradient of phase S_j with averaging over the cone cross section in plane z_j

$$s_j^x = \iint_{R(z_j)} dx dy \frac{\partial S_j}{\partial x} = \int_{-R}^R dy (S_j(x_R, y) - S_j(-x_R, y)), \quad x_R = \sqrt{R^2 - y^2} \quad (1.1.24)$$

where R is the cone radius in the taken cross section. The origin of coordinate system in each cross section coincide with the axis of the cone.

The next problem is simulation of downward propagation of the reference wave. Taking a reference source as a point and disregarding bending of rays due to atmospheric turbulence, fluctuations of optical path length of a beam in point

with coordinates $(\bar{\rho}, 0)$ can be written as

$$\tilde{l}(\bar{\rho}) = -\bar{\rho} \frac{\bar{\rho}_b}{L} + \int_0^L \tilde{n}(\bar{\rho} + (\bar{\rho}_b - \bar{\rho}) \cdot z/L, z) dz. \quad (1.1.25)$$

This equation obtained with the condition

$$\frac{(\bar{\rho} - \bar{\rho}_b)^2}{L^2} \ll 1, \quad (1.1.26)$$

i.e., in paraxial approximation.

Due to this condition was developed the well-known conclusion that the general tilt cannot be compensated for by an adaptive optics system with an artificial guide star. Let us assume that an «inhomogeneity» (a thin lens) is placed right before the telescope aperture, i.e.,

$$\tilde{n}(\bar{\rho}, z) = \bar{\alpha} \bar{\rho} \cdot \delta(z). \quad (1.1.27)$$

Using simple geometrical schemes it can be shown that a beam is formed by the lens in a point

$$\bar{\rho}_b = \bar{\alpha} \cdot L \quad (1.1.28)$$

and

$$\tilde{l}(\bar{\rho}) = -\bar{\rho} \frac{\bar{\alpha} L}{L} + \int_0^L \bar{\alpha} \bar{\rho} \cdot \delta(z) \cdot dz = -\bar{\alpha} \bar{\rho} + \bar{\alpha} \bar{\rho} = 0. \quad (1.1.29)$$

Eq. (1.1.25) is the base of numeric simulation. According to the splitting algorithm /11/ randomly-inhomogeneous field of the index of refraction is represented by a series of phase screens. This representation is equivalent to the following description of $\tilde{n}(\bar{\rho}, z)$:

$$\tilde{n}(\bar{\rho}, z) = \sum_{j=1}^{N_z} S_j(\bar{\rho}) \cdot \delta(z_j) \quad (1.1.30)$$

Substituting this equation into Eq. (1.1.25) we obtain

$$\tilde{l}(\bar{\rho}) = -\bar{\rho} \frac{\bar{\rho}_b}{L} + \sum_{j=1}^{N_z} S_j(\bar{\rho} + (\bar{\rho}_b - \bar{\rho}) \cdot z_j/L) \quad (1.1.31)$$

Transverse coordinates are also represented by discrete analogues, i.e., phase distortions are known only in nodes of the grid

$$S_{l,m,j} = S(x_l, y_m, z_j). \quad (1.1.32)$$

In the considered problem it is necessary to interpolate these values to an any arbitrary point. Simple two-dimensional interpolation is sufficient for our problem. Interpolation is performed according to the formulae

$$\begin{aligned} S(x, y) &= S(x, y_m) + \frac{S(x, y_{m+1}) - S(x, y_m)}{\Delta y} \cdot (y - y_m); \\ S(x, y_m) &= S(x_l, y_m) + \frac{S(x_{l+1}, y_m) - S(x_l, y_m)}{\Delta x} \cdot (x - x_l). \end{aligned} \quad (1.1.33)$$

Here a pair of indexes (l, m) corresponds to the left low corner of a cell where a point is located with coordinates $\bar{\rho} = (x, y)$. Optical difference of the paths for a nodes of computational grid is calculated according to Eq. (1.1.31) written in the form

$$\tilde{l}_{l,m} = \tilde{l}(\bar{\rho}_{l,m}) = -\bar{\rho}_{l,m} \frac{\bar{\rho}_b}{L} + \sum_{j=1}^{N_z} S_j(\bar{\rho}_{l,m} + (\bar{\rho}_b - \bar{\rho}_{l,m}) \cdot z_j/L). \quad (1.1.34)$$

Interpolation is performed according to Eq. (1.1.33).

We have considered three possible models of a reference wave. The model of the beam propagating in the opposite direction was formulated so as to minimize the effect of isoplanarity, i.e., paths of a reference and corrected beams in absence of aberrations coincided. Due to this fact we investigate actually the limits of phase correction efficiency.

The effect of wave diffraction on turbulent inhomogeneities can be disregarded when vertical paths are considered so efficiency of phase and amplitude-phase correction in adaptive telescopes is almost the same. The main source of aberrations is effect of anisoplanarity, i.e., the factor purely geometrical.

1.2. Wave front sensor

Information concerning inhomogeneities of the index of refraction on the path is carried by the radiation of a reference source. To extract this information we should use some electro-optics device. Commonly, devices of this kind are referenced to as wave front sensors. Numerical simulation of the sensors is considered in the present paragraph.

Generally, the problem of their simulation can be formulated in the following manner. A complex amplitude of a field obtained as a result of numeric simulation of a beam propagation is represented in nodes of a computational grid

$$U_{I,J} = U(\rho_{I,J}), \quad I, J = 0, 1, \dots, N-1 \quad (1.2.1)$$

It is required to define a two-dimensional function Φ which is estimation of a wave front of the given wave. The precision of this function estimation should be a characteristic of spatio-temporal resolution of a device that we simulate. For an ideal device this estimation should meet the following condition

$$\arg(U_{I,J} \cdot \exp(-i\phi_{I,J})) = \arg(U_{I,J} \cdot \exp(-ik\theta_{I,J})) = \text{const}. \quad (1.2.2)$$

So the estimation differs from a real quantity only by a constant.

Ideal quadrature wave front sensor

One of the problem of modern adaptive optics is comparison of full-field control with phase-only control. To accomplish this problem, principally, we need only a model of some ideal sensor. In numerical experiments we can obtain the real part $\text{Re}E = A \cos\varphi$ of a field complex amplitude as well as its second quadrature component $\text{Im}E = A \sin\varphi$, so this sensor can be called a quadrature sensor. Phase in each node of the grid is computed as a main value of an argument of complex amplitude $\arg(E)$. The possible values of $\text{Arg}(E)$ is limited to the interval $[0, 2\pi]$ so if an amplitude of aberration is greater than λ the lines of discontinuation appear inevitably. When these lines are closed the discontinuities can be removed by addition of $2\pi n$ in a region bounded by the line.

Because direct detection of quadrature components of a field is practically impossible in optical range, phase measurements by sensors are based on intensity

measurements, so we have to make some transformation of the wave (diffraction or interference) after which the distribution of intensity is analyzed mathematically, as a result we obtain the estimation of two-dimensional distribution of the wave front.

An ideal wave front sensor

There are two approaches to the problem of wave front detection. The first is based on measurements of phase differences, the second on registration of local tilts. The detection of differences is performed with the use of interference transformation and, correspondingly, an interferometer is used as the optical component of a sensor. In adaptive optics systems commonly used interferometers of transverse shear, where the phase difference between two small squares is registered. In idealized case the phase difference is detected between two spatially separated points.

The technique of numerical simulation allows one to form two-dimensional array of phase differences between neighboring nodes of the grid along OX and OY axis. The elements of the array can be written as

$$\begin{aligned}\Delta_{I,J}^x &= \arg(U_{I+1,J} \cdot U_{I,J}^*), \\ \Delta_{I,J}^y &= \arg(U_{I,J+1} \cdot U_{I,J}^*).\end{aligned}\quad (1.2.3)$$

To simulate errors of a sensor, noise can be superimposed additively on these differences

$$\begin{aligned}\Delta_{I,J}^x &= \arg(U_{I+1,J} \cdot U_{I,J}^*) + \mu_{I,J}^x; \\ \Delta_{I,J}^y &= \arg(U_{I,J+1} \cdot U_{I,J}^*) + \mu_{I,J}^y.\end{aligned}\quad (1.2.4)$$

Because complex amplitude is defined in nodes of a discrete grid, the most convenient is a direct method of phase reconstruction based on two-dimension discrete Fourier transform (DFT) [12, 13, 14]. The whole number of differences is two times greater than the number of points where the phase is computed so the problem is excessive. Usually, the following parameter is minimized

$$\sum_{I,J} \left[(\phi_{I+1,J} - \phi_{I,J}) - \Delta_{I,J}^x \right]^2 + \left[(\phi_{I,J+1} - \phi_{I,J}) - \Delta_{I,J}^y \right]^2 \rightarrow \min \quad (1.2.5)$$

or

$$\left\langle \sum_{I,J} (\phi_{I,J} - \hat{\phi}_{I,J})^2 \right\rangle \rightarrow \min. \quad (1.2.6)$$

Here angular brackets denote statistical averaging over the ensemble of noise, $\phi_{I,J}$ is the sought for phase estimation defined in nodes (i, j), $\hat{\phi}_{I,J}$ its precise value. In the both cases the solving of the set of linear equations is required

$$\phi_{I+1,J} + \phi_{I-1,J} + \phi_{I,J+1} + \phi_{I,J-1} - 4\phi_{I,J} = \Delta_{I,J}^x + \Delta_{I,J}^y - \Delta_{I-1,J}^x - \Delta_{I,J-1}^y = f_{I,J} \quad (1.2.7)$$

The unknown and known functions are represented as a Fourier series of the form

$$\Phi_{L,M} = \frac{F_{L,M}}{2(\cos(2\pi L/N) + \cos(2\pi M/N) - 2)}. \quad (1.2.8)$$

Where Φ is two dimension discrete Fourier transform (DFT) of phase array ϕ and is DFT of the right part of the original equation. For $L = M = 0$ the denominator is equal to zero that means that the problem is solved with precision up to a constant.

The values of the sought for function (wave front) are unknown at the boundaries of the region, so the boundary condition should be formulated for differences. These conditions are included already in the right-hand part of system (1.2.7) and associated with values of wave front in points beyond the boundaries of the grid region

$$\begin{aligned} \Delta_{N-1,J}^x &= \phi_{N,J} - \phi_{N-1,J}; \quad \Delta_{-1,J}^x = \phi_{0,J} - \phi_{-1,J}, \quad J = 0, \dots, N-1; \\ \Delta_{I,N-1}^y &= \phi_{I,N} - \phi_{I,N-1}; \quad \Delta_{I,-1}^y = \phi_{I,0} - \phi_{I,-1}, \quad I = 0, \dots, N-1. \end{aligned} \quad (1.2.9)$$

Definition of the boundary condition is dependent on the method of the function continuation beyond the region of definition. Any function defined on the grid with number of nodes $N \times N$ can be supplemented up to periodicity at least in one of the following two ways. First, the function is continued periodically without any transformation

$$\begin{aligned} \phi_{I-N,J} &= \phi_{I,J} = \phi_{I+N,J}, \\ \phi_{I,J-N} &= \phi_{I,J} = \phi_{I,J+N}. \end{aligned} \quad (1.2.10)$$

In this case the function is continuous only over a period. A break of continuity is possible at the end of a period. Phase differences can be calculated at the borders

through the known values by the following formulae:

$$\begin{aligned}\Delta_{-1,J}^x &= \Delta_{N-1,J}^x = \sum_{I=0}^{N-2} \Delta_{I,J}^x, \\ \Delta_{I,-1}^y &= \Delta_{I,N-1}^y = \sum_{J=0}^{N-2} \Delta_{I,J}^y.\end{aligned}\tag{1.2.11}$$

Next method of continuation is definition of a new discrete function on a grid with doubled number of nodes by mirror reflection of an original function /15, 16/. The obtained function is periodical with a period $2N$. Only one quarter of the area is used that corresponds to the initial grid with $N*N$ nodes.

The same system of equations is solved in both cases so the result should be the same, at least when noise is absent. The first method is more economical, because Fourier transform is performed on the grid with less number of nodes.

From the above we can conclude that solving Eqs. (1.2.7) with a right hand part defined by Eq. (1.2.3) one can obtain wave front with precision up to a constant. Definition of noise according to Eq. (1.2.4) facilitates simulation of measurement errors. All in all, this model corresponds to interferometric sensor with resolution equal to a distance between nodes.

From the other hand, the algorithm allows one to solve the problem of unwrapping of a wave front which appears in a model of an ideal quadrature sensor, but only when all contours of discontinuity is closed.

A sensor of local tilts

Let us consider a model of a Hartmann-Shack sensor. The method formulated by Hartmann /17/ is based on measurement of local tilts on subapertures and subsequent calculation of a phase map over the whole aperture.

Nowadays Hartmann-Shack sensor is the most common in adaptive optics applications. Geometry of the sensor is illustrated in Fig. 1. The sensor is a set of focusing lenslets, a matrix of photodetectors is placed in a focal plane of lenslets. Light amplifiers are used usually to increase the intensity of light incident on the sensor.

The sensor operates in the following way. Each subaperture focuses a portion of light into a photodetector plane. Shifts of focal spots is obtained using signals

from photodetectors. It is assumed that these shifts are proportional to average local tilt of a wave front in bounds of corresponding subaperture. When the matrix with large number of photosensitive elements is used, the shift of focal spot is defined as a shift of its centroid.

We have realized numerically two models of Hartmann-Shack sensor /18/.

The first method of the sensor simulation

This method is based on a direct calculations of intensity distribution in a focal spot for each of subapertures and subsequent estimation of centroid shift.

According to the method developed small parts corresponding to subaperture areas are cut out from the initial array of complete amplitude. The obtained arrays include very few elements so it is convenient to supplement them by zeros, in this way we can obtain intensity distribution on more dense grid. The input pupil of the sensor is circular so we should mask correspondingly distribution of the intensity. An amplitude mask is also superimposed on each subaperture.

The next step of the algorithm is computation of intensity in a focal plane of a subaperture.

The important factor that influence the error of measurements is a shot noise that can be accounted for by quantum origin of light and by a dark current of a photodetector. Simulating numerically Hartmann-Shack sensor it is convenient to use an input parameter mean number of photons $\langle N_p \rangle$ incident on a subaperture during the time of exposure. Each node of computational grid corresponds to a small area of photodetector. For each area the mathematical

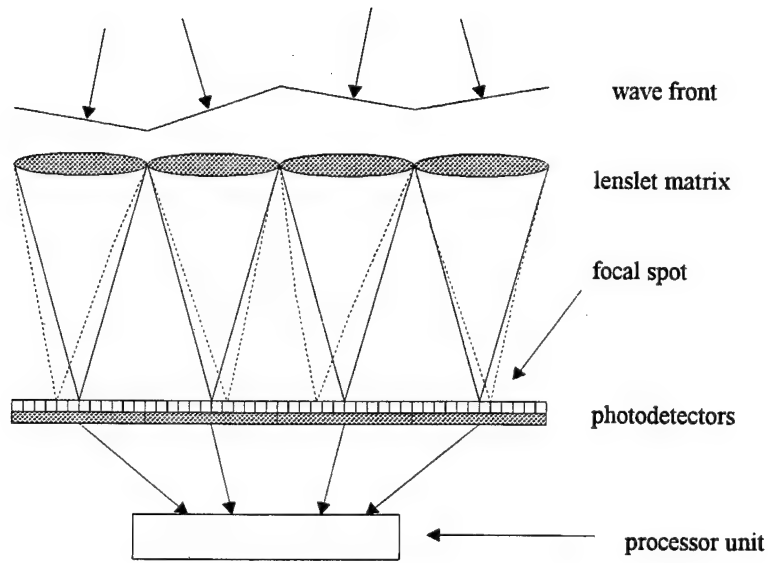


FIG.1 Schematic representation of a wave front sensor

expectation of a photoelectron number $\langle n_p \rangle$ is calculated as a product of $\langle N_p \rangle$ and a portion of beam energy incident on the area. Using the calculated mean $\langle n_p \rangle$ we generate random values n_p according to Poisson statistics. The shift of focal spot $\Delta \bar{\rho}$ is estimated as a shift of centroid of the distribution $n_p(x_I, y_I)$ after that the local tilt is calculated as a ratio of $\Delta \bar{\rho}$ and focal length f

$$\bar{s} = \Delta \bar{\rho}_c / f \quad (1.2.12)$$

The second method of the sensor simulation

In application of the second method calculation of intensity distribution in focal plane of a sensor subapertures is not necessary. The method is based on the direct estimations of the centroid shift. In this case the shift is taken as a weighted on intensity I mean over subaperture A gradient of wave front ϕ . Using the parabolic equation it is easy to obtain the well-known equation

$$\bar{\rho}_c = \frac{kf}{P} \iint_A I(\bar{\rho}) \bar{\nabla} \phi d^2 \rho. \quad (1.2.13)$$

Here P is the whole power of the beam incident on the subaperture. Difficulty in application of the equation associated with taking phase derivative, i.e., if we know complex amplitude it does not mean that we have a continuous phase surface. To avoid this difficulty we should express a weighted phase gradient through gradients of imaginary and real parts of a complex amplitude E

$$I(\bar{\rho}) \bar{\nabla} \phi - |E|^2 \bar{\nabla} \text{arctg}(\text{Im } E / \text{Re } E) = (\text{Re } E) \bar{\nabla}(\text{Im } E) - (\text{Im } E) \bar{\nabla}(\text{Re } E). \quad (1.2.14)$$

After that we obtain the following equation for a local tilt estimation:

$$\bar{s} = \frac{1}{P} \iint_A [(\text{Re } E) \bar{\nabla}(\text{Im } E) - (\text{Im } E) \bar{\nabla}(\text{Re } E)] d^2 \rho \quad (1.2.15)$$

In our numeric model calculation of derivatives is organized with the use of DFT performed over the whole grid, after that the estimations for each of subapertures are obtained. This technique allows us to minimize the number of numerical calculations.

Reconstructed wave front can also be obtained by different methods. There are two main approaches to this problem. According to the **first approach** phase differences are calculated through local tilts after that an algorithm is used

analogous to algorithms employed in interferometric sensors. According to the second a wave front is written as a sum of some functions. For this sum local tilts should be the same as calculated earlier local tilts.

When we use a modal reconstruction over a sensor aperture the sought for distribution is a series of polynomials Z_l

$$\phi(\vec{\rho}) = \sum_{l=1}^{N_z} a_l \cdot Z_l(\vec{\rho}). \quad (1.2.16)$$

When the difference is minimized between local tilts of this distribution and tilts obtained in the wave front sensor

$$\sum_{m=1}^M \left[\sum_{l=1}^{N_z} a_l \vec{Z}_{lm} - \vec{s}_m \right]^2 \rightarrow \min. \quad (1.2.17)$$

Here \vec{Z}_{lm} is the local tilt of the l th function of the basis over the m th subaperture. The components of local tilts can readily be computed as coefficients of linear approximation of function. The problem of minimization is solved by a common method, i.e., by taking partial derivative with respect to the coefficients of the series and equating these derivative with zero.

$$\frac{\partial}{\partial a_k} \sum_{m=1}^M \left[\sum_{l=1}^{N_z} a_l \vec{Z}_{lm} - \vec{s}_m \right]^2 = 0. \quad (1.2.18)$$

As a result the system of linear equation is obtained which can be written in a matrix form as

$$\|A_k\| \cdot \|a_l\| = \|B_k\|, \quad (1.2.19)$$

where

$$A_{kl} = \left(\sum_{m=1}^M \vec{Z}_{lm} \cdot \vec{Z}_{km} \right), \quad B_k = \sum_{m=1}^M \vec{s}_m \cdot \vec{Z}_{km}. \quad (1.2.20)$$

The system has a following solution

$$\|a_l\| = \|A_{kl}\|^{-1} \|B_k\| \quad (1.2.21)$$

The reverse matrix is calculated numerically when sensor data are initialized and the reverse matrix once calculated is used after that at each subsequent exposure.

Zernike polynomials are use commonly as the basis of expansion and we also use them.

The second method of a wave front reconstruction is based on a zonal

algorithm. The first step of the method is calculation of phase difference Δ between the centers of neighboring subapertures

$$\Delta_{km} = \frac{1}{2}(\vec{g}_k + \vec{g}_m)(\vec{\rho}_k - \vec{\rho}_m),$$

where ρ_k and ρ_m are coordinates of the centers of the m th and k th subapertures, g_k and g_m are estimations of local tilts over these subapertures. Vector description of algorithms allows one to use them practically for any geometry of subapertures.

Testing of the sensor numeric model is performed by the following method. A given phase was defined as a sum of the first ten Zernike polynomials. Hartmann-Shack sensor was simulated according to technique described earlier. Errors of reconstruction of polynomial coefficients were less than 1%.

1.3. Wave front correctors

Because a corrector of the wave front defines a spatial resolution of an adaptive system, it can be considered as a key element of the loop.

The mirrors are commonly used as correctors in modern systems of adaptive optics. The two main types of mirrors are segmented and flexible. The mirrors differ by a number of degrees of freedom, material, geometry of driver and so on. These two types of correctors are considered in the present paragraph of the report.

Modal correctors

A modal corrector is a hypothetical mirror, its response functions are components of some basis of expansion, usually, Zernike polynomials. There is no such a device, but estimations of its efficiency is interesting from theoretical point of view, as well as from practical. For example, some flexible mirrors are developed with an interface that allows one to assess the quality of reproduction of the lowest Zernike polynomials /19/. From the other hand, the output parameters of the algorithm of a wave front reconstruction described in the previous section of the report, are coefficients of aberrations. And to formulate requirements to a mirror it is possible to estimate the number of these aberrations. Moreover, statistics of Zernike polynomials are well known for turbulent distortions /20, 21, 22, 23, 24/ and in some cases allows one to obtain simple expressions for estimations of control efficiency /25, 26, 27, 28, 29/.

In the adaptive optics system with a modal corrector the corrected wave front is computed as a difference between the initial wave front and a truncated series of Zernike polynomials

$$\Delta\phi(\vec{\rho}) = \phi(\vec{\rho}) - \sum_{l=1}^L a_l Z_l(\vec{\rho}) \quad (1.3.1)$$

The coefficients of the series are found from the condition of the minimum of approximation error

$$\int W(\vec{\rho}) \left[\phi(\vec{\rho}) - \sum_{l=1}^L a_l Z_l(\vec{\rho}/R) \right]^2 d^2\rho \rightarrow \min \quad (1.3.2)$$

If an aperture function corresponds to a circle

$$W(\vec{\rho}) = \begin{cases} 1, \rho \leq R, \\ 0, \rho > R, \end{cases} \quad (1.3.3)$$

then from orthogonality of Zernike polynomials in a circle it follows that the sought for coefficients can be found as coefficients of expansion

$$a_l = \frac{\int_{\rho < R} \phi(\vec{\rho}) \cdot Z_l(\vec{\rho}) \cdot d^2\rho}{\int_{\rho < R} Z_l^2(\vec{\rho}) \cdot d^2\rho} \quad (1.3.4)$$

In the opposite case the problem is solved by a variational method from which the system of equations follows

$$\|A_{kl}\| \cdot \|a_l\| = \|B_k\| \quad (1.3.5)$$

where

$$A_{kl} = \int W(\vec{\rho}) \cdot Z_k(\vec{\rho}/R) \cdot Z_l(\vec{\rho}/R) d^2\rho, \quad B_k = \int W(\vec{\rho}) \cdot Z_k(\vec{\rho}/R) \cdot \phi(\vec{\rho}) d^2\rho \quad (1.3.6)$$

In a numeric model all functions are defined by their discrete analogues and integrals are changed for corresponding sums

$$A_{kl} = \sum_{I,J} W(\vec{\rho}_{I,J}) Z_k(\vec{\rho}_{I,J}/R) Z_l(\vec{\rho}_{I,J}/R), \quad B_k = \sum_{I,J} W(\vec{\rho}_{I,J}) Z_k(\vec{\rho}_{I,J}/R) \phi(\vec{\rho}_{I,J}) \quad (1.3.7)$$

Solution of Eq. (1.3.5) yields the following parameter that should be minimized

$$\sigma^2 = \sum W_{I,J} \left[\phi_{I,J} - \sum_{l=0}^L a_l Z_l(\vec{\rho}_{I,J}/R) \right]^2 \quad (1.3.8)$$

Deformable mirrors

In the modern scientific literature many types of deformable mirrors are described. They differ by number and construction of actuators, by a method of actuators clumping on the mirror plate and so on. The most common are mirrors with discrete points of application of deforming forces or moments of forces /30/. So we consider this type of mirror in more details. Usually this mirror is described through given response functions. The surface of mirror is defined as a weighted sum of this functions

$$S(\vec{\rho}) = \sum_{l=1}^L a_l \cdot f_l(\vec{\rho} - \vec{\rho}_l) \quad (1.3.9)$$

where a_l is a deformation of reflecting surface in a point of l th actuator fastening. The response functions can be obtained experimentally or found by solving corresponding problem of mechanics. There are shown by some authors that Gaussian response functions

$$f(\vec{\rho}) = \exp\left(-\frac{\rho^2}{w^2}\right) \quad (1.3.10)$$

ensure good correspondence with experimental data. The half width w is obtained from experimental data. The typical value of this function is $0.7 - 0.8 d$, where d is a distance between actuators.

To obtain a reproduction of a given surface by a mirror the problem of minimization (Eq. (1.3.8)) was written in a following form

$$\sigma^2 = \int W(\vec{\rho}) \left(\phi(\vec{\rho}) - \sum_{l=1}^L a_l f(\vec{\rho} - \vec{\rho}_l) \right)^2 d^2\rho \rightarrow \min \quad (1.3.11)$$

To decrease volume of calculations the response function is defined as truncated Gaussian function

$$f(\vec{\rho}) = \begin{cases} \exp(-\rho^2/w^2), & \rho \leq 2w \\ 0, & \rho > 2w \end{cases} \quad (1.3.12)$$

Correspondingly, the elements of matrix (1.3.5) are calculated as

$$\begin{aligned} A_{kl} &= \sum_{|\vec{\rho}_{I,J} - \vec{\rho}_k| < 2w} W(\vec{\rho}_{I,J}) \cdot f_k(\vec{\rho}_{I,J} - \vec{\rho}_k) \cdot f_l(\vec{\rho}_{I,J} - \vec{\rho}_k), \\ B_k &= \sum_{|\vec{\rho}_{I,J} - \vec{\rho}_k| < 2w} W(\vec{\rho}_{I,J}) \cdot f_k(\vec{\rho}_{I,J} - \vec{\rho}_k) \cdot \phi(\vec{\rho}_{I,J}), \end{aligned} \quad (1.3.13)$$

The actuators were fastened in nodes of an equidistant grid. Coordinates of nodes (x_l, y_l) , $l = 1, \dots, L$, was calculated according to the formula

$$\begin{aligned} x_l &= -R + [l/\sqrt{L}] \cdot d, \\ y_l &= -R + \{l/\sqrt{L}\} \cdot \sqrt{L} \cdot d. \end{aligned} \quad (1.3.14)$$

Here the entire part of a variable is marked by square brackets and its submultiple by curly brackets, R is a radius of the corrector.

A segmented mirror

Modern segmented mirrors differ by the two main parameters: by form of segments and by the number of degrees of freedom for an element. The whole number of elements is also varied.

The form of elements is usually square or hexagonal. The number of freedom for an element differ from one (control of piston) to three (control of piston, tip, and tilt).

Mathematics description of the surface S of such a mirror is also possible with the use of response functions.

$$S(\vec{\rho}) = \sum_{i=1}^L a_i \cdot w(\vec{\rho} - \vec{\rho}_i) \cdot f_i(\vec{\rho} - \vec{\rho}_i) \quad (1.3.15)$$

where response functions f_i are defined in a form

$$\begin{aligned} f_i(\vec{\rho}) &= C_i, \\ f_i(\vec{\rho}) &= A_i x + B_i y, \\ f_i(\vec{\rho}) &= A_i x + B_i y + C_i, \end{aligned} \quad (1.3.16)$$

The first formula corresponds to an element with one degree of freedom, the second to an element with two degrees of freedom and so on.

An aperture function of the corrector is equal to unity inside the corrector aperture and to zero behind the aperture.

$$w(\vec{\rho}) = \begin{cases} 1, & \vec{\rho} \in A \\ 0, & \vec{\rho} \notin A. \end{cases} \quad (1.3.17)$$

For a corrector with square elements definition of the aperture function is simple

$$w(\vec{\rho}) = \begin{cases} 1, & |x| \leq d/2 \wedge |y| \leq d/2 \\ 0, & |x| > d/2 \vee |y| > d/2, \end{cases} \quad (1.3.18)$$

where d is a size of an element. More difficult is definition of an aperture function for a corrector with hexagonal elements. Difficulty arouses especially when the corrector with a given number of actuators should be inscribed in an aperture with a given size.

In the algorithm developed by us this problem is solved in a following way. The input parameters of the procedure are radius of the corrector aperture R and number of the rings N of elements. One ring corresponds to a 7 - element

corrector, 2 to 19 - element corrector, 3 to 37 - element corrector and so on. The first step is definition of the radius of a circle r circumscribed about an element. The circle is so calculated that an aperture of the radius R would be entirely filled by elements. We obtained the following formula:

$$r = \frac{R}{3 \cdot [(N+1)/2 - 1]} \quad \text{for a even } N, \quad (1.3.19)$$

and

$$r = \frac{R}{\sqrt{3/4 + (3/2 \cdot N + 1/2)^2}} \quad \text{for an odd } N$$

After that the coordinates of centers of segments are calculated according the following iterational formula

$$\begin{aligned} \bar{\rho}_{m,k} &= \begin{cases} m \cdot \bar{\Delta}_{m,k}, & \{k/m\} = 0 \\ \bar{\rho}_{m,k-1} + \bar{\Delta}_{m,k}, & \{k/m\} \neq 0 \end{cases}, \quad m = 1, \dots, N, \quad k = 0, \dots, 6m-1; \\ \bar{\Delta}_{m,k} &= \sqrt{3} r \cdot (\bar{e}_x \cos \varphi_{m,k} + \bar{e}_y \sin \varphi_{m,k}); \quad \varphi_{m,k} = \begin{cases} \frac{\pi k}{3m}, & \{k/m\} = 0 \\ \frac{\pi k}{3m} + \frac{2\pi}{3}, & \{k/m\} \neq 0 \end{cases}; \end{aligned} \quad (1.3.20)$$

where m is a number of a ring, k is a number of a segment inside a ring, by curly brackets is marked fractional part of variables.

To define if a point of the grid is inside a segment we employ a following algorithm. The length of a line is calculated which connects the center and border of a segment and runs through the chosen point with coordinates (x, y) :

$$\rho_{\max}(x, y) = \frac{\sqrt{3} r}{2 \cos(\varphi_1 - \frac{\pi}{3} \cdot [\varphi_1 / \frac{\pi}{3}] - \frac{\pi}{6})}, \quad \varphi_1 = \arctan_2(|x|, y); \quad (1.3.21)$$

An aperture function of a segment is defined as

$$w(\bar{\rho}) = \begin{cases} 1, & \rho \leq \rho_{\max}(\bar{\rho}) \\ 0, & \rho > \rho_{\max}(\bar{\rho}) \end{cases}, \quad \bar{\rho} = (x, y) \quad (1.3.22)$$

The control vector $\{A_l, B_l, C_l\}$ is found as a result of minimization of approximation errors

$$\sigma_l^2 = \int W(\bar{\rho}) w(\bar{\rho} - \bar{\rho}_l) (f_l(\bar{\rho} - \bar{\rho}_l) - \phi(\bar{\rho}))^2 d^2 \rho \rightarrow \min \quad (1.3.23)$$

This problem is also can be solved by the least squares method

Statical model of a flexible mirror

In numerical experiments as a flexible mirror we also used the model of a thin homogeneous plate. Static deformations of the plate were described by equation of biharmonic type

$$D \left(\frac{\partial^4 W}{\partial x^4} + \frac{\partial^4 W}{\partial x^2 \partial y^2} + \frac{\partial^4 W}{\partial y^4} \right) = f(x, y), \quad (1.3.24)$$

where (x, y) are the coordinates in the plane of the plate, D is the cylindrical stiffness, and f is the lateral load. At the points of fastening of the mirror on the frame (at these points the plate cannot be shifted, and deformations appear when tilting the mirror) the boundary conditions can be written in the form:

$$W|_{(x_i, y_i)} = \frac{\partial W}{\partial n} \Big|_{(x_i, y_i)} = 0, \quad (1.3.25)$$

while at the hinged point (where tilting causes no deformations)

$$W|_{(x_i, y_i)} = D \left(\frac{\partial^2 W}{\partial n^2} + \sigma \frac{\partial^2 W}{\partial \tau^2} \right) \Big|_{(x_i, y_i)} = 0 \quad (1.3.26)$$

Here $\partial/\partial n$ and $\partial/\partial \tau$ are the normal and tangential derivatives with respect to the plate plane, and σ is the Poisson coefficient.

Numerical solution of Eq. (1.3.24) was found by the finite-element method [31]. According the method, the plate was divided into a set of elements, with the local coordinate system $(O\xi, O\eta)$ affixed to each element. Deformations of each element were described by the vector

$$\vec{W} = \begin{Bmatrix} \vec{\xi} \\ \vec{\varphi} \\ \vec{\eta} \end{Bmatrix}$$

where $\vec{\xi}$ is the vector of lateral shifts of the element angular points (nodes of a computation grid), $\vec{\varphi}$ and $\vec{\eta}$ are the vectors of tilt angles with respect to the $O\xi$ and $O\eta$ axes. The vector \vec{W} has $3N_e$ components, where N_e is the number of

nodes of a grid bounding the element.

The vector of generalized forces \bar{Q} is associated with the vector of generalized coordinates \bar{W} and has the form

$$\bar{Q} = \begin{Bmatrix} \bar{P} \\ \bar{N} \\ \bar{T} \end{Bmatrix},$$

where \bar{P} is the vector of shearing forces, \bar{N} and \bar{T} are the vectors of deflection moments with respect to the axes of the local coordinate system. The relation between \bar{W} and \bar{Q} , found by the virtual displacement method, has the form [31/

$$[k]\bar{W} - \bar{f} = \bar{Q}. \quad (1.3.27)$$

The first term in the left-hand side of Eq. (1.3.27) describes the generalized forces of elastic deformations ($[k]$ is the stiffness matrix of an element), and the second term describes the external forces. In the right-hand side of Eq. (1.3.27), the forces of interaction between the elements are involved. The stiffness matrix $[k]$ is found as an integral of the element potential energy density, in this case the calculation is significantly simplified with limitations on the shape of deflection. For the deflection shape described by a finite power series, the matrix $[k]$ was calculated and presented in Ref. 31:

Taking into account the conditions of element conjugation that follow from the requirement for the continuity of the field of model displacements as a whole and equilibrium of interaction forces between elements, an equation describing static deformation of the whole model can be derived

$$[K]\bar{W} = \bar{F}. \quad (1.3.28)$$

Here \bar{F} is the vector of external forces (the vector is $3N_m$ -dimensional, where N_m is the number of nodes of the model). The stiffness matrix of the plate $[K]$ also can be found from the conditions of element conjugation, with the order of the matrix being $3N_m \times 3N_m$. Here, it should be emphasized that even for rare grid the operation with the matrix $[K]$ is difficult because of a large number of its

elements (this concerns mainly the operations of matrix inversion and data transfer from a hard disk to a random-access memory; the last procedure requires too much time). Thus for the grid 9×9 ($N_m = 81$) the matrix $[K]$ is of order 243×243 .

The order of the stiffness matrix $[K]$ can be decreased¹⁰ (reduction is accomplished), and operations with it are simplified if only transverse forces are exerted to the model, i.e., the vector \bar{F} included in Eq. (1.3.28) is of the form

$$\bar{F} = \begin{Bmatrix} \bar{P} \\ 0 \\ 0 \end{Bmatrix}.$$

In this case the stiffness matrix components to be multiplied by the zero components of the \bar{F} vector can be excluded beforehand. The second reduction of the matrix $[K]$ is carried out using the data on the geometry of actuator arrangement, assuming that at the points where the actuators are absent external forces do not act on the model. As a result of reduction, the order of the matrix is decreased down to $(N_m - N_{act}) \times N_{act}$ (N_{act} is the number of actuators), i.e., for 9×9 grid the stiffness matrix for a mirror with five actuators would be of the order 76×5 , that is, much lower than before the reduction.

Numerical model of a dynamic mirror

In the design of an adaptive optical system we have constructed a numerical model of a dynamic mirror enabling us to record the transient processes under deformation of a flexible plate. In this case deflection of the reflecting surface $W(x, y)$ was described by the matrix equation which, as equation (1.3.28), was obtained on the basis of the virtual work principle /31/

$$[M] \ddot{W} + [G] \dot{W} + [K] W = \bar{F}. \quad (1.3.29)$$

Here $[M]$, $[G]$, and $[K]$ are the inertia, oscillation damping, and stiffness matrices, respectively. The system of equations (1.3.29) was solved by the Runge-Kutta method /32/. The result of the system solution was the dynamic

field of lateral shifts of the model nodes, which describes the movements of the plate under the action of given forces. On the basis of this computational scheme the models of a mirror shown in Fig. 2a and b were constructed.

The transient processes illustrated in Figs. 3 and 4 occur when reproducing the given surface by the dynamic corrector. Shown here are the shifts of the points arranged on the mirror radius and the standard deviation $\varepsilon(t)$ of the corrector surface $W(x, y, t)$ from the given profile $\varphi(x, y)$ defined by the formula

$$\varepsilon(t) = \frac{\iint (\varphi(x, y) - W(x, y, t))^2 \rho(x, y) dx dy}{\iint \varphi(x, y)^2 \rho(x, y) dx dy},$$

where ρ is the weighting function.

Let us consider the accuracy of parabolic surface approximation by a flexible mirror. The action \bar{F} was determined by the least-squares method. In Eq. (1.3.28) the vector \bar{F} was introduced as follows (step action):

$$\bar{F} = \begin{cases} 0, & t < 0, \\ (f_1, f_2, \dots, f_n), & t \geq 0. \end{cases}$$

Here f_i are the components of the vector \bar{F} , and n is the number of actuators.

Because the damping coefficient was chosen small enough, it is practically impossible to see the damping of surface oscillations in the figures. The amplitude of oscillations of the function ε is small in comparison with its values, but without damping the accuracy of surface reproduction is insufficient (for a similar static mirror in focusing reproduction ε is 0.10–0.12, see Ref. 33). The data presented demonstrate the increase of frequency with the decrease of the distance between the clamped points and points of force application.

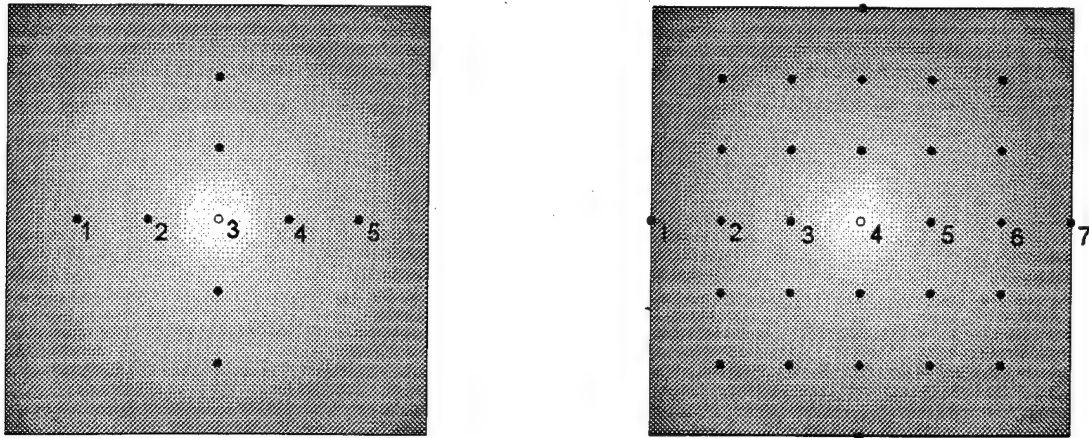


FIG. 2. Models of a flexible dynamic mirror: points of actuator locations (●) and points of mirror clamping on a frame (○) are shown. The serial numbers of points where surface displacements were registered are shown on the models.

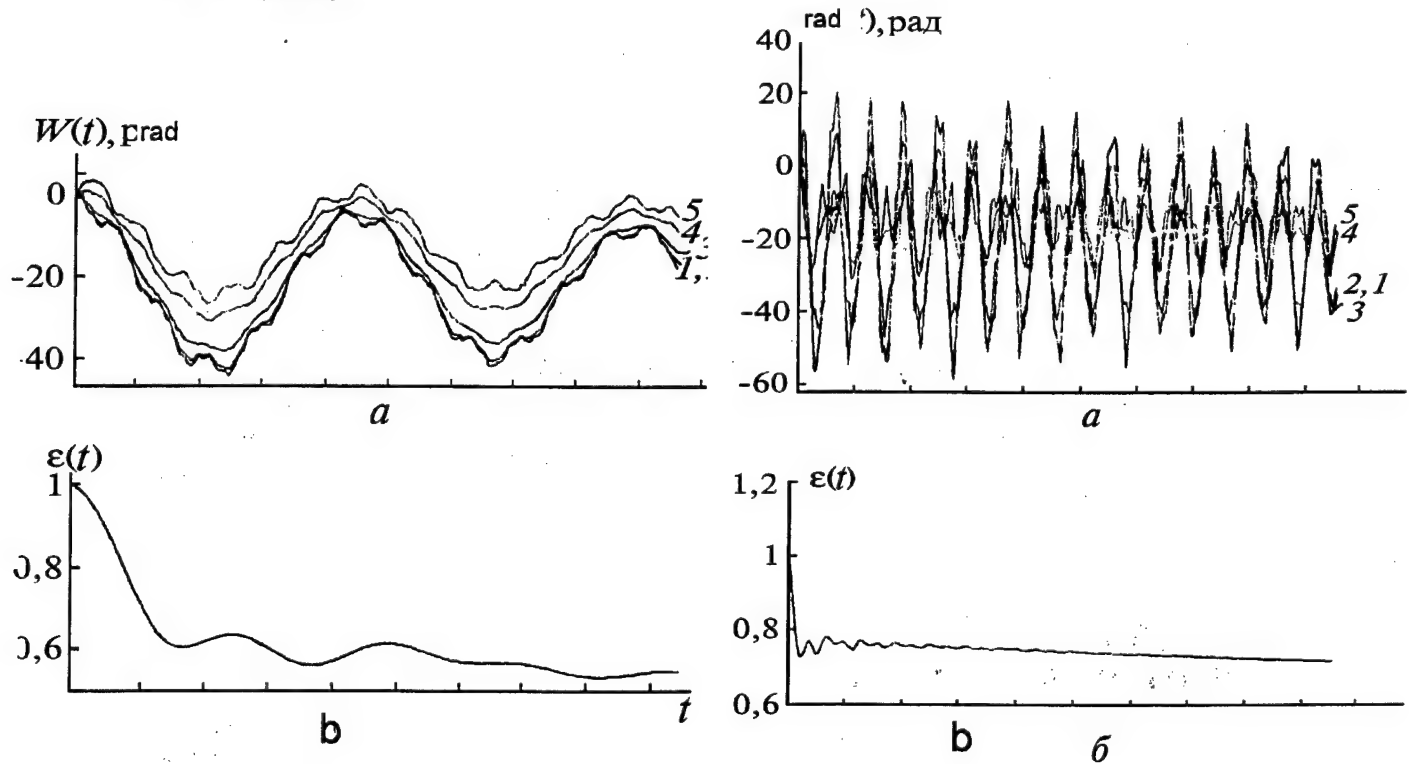


Fig. 3

Fig. 4

FIG. 3. Transient processes for the model of a mirror shown in Fig. 2a: shifts of reflecting surface at points 1–5 (a) and rms error $\varepsilon(t)$ (b).

FIG. 4. Transient processes for the model of a mirror shown in Fig. 2b.

Earlier we considered the use of dynamic mirror in multidither algorithm /33/. In this case the necessity of signal filtration for separation of variations of sensing radiation before completion of transient processes was shown. At present the efficiency of the phase conjugation algorithm with account of natural oscillations of reflecting surface of a corrector is investigated. Changing the method of force application to a mirror, we are supposed to decrease the influence of transient processes on a control algorithm. As an illustration, the oscillation of the surface driven by smoothly increasing components of the vector \vec{F} rather than by its step components is shown in Fig. 5. The significant decrease in the oscillation amplitude is observed.

1.4. Computer codes

Based on the numerical algorithms considered in the previous paragraphs, we have developed the program package for simulating the operation of an atmospheric adaptive optical system. When conducting numerical experiments the software package provides the following possibilities:

- setting of conditions of beam propagation (propagation in linear medium, under conditions of thermal blooming, in the turbulent atmosphere, under joint action of both latter factors);
- setting of the experimental geometry (vertical, slant, and horizontal paths);
- setting of the components of the adaptive system (the type of an adaptive mirror and a wave-front sensor);
- selection of the algorithm for beam control (phase conjugation, inversion of wave front);
- use of the set of service functions (solution of the problem and recording of amplitude and phase distributions at each step as well as with the subsequent plotting of dynamics, graphic representation of the results on a display screen and/or on a printer).

As a separate program unit with a built-in interface, the package includes the model of a flexible static mirror constructed on the basis of the finite-

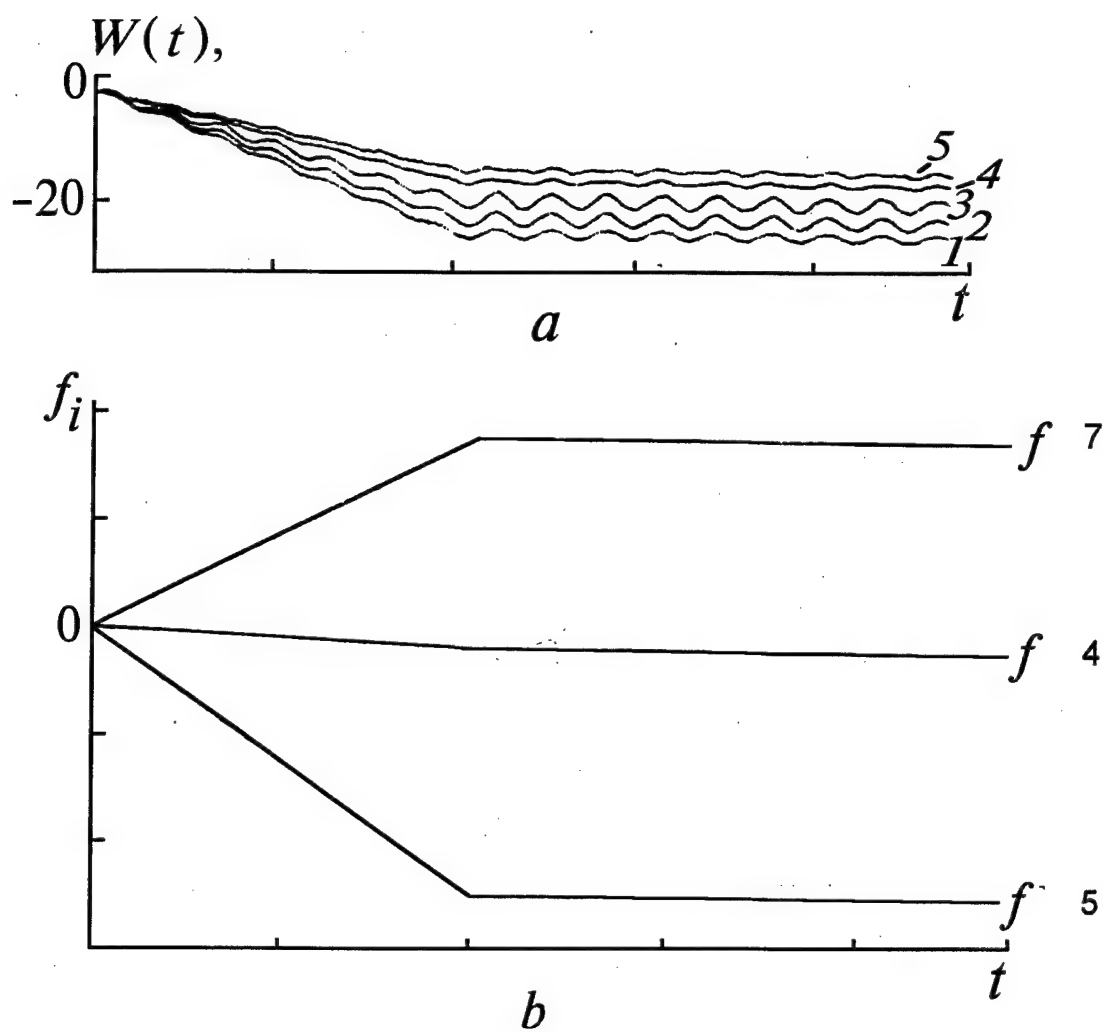


Fig. 5a. Oscillations of the mirror, the model corresponds to Fig. 2b.

Fig. 5b. Loading of the mirror surface, forces applied in points 4, 5, 7

element method /31/. The mirror parameters are set before running the basic program. When forming the adaptive system element base the mirror is included into the full model.

The developed program package is adapted to WINDOWS what makes it possible to use the VISUAL BASIC language² supported by this system. VISUAL BASIC enables one to implement the program control and parameter input/output operations of the form convenient for an user. At the same time, the basic computational procedures are written in FORTRAN language, what provides higher speed of operation as compared with VISUAL BASIC and has a wider set of built-in functions. The interaction is performed using the dynamic DLL library in which some subroutines written in FORTRAN are stored.

Setting of propagation conditions and forming the element base of an adaptive system

The parameters of an adaptive system are set by means of a specially developed graphic interface. In this case the program can be controlled using a computer keyboard or a mouse. Figure 6 shows the principal window of interface appearing on the display screen when making reference to the program. The column with the keys of the parameters setting occurs in the right-hand part of the window. They serve for initiating the following functions.

Key group **Prop** is intended for the selection of the beam propagation conditions (propagation under conditions of thermal blooming, in the turbulent atmosphere, vacuum, or with simultaneous consideration of turbulence and nonlinearity).

Key group **Correct** is intended for the selection of the algorithm of compensation for distortions. It is possible to consider the beam propagation in the absence of correction as well as to realize the control based on the algorithm of wave front inversion or phase conjugation.

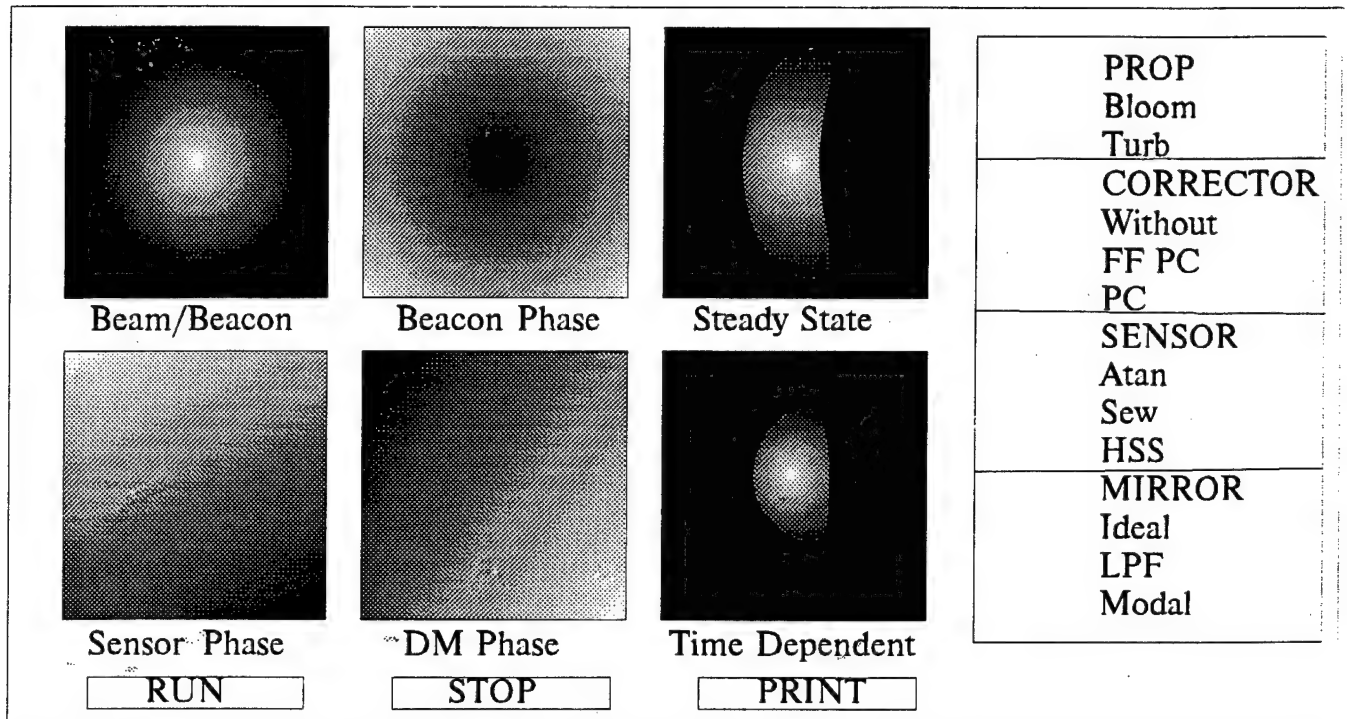


Fig. 6.

Key group **Sensor** is intended for selection of the wave-front sensor (an ideal sensor, a possibility to supplement an ideal device with the algorithm of joining of phase surface, and introduction of a Hartmann sensor into the system).

Group **Mirror** is intended for selection of an adaptive mirror.

Six half-tone figures occur in the central part of the interface main window. These figures show:

- 1) intensity of the basic or reference beam (according to the user's choice) in the plane of the emitter aperture;
- 2) phase distribution of the reference beam;
- 3) beam intensity distribution in the observation plane at thermal blooming;
- 4) phase distribution recorded by the wave-front sensor;
- 5) phase surface reproduced by an adaptive mirror;
- 6) running distribution of beam intensity in the observation plane.

The output to supplementary windows of the interface, by means of which the beam parameters (power, radius, wavelength) are set as well as the atmospheric parameters (wind velocity, turbulence intensity, absorption coefficient, and so on) is done via the menu of the main window.

Setting parameters of a flexible mirror

As was noted above the setting of parameters of the flexible static mirror in the above considered program package is formulated as a separate block. The basic interface windows are described in the present section.

With the call to the program, the first window appears in the display screen (Fig. 7), which provides for

- output of parameters of the mirror model recorded beforehand (the key "Current version of the mirror");
- calculation and recording of the rigidity matrix of a new model of the mirror (the key "New version of the mirror");
- completion of the program operation (the key "Exit").

STATICAL MIRROR

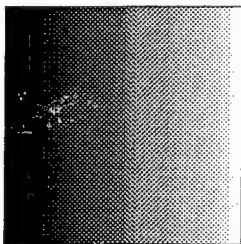
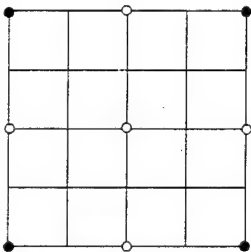
current version of mirror

current version of mirror

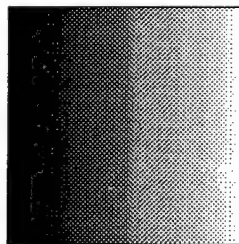
current version of mirror

Fig. 7

DEMO



material	copper
dimension of the grid	5 * 5
number of actuators	4
coordinates of actuators	



reproduction of polynimials

tilt

coma

defocusing

sph. aberrat.

Fig. 8.

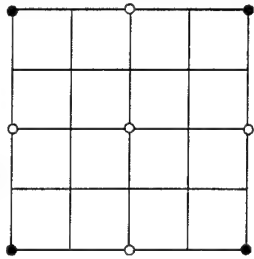
MAIN PANEL	
Material of mirror <div style="display: flex; justify-content: space-around; margin-bottom: 5px;"> <div style="border: 1px solid black; padding: 2px 10px; background-color: #cccccc;">copper</div> <div style="border: 1px solid black; padding: 2px 10px; background-color: #cccccc;">tin</div> <div style="border: 1px solid black; padding: 2px 10px; background-color: #cccccc;"></div> </div> <div style="display: flex; align-items: center; margin-bottom: 5px;"> <div style="border: 1px solid black; padding: 0 5px;">←</div> <div style="border: 1px solid black; padding: 2px 20px; flex-grow: 1; text-align: center;">dimension of the grid</div> <div style="border: 1px solid black; padding: 0 5px;">→</div> </div> <div style="background-color: #cccccc; padding: 2px 5px; margin-bottom: 5px; text-align: center;">position of actuators</div> <div style="background-color: #cccccc; padding: 2px 5px; margin-bottom: 5px; text-align: center;">position of fixed points</div> <div style="background-color: #cccccc; padding: 2px 5px; margin-bottom: 5px; text-align: center;">realization of the model</div> <div style="background-color: #cccccc; padding: 2px 5px; margin-bottom: 5px; text-align: center;">DEMO</div> <div style="background-color: #cccccc; padding: 2px 5px; margin-bottom: 5px; text-align: center;">DONE</div> <div style="background-color: #cccccc; padding: 2px 5px; margin-bottom: 5px; text-align: center;">exit</div>	Geometry of mirror  <div style="border: 1px solid black; padding: 10px; margin-top: 10px; min-height: 100px;"> current status </div>

Fig. 9.

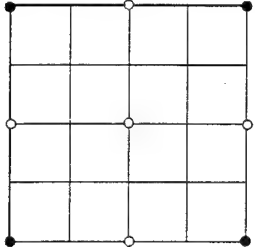
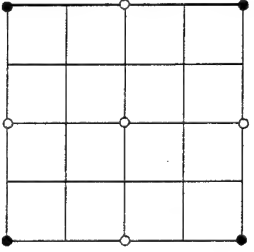
Position of actuators 	Geometry of the mirror 								
current status									
<table border="1" style="width: 100%; border-collapse: collapse;"> <tbody> <tr> <td style="padding: 5px;">material</td> <td style="padding: 5px;">copper</td> </tr> <tr> <td style="padding: 5px;">dimension of the grid</td> <td style="padding: 5px;">5 * 5</td> </tr> <tr> <td style="padding: 5px;">number of actuators</td> <td style="padding: 5px;">4</td> </tr> <tr> <td style="padding: 5px;">coordinates of actuators</td> <td></td> </tr> </tbody> </table>		material	copper	dimension of the grid	5 * 5	number of actuators	4	coordinates of actuators	
material	copper								
dimension of the grid	5 * 5								
number of actuators	4								
coordinates of actuators									
<div style="background-color: #cccccc; padding: 5px 20px; display: inline-block;">DONE</div>									

Fig. 10.

As a result of the call to the block for reading the rigidity matrix parameters, the panel DEMO appears in the screen (Fig. 8). In the left upper corner of this panel the diagram of the mirror is given. The points of actuator fastening are denoted by circles, the points of mirror fastening to the base are denoted by squares. Besides, the panel shows such parameters as the material of the plate, the number of actuators and points of fastening as well as the dimension of the computation grid. This block makes it possible to assess the quality of reproducing the lowest Zernike polynomials with the mirror (the keys "defocusing," "astigmatism," "coma," "sph. aberration"). When pressing these keys the image of the reproduced polynomial and the mirror surface appears at the lower left, the screen shows the value of the rms error of reproduction.

If the other rigidity matrix should be given, the program block is controlled by means of the interface panel "Main Panel" (Fig. 9). Here the user can select material of the plate and set the dimension of the computation grid (maximum size is 21×21). The number of mirror actuators, which cannot exceed the number of nodes, also depends on the latter parameter. The program operation is facilitated by the instructions at the screen.

Setting of the geometry of actuators location is done with the panel given in Fig. 10. In the left-hand part of Fig. 10, the calculating grid is presented where the points of possible location of actuators are denoted by the squares. To set the point, the mouse cursor is positioned on the chosen square. The position of actuators is set by single press and cancelled by double press. The geometry of points of mirror fastening to the support is set analogously.

Once the parameters are set the reference is made to the FORTRAN program for calculating and recording the rigidity matrix. The results of calculations can be seen upon calling to the panel DEMO.

In addition to the programs described the work is in progress to make the block for calculating the deformations of dynamic mirror and its graphic interface.

References to Chapter I

1. J.Herrmann, J. Opt. Soc. Am., Vol. 67, P.290-295 (1977).
2. V.P.Lukin, Kvant. Elektron., Vol. 4, P.923-927 (1977).
3. M.A. Vorontsov, Kvant. Elektron., Vol. 6, P.2078-2083 (1979).
4. L.A. Thompson, C.S. Nature (London), Vol. 328. No. 16. P.229-231 (1987).
5. H.W.Babcock, Publ. Astron. Soc. Pac., Vol. 65, P.229-236 (1953).
6. V.P. Linnik, Opt. Spektrosk., No.4, P.401-402 (1957)
7. D.Korff, G.Dryden, and R.P.Leavitt, J. Opt. Soc. Am. Vol.65. P.1321-1330 (1975).
8. D.L. Fried, J. Opt. Soc. Am. Vol. 72, P.52-61 (1982).
9. E.A. Vitrichenko, V.V. Voitsekhovich, and M.I. Mishenko. Preprint No. 790, Institute of Space Research of the Academy of Sciences, Moscow (1983), 17 pp.
10. E.A. Vitrichenko and M.I. Mishenko. Preprint No. 810, Institute of Space Research of the Academy of Sciences, Moscow (1983), 11 pp.
11. J.A.Fleck, J.R.Morris, and M.D.Feit, Appl. Phys. Vol.10. P.129-139 (1976).
12. K.Freischlad and C.L.Koliopoulos, Proc.SPIE. Vol.551. P.74-80 (1985).
13. Hiroaki Takajo and Tohru Takahashi, J. Opt. Soc. Am. A. Vol.5. P.1818-1827 (1988).
14. Hiroaki Takajo and Tohru Takahashi, J. Opt. Soc. Am. A. Vol.5. No. 3. P.416-425 (1988).
15. A.N. Bogaturov, Izv. Vyssh. Uchebn. Zaved. SSSR, Ser. Fizika, Vol. XXVIII. P.86-95 (1985)
16. Hiroaki Takajo and Tohru Takahashi, J. Opt. Soc. Am. A, Vol.5. P.1818-1827 (1988).
17. J. Hartmann, Objektivuntersuchungen. Zt.Instrumentenk. Vol.24 (1904).
18. V.P.Lukin, N.N.Mayer, and B.V.Fortes, Atmos. Oceanic Opt. Vol. 5. P.1241-1251. (1992)
19. V.P.Kandidov, I.V. Larionova, and V.V. Popov, Atmos. Oceanic Opt. Vol. 2. P.836-842 (1989).
20. D.L.Fried, J. Opt. Soc. Am. Vol.55. P.1426-1435 (1965).

21. C.B.Hogge and R.R.Butts, IEEE Trans. Ant. Prop. Vol. AP-24. P.144-154 (1976).
22. R.J.Noll, J. Opt. Soc. Am. Vol.66, P.207-211 (1976).
23. G.C.Valley and S.M.Wandzura, J. Opt. Soc. Am.
24. K.V. Shishakov and V.I. Shmal'gauzen, Atmos. Oceanic Opt. Vol. 3. P. 1244-1248 (1990).
25. J.Winocur, Appl.Opt. Vol.21. P.433-438 (1982).
26. J.H.Churnside, M.T.Tavis, and H.T.Yura, Opt.Lett. Vol.10. P.258-260 (1985).
27. P.H.Hu, J.Stone, and T.Stanley, J. Opt. Soc. Am. A. Vol.6. P.1595-1608 (1989).
28. V.P.Lukin, Kvant. Elektron., Vol.10. P.993-1001 (1983).
29. E.A. Vitrichenko and V.V. Voitsekhovich. Preprint No. 881, Institute of Space Research of the Academy of Sciences, Moscow (1984), 22 pp.
30. P.K.Mehta, Opt. Eng. Vol.29. P.1213-1222 (1990).
31. V.P. Kandidov, S.S. Chesnokov, and V.A. Visloukh, Finite element Method as applied to problems of mechanics, Moscow, Moscow State University Printing House, 1975, 376 pp.
32. D. Potter, Computational Physics, Moscow, Mir Publishers, 1975, 376 pp.
33. F.Yu. Kanev, L.I. Lavrinova, and V.P. Lukin, Atm. Oceanic Opt., Vol. 6. P. 962-968 (1993).

CHAPTER 2. PARTIAL CORRECTION FOR TURBULENT DISTORTIONS IN TELESCOPE

In order to provide complete compensation for turbulent distortions in the visible range at the aperture dimensions typical for modern telescopes (6–10 m) one needs for the development of adaptive systems with hundreds of control channels. More simple adaptive systems providing a complete compensation in the infrared range can give an essential advantage in angular resolution in the visible range too. In this case the image brightness characterized by the Strehl ratio remains much less than that in the diffraction-limited case, i.e., the system provides only partial compensation. In this section we present the results of numerical calculations of the partially corrected point spread function (PSF) and discuss possible approaches to composing the adaptive system configuration.

The spatial frequency spectrum of turbulent distortions is sufficiently wide, and although the lowest frequency wavefront aberrations (slopes and quadratic aberrations) give the largest contribution to the phase fluctuation variance for a telescope of large aperture a compensation for these aberrations does not improve the image quality essentially. Therefore to achieve a sufficiently high level of compensation the wavefront correctors with a large number of degrees of freedom ought to be used.

The complexity and cost of such devices grows rapidly with requirements to their spatial resolution. Therefore it is necessary to choose such a configuration of the corrector which, on the one hand, should not lead to excessive complication and cost rise of an adaptive optical system (AOS) and, on the other hand, should be able to provide a sufficient increase in the image quality.

Moreover, as the compensation efficiency depends also on the operation of other units of AOS, the characteristics of a compensating device (configuration, spatial resolution, and frequency range) must be coordinated and balanced with the parameters of other units of the adaptive optical system, for example, a reference source and wavefront sensor.

The topic of partial compensation has received plenty of attention in the literature [1,2,3,4]. In Ref.1 was performed some one-dimensional numerical simulation to test atmospheric wave front correction when the active element is not matched to the correlation scale in the pupil. The results demonstrated that substantial seeing improvement can be obtained with an adaptive optical system having a limited number of active elements. However, the Gaussian model for the atmosphere used in Ref.1 is a substantial simplification and is certainly not accurate at all scales. Results of Ref.2 illustrate that even a modest number of actuators can produce an image with essentially diffraction-limited resolution superimposed upon a background of scattered light. In Ref.3 the use of limited degree-of-freedom adaptive optics in conjunction with statistical averaging and linear image reconstruction algorithm is considered.

Here we expand consideration of partial compensation and present the partially compensated PSF for various kinds of corrector, for quantum noise effect and for cone anisoplanatism.

TABLE I. Values of the coefficients C_N

N	1	3	6	10	15	21
C_N	1.03	0.134	0.0648	0.0401	0.0279	0.0208

For large values of N an approximate formula can be written

$$C_N \approx 0.2944 N^{-\sqrt{3}/2}.$$

This theoretical results allow one to estimate the variance of residual distortions for a given parameter N of a modal corrector and vice versa, for a given level of the residual distortions, to determine the number of polynomials which ought to be compensated for. For example, to reach the level of residual distortions corresponding to the criterion $\lambda/6$ ($\sigma_N^2 \approx 1$) we obtain the estimation

$$N = 0.244 (D/r_0)^{1.92}. \quad (2.1.2)$$

Table II illustrates the dependence of N on the normalized aperture diameter.

TABLE II. Dependence of the number of modes N on the normalized aperture diameter

D/r_0	10	20	30	40	50
N	20	78	170	295	454

For such a number of degrees of freedom of the modal corrector the Strehl ratio approximately equals to

$$S = \exp(-\sigma_N^2) = 1/e \approx 0.37. \quad (2.1.3)$$

Obviously the bimorphic mirrors available now [9] are not able to provide such compensation level in the visible range (when the most probable value of $D/r_0 = 40-50$) but their use for the compensation in the infrared range (for $D/r_0 = 10-15$) seems to be quite reasonable. Moreover, as it will be shown below, and for higher values of the residual error variance the angular resolution close to the diffraction one (defined as the width of PSF at half maximum) can be obtained.

Calculations of the optical transfer function (OTF) for the modal compensation were performed in a number of papers (for example, in Ref./7/) but the OTF bears no direct information on the angular resolution. Let us consider the results of the numerical experiment we have carried out using our own software.

Turbulent distortions were simulated in approximation of a phase screen with a given parameter r_0 . Intensity fluctuation did not allowed for. For computations we employed 128×128 mesh of discretization and performed averaging over 100 random phase screens. Phase screens were generated and PSF was calculated with the use of discrete Fourier transform. Detailed description of the procedure of image forming simulation in the system "atmosphere – telescope" can be found in Ref. /10/.

The wavefront distortions were considered known (the model of an "ideal" sensor was used). A control by the corrector was determined on the base of minimization of integrated square error of the compensation. Calculations was performed for several values of the normalized aperture diameter $D/r_0 = 10, 20, 30$. The simulation of the modal compensation was performed for the values $N = 3, 10, 15, 21, 28$ that corresponds to compensation for the wavefront aberrations from 1st to 5th radial degrees inclusive.

Figure 1 (page 52) presents PSFs of a modal adaptive optical system obtained by simulation. The partially corrected PSF consists of two components. The width of the first component is equal approximately to the turbulent PSF and the angular size of the second component is diffraction-limited. Figure 2 (page 53) presents the radial cross-sections of the normalized PSF as functions of the telescope normalized diameter and the compensation parameter N .

According to the data of Table II to obtain the perfect correction of distortions for $D/r_0 = 20$ one need a modal corrector with $N = 78$. But even with $N = 10$ the first diffraction rings are seen in the central part of PSF, though intensity of the central maximum of PSF is 66 times less than that for diffraction-limited case ($SR = 0.015$).

Let us consider radial cross-sections normalized on the axial values of PSF which represented in Fig.2. Normalization of such kind allows one to consider the structure of PSF at different levels of residual error. Strehl ratio is shown in the legend of Fig. 2. At $D/r_0 = 10$ and $N = 21$ we obtain $SR = 0.44$. The data of Table 1 allow one to conclude that to obtain $SR = 0.37$ at $D/r_0 = 10$ we should take $N = 20$. So the results of numerical experiments correspond to analytical estimations.

It is interesting to consider how the parameter characterizing the contrast of PSF changes with increase of the aperture diameter and number of corrected distortions. Let us define the contrast as a ratio of the axial intensity to the intensity of the first diffraction ring. When two point objects are located at the angular distance about λ/D the contrast determines the ratio of intensities at this the dim object is seen with the background of the bright one.

In Fig.3 the dependence of the contrast on Strehl ratio is represented for modal correction. It is seen that at equal Strehl ratios the contrast is greater for large apertures. So a sharp diffraction circle appears earlier, i.e., at the higher level of turbulent distortions (the residual aberrations are high). The possible explanation is: at the lower level of intensity the turbulent components of the partially corrected PSF and its diffraction-limited part are characterized by the greater contrast for the same values of SR . It is seen that the high contrast diffraction limited core is observed up to the values of the Strehl ratio of the order of 0.01. This fact is not obvious and could be established only by direct calculation of the PSF.

Really, it could have been expected that a decrease in the axial image intensity by the factor of 10 leads to its, approximately threefold broadening, since the intensity is inversely proportional to the square of effective dimension with the invariable "form" of the intensity distribution in the image plane. However, when compensating for the lowest aberrations the spatial spectrum of wavefront distortions changes essentially. The small-scale aberrations not compensated for cause a redistribution of the corrected PSF power in the far "wings" (as

compared with the turbulent PSF for the same phase distortion variance). In this case the effective dimension of image is more than it could have been expected but the width of PSF at half maximum only slightly differs from the diffraction one. This gives a possibility to carry out astronomic observations connected with the measurement of object angular positions with the accuracy close to the diffraction one, even for the comparatively "poor" (by the Strehl ratio) compensation.

The following practical conclusions can be drawn. The use of bimorphic mirrors (the most close to a modal corrector by their characteristics) can be recommended at the first stages of the development of adaptive optics. Bimorphic mirrors will be able to provide a high level of the compensation in the far and middle infrared ranges and will provide partial correction in the near infrared range. It is hardly worth expecting the creation of bimorphic correctors in the visible region unless a good mirror is manufactured with about 100 to 200 control channels. Imaging binary stars with widely different brightness, and searching for planets may not be practical with partially compensated system.

Zonal and segmented correctors

Resolution close to the diffraction limited one, at small values of Strehl ratio, is also achievable with other types of wavefront correctors. Let the deformable mirrors of a zonal type and segmented correctors be considered from this point of view.

In contrast to the modal corrector it is characteristic of zonal correctors that application of a signal at one of the control points effects the shape of deformable mirror surface only in the part, under the influence of a given control channel. The deformable mirrors actuated with the piezoelectric elements stack to the rear side of the mirror are most widely used correctors of the zonal type. The "effect zone" dimension of a control element is determined by the distance from the nearest adjacent drive. Outside this zone the "response" of a mirror plate rapidly decreases.

Segmented adaptive mirrors also can be referred to the zonal class in the sense that the control of one mirror element does not affect the state of the rest its segments provided that no special connection is arranged. A distinguishing peculiarity of segmented mirrors is the presence of the surface breaks which are caused by the non-joint of adjacent segment edges.

For zonal type correctors /11,12/ as well as for the segmented mirrors /15/ the residual error variance of the phase correction is described by the formula

$$\sigma^2 = C (d/r_0)^{5/3}, \quad (2.1.4)$$

where d is the corrector characteristic scale, i.e., the distance between the control points of a zonal corrector or dimension of a segmented mirror element, and the coefficient C depends on the peculiarities of a corrector performance.

This expression is obtained within the Kolmogorov turbulence theory and can be used in the case when the outer turbulence scale exceeds the corrector scale d . Otherwise this formula overestimates residual distortions.

The value of the coefficient C for a segmented corrector can be estimated approximately based on the modal compensation theory considered in the previous section neglecting the fact that the shape of a controlled element is different from a circle. Since, for the isotropic turbulent distortions the variance of the residual correction error coincides with the variance of errors on a separate segment then $C = 1.03$ for the control of a segment location and $C = 0.134$ for the control of location and slopes of segments. For a deformable mirror with the Gaussian response function the estimation $C = 0.2$ can be used /7/.

The number of control elements, which are necessary for obtaining a given level of residual distortions can be estimated by the following formula

$$N = \left(\frac{D}{d}\right)^2 = (D/r_0)^2 (C/\sigma^2)^{6/5}. \quad (2.1.5)$$

Table III presents the estimations of the number of elements N for both corrector types calculated for the level of residual distortions corresponding to $\sigma^2 = 1$. The upper line of the Table presents the values of the aperture normalized diameter

(10 ... 50). Next two lines correspond to a segmented corrector, and the last line corresponds to a flexible mirror.

TABLE III. Estimations of the number of corrector elements N

D/r_0	10	20	30	40	50
$C = 1.03$	104	414	932	1657	2590
$C = 0.134$	9	36	81	143	224
$C = 0.2$	14	58	130	232	362

In Fig 4. the results of simulation are presented for a segmented mirror taking $D/d = 11$. Such spatial resolution is sufficient for the complete correction at $D/r_0 \approx 30$, but even for $D/r_0 = 50$ normalized PSF is, practically, diffraction limited in the boundaries of the first bright ring. At the same time Strehl ratio equals to 0.1, i.e., axial intensity is on the order of magnitude less than diffraction limited value.

Similar calculations were performed for a deformable mirror with the Gaussian response function. Results of this calculations are presented in Fig. 5. According to Table III resolution with $N = 9$ is sufficient for the complete correction only with $D/r_0 = 20$ but with $D/r_0 = 50$ diffraction core is developed in PSF with contrast close to 6.

Summing up the considered aspect of the partial correction we note that the appearance of a sharp diffraction core against the background of a turbulence distorted image occurs earlier (for large residual distortions) at higher level of the initial turbulent aberrations. It is explained by the fact that at lower intensity of the turbulent component in the partially corrected PSF its diffraction-limited part is characterized by a greater contrast for the same value of the Strehl ratio S .

For example, if for an uncorrected image the Strehl ratio S is 0.001 then the partial correction increasing the image axial intensity up to the level $S = 0.01$ leads to appearance of diffraction component of a PSF with the contrast parameter (ratio of the axial intensity to the intensity at the level of the first diffraction ring) of the order of 10. To obtain the same contrast at the initial

distortion level corresponding to $S = 0.01$ it is necessary to compensate for turbulent distortions up to the level corresponding to $S = 0.1$ that is reached at an essentially lower value of the variance of phase residual distortion.

It may be expected that already at the first stages of the development of adaptive optics for telescope it will be possible to achieve the angular resolution close to the diffraction one even at low values of the Strehl ratio. Although in this case a power portion concentrated in the diffraction circle will be much less than its diffraction-limited value the advantage as compared with an uncorrected image can be essential. First of all, this will provide a possibility to carry out accurate angular measurements in the visible region.

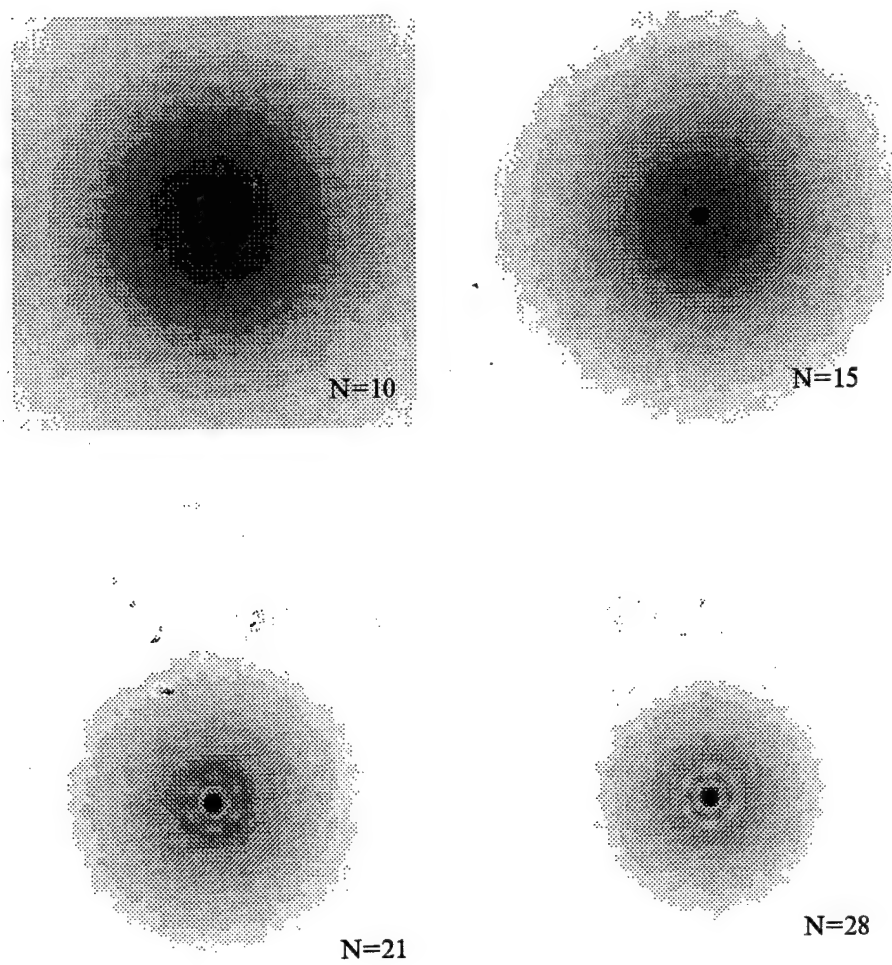


FIG. 1. Two-dimensional intensity distribution of PSF for the modal compensation. Value of the aperture normalized diameter is $D/r_0 = 20$.

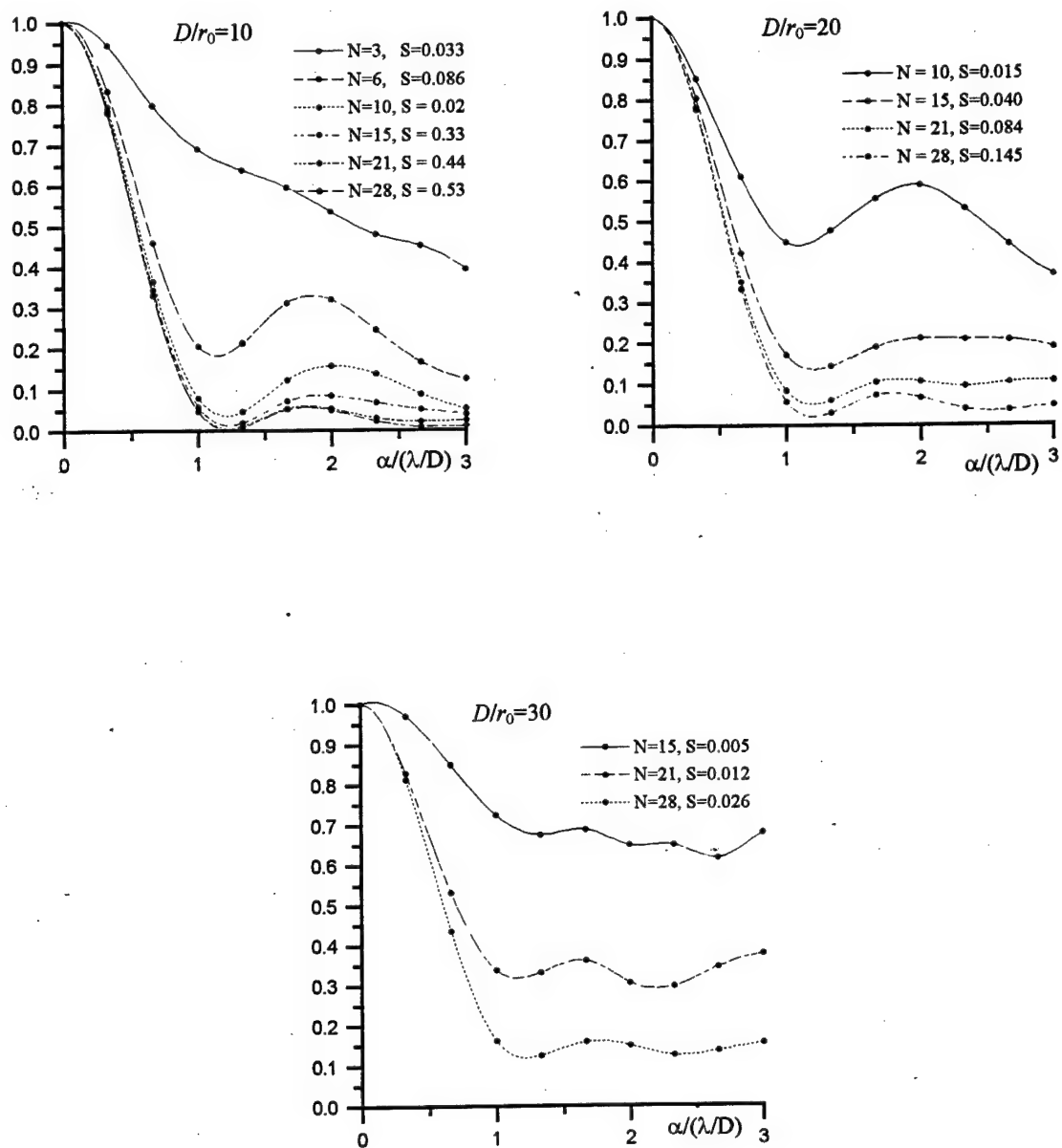


FIG. 2. PSFs, when a modal corrector is used. Parameter N corresponds to the number of Zernike polynomials. PSF is normalized to the axial value. S is the Strehl ratio.

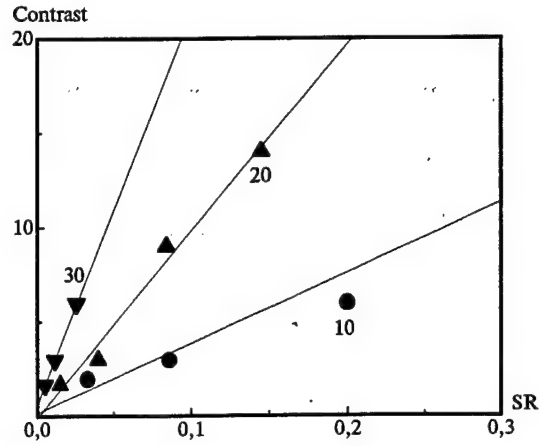


FIG. 3. The dependence of the contrast on Strehl ratio for modal correction. $D/r_0 = 10, 20, 30$.

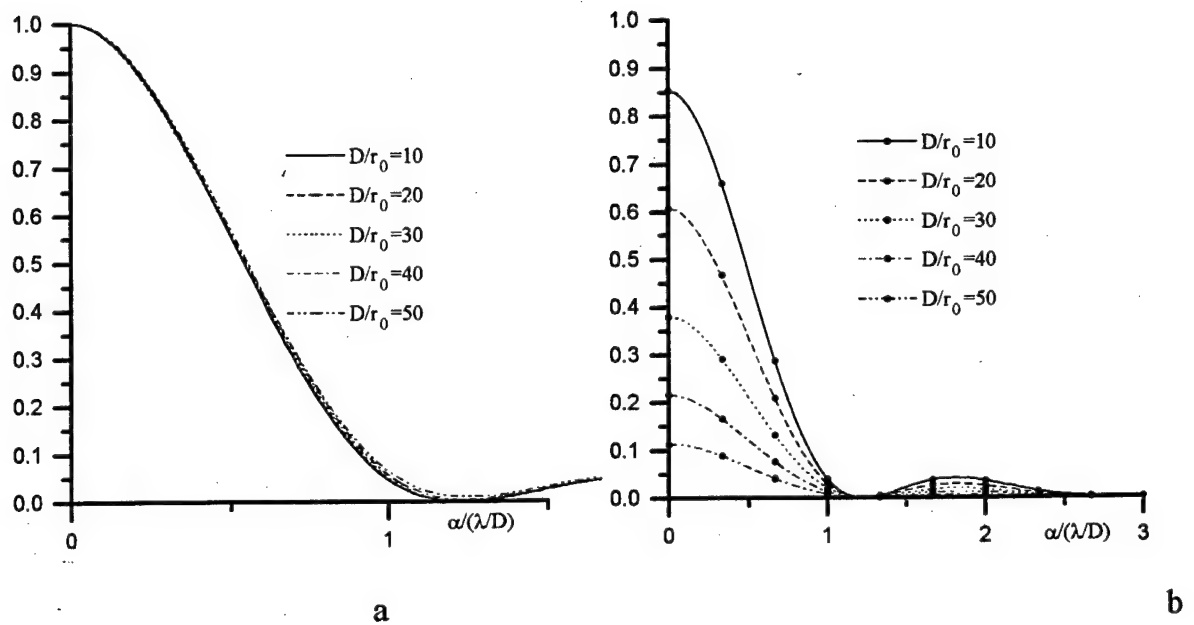


FIG. 4. PSF, when the segmented adaptive mirror with 84 elements of hexagonal form is used. Every segment is controlled by the position and slopes. *a* — PSF is normalized by its axial value. *b* — PSF is normalized by the diffraction maximum.

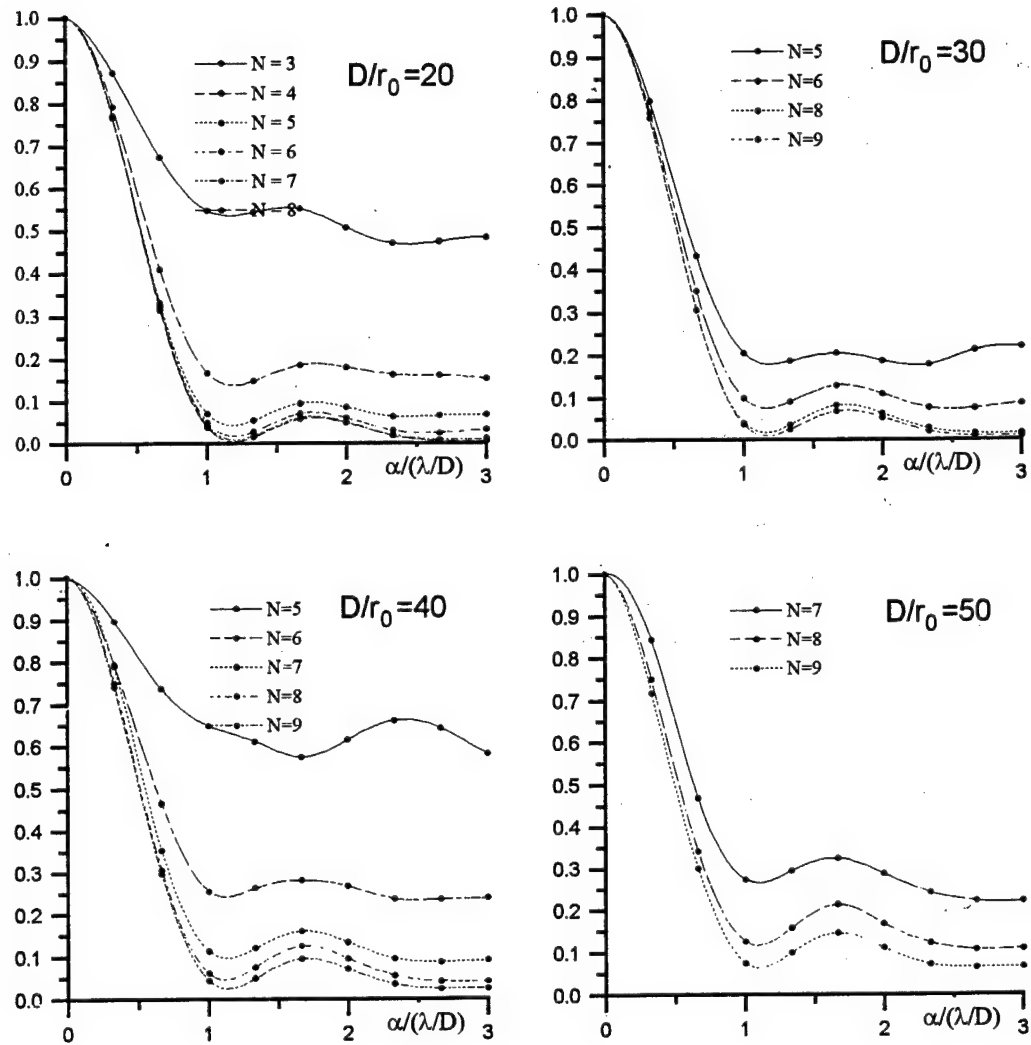


FIG. 5. PSF, when a flexible adaptive mirror with the Gaussian reference function is used. Parameter N corresponds to a number of the control points at the aperture diameter. PSF is normalized by its axial value.

2.2 Hartmann sensor and partial correction

Even if we have got a wavefront corrector with a sufficiently high spatial resolution the performance of an adaptive correction is impossible without a device measuring aberrations of the optical wave to be corrected. Since, the correction quality will be determined by the weakest member of the chain "measurement-compensation" during the development of an adaptive system one should make a choice balancing the characteristics of both a corrector and wavefront sensor.

Measurement of atmospheric aberrations of optical waves coming from astronomic objects in a real time has a set of specific peculiarities. First of all, these are fast temporal variability of aberrations and low level of the light flux /16,17/. Other peculiarity is a wide spatial spectrum of distortions. This spectrum is characterized by the presence of both small-scale and large-scale distortions that impose higher requirements to the dynamic range of wavefront distortion sensor (WFS). At present the Shack-Hartmann /8/ sensors are most widely used. Prototype of this sensor is the known classic Hartmann sensor widely used in the problems on testing astronomic optics.

Numerical model of the Shack-Hartmann sensor with a modal algorithm of retrieving from the Zernike polynomials /10/ is included as a component in the applied software we have developed to study the problems on adaptive formation of beams and images in the atmosphere. This model allows us to investigate the accuracy of measurements of the wavefront aberrations depending on the number of subapertures, quantum noise level, relationship between subaperture dimension and coherence radius, and estimating algorithm.

For this sensor spatial resolution is defined by the subaperture size and temporal resolution by the time of exposure. The product of subaperture area, exposure time, and intensity of reference signal defines the number of photoelectrons $\langle N_{ph} \rangle$ at the output of the sensor. This number is a parameter which defines signal to noise ratio.

Let us consider the effect of photon noise on the correction quality. In numeric experiments we will use a model of Shack-Hartmann sensor with 10×10 array of subapertures. To reconstruct a map of aberrations let us employ a modal reconstruction algorithm calculating 28 Zernike polynomials. Let us assume that ideal corrector reproduces exactly all aberrations and the aperture diameter is equal to $10r_0$. So the radius of subapertures is equal to the coherence length. The delay of correction is assumed to be zero. Turbulent distortions are simulated in phase screen approximation, no intensity fluctuations are allowed for.

PSFs computed in this numeric experiment are shown in Fig. 6. Average number of photons $\langle N_{ph} \rangle$ incident on a sensor subaperture at exposure time varied in the interval 5–100. In the figure PSFs are shown for $\langle N_{ph} \rangle = 5, 10, 100$. For $\langle N_{ph} \rangle = 100$ Strehl ratio is equal to 0.38. This value is close to the result obtained for a modal corrector with the same number of corrected aberrations ($N = 28$) when the model of an ideal sensor was used ($SR = 0.53$). The difference can be induced by a small error due to noise. At $\langle N_{ph} \rangle = 5$ the axial value of PSF decreases almost twice and $SR = 0.19$. It can readily be seen from the comparison of PSFs normalized on axial value that the radius of PSFs changes only a little and the contrast is still equal to 10 even at this level of noise. Further decrease of reference wave intensity results in sharp increase of variance σ^2 of residual phase distortions and decrease of SR .

So the increase of phase aberrations along with decrease of a reference source brightness results in a two-component structure of corrected PSF. We can see a turbulent circle and diffraction core.

These requirements to the intensity level determine the minimal brightness of a reference source, and in combination with the isoplanatism angle value and distribution of stars with such brightness over the celestial sphere determine the portion of this sphere area where the effective compensation for turbulent distortions is possible. Different estimations show that this portion does not exceed several percent and depends on operation wavelength and turbulence

altitude profile. To provide the qualitative compensation on all area of the celestial sphere it is necessary to create an artificial reference source.

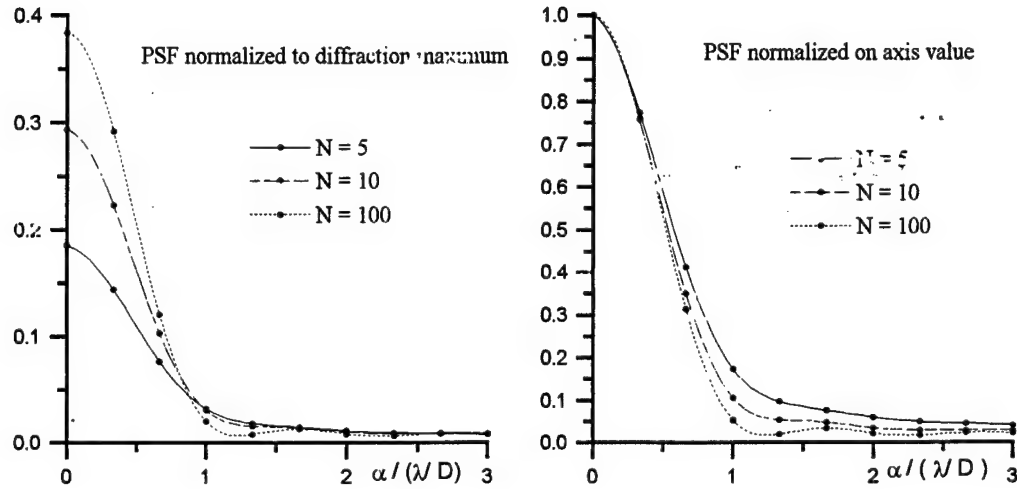


FIG. 6. Results of the simulation of an adaptive telescope with the Shack-Hartmann sensor. Normalized diameter of the aperture is $D/r_0 = 10$. Dimensions of the sensor lens diaphragm are 10×10 . Estimation of the wavefront aberrations was performed by the modal algorithm (28 Zernike polynomials). Parameter N corresponds to the average-statistical number of photons at the subaperture during one exposure.

2.3 Cone anisoplanatism and partial correction

Two basic types of the anisoplanatism are distinguished in the image correction schemes used at present: the angular anisoplanatism and cone anisoplanatism. The first one occurs for the object image correction using reference wave from a star located at a certain angular distance from this object. When correcting image of an extended object the angular anisoplanatism manifests itself in the fact that only a part of the object laying within isoplanatism zone is sharp.

Cone anisoplanatism takes place when a laser guide star (LGS) is used as a reference source. In this case the source angular position, as a rule, coincides with the angular position of the observed object, but the latter is at infinity and the LGS altitude is limited within the effectively scattering atmosphere. In contrast to the "classic" angular anisoplanatism the angle between the beam paths of the reference and corrected waves changes as a function of distance between the considered point and the center of receiving aperture.

Let us consider the effect of this error on PSF. We assume the infinite spatio-temporal resolution of the adaptive optics system, absence of noise, and the cone anisoplanatism as the main source of errors. The atmosphere is stimulated by a number of phase screens. Passing of a wave through the phase screens is computed in geometric optics approximation not allowing for diffraction effects and intensity fluctuations. We assume that the angle of arrival fluctuations are corrected with the use of a bright natural star.

The altitude profile of turbulence intensity we take corresponding to Gurvich's model of «the best conditions». Aperture diameter is $D = 10\text{m}$, that correspond to the diameter of Keck telescope and Russian telescope AST-10 (presently under development). The altitude of an artificial beacon H was taken equal to 10 and 100 km, that correspond to schemes with Rayleigh and sodium beacons. Above this we varied wavelength in the interval from 1 to 5 μm in the case of Rayleigh beacon ($H = 10\text{ km}$) and from 0.5 to 2 μm in the case of a sodium beacon ($H = 100\text{ km}$).

Figure 7 presents the PSF for this versions of the LGS. It is clear that the use of Rayleigh reference source is effective in the infrared range only (small values of D/r_0). Use of the sodium LGS allows one to obtain good correction quality in the infrared range and makes it possible to provide nearly diffraction limited angular resolution under the condition of partial compensation in the visible region of spectrum.

In the visible range the radius of PSF is also close to diffraction limited one with $SR = 0.23$ and contrast greater than 10. Taking into account the fact that angular coordinate is normalized on the ratio λ/D one can conclude that in optical range the angular resolution is higher as compared with IR region.

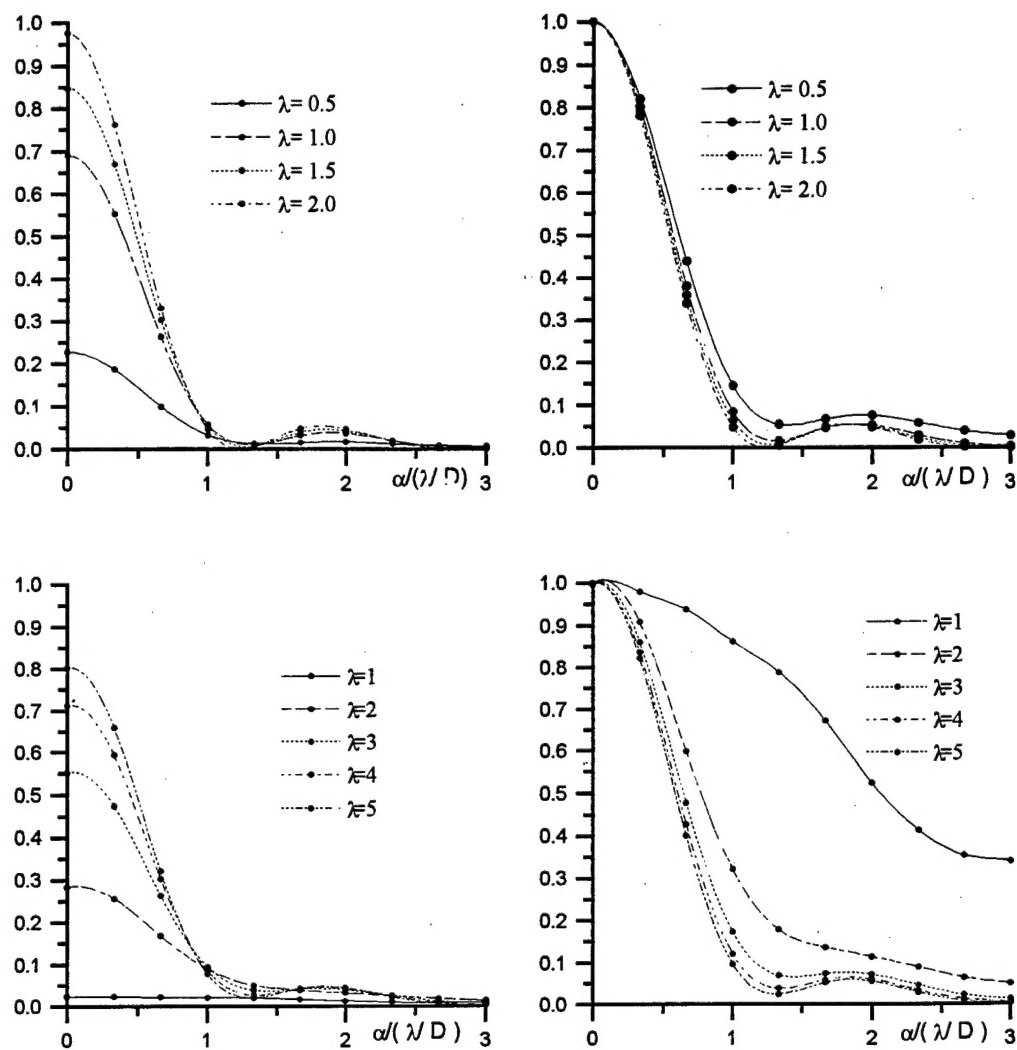


FIG. 7. PSFs of the 10-meter telescope at different wavelengths for the adaptation using a laser guide star. Upper plots are for the sodium LGS ($H = 100$ km), the lower plots are for the Rayleigh LGS ($H = 10$ km). At the left plots the PSF is normalized to the diffraction maximum, at the right plots the PSF is normalized to its axial value. The wavelength λ is given in μm .

CONCLUSION

Let us sum up the analysis of partial correction for turbulent aberrations. We have considered three variants of the idealized adaptive system. In each case we allowed for only one factor influencing residual distortions of PSF. In the first variant the spatial resolution of the corrector was taken as such a factor, noise of the sensor was taken in the second variant, and cone anisoplanatism in the third. In all cases we found out that radius of PSF increases relatively slowly and the width of PSF is almost diffraction limited for large residual distortions.

These results are analogous with the results of uncorrected PSF for finite outer scale of turbulence. Partial correction is, first of all, correction for the lowest aberrations which correspond to large scale inhomogeneities of the atmosphere. Particularly it is true in the case when the main factor is a finite spatial resolution of correcting device. Aberrations induced by inhomogeneities with size greater than size of a corrector element can be compensated and the spectrum of residual aberrations is the same as a spectrum with outer scale equal to the size of an element.

From the stated above the case of diffraction core appearance is clear. Explanation can be found in analysis of phase structure function, OTF and PSF. Phase structure function $D(\rho)$ saturates at level $2\sigma_\phi^2$ with the value of argument ρ about turbulence outer scale L_0 or corrector element size d . Atmospheric optical transfer function $\tau(\rho) = \exp(-D(\rho)/2)$ decreases to value $\exp(-\sigma_\phi^2)$ and saturates too. So OTF consists of the narrow peak OTF_1 with the width about L_0 or d and wide component OTF_2 :

$$OTF = OTF_1 + OTF_2$$

PSF is Fourier transform (FT) of OTF so $PSF = FT(OTF_1 + OTF_2) = PSF_1 + PSF_2$. Since width of Fourier transform is inversely proportional to original function, narrow component OTF_1 transforms to wide component PSF_1 (turbulent seeing), and wide component OTF_2 transforms to narrow component PSF_2 (diffraction core).

REFERENCES TO CHAPTER 2

1. P.Nisenson and R.Barakat, J. Opt. Soc. Am. **A4**, 2249–2253 (1987).
2. R.C. Smithson and M.L. Peri J. Opt. Soc. Am., **A6**, 92–97 (1989).
3. M.C. Roggemann, Appl. Opt., **30**, 4227–4233 (1991).
4. J.M. Beckers and F. Merkle, Astrophysics and space science **160**, 345–351 (1989).
5. D.L. Fried, J. Opt. Soc. Am. **55**, 1426–1435 (1965).
6. R.J. Noll, J. Opt. Soc. Am. **66**, 207–211 (1976).
7. J.Y. Wang and J.K. Markey, J. Opt. Soc. Am. **68**, No. 1, 78–88 (1978).
8. J. Winocur, Appl. Opt. **21**, 433–438 (1982).
9. F.Roddier, M.Northcott and J.E. Graves Pub.Astr.Soc.Pac., 131–149, January (1991).
10. B.V.Fortes and V.P.Lukin, Anton Kohnle, Walter Miller, Editors, Proc. SPIE **1668**, 477–488 (1992).
11. M.A. Ealey and J.F. Washeba Opt.Eng., **29**, 1191–1198 (1990).
12. M.A. Ealey and J.A. Wellman Active and adaptive optical components, Mark A. Ealey, Editor, Proc.SPIE **1543**, 36–51 (1991).
13. R.K. Tyson, Opt. Eng. **29**, 1165–1173 (1990).
14. R.B. Shack and B.C. Platt, J. Opt. Soc. Am. **61**, 1586 (1971).
15. B. Hurlburd and D.Sandler Opt.Eng. **29**, 1186–1190 (1991).
16. E.P. Wallner J. Opt. Soc. Am. **A73**, 1771–1776, 1983
17. B.M. Welsh, B.L.Ellenbroek, M.C. Roggermann and T.L.Pennington, Appl. Opt. **34**, 4186–4195 (1995).